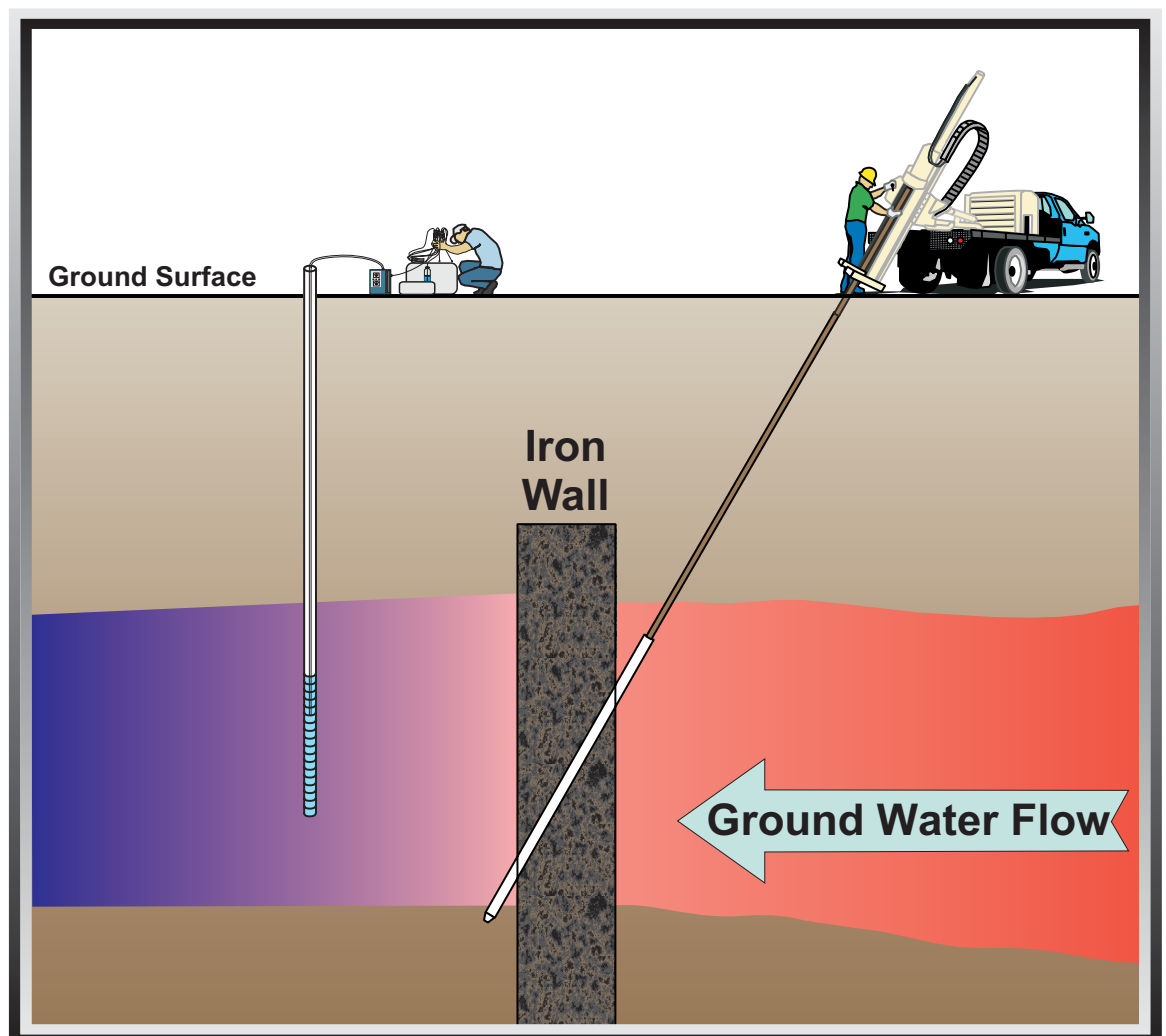


Capstone Report on the Application, Monitoring, and Performance of Permeable Reactive Barriers for Ground-Water Remediation:

Volume 1

Performance Evaluations at Two Sites



Capstone Report on the Application, Monitoring, and Performance of Permeable Reactive Barriers for Ground-Water Remediation:

Volume 1 – Performance Evaluations at Two Sites

Richard T. Wilkin and Robert W. Puls
Ground Water and Ecosystems Restoration Division
National Risk Management Research Laboratory
Ada, Oklahoma 74820

National Risk Management Research Laboratory
Office of Research and Development
U.S. Environmental Protection Agency
Cincinnati, OH 45268

Notice

The U.S. Environmental Protection Agency through its Office of Research and Development funded the research described here. It has been subjected to the Agency's peer and administrative review and has been approved for publication as an EPA document. Mention of trade names or commercial products does not constitute endorsement or recommendation for use.

All research projects making conclusions or recommendations based on environmentally related measurements and funded by the Environmental Protection Agency are required to participate in the Agency Quality Assurance Program. This project was conducted under an approved Quality Assurance Project Plan. The procedures specified in this plan were used without exception. Information on the plan and documentation of the quality assurance activities and results are available from the Principal Investigator.

Foreword

The U.S. Environmental Protection Agency (EPA) is charged by Congress with protecting the Nation's land, air, and water resources. Under a mandate of national environmental laws, the Agency strives to formulate and implement actions leading to a compatible balance between human activities and the ability of natural systems to support and nurture life. To meet this mandate, EPA's research program is providing data and technical support for solving environmental problems today and building a science knowledge base necessary to manage our ecological resources wisely, understand how pollutants affect our health, and prevent or reduce environmental risks in the future.

The National Risk Management Research Laboratory (NRMRL) is the Agency's center for investigation of technological and management approaches for preventing and reducing risks from pollution that threatens human health and the environment. The focus of the Laboratory's research program is on methods and their cost-effectiveness for prevention and control of pollution to air, land, water, and subsurface resources; protection of water quality in public water systems; remediation of contaminated sites, sediments and ground water; prevention and control of indoor air pollution; and restoration of ecosystems. NRMRL collaborates with both public and private sector partners to foster technologies that reduce the cost of compliance and to anticipate emerging problems. NRMRL's research provides solutions to environmental problems by: developing and promoting technologies that protect and improve the environment; advancing scientific and engineering information to support regulatory and policy decisions; and providing the technical support and information transfer to ensure implementation of environmental regulations and strategies at the national, state, and community levels.

This publication has been produced as part of the Laboratory's strategic long-term research plan. It is published and made available by EPA's Office of Research and Development (ORD) to assist the user community and to link researchers with their clients. The purpose of this document is to provide detailed performance monitoring data on full-scale Permeable Reactive Barriers (PRBs) installed to treat contaminated ground water at two different sites. This report will fill a need for a readily available source of information for site managers and others who are faced with the need to remediate ground water contaminated by chlorinated solvents, chromium, arsenic, nitrates, and other organic and inorganic compounds and are considering the use of this cost-effective technology. The PRBs discussed in this report are among the oldest full-scale systems available for study and provide an opportunity to analyze the performance of systems with more than five years of field history. In addition, the PRBs examined here have contrasting design and hydrogeochemical characteristics that are useful in the context of gaining insight about the factors that govern PRB longevity and long-term performance. The information provided in this document will be of use to stakeholders such as state and federal regulators, Native American tribes, consultants, contractors, and other interested parties.



Ground Water and Ecosystems Restoration Division
National Risk Management Research Laboratory

Abstract

Research results discussed in this report explore the geochemical and microbiological processes within zero-valent iron Permeable Reactive Barriers (PRBs) that may contribute to changes through time in iron reactivity and decreases in reaction zone permeability. Two full-scale PRBs were evaluated in this study: the U.S. Coast Guard Support Center PRB located near Elizabeth City, North Carolina, and the Denver Federal Center PRB in Lakewood, Colorado. Detailed water sampling and analysis, core sampling, and solid-phase characterization studies were carried out to: i) evaluate spatial and temporal trends in contaminant concentrations and key geochemical parameters; ii) characterize the type and nature of surface precipitates forming over time in the reactive barriers; and iii), identify the type and extent of microbiological activity within and around the reactive barriers.

Trends in geochemical parameters (e.g., pH and oxidation-reduction potential) may signal changes in system performance, but no clear correlations between these parameters and decreased system performance have been observed to date at the sites studied. Long-term trends in geochemical parameters are consistent with contaminant removal trends observed at both sites. Spatial and temporal variations in the concentration distribution of terminal electron accepting species (e.g., sulfate), specific conductance, and Eh suggest that both anaerobic iron corrosion and microbial activity play important roles in controlling the oxidation-reduction potential in iron barriers. Low Eh values (≤ 100 mV relative to the standard hydrogen electrode) and decreases in the specific conductance of ground water between upgradient contaminant plumes and sampling points within reactive iron media are consistently observed in normally operating PRB systems.

The rate of mineral and biomass buildup was evaluated at both sites. The principal factors that determine the amount of mineral precipitation in zero-valent iron PRBs are flow rate, ground-water chemistry, and microbial activity. After five years of operation, the Elizabeth City and Denver Federal Center reactive barriers have developed consistent patterns of spatially variable mineral precipitation and microbial activity. The development of precipitation and biomass fronts result from abrupt geochemical changes that occur at upgradient interface regions coupled with ground water solute transport. Upgradient regions at both sites investigated in this study have witnessed the greatest accumulation of mineral mass and biomass. However, neither of the sites of this study show complete filling of available pore space after five years, suggesting that flow characteristics should not be affected by the accumulation of authigenic components. For zero-valent iron systems, the reactive media is a long-term sink for C, S, Ca, Si, Mg, and N. Porosity loss in the iron media due to precipitation of inorganic carbon and sulfur minerals can be estimated by integrating the concentrations of inorganic carbon and sulfur as a function of distance in the iron and estimating the volume loss by using the molar volumes of zero-valent iron, calcium carbonate, iron carbonate, and iron sulfide. Porosity loss estimates have ranged from about 1% to 4% per year in this study. Based on these estimates, the average porosity of the PRB at Elizabeth City, for example, would not be expected to approach that of the surrounding aquifer for 15 to 30 years. As corrosion minerals form on the surface of the iron media, reactive surfaces are coated, presumably decreasing the effective reactive surface area. However, corrosion products formed include some minerals which themselves are highly reactive and capable of transforming inorganic and organic contaminants into immobile or non-toxic forms. This phenomenon must also be factored into lifetime projections.

While long-term performance observations of the Elizabeth City and Denver Federal Center site are now past five years, there has still not been sufficient time to adequately predict the lifetime of these PRBs or most other PRBs. It is clear that lifetimes exceeding 10 years are reasonable to expect under some conditions and that PRBs may function adequately for much longer. Continued studies are needed to better predict longevity based on ground-water composition, flow rate and contaminant flux.

Table of Contents

Notice	ii
Foreword	iii
Abstract	iv
Table of Contents	v
Figures	vii
Tables	xii
Acknowledgments	xiv
1.0 Introduction	1
1.1 Federal Tri-Agency Initiative	2
1.1.1 DoD Studies	2
1.1.2 DOE Studies	3
1.1.3 EPA Studies	3
2.0 Site Descriptions	5
2.1 U.S. Coast Guard Support Center	5
2.2 Denver Federal Center	5
3.0 Elizabeth City PRB Monitoring Results	9
3.1 Ground Water Monitoring	9
3.1.1 Contaminant Behavior	9
3.1.2 Geochemical Parameters	13
3.1.3 Dissolved Cations and Anions	18
3.2 Core Sampling at Elizabeth City	25
3.2.1 Carbon Analysis	25
3.2.2 Sulfur Analysis	33
3.2.3 Cr Extractions	39
3.2.4 X-ray Diffraction Analysis	39
3.2.5 Scanning Electron Microscopy	41
3.2.6 Microbial Characterization	46
3.3 Summary of Results from the Elizabeth City Site	52
4.0 Denver Federal Center Monitoring Results	53
4.1 Ground Water Monitoring	53
4.1.1 Gate 1 Contaminant Behavior	53
4.1.2 Gate 2 Contaminant Behavior	58
4.1.3 Gate 3 Contaminant Behavior	58
4.1.4 Geochemical Parameters	58
4.1.5 Hydrogen Gas Concentrations	62
4.1.6 Dissolved Cations and Anions	64
4.2 Core Sampling at the Denver Federal Center	68
4.2.1 Carbon Analysis	71
4.2.2 Sulfur Analysis	71
4.2.3 X-ray Diffraction Analysis	71
4.2.4 Scanning Electron Microscopy	71
4.2.5 Microbial Characterization	80
4.3 Summary of Results from the Denver Federal Center Site	82

5.0 Factors Affecting Longevity and Performance	87
5.1 Fe ⁰ Dissolution	87
5.2 Anion Composition	89
5.2.1 Bicarbonate Reactions	89
5.2.2 Sulfate Reactions	96
5.2.3 Nitrate Reactions	97
5.2.4 Reactions with Silica	97
5.2.5 Reactions with Oxygen	98
5.3 Mineral Precipitation	99
5.3.1 Pore Volume Reduction	99
5.3.2 Loss of Reactivity.	103
5.4 Microbial Activity	104
5.5 Hydrogeological Issues	107
6.0 State of Permeable Reactive Barrier Technology and Lessons Learned from Long-Term Performance Monitoring	111
6.1 Permeable Reactive Barriers: An Accepted Remedial Option for Containment & Treatment of Contaminated Ground Water	111
6.2 Lessons Learned: Site Characterization and PRB Construction	112
6.3 Lessons Learned: Long-term Performance Assessments of PRBs	112
6.3.1 Recommendations for Future Research.	113
7.0 References	115
Appendix A	121
Appendix B	135

Figures

Figure 2.1	Plan view map of the PRB at the U.S. Coast Guard Support Center, Elizabeth City, NC	7
Figure 2.2	Plan view map of the PRB at the Denver Federal Center, Lakewood, CO (after McMahon et al., 1999)	8
Figure 2.3	Schematic cross-section of the Denver Federal Center funnel-and-gate system (after McMahon et al., 1999)	8
Figure 3.1	Concentrations of contaminants through time in monitoring wells located hydraulically upgradient of the Elizabeth City PRB	10
Figure 3.2	Concentrations of TCE ($\mu\text{g/L}$) through time in monitoring wells located hydraulically downgradient of the Elizabeth City PRB	13
Figure 3.3	Cross-sectional profiles showing total chromium concentrations (mg/L) in transects 1, 2, and 3 (Elizabeth City PRB)	14
Figure 3.4	Cross-sectional profiles showing TCE concentrations ($\mu\text{g/L}$) in transects 1, 2, and 3 (Elizabeth City PRB)	15
Figure 3.5	Cross-sectional profiles showing cis-DCE concentrations ($\mu\text{g/L}$) in transects 1, 2, and 3 (Elizabeth City PRB)	16
Figure 3.6	Cross-sectional profiles showing VC concentrations ($\mu\text{g/L}$) in transects 1, 2, and 3 (Elizabeth City PRB)	17
Figure 3.7	Cross-sectional profiles showing pH distributions in transects 1, 2, and 3 (Elizabeth City PRB)	19
Figure 3.8	Cross-sectional profiles showing Eh distributions (mV) in transects 1, 2, and 3 (Elizabeth City PRB)	20
Figure 3.9	Cross-sectional profiles showing specific conductance distributions ($\mu\text{S/cm}$) in transects 1, 2, and 3 (Elizabeth City PRB)	21
Figure 3.10	Cross-sectional profiles showing calcium concentrations (mg/L) in transects 1, 2, and 3 (Elizabeth City PRB)	22
Figure 3.11	Cross-sectional profiles showing magnesium concentrations (mg/L) in transects 1, 2, and 3 (Elizabeth City PRB)	23
Figure 3.12	Cross-sectional profiles showing sodium concentrations (mg/L) in transects 1, 2, and 3 (Elizabeth City PRB)	24
Figure 3.13	Cross-sectional profiles showing potassium concentrations (mg/L) in transects 1, 2, and 3 (Elizabeth City PRB)	26
Figure 3.14	Cross-sectional profiles showing chloride concentrations (mg/L) in transects 1, 2, and 3 (Elizabeth City PRB)	28
Figure 3.15	Cross-sectional profiles showing sulfate concentrations (mg/L) in transects 1, 2, and 3 (Elizabeth City PRB)	29

Figure 3.16 Cross-sectional profiles showing alkalinity distributions (mg/L) in transects 1, 2, and 3 (Elizabeth City PRB)	30
Figure 3.17 Cross-sectional profiles showing nitrate concentrations (mg/L) in transects 1, 2, and 3 (Elizabeth City PRB)	31
Figure 3.18 Cross-sectional profiles showing silica concentrations (mg/L) in transect 2 (Elizabeth City PRB)	33
Figure 3.19 Coring locations and monitoring well locations at the Elizabeth City PRB (plan view)	34
Figure 3.20 Cross-sectional profile showing concentration distribution of inorganic carbon in the solid phase ($\mu\text{g/g}=\text{ppm}$), Elizabeth City PRB (June 2002)	36
Figure 3.21 Concentrations of inorganic carbon ($\mu\text{g/g}$) in core materials through time, Elizabeth City PRB	37
Figure 3.22 Cross-sectional profile showing concentration distribution of sulfur in the solid phase ($\mu\text{g/g}=\text{ppm}$), Elizabeth City PRB (June 2002)	38
Figure 3.23 Powder X-ray diffraction data from fine-grained materials removed via sonication from cores collected at the Elizabeth City PRB: a) core EC060300-4; b) core EC050801-3	40
Figure 3.24 Scanning electron micrographs of samples from the Elizabeth City PRB: a) sample EC060300-4-1; b) sample EC060300-4-3; c) EC060300-4-7	42-44
Figure 3.25 Iron concentration versus oxygen concentration in iron grains and surface precipitates (SEM-EDX)	46
Figure 3.26 Element concentrations in surface precipitates from the Elizabeth City PRB	48
Figure 3.27 Cross-sectional profile showing concentration distribution of biomass (from PLFA data) in picomoles per gram, Elizabeth City PRB (June 2002)	49
Figure 3.28 Histograms of microbial biomass concentrations (from PLFA data) in picomoles per gram in aquifer materials, iron from near the upgradient aquifer/iron interface, and iron from near the downgradient aquifer/iron interface	50
Figure 3.29 Pie graphs showing structural distribution of PLFA compounds (average values) at the Elizabeth City site	51
Figure 4.1 Coring locations and monitoring well locations at the Denver Federal Center, gate 1 (plan view)	54
Figure 4.2 Coring locations and monitoring well locations at the Denver Federal Center, gate 2 (plan view)	55
Figure 4.3 Coring locations and monitoring well locations at the Denver Federal Center, gate 3 (plan view)	56
Figure 4.4 Concentrations of contaminants through time in monitoring wells from the Denver Federal Center, gate 1 (data from FHWA): a) well GSA-21 (upgradient); b) well C1-11 (iron wall); c) well GSA-20 (downgradient)	57

Figure 4.5	Concentrations of contaminants through time in monitoring wells from the Denver Federal Center, gate 2 (data from FHWA): a) well GSA-26 (upgradient); b) well C2-I2 (iron wall); c) well GSA-25 (downgradient)	59
Figure 4.6	Depth-resolved concentrations of a) contaminants ($\mu\text{g/L}$) and b) sulfate, calcium, and iron (mg/L) in wells GSA-26 and GSA-25 from the Denver Federal Center (gate 2)	60
Figure 4.7	Concentrations of contaminants through time in monitoring wells from the Denver Federal Center, gate 3 (data from FHWA): a) well GSA-31 (upgradient); b) well C3-I2 (iron wall); c) well GSA-30 (downgradient)	61
Figure 4.8	Average pH values through time in wells from upgradient, iron wall, and downgradient positions relative to gate 1, gate 2, and gate 3 at the Denver Federal Center	62
Figure 4.9	Average specific conductance values ($\mu\text{S/cm}$) through time in wells from upgradient, iron wall, and downgradient positions relative to gate 1, gate 2, and gate 3 at the Denver Federal Center	63
Figure 4.10	Average Eh (V) values through time in wells from upgradient, iron wall, and downgradient positions relative to gate 1, gate 2, and gate 3 at the Denver Federal Center	63
Figure 4.11	Concentrations of dissolved hydrogen (log molar) as a function of sampling position and time in gate 1 at the Denver Federal Center. Also shown are the concentration ranges of dissolved hydrogen measured in the iron media in gate 2 and gate 3	64
Figure 4.12	Average (± 1 s.d.) concentrations of Na, K, Ca, Mg, sulfate, bicarbonate, chloride, and silica (mg/L) as a function of sampling position in gate 1 at the Denver Federal Center	65
Figure 4.13	Average (± 1 s.d.) concentrations of Na, K, Ca, Mg, sulfate, bicarbonate, chloride, and silica (mg/L) as a function of sampling position in gate 2 at the Denver Federal Center	66
Figure 4.14	Average (± 1 s.d.) concentrations of Na, K, Ca, Mg, sulfate, bicarbonate, chloride, and silica (mg/L) as a function of sampling position in gate 3 at the Denver Federal Center	67
Figure 4.15	Picture showing cemented nodules recovered from core collected at the Denver Federal Center	69
Figure 4.16	Picture showing the appearance of cores collected at the Denver Federal Center, from gate 2 near the upgradient peagravel/iron interface	69
Figure 4.17	Concentration distribution of solid phase inorganic carbon in angle cores collected from gate 1 at the Denver Federal Center	72
Figure 4.18	Concentration distribution of solid phase inorganic carbon in angle cores collected from gate 2 at the Denver Federal Center	72

Figure 4.19 Concentration distribution of solid phase inorganic carbon in a vertical core collected from gate 2 at the Denver Federal Center	73
Figure 4.20 Concentration distribution of solid phase sulfur in angle cores collected from gate 1 at the Denver Federal Center	73
Figure 4.21 Concentration distribution of solid phase sulfur in angle cores collected from gate 2 at the Denver Federal Center	74
Figure 4.22 Inorganic carbon concentrations versus total sulfur a) Elizabeth City core materials; b) Denver Federal Center	75
Figure 4.23 Powder X-ray diffraction data from fine-grained materials removed via sonication from cores collected at the Denver Federal Center PRB (core C2-3-71801)	76
Figure 4.24 Scanning electron micrographs of samples from the Denver Federal Center PRB:a) sample C2-17-71300-2; b) sample C2-17-71300-7; c) sample C1-2-71000-3	77-79
Figure 4.25 Concentration of microbial biomass (from PLFA data) in picomoles per gram in iron from near the upgradient peagravel/iron interface and iron from near the downgradient peagravel/iron interface: a) gate 1; b) gate 2	82
Figure 4.26 Concentration distribution of solid phase sulfur and microbial biomass (from PLFA data) in a vertical core collected from gate 2 at the Denver Federal Center (vertical cores C2-1-71901, C2-2-71901, and C2-3-71901)	83
Figure 4.27 Pie graphs showing average structural distribution of PLFA compounds in core materials from the Denver Federal Center	84
Figure 5.1 Redox –pH diagram showing composition of ground water from the Elizabeth City iron wall compared to equilibrium trends for the Fe^0 - $Fe(OH)_3$, Fe^0 - Fe_3O_4 , and Fe^{2+} - $Fe(OH)_3$ couples	88
Figure 5.2 Redox-pH diagram for the Fe- H_2O system at 25 °C, showing speciation of iron (dashed lines) and stability fields of iron-bearing minerals (solid lines).....	90
Figure 5.3 Redox-pH diagram for the Fe- CO_2 - H_2O system at 25 °C, showing speciation of iron (dashed lines) and stability fields of iron-bearing minerals (solid lines).....	90
Figure 5.4 Redox-pH diagram for the Fe-S- CO_2 - H_2O system at 25 °C, showing speciation of iron (dashed lines) and stability fields of iron-bearing minerals (solid lines).....	91
Figure 5.5 Redox-pH diagram for the Fe-S- CO_2 - H_2O system at 25 °C, showing speciation of iron (dashed lines) and stability fields of iron-bearing minerals (solid lines).....	91
Figure 5.6 Redox-pH diagram for the Fe- CO_2 - H_2O system at 25 °C, showing speciation of iron (dashed lines) and stability fields of iron-bearing minerals (solid lines).....	92

Figure 5.7	Redox-pH diagram for the Fe-CO ₂ -H ₂ O system at 25 °C, showing speciation of iron (dashed lines) and stability fields of iron-bearing minerals (solid lines).....	92
Figure 5.8	Upgradient ground-water compositions (molar ratios) and TDS values for the Elizabeth City and Denver Federal Center PRB sites	93
Figure 5.9	Comparison of total dissolved solids concentrations at PRB sites studied in the Tri-Agency initiative	93
Figure 5.10	Solubility diagram showing the stability field of carbonates as a function of pH and log activities of Ca, Fe, Mg, and dissolved inorganic carbon compared to ground-water compositions from upgradient, iron wall, and downgradient sampling locations (Elizabeth City PRB)	95
Figure 5.11	Saturation indices of magnesium-bearing phases (brucite, Mg(OH) ₂ ; sepiolite, Mg ₄ (OH) ₂ Si ₆ O ₁₅ ·H ₂ O) as a function of pH in ground water from upgradient, iron wall, and downgradient sampling locations (Elizabeth City PRB)	98
Figure 5.12	Conceptual model of the impact of mineral and biomass accumulation to PRB hydraulic performance	99
Figure 5.13	Fractional porosity reduction as a function of inorganic carbon concentration in the solid phase.	100
Figure 5.14	Fractional porosity reduction as a function of sulfur concentration in the solid phase.	102
Figure 5.15	Fractional porosity reduction as a function of the positive molar volume change as iron metal reacts to form magnetite, hematite, goethite, and ferrihydrite	102
Figure 5.16	Concentration versus time in batch tests: a) chromium; b) TCE	105
Figure 5.17	Comparison of PLFA distribution in four iron walls	107
Figure 5.18	Water levels in Elizabeth City monitoring wells	109

Tables

Table 2.1	Comparison of PRBs investigated in this study	6
Table 3.1	Contaminant concentrations in ground water upgradient of the Elizabeth City PRB	11
Table 3.2	Contaminant concentrations in ground water downgradient of the Elizabeth City PRB	12
Table 3.3	Geochemical parameters in upgradient, iron wall, and downgradient locations, Elizabeth City PRB	18
Table 3.4	Changes in concentrations of metals in transect 2 as a function of time and depth below ground surface	27
Table 3.5	Changes in concentrations of anions in transect 2 as a function of time and depth below ground surface	32
Table 3.6	Cores collected for analysis at the Elizabeth City PRB	35
Table 3.7	Results of powder X-ray diffraction analysis of core materials from the Elizabeth City PRB	41
Table 3.8	Pearson's correlation matrix of element concentrations determined by SEM-EDX analysis	46
Table 3.9	Summary of PLFA data from the Elizabeth City PRB	47
Table 4.1	Cores collected for analysis at the Denver Federal Center PRB	70
Table 4.2	Results of powder X-ray diffraction analysis of core materials from the Denver Federal Center PRB	76
Table 4.3	Results of SEM-EDX analysis of core materials from The Denver Federal Center PRB	80
Table 4.4	Summary of PLFA data from the Denver Federal Center PRB	81
Table 5.1	Mineral precipitates identified in iron walls	94
Table 5.2	Molar volume and density of mineral precipitates	101
Table 5.3	Core samples used in batch reactivity tests	103
Table 5.4	Water compositions used in batch reactivity tests	104
Table 5.5	Summary of rate data for reactions of TCE and 1,1,1-TCA with zero-valent iron (unreacted and from field PRBs)	106

Appendix A-1: Inorganic carbon and sulfur concentrations in cores collected from the Elizabeth City and Denver Federal Center PRB sites	122-126
Appendix A-2: Reduced Sulfur Speciation in Elizabeth City and Denver Federal Center Cores	127
Appendix A-3: Inorganic Carbon and Sulfur Concentrations in Denver Federal Center Cores	128-133
Appendix B-1: Phospholipid fatty-acid (PLFA) extract data from cores collected from the Elizabeth City and Denver Federal Center PRB sites	136-140

Acknowledgments

The authors would like to acknowledge all of the participants of the Tri-Agency PRB research initiative, in particular Arun Gavaskar (Battelle), Bruce Sass (Battelle), Neeraj Gupta (Battelle), Woong-Sang Yoon (Battelle), Libby West (Oak Ridge National Laboratory), Nic Korte (Oak Ridge National Laboratory), Liyuan Liang (Cardiff University), and Matt Turner (Interstate Technologies Regulatory Cooperation). Members of the Permeable Reactive Barriers Research Team contributed to the research described in this report, especially S. Acree, F. Beck, P. Clark, K. Jones, M. McNeil, C. Paul, and C. Su. Mantech Environmental Research Services Corporation provided analytical support both in the field and in the laboratory. T. Sivavec (General Electric Corporate) provided X-ray photoelectron spectroscopic analysis of iron core materials. We thank R. Ford (U.S. EPA) for many discussions throughout this study and D. Myers (East Central University) for the scanning electron microscopy. Shim Myung-Hwa, a visiting student from the Kwangju Institute of Science and Technology (South Korea), is acknowledged for her help on parts of this study. Martha Williams (CSC) provided support in document preparation. J.P. Messier (U.S. Coast Guard Support Center) is thanked for providing site assistance at the Elizabeth City site and C. Eriksson (Pacific Western Technologies, Ltd.), J. Jordon (Pacific Western Technologies, Ltd.), and M. Gasser (Pacific Western Technologies, Ltd.) are thanked for site assistance at the Denver Federal Center site. We also acknowledge the U.S. Coast Guard for access to the Elizabeth City site and the Federal Highway Administration and General Services Administration for access to the Denver Federal Center site. Reviews of the document were provided by Eric Reardon (University of Waterloo), Liyuan Liang (Cardiff University), Steve Shoemaker (Dupont), Robert Powell (Powell and Associates), Carl Eriksson (Pacific Western Technologies, Ltd.), and Thomas Holdsworth (U.S. EPA); their thoughtful comments are appreciated.

1.0 Introduction

The permeable reactive barrier (PRB) technology has gained acceptance as an effective ground-water remediation strategy for the treatment of a variety of chlorinated organic and inorganic compounds. The technology combines subsurface fluid-flow management with contaminant treatment by chemical, physical or biological processes, or by combinations of these three principal process categories. The PRB methodology has advantages over traditional pump-and-treat systems in that it is passive and a large plume can be treated in a cost-effective manner. More than one hundred implementations of the technology worldwide have proven that passive reactive barriers can be cost-effective and efficient approaches to remediate a variety of compounds of environmental concern. Yet, few case studies are available that evaluate the long-term performance of these *in-situ* systems, especially with respect to the long-term efficiency of contaminant removal, the buildup of mineral precipitates, and the buildup of microbial biomass (e.g., O'Hannesin and Gillham, 1998; McMahan et al., 1999; Puls et al., 1999a; Vogan, 1999; Phillips et al., 2000; Gavaskar et al., 2002; Liang et al., 2002; Wilkin et al., 2002).

Granular iron is most often used as a reactive media in full-scale site remediation efforts using the PRB technology. The prevalent use of zero-valent iron mainly stems from its low cost (approx. \$350 to \$450 per ton in 2002), availability, and documented ability to degrade a wide variety of contaminant types. In the case of chlorinated volatile organic compounds such as perchloroethylene (PCE) and trichloroethylene (TCE), contaminant removal by zero-valent iron may be due to direct electron transfer, reaction with Fe^{2+} produced during anaerobic iron corrosion, or due to catalytic hydrogenation reactions (e.g., Matheson and Tratnyek, 1994; Gillham and O'Hannesin, 1994; Johnson and Tratnyek, 1994; Roberts et al., 1996; Orth and Gillham, 1996; Fennelly and Roberts, 1998). In the case of inorganic contaminants such as U, Cr, and As, contaminant removal may be achieved through reductive precipitation or adsorption (e.g., Cantrell et al., 1995; Blowes et al., 1997, 2000; Powell et al., 1998; Fiedor et al., 1998; Lackovic et al., 2000; Morrison et al., 2001, 2002). New insight regarding the reactive behavior of zero-valent iron and a more detailed understanding of reaction kinetics and reaction pathways involving zero-valent metals continues to emerge from laboratory studies (e.g., Burris et al., 1995; Agrawal and Tratnyek, 1996; Wüst et al., 1999; Deng et al., 1999; Su and Puls, 1999; Nam and Tratnyek, 2000; Schlicker et al., 2000; Arnold and Roberts, 2000; Farrell et al., 2000; Ruiz et al., 2000; Su and Puls, 2001; Melitas et al., 2001; Scherer et al., 1998; Lien and Wilkin, 2002; Alowitz and Scherer, 2002; Köber et al., 2002).

In addition to reaction processes involving contaminant species, zero-valent iron also impacts the biogeochemical behavior of the typically more concentrated assortment of ground-water solutes. Reaction processes that involve the major anionic (e.g., Cl^- , SO_4^{2-} , HCO_3^-) and major cationic ground-water components (e.g., Ca^{2+} , Mg^{2+}) govern the kinetics and pathways of iron corrosion, mineral precipitation, microbial activity, and gas production within and around the reactive media (e.g., Reardon, 1995). The cumulative effect of these processes through time can lead to changes in the reactivity, porosity, and hydraulic permeability of a PRB.

Research results described in this report explore the geochemical and microbiological processes occurring within zero-valent iron PRBs that may contribute to changes in iron reactivity and decreases in reaction zone permeability that, in turn, may eventually lead to system failure or plugging. Field studies were carried out at two geographically, hydrogeologically, and geochemically distinct iron barrier installation sites (U.S. Coast Guard Support Center, Elizabeth City, NC; and Denver Federal Center, Lakewood, CO). The research approach consisted of intensive ground-water sampling, mineralogical and microbiological characterization of core materials, and geochemical modeling to compare expected trends in the type and mass of mineral precipitates with observations from the field. Specific objectives of this research project were to:

- 1) Evaluate spatial and temporal trends in contaminant concentrations and key geochemical parameters that may impact reactivity and steady system performance.
- 2) Characterize the type and properties of surface precipitates forming over time at the upgradient aquifer/iron interface, within the iron media, and at the downgradient/iron interface.
- 3) Develop conceptual models that predict the type and rate of precipitate formation based on iron characteristics and water chemistry.

-
- 4) Identify the type and extent of microbiological activity at the upgradient aquifer/iron interface, within the iron media, and at the downgradient/iron interface.
 - 5) Define practical and cost-effective protocols for long-term performance assessments at permeable reactive barrier installations.

A detailed analysis of the rate of surface precipitate buildup in PRBs is critical for understanding how long these systems will remain effective and what methods may be employed to extend their lifetime or improve their performance (e.g., Geiger et al., 2002). Different types of minerals and surface coatings have been observed to form under different geochemical conditions that would appear to be dictated by aquifer chemistry and the composition of the permeable reaction zone (Powell et al., 1995; Mackenzie et al., 1999; Puls et al., 1999b; Liang et al., 2000; Phillips et al., 2000; Bonin et al., 2000; Roh et al., 2000; Wilkin et al., 2002; Furukawa et al., 2002). Furthermore, microbiological impacts are also important to understand in order to better predict how long these systems will remain effective in the subsurface (Matheson, 1994; Weathers et al., 1997; Till et al., 1998; Gu et al., 1999, 2002; Scherer et al., 2000; Gandhi et al., 2002). The presence of a large reservoir of iron coupled with plentiful substrate availability in the form of hydrogen supports the metabolic activity of iron-reducing, sulfate-reducing, and/or methanogenic bacteria. This enhanced microbial activity may beneficially influence zero-valent iron reductive dehalogenation reactions through favorable impacts to the iron surface or through direct microbial transformations of the target compounds. However, this enhancement may come at the expense of faster corrosion leading to faster precipitate buildup and potential biofouling of the permeable treatment zone.

1.1 Federal Tri-Agency Initiative

Research described in this report was carried out as part of a Tri-Agency cooperative effort between the United States (U.S.) Department of Defense (DoD), the U.S. Department of Energy (DOE), and the U.S. Environmental Protection Agency (EPA). This collaborative initiative allowed the three federal agencies to leverage technical and funding resources and to share experiences at over 10 PRB installations across the U.S. The primary goal of the research initiative was to evaluate the longevity and hydraulic performance of zero-valent iron PRBs in various hydrogeological and geochemical settings. Members of the Tri-Agency initiative met periodically and conducted regular conference calls to discuss research progress. Results of research projects conducted by members of the Tri-Agency effort are reported in Gavaskar et al. (2002), Liang et al. (2002), and Wilkin et al. (2002). A combined final product outlining conclusions of the Tri-Agency study is expected in 2003.

This report provides a detailed exploration of long-term monitoring results obtained over the initial 5-year operation period of PRBs at the U.S. Coast Guard Support Center (Elizabeth City, NC) and the Denver Federal Center (Lakewood, CO). Results of the study are presented in two volumes. Volume 1 (this volume) presents a performance assessment and data on the geochemical and microbiological factors that impact the performance of zero-valent iron PRBs. Volume 2 presents ground water monitoring practices and procedures employed in this study as well as soil core collection, preservation, and analysis methods. The remainder of this section presents the general scope and major conclusions of the DoD, DOE, and EPA contributions to the Tri-Agency collaborative effort.

1.1.1 DoD Studies

Results of the DoD study on PRB longevity and hydraulic performance are reported in Gavaskar et al. (2002). Field data were collected and analyzed from PRBs at several DoD sites. The longevity evaluation focused primarily on PRBs at the Moffett Field former Naval Air Station (CA) and the former Lowry Air Force Base (CO). Both PRBs have a funnel-and-gate design and were installed prior to 1996. The longevity evaluation consisted of geochemical monitoring and modeling of ground water, iron core collection and analysis, and accelerated column tests. Hydraulic performance was also studied at the Seneca Army Depot (NY, installed 1998) and the Dover Air Force Base (DE, installed 1997). Methodologies used for the hydraulic performance testing were water level measurements and a variety of available *in-situ* flow sensors.

Five years after installation of the Moffett Field PRB, concentrations of TCE, PCE, and cis-1,2 dichloroethylene (cis-DCE) in effluent ground water from the reactive cell were all below their respective maximum concentration levels (MCLs). Treatment of contaminants occurred mainly in the upgradient region of the reactive media. As of 2001, a clean front of ground water had not been identified in the downgradient aquifer, although there was an indication that a clean front would occur in the future. Similar results with respect to contaminant treatment were observed at the former Lowry Air Force Base (AFB). At the Moffett Field and Lowry AFB sites, concentrations of dissolved calcium, iron, magnesium, sulfate, nitrate, alkalinity, silica, and total dissolved solids flowing to the PRBs were significantly reduced in effluent ground water compared to influent ground water. At both sites, pH values within the reactive media rose to levels as high as 11.5 and ORP values dropped to as low as -821 mV. Solid-phase characterization studies were carried out to evaluate the mineralogy of precipitates that formed in the reactive media.

Careful and periodic water level measurements were found to give the best results with respect to hydraulic performance monitoring. *In-situ*, direct-flow measurements in some cases gave flow direction results that were contradictory from those indicated by water level measurements. This was thought to be due to the fact that *in-situ* techniques were point estimates and more indicative of localized flow conditions, whereas water level trends are more indicative of the overall flow regime around the PRBs studied. Estimated effective residence times varied from about 9 days at the Moffett Field site to about 25 days at the Lowry AFB.

1.1.2 DOE Studies

Results of the DOE study are presented in two reports (Liang et al., 2002; Moline et al., 2002) and recent publications (e.g., Kamolpornwijit et al., 2003; Liang et al., 2003). The DoE study focused on PRBs in Monticello, Utah and at the Y-12 Pathway-2 in Oak Ridge, Tennessee. The Monticello site was a former vanadium and uranium ore-processing mill. A zero-valent iron funnel-and-gate system was installed in July 1999 to treat uranium-contaminated ground water. The Y-12 Pathway-2 PRB was installed in November 1997 as a trench that was intended to capture shallow ground-water flow contaminated with uranium. The DOE study consisted of geochemical and hydrogeologic monitoring, core sampling, column tests, and geochemical modeling.

Slug tests at the Monticello barrier in wells immediately upgradient of the PRB resulted in hydraulic conductivity values of 3.1 to 27 m/d. Colloidal borescope measurements showed average particle velocities ranging from 4.3 to 43 m/day. The borescope measurements showed evidence of vertical variability in flow conditions within each of the wells tested. A multiparameter tracer test conducted one year after the PRB was installed resulted in upgradient seepage velocities of 0.36 to 3.6 m/d. Tracer tests were conducted by injecting anionic tracers (bromide, iodide) or dissolved gas tracers (helium, neon, argon), and monitoring their appearance in a network of adjacent monitoring wells. Within the PRB at Monticello, considerable lateral transport was observed.

The DOE report indicates that flow directions and velocities are dependent on the type of tracer test used. A general conclusion presented was that an analysis of water levels provides information about average gradients but may be difficult to interpret within the context of site heterogeneity. Potentiometric surfaces have the most value for regional conceptualization of water flow patterns and for delineating gross features such as ground-water mounding. On the other hand, tracer tests provide definitive results on a more local scale, but the scale of the measurement needs to be considered when interpreting such data or when extrapolating trends to adjacent aquifer regions (Moline et al., 2002).

Liang et al. (2002; 2003) used the geochemical equilibrium model PHREEQC to evaluate mineral saturation indices in waters from several sites including the Monticello and Y-12 Plant PRBs. This analysis was carried out to understand the types and quantities of minerals that might form as water passes through and chemically equilibrates with the reactive medium. The results of the modeling show that the buffering capacity and flow rate of the influent ground water is important in determining the equilibrium pH in the Fe⁰ media and in effluent water from Fe⁰ columns. The predicted spatial distribution of secondary minerals based on pore water chemistry provides a direct indication of changing flow characteristics over time and has been shown to be in agreement with the results of tracer testing at the Y-12 site. Column tests were carried out at the Y-12 Plant site to examine iron deterioration processes, changes to influent water chemistry after reaction with iron metal, and mineral precipitation processes. Column tests were run for over 14 months. In the column experiments, *in-situ* ground water was used as the input fluid. Two different flow rates were used (0.09 and 1.8 m/day) to test the effect of seepage velocity on geochemical performance. Results of the column tests showed that heterogeneous flow (preferential flow) conditions developed as a result of mineral precipitation and gas production in the column. Tracer tests in the columns showed that pH and hydrologic residence time were closely linked. Therefore, pH may be a key indicator of residence time in PRB installations.

1.1.3 EPA Studies

Preliminary results of EPA's long-term performance study were reported in Wilkin et al. (2002). Geochemical and microbiological factors that control long-term performance of PRBs were evaluated at the Elizabeth City, NC and the Denver Federal Center, CO sites. These ground-water treatment systems use zero-valent iron granules (Peerless Metal Powders, Inc.) to intercept and remediate chlorinated volatile organic compounds at the Denver Federal Center (funnel-and-gate system) and overlapping plumes of hexavalent chromium and chlorinated compounds at Elizabeth City (continuous wall system). Zero-valent iron at both sites is a long-term sink for C, S, Ca, Si, N, and Mg. Based on an analysis of mineral precipitate abundance in core materials, after about four years of operation the average rates of inorganic carbon (IC) and sulfur (S) accumulation were determined to be 0.09 and 0.02 kg/m²y, respectively, in the Elizabeth City PRB where upgradient waters contain <400 mg/L of total dissolved solids (TDS). At the Denver Federal Center site, upgradient ground water contains 1000-1200 mg/L TDS and rates of IC and S accumulation were determined to be as high as 2.16 and 0.80 kg/m²y, respectively. At both sites, consistent patterns of spatially variable mineral precipitation and microbial activity were observed. Mineral precipitates and microbial biomass accumulate the fastest near the upgradient aquifer-Fe⁰ interface. After four years, maximum net reductions in porosity, due to the

accumulation of sulfur and inorganic carbon precipitates, range from 0.032 at Elizabeth City to 0.062 at the Denver Federal Center (gate 2). While pore space has been lost due the accumulation of authigenic components, neither site showed evidence of pervasive pore clogging after four years of operation.

The following sections of this report provide descriptions of the Elizabeth City and the Denver Federal Center PRB sites, and results and analysis of the first five-year monitoring period for contaminant distributions, ground-water chemistry, as well as mineralogical and microbiological characterization of material that has accumulated within the reactive barriers.

2.0 Site Descriptions

The U.S. Coast Guard Support Center (USCG-SC) site near Elizabeth City, North Carolina, and the Denver Federal Center (DFC) in Lakewood, Colorado were evaluated in the EPA portion of the Tri-Agency PRB initiative. Both of these PRB installations are among the oldest full-scale systems available for study. The Elizabeth City PRB was installed in June 1996, and the Denver Federal Center system was installed in October 1996. The two sites are of similar age; they use the same type of iron (Peerless Metal Powders, Inc.), yet they have contrasting ground-water chemistry and different design configurations (continuous wall configuration at Elizabeth City vs. funnel-and-gate design at the Denver Federal Center). Table 2.1 provides a general comparison of the PRBs at Elizabeth City and the Denver Federal Center.

2.1 U.S. Coast Guard Support Center

The USCG-SC is located about 100 km south of Norfolk, Virginia and 60 km inland from the Outer Banks region of North Carolina. The base is situated on the southern bank of the Pasquotank River, about 5 km southeast of Elizabeth City, North Carolina. A hard-chrome plating shop was in operation for more than 30 years in Hangar 79, which is only 60 m south of the river (Figure 2.1). Following its closure in 1984, soils beneath the shop were found to contain chromium concentrations up to 14,500 mg/kg. Subsequent site investigations by U.S. EPA personnel identified a chromate plume extending from beneath the shop to the river. The plume has high (>10 mg/L) concentrations of chromate, elevated sulfate (to 150 mg/L), and minor amounts of volatile chlorinated organic compounds: TCE, cis-DCE, and vinyl chloride (VC). The plating shop soils and related ground-water contamination are referred to as solid waste management unit (SWMU) number 9 by the state of North Carolina and the USCG. Sampling results from a monitoring network consisting of more than 40 monitoring wells and about 100 Hydropunch™ and Geoprobe™ monitoring points indicate that the Cr(VI) plume is about 35 m wide, extends to 6.5 m below ground surface and extends laterally about 60 m from the hangar to the Pasquotank River (Figure 2.1). Multilevel samplers installed near the barrier wall location indicate that the bulk of the contamination resides from 4.5 to 6.5 m below ground surface.

The site geology has been described in detail elsewhere (e.g., Puls et al., 1999b), but essentially consists of typical Atlantic coastal plain sediments, characterized by variable sequences of surficial sands, silts and clays. In general, the upper 2 m of the aquifer consists of sandy- to silty-clays that pinch out toward the north, or near the Pasquotank River, where sandy-fill predominates. Fine-sands, with varying amounts of silt and clay, and silty-clay lenses form the rest of the shallow aquifer.

Ground-water flow velocity is extremely variable with depth, with a highly conductive layer at roughly 4.5 to 6.5 m below ground surface. As noted above, this layer coincides with the highest aqueous concentrations of chromate. The ground-water table ranges from about 1.5 to 2.0 m below ground surface and the average horizontal hydraulic gradient varies from 0.0011 to 0.0033. Slug tests conducted on monitoring wells with 1.5 m screened intervals between 3 and 6 m below ground surface indicate hydraulic conductivity values of between 0.3 to 8.6 m/d. A multiple borehole tracer test in wells screened between 3.9 to 5.9 m below ground surface was conducted. Ground-water velocities between about 0.13 and 0.18 m/d were measured in this test. Assuming an average hydraulic gradient of 0.0023 and an effective porosity of 0.38, these flow velocities correspond to an average hydraulic conductivity of about 26 m/d.

In June of 1996, a 46 m long, 7.3 m deep, and 0.6 m wide permeable reactive barrier (continuous wall configuration) of zero-valent iron (Peerless Metal Powders, Inc.) was installed approximately 30 m from the Pasquotank River (Figure 2.1; Blowes et al., 1999a,b). The reactive wall was designed to remediate hexavalent chromium-contaminated ground water and portions of the larger overlapping plume of volatile chlorinated organic compounds. A detailed monitoring network of over 130 subsurface sampling points was installed in November of 1996 to provide detailed information on spatial and temporal changes in pore water geochemistry and hydrology (Blowes et al., 1999a; Puls et al., 1999a).

2.2 Denver Federal Center

The Denver Federal Center (DFC) is located about 10 km west of downtown Denver, Colorado. Aquifer materials at the site consist of alluvial sediments that overlie the Denver Formation. The Denver Formation is Paleocene to Late Cretaceous in age and consists of brown, yellowish-brown, gray, and blue-gray intercalated sandstone, claystone, siltstone, shale and conglomerate containing olive-brown andesitic sandstone beds. It lies about 2 to 14 m below ground

Table 2.1. Comparison of PRBs Investigated in this Study

	Contaminants	PRB Configuration	Date Installed	Iron Dimensions	Iron Volume	Ground water, SC ($\mu\text{S/cm}$)	Ground water, pH	Ground water, DO (mg/L)	
U.S. Coast Guard Support Center	Cr(VI) TCE, cis-DCE	Continuous wall	6/96	46 m length 7.3 m deep 0.6 m wide	150 m ³	307±149 (n=18)	5.86±0.25 (n=18)	0.7±0.5 (n=17)	
Denver Federal Center	TCE, TCA, cis-DCE	Funnel-and-gate	10/96	Gate 1	12.2 m length 8.5 m deep 1.8 m wide	187 m ³	1236±65 (n=3)	7.14±0.15	0.5±0.2
				Gate 2	12.2 m length 9.5 m deep 1.2 m wide	139 m ³	1358±10 (n=3)	7.19±0.08	0.2±0.1
				Gate 3	12.2 m length 7.3 m deep 0.6 m wide	53 m ³	1306±10 (n=2)	7.06±0.07	<0.05

Notes: Geochemical parameters from Elizabeth City are average values (± 1 s.d.) from upgradient monitoring well MW48. All parameters monitored quarterly from 2/97 to 8/01 and biannually since 8/01. Geochemical parameters from DFC gates 1, 2, 3 are average values of wells GSA21, GSA 26, and GSA31 from 7/00 to 7/01. SC is specific conductance. DO is dissolved oxygen. DFC gate 4 was not studied in this investigation.

surface at the DFC and can attain a thickness of up to about 260 m. The Denver Formation has been divided into two zones, the upper weathered zone and a lower unweathered zone. These two zones are lithologically similar but differ in color. The upper weathered zone is up to 7 m thick and exhibits a grayish brown color with yellowish orange staining while the lower unweathered zone has a diagnostic blue color, commonly called “Denver Blue.”

There are two separate deposits of alluvial sediments in the vicinity of the DFC. The Verdos Alluvium of Pleistocene age is a poorly sorted, stratified gravel containing lenses of sand, silt, and clay. In some surface-drainages, the Denver Formation may be overlain by the Piney Creek Alluvium, which consists of well-stratified sands, silts and clays with interbedded gravels.

Ground water in the alluvial sediments at the site generally moves from west to east with an average hydraulic velocity of about 0.3 m per day and a range between about 0.03 and 0.5 m per day (Pacific Western Technologies, 2000). Shallow ground water is contaminated with volatile organic compounds including TCE, cis-DCE, VC, 1,1,1-trichloroethane (1,1,1-TCA), and 1,1-dichloroethylene (1,1-DCE). At the eastern boundary of the site, maximum concentrations entering gate 2 of TCE, cis-DCE, 1,1,1-TCA, and 1,1-DCE were about 80 $\mu\text{g/L}$, 1.6 $\mu\text{g/L}$, 200 $\mu\text{g/L}$, and 230 $\mu\text{g/L}$, respectively, when the PRB was constructed in November 1996 (FHWA, personal communication, 2002). At least one source of

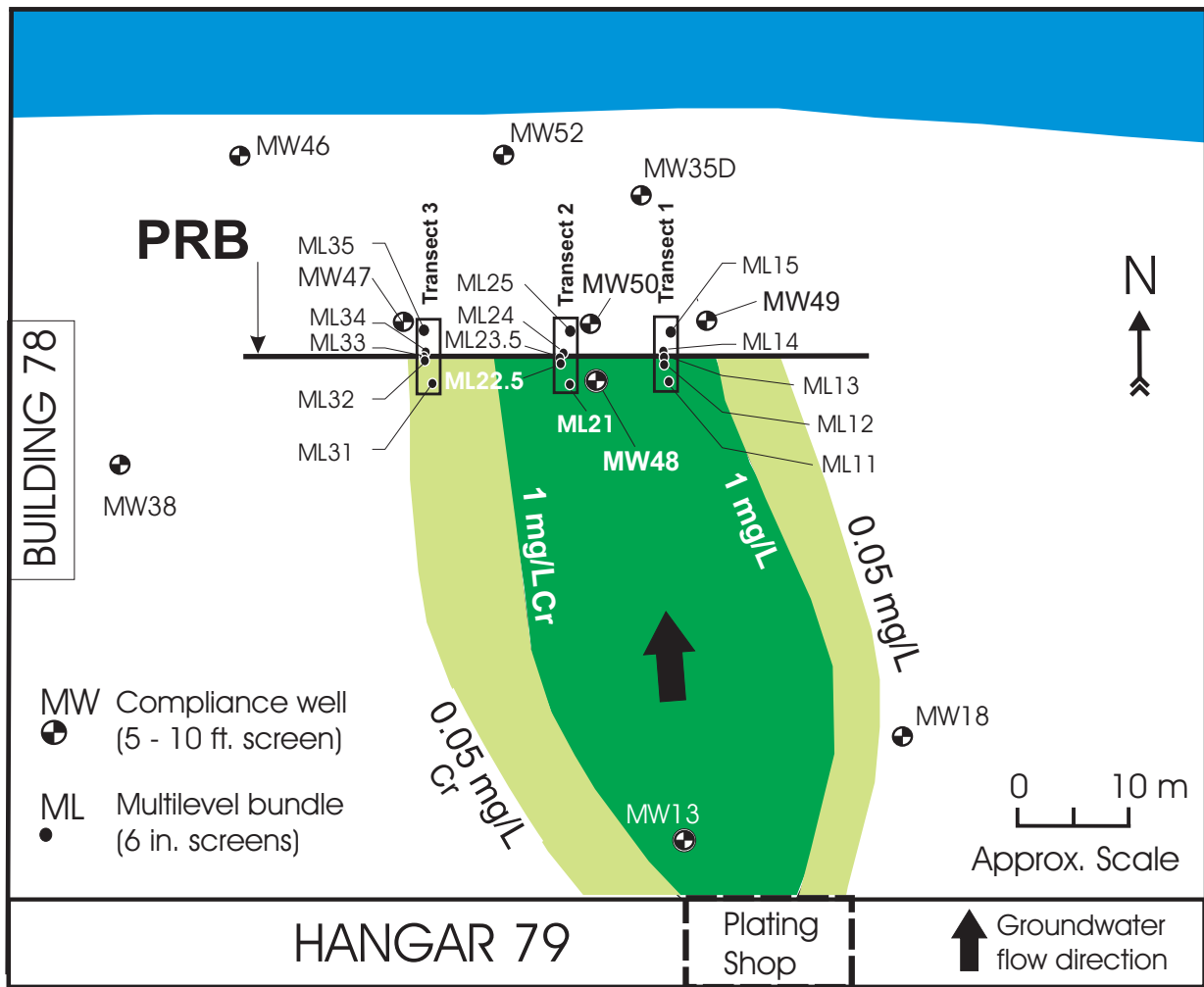


Figure 2.1 Plan view map of the PRB at the U.S. Coast Guard Support Center, Elizabeth City, NC.

these volatile organic compounds was a leaking underground storage tank located near Building 52 that was used by the Federal Highway Administration (FHWA) to store waste, primarily 1,1,1-TCA. Ground-water flow from the aquifer discharges into McIntyre Gulch (Figure 2.2). McIntyre Gulch is a deep channel that penetrates the aquifer along the southern edge of the contaminant plume. Downing Reservoir is too shallow to be influenced by the aquifer, but the reservoir stage does affect the ground-water level.

In the fall of 1996, FHWA and the General Services Administration (GSA) installed a permeable reactive barrier at the eastern edge of the DFC property along north-south trending Kipling Street (Figure 2.2). In contrast to the continuous wall design used at the USCG-SC, the DFC PRB has a funnel-and-gate design configuration. The funnel component of the PRB employs metal sheet pile that was driven into unweathered bedrock of the Denver Formation or into resistant, weathered layers of the Denver Formation. The depth of penetration of the funnel ranged from about 7 to 10 m (Figure 2.3). The PRB has 4 reactive gates, each 12.2 m long, 9.5 m deep, and from 1.8 m to (gate 1) to 0.6 m (gates 3 and 4) wide (Table 2.1). The design thickness varied because of anticipated differences of contaminant fluxes to the PRB at different locations. Peagravel zones (0.6 to 1.2 m) were installed immediately upgradient and downgradient of the reactive iron zones to improve hydraulic connection between the aquifer and the PRB.

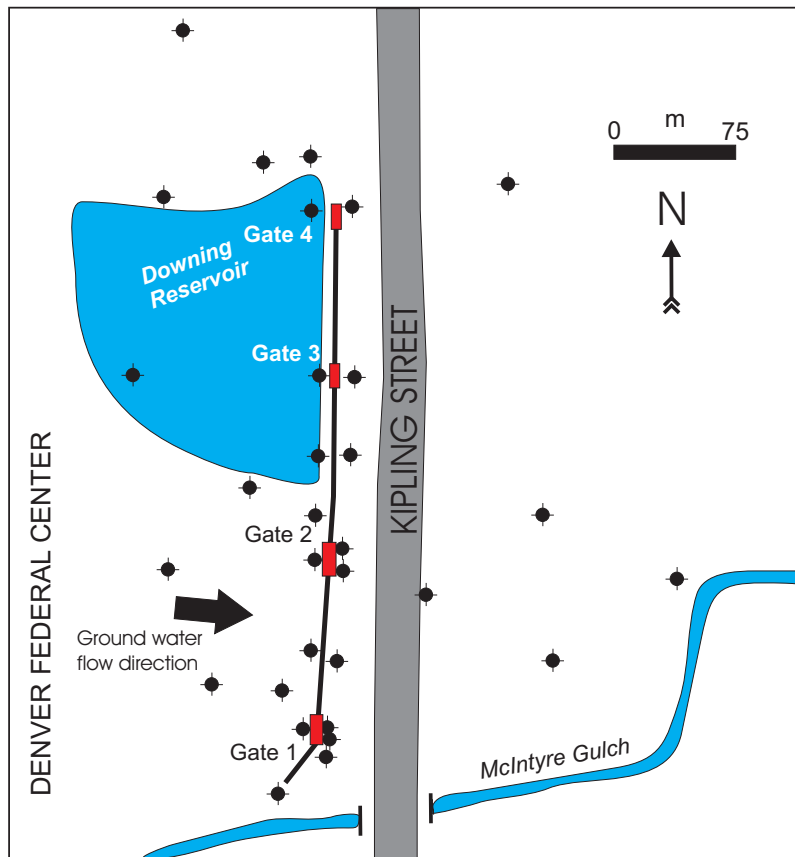


Figure 2.2 Plan view map of the PRB at the Denver Federal Center, Lakewood, CO (after McMahon et al., 1999).

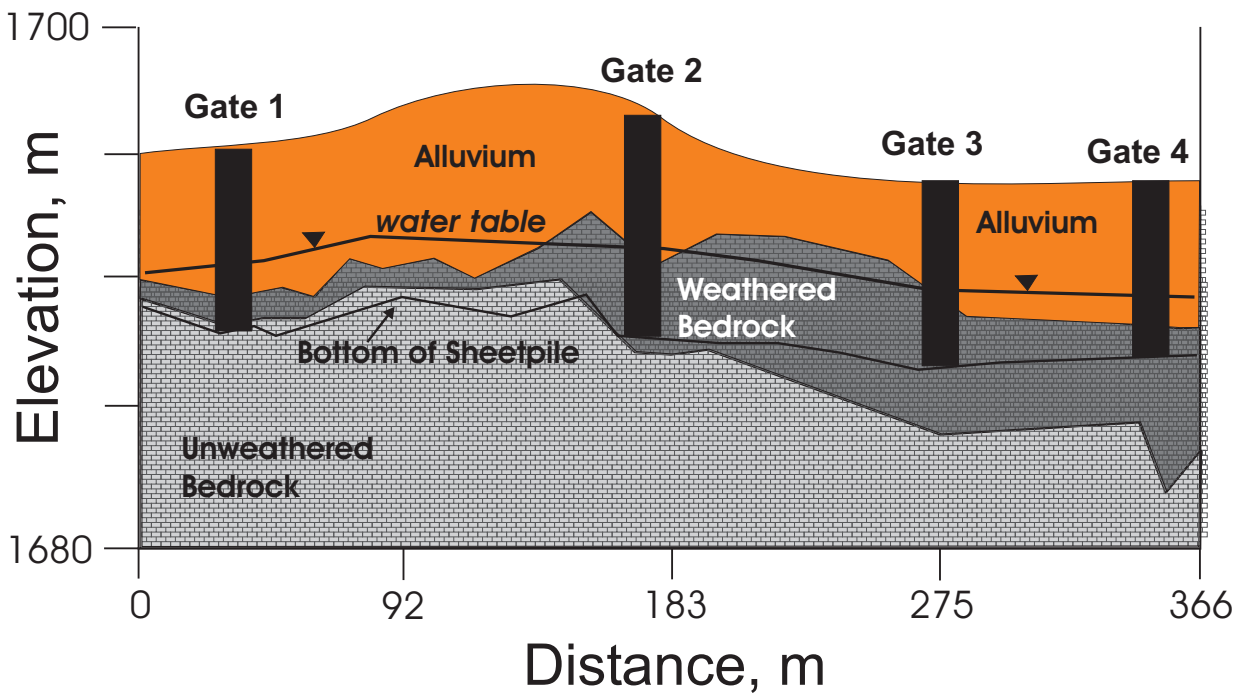


Figure 2.3 Schematic cross-section of the Denver Federal Center funnel-and-gate system (after McMahon et al., 1999).

3.0 Elizabeth City PRB Monitoring Results

3.1 Ground Water Monitoring

Ten ground-water monitoring wells (two-inch PVC) located upgradient and downgradient of the iron wall were sampled on a quarterly basis from February 1997 to August 2001. Beginning in August 2001, sampling of these 10 compliance wells switched to a biannual schedule. In order to obtain more detailed spatial information on ground-water geochemistry and contaminant distributions in the subsurface, up to 130 multilevel well bundles were sampled on an annual basis. The monitoring well network at the Elizabeth City site is described in Blowes et al. (1999b). The locations of the monitoring wells and the multilevel well bundles in relation to the PRB at the Elizabeth City site are shown in Figure 2.1.

Methods of ground-water and soil core sampling, preservation and analysis, in addition to Quality Assurance/Quality Control (QA/QC) procedures used in this five-year investigation of PRB performance are described and discussed in Volume 2 of this EPA Report series.

3.1.1 Contaminant Behavior

Ground-water contaminants near the PRB location at the Elizabeth City site are hexavalent chromium, TCE, cis-DCE, and VC. Figure 3.1 shows the time-dependent variations in the concentrations of chromium, TCE, and cis-DCE in monitoring wells MW48 and MW13, wells located upgradient of the PRB (see Figure 2.1). The concentration trends evident in these upgradient wells are non-steady state, particularly for TCE in MW48 (Figure 3.1). Concentrations of TCE in well MW48 have increased with time suggesting that the flux of TCE to the center portion of the reactive barrier also has increased over the initial five-year period of operation. Average, minimum, and maximum contaminant concentrations determined at upgradient monitoring points are listed in Table 3.1. The greatest concentrations of chromium and volatile organic compounds are present in ML21, the multilevel well bundle located just upgradient of and near the mid-point of reactive barrier. In ML21, the maximum TCE concentration observed was 42,400 µg/L at a depth of 6.4 m below ground surface (Table 3.1). Note that this concentration is much greater than the average, depth-integrated concentration of 2,585 µg/L from ML21, and the average TCE concentration in the proximate well MW48 (716 µg/L), which is screened over a 10 ft interval from 4.3 m to 7.3 m below ground surface. The detection of TCE degradation products, cis-DCE and VC, in upgradient monitoring wells suggests that partial anaerobic bioattenuation of TCE is occurring in the plume before it reaches the PRB.

The concentration of chromium entering the PRB is greatest near ML21 (average concentration 0.82 mg/L) and least near ML31 on the west side of the PRB (average concentration 0.032 mg/L). Taking an average chromium concentration of 0.5 mg/L over the depth interval from 3 m to 6 m below ground surface and an average flow velocity of 0.16 m/d, it is estimated that the reactive wall removes about 4.1 kg Cr per year. Over the first five years of operation an estimated 21 kg of chromium has been removed from the ground-water plume and sequestered into immobile forms in the solid phase.

Table 3.2 lists the concentrations of contaminants in monitoring wells located downgradient of the Elizabeth City PRB. Over the five year period from 1996 to 2001, there were a total of 150 sampling events in downgradient monitoring wells MW47, MW49, MW50, and in the multilevel well bundles ML15, ML25, and ML35. Chromium was detected in 13 sampling events or in about 9% of the sampling events of wells located in downgradient positions. The highest concentration of chromium observed in a well downgradient of the PRB from 1996 to 2001 was 0.005 mg/L, significantly below the MCL and target treatment level for chromium of 0.050 mg/L. Where influent concentrations of chromium were the greatest, the best performance was observed in that 0 samples of 32 from multilevel well bundle ML25 showed detectable concentrations of chromium. The monitoring results presented in Table 3.2 show the sustained performance of the PRB for removing chromium from the ground-water plume. A trend of increasing chromium concentrations at downgradient locations is not evident after five years of operation.

Average, minimum, and maximum concentrations of TCE, cis-DCE, and VC in downgradient monitoring wells are shown in Table 3.2. Inspection of the data in Table 3.2 reveals that average TCE concentrations in wells downgradient of the PRB have been significantly reduced compared to locations upgradient of the PRB, although average concentrations in downgradient monitoring wells MW49, MW50, and multilevel well bundle ML25 are above the MCL of 5 µg/L. Monitoring

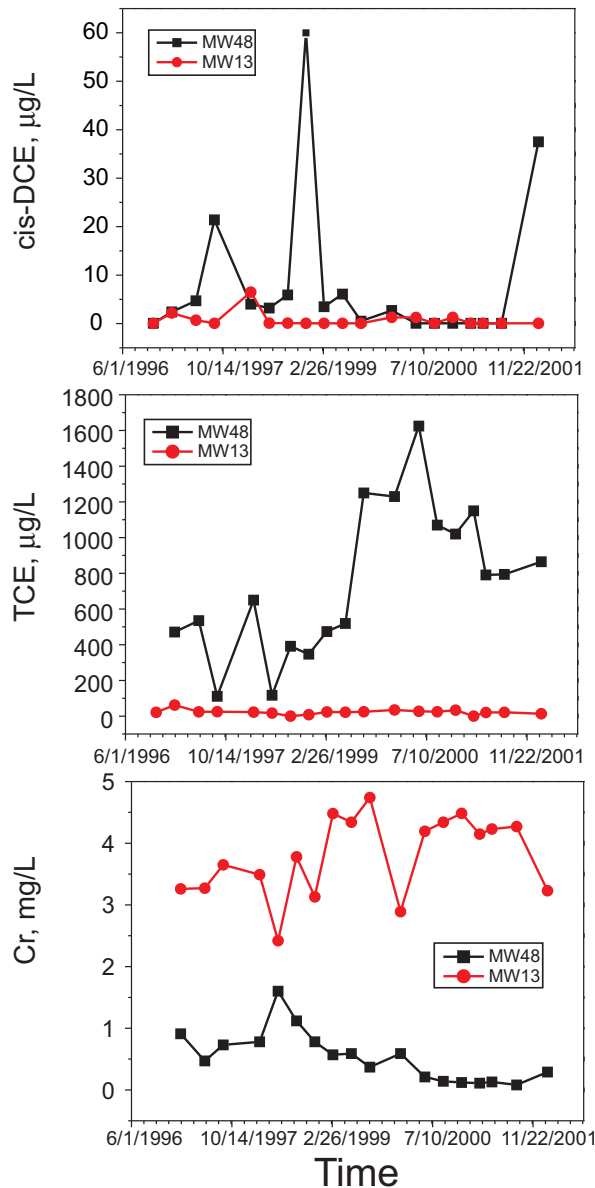


Figure 3.1 Concentrations of contaminants through time in monitoring wells located hydraulically upgradient of the Elizabeth City PRB (screened interval in MW48 and MW13 is 4.3 to 7.3 m below ground surface).

well MW50, in particular, has typically shown TCE concentrations above 100 µg/L, especially prior to 2000 (Figure 3.2). Well MW50 is screened over a 5-foot interval from 7.6 m to 9.1 m below ground surface, a depth interval that extends below the PRB (maximum depth 7.3 m). Some underflow of the chlorinated solvent plume, therefore, is evident in the central portion of the PRB. This may have been caused by the disturbance of an unrecognized TCE source near the PRB and/or a large influx of recharge water into the aquifer near the PRB following installation and prior to repaving of the parking lot covering the excavation site.

Monitoring results from multilevel bundles ML21 and ML25 indicate that concentrations of cis-DCE have been reduced from an average of 154 µg/L in upgradient ground water to an average concentration of 14 µg/L in downgradient ground water. Similarly concentrations of VC have been reduced by the PRB. The average VC concentration in multilevel well bundles ML21 and ML31 was 31 µg/L and 22 µg/L, respectively, from 1997 to 2001 (Table 3.1). In downgradient multilevel well positions ML25 and ML35, VC was detected in about 45% to 55% of the sampling events. When detected the average VC concentration in multilevel well bundles ML25 and ML35 was 4.3 µg/L and 2.3 µg/L, respectively. In general, concentrations of cis-DCE and VC decrease by about an order of magnitude as a consequence of processes that take place within the PRB.

Table 3.1. Contaminant Concentrations in Ground Water Upgradient from the PRB at Elizabeth City

Well		n _{total}	n _{detected}	Average	Minimum	Maximum
MW48	Cr (mg/L)	18	18	0.53	0.08	1.6
	TCE (µg/L)	17	17	716	111	1625
	cis-DCE (µg/L)	18	12	8.31	<0.1	60
	VC (µg/L)	18	3	4.0	<0.1	5.8
MW13	Cr	18	18	3.8	2.9	4.7
	TCE	18	18	17	<0.1	62
	cis-DCE	18	6	0.8	<0.1	6.5
	VC	18	0	--	<0.1	<0.1
ML11	Cr	32	25	0.75	<0.002	2.5
	TCE	32	24	31	<0.1	89
	cis-DCE	32	28	11	<0.1	56
	VC	32	2	1.5	<0.1	1.5
ML21	Cr	32	25	0.82	<0.002	3.43
	TCE	32	30	2585	<0.1	42400
	cis-DCE	32	15	154	<0.1	384
	VC	32	12	31	<0.1	52
ML31	Cr	30	17	0.03	<0.002	0.08
	TCE	30	30	249	2.6	1160
	cis-DCE	30	16	34	<0.1	103
	VC	30	16	22	<0.1	43

Notes: n_{total} is the total number of samples analyzed; n_{detected} is the number of samples in which the contaminant was detected. Entries for ML11, ML21, and ML31 (multilevel bundles) are averages of all sampling depths. MW48 and MW13 data span the time period of November 1996 to February 2002. ML11 and ML31 data were collected in 1997, 1998, and 2000 (annually). ML21 data were collected in 1997, 1998, 1999, 2000, and 2001 (annually). Values below the analytical detection limit were excluded from the average calculation. Concentration units: Cr (mg/L), TCE (µg/L), cis-DCE (µg/L), VC (µg/L).

A more detailed picture of contaminant behavior can be reached by inspecting 2-dimensional concentration profiles, constructed by contouring monitoring data from the multilevel well bundles. Figures 3.3 through 3.18 show cross-sectional profiles of various dissolved solutes and geochemical parameters determined on an annual basis at Elizabeth City from 1997 to 2001. The locations of transects 1, 2, and 3 are shown in Figure 2.1. For each transect in the cross-sectional profiles, the position of the PRB is referenced to the position of the furthest upgradient multilevel well bundle (i.e., ML11, ML21, and ML31). The distribution of subsurface sampling points is shown for transect 3 in the lower left hand corner of Figure 3.3 to provide an indication of the density of sampling data used to construct the contour diagrams.

Cross-sectional profiles for dissolved chromium are shown in Figure 3.3. Long-term trends indicate that chromium continues to be removed from the ground-water plume after five years of operation. In general, depth-dependent concentration profiles have remained consistent with time. However, the dissolved chromium plume appears to be migrating to shallower depths at a rate of about 15 cm/y in the vicinity of transect 2 (Figure 3.3). In the vicinity of transect 1 there appears to be no vertical movement of the dissolved chromium plume. The upward movement of the plume in the vicinity of transect 2 may be linked to the emergence of the deep TCE plume as described below.

More complicated transport behavior is evident for TCE based upon monitoring results from the multilevel well bundles. There are two separate TCE plumes, one shallow that coincides with the chromium plume (approx. 4 to 6 m below ground surface). This shallow plume containing TCE (plus cis-DCE and VC) is present in each of the three multilevel well transects. A second deeper plume containing TCE (minus cis-DCE and VC) appears only upgradient of the PRB in the vicinity of transect 2 (Figure 3.4). The shallow TCE plume is most concentrated and most shallow near transect 3, unlike

Table 3.2. Contaminant Concentrations in Ground Water Downgradient from the PRB at Elizabeth City

Well		n_{total}	$n_{detected}$	Average	Minimum	Maximum
MW47	Cr (ppm)	18	2	0.002	<0.002	0.002
	TCE ($\mu\text{g/L}$)	18	15	6.0	<0.1	30.2
	cis-DCE ($\mu\text{g/L}$)	18	17	7.0	<0.1	19.7
	VC ($\mu\text{g/L}$)	18	11	5.5	<0.1	10.4
MW49	Cr	18	4	0.003	<0.002	0.004
	TCE	18	11	9.0	<0.1	41
	cis-DCE	18	4	1.6	<0.1	2.6
	VC	18	8	5.0	<0.1	7.0
MW50	Cr	18	4	0.003	<0.002	0.003
	TCE	18	18	204	<0.1	548
	cis-DCE	18	17	15	<0.1	35
	VC	18	14	7	<0.1	18
ML15	Cr	32	2	0.004	<0.002	0.005
	TCE	32	8	1.8	<0.1	4.9
	cis-DCE	32	9	1.5	<0.1	1.9
	VC	32	8	2.1	<0.1	7.8
ML25	Cr	32	0	--	<0.002	<0.002
	TCE	32	15	16	<0.1	81.6
	cis-DCE	32	30	14	<0.1	74.6
	VC	32	18	4.3	<0.1	10
ML35	Cr	32	1	0.005	<0.002	0.005
	TCE	32	12	3.6	<0.1	9.1
	cis-DCE	32	14	4.3	<0.1	13
	VC	32	14	2.3	<0.1	4.2

Notes: n_{total} is the total number of samples analyzed; $n_{detected}$ is the number of samples in which the contaminant was detected. Entries for ML15, ML25, and ML35 (multilevel bundles) are averages of all sampling depths. MW47, MW49, and MW50 data span the time period of November 1996 to February 2002. ML15 and ML35 data were collected in 1997, 1998, and 2000 (annually). ML25 data were collected in 1997, 1998, 1999, 2000, and 2001 (annually). Values below the analytical detection limit were excluded from the average calculation. Concentration units: Cr (mg/L), TCE ($\mu\text{g/L}$), cis-DCE ($\mu\text{g/L}$), VC ($\mu\text{g/L}$).

chromium, which is most concentrated near transect 2. These relationships suggest that rather than sharing identical sources, chromium and TCE are more likely being transported in a hydrologically favorable zone. Comparing both TCE plumes, the highest TCE concentrations are found in the deep plume at a depth range from about 6 to 7 m below ground surface immediately upgradient of the PRB near transect 2. Over this depth interval, TCE concentrations increased almost tenfold from 4,320 $\mu\text{g/L}$ in 1997 to 42,400 $\mu\text{g/L}$ in 2001. In downgradient multilevel well bundle ML25, TCE concentrations are below 10 $\mu\text{g/L}$ in all but five samples collected between 1997 and 2001. However, TCE contamination extends beneath the maximum depth of the PRB near transect 2 and this explains the higher TCE concentrations detected in MW50 (Figure 3.2).

Unlike TCE, the occurrences of cis-DCE and VC are generally restricted to the shallow plume or to depths of about 4 to 6 m below ground surface (Figures 3.5 and 3.6). In the vicinity near transect 1, concentrations of cis-DCE are reduced to below detection limits as the contaminant plume passes through the PRB. In this region, the maximum concentration of cis-DCE observed upgradient of the PRB was 260 $\mu\text{g/L}$ (Figure 3.5). The concentration of cis-DCE in regions immediately upgradient of the PRB increased from 1997 to 2000. The fact that neither cis-DCE nor VC are present in the

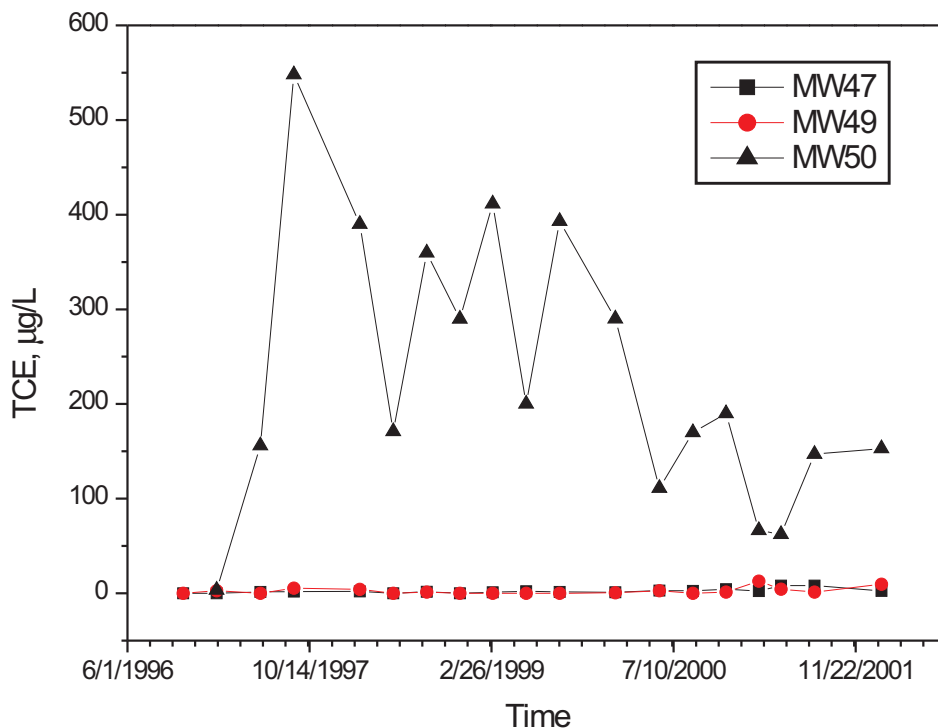


Figure 3.2 Concentrations of TCE ($\mu\text{g/L}$) through time in monitoring wells located hydraulically downgradient of the Elizabeth City PRB (screened intervals: MW47, 4.3-7.3 m; MW49, 4.3-7.3 m; MW50, 7.6-9.1 m).

deeper plume near transect 2 suggests that appreciable bioattenuation of TCE in this area has not occurred. In transects 2 and 3, concentrations of cis-DCE above $10 \mu\text{g/L}$ are sporadic in downgradient regions; however, with time, concentrations of cis-DCE appear to increase in regions downgradient of transect 2.

3.1.2 Geochemical Parameters

In this section, results for three geochemical parameters are presented and discussed: pH, Eh, and specific conductance. Table 3.3 lists average values for these parameters from the upgradient (ML11, ML21, and ML31), downgradient (ML15, ML25, and ML35), and iron wall (ML14, ML24, and ML34) multilevel samplers. The results of all field analyses are averaged to provide an overall view of the PRB impact to ground water chemistry. At Elizabeth City, the pH of ground-water entering the PRB is approximately 6, but varies in time and space from about 5.4 to 6.6. The pH increases to an average value of 9.5 within the iron media, and then decreases to a value of 7.7 in the aquifer approximately 0.5 m downgradient of the PRB. This trend in pH clearly shows that the PRB has an impact on the aqueous chemistry of the downgradient aquifer (Table 3.3). Similarly the Eh of water entering the PRB is moderately oxidizing (approx. 218 mV) and becomes moderately to highly reducing within the reactive media (approx. -260 mV). Moderately reducing water emerges from the PRB (approx. -2 mV). The decrease in Eh and increase in pH across the flow path are expected trends that result from the corrosion of iron in water as discussed in detail in a following section of this report. The specific conductance of ground water downgradient of the PRB is approximately 15% to 30% lower than that of upgradient ground water due to partitioning of dissolved solutes into the solid phase within the reactive media. Interestingly, dissolved oxygen results (data not shown) show essentially no variability between upgradient, iron, and downgradient positions. The reasons for this are likely due to the difficulty in obtaining highly accurate DO concentrations at low levels and in the presence of ferrous iron.

Long-term trends in pH, Eh, and specific conductance are shown in Figures 3.7-3.9. In transect 2, the high pH zone caused by corrosion of the zero-valent iron has remained largely unchanged in space over the initial five-year period of operation (Figure 3.7). This result indicates that the zero-valent iron at Elizabeth City still retains some degree of reactivity even after five years of subsurface exposure. The pH values measured in upgradient regions have remained

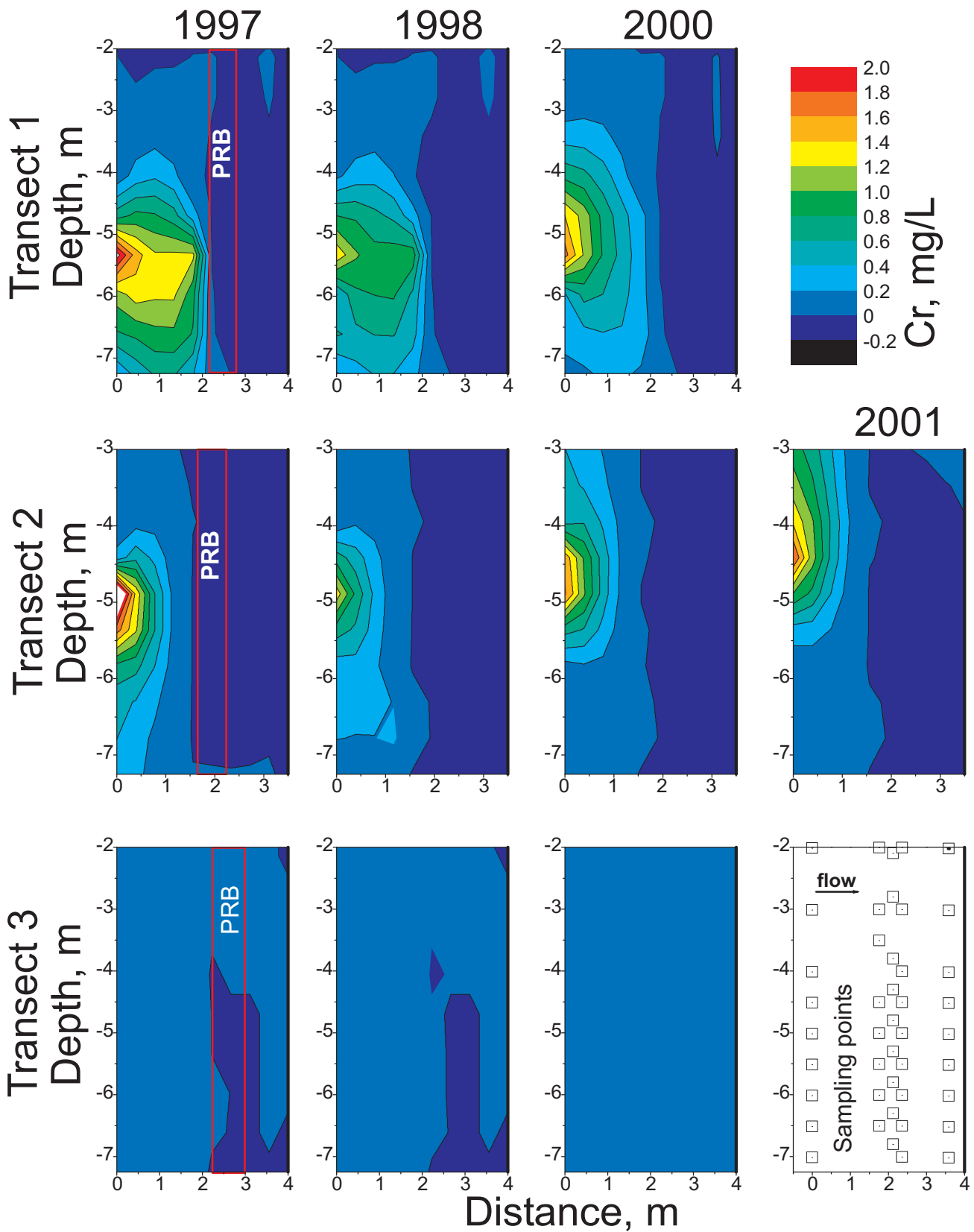


Figure 3.3 Cross-sectional profiles showing total chromium concentrations (mg/L) in transects 1, 2, and 3, Elizabeth City PRB.

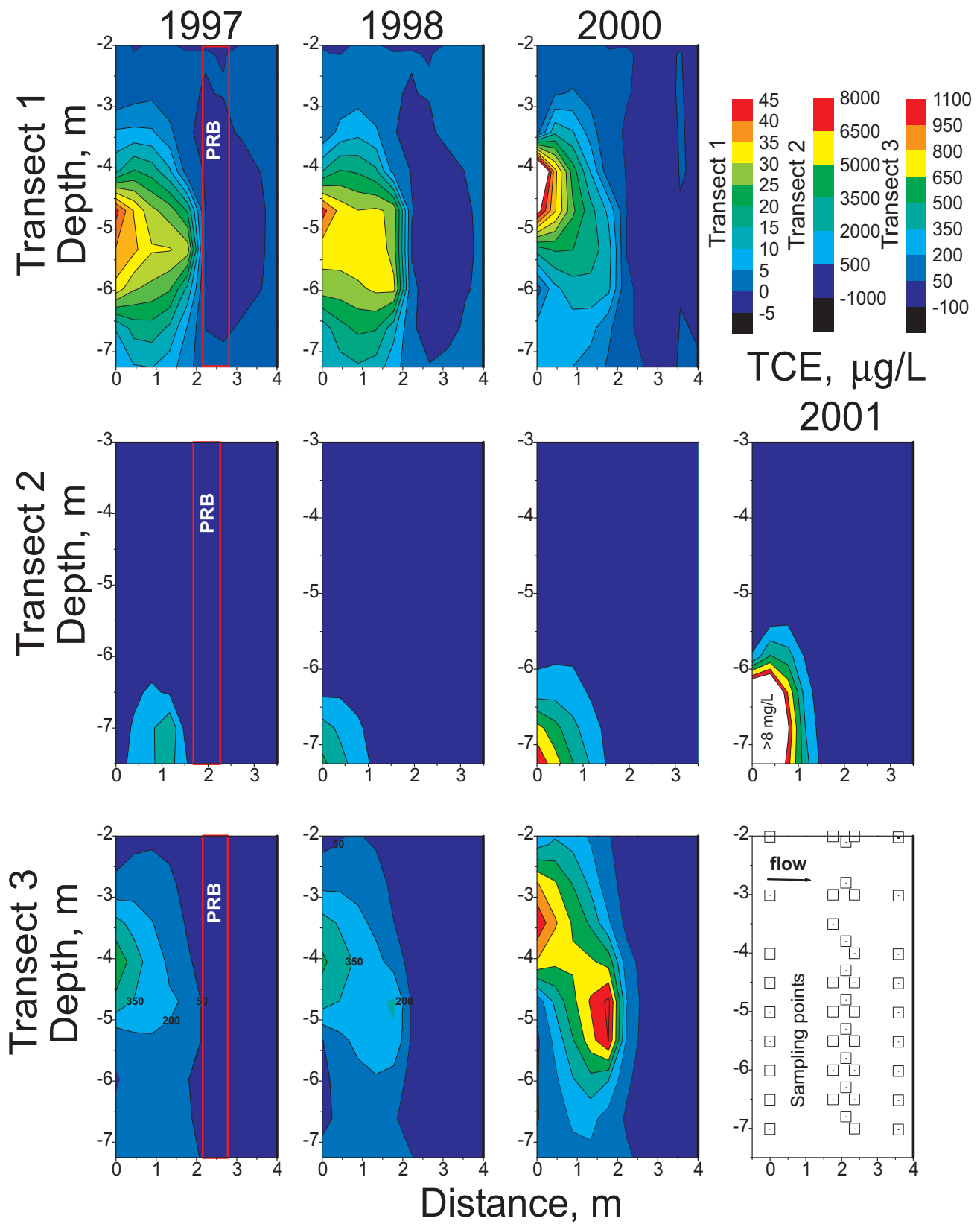


Figure 3.4 Cross-sectional profiles showing TCE concentrations ($\mu\text{g/L}$) in transects 1, 2, and 3, Elizabeth City PRB.

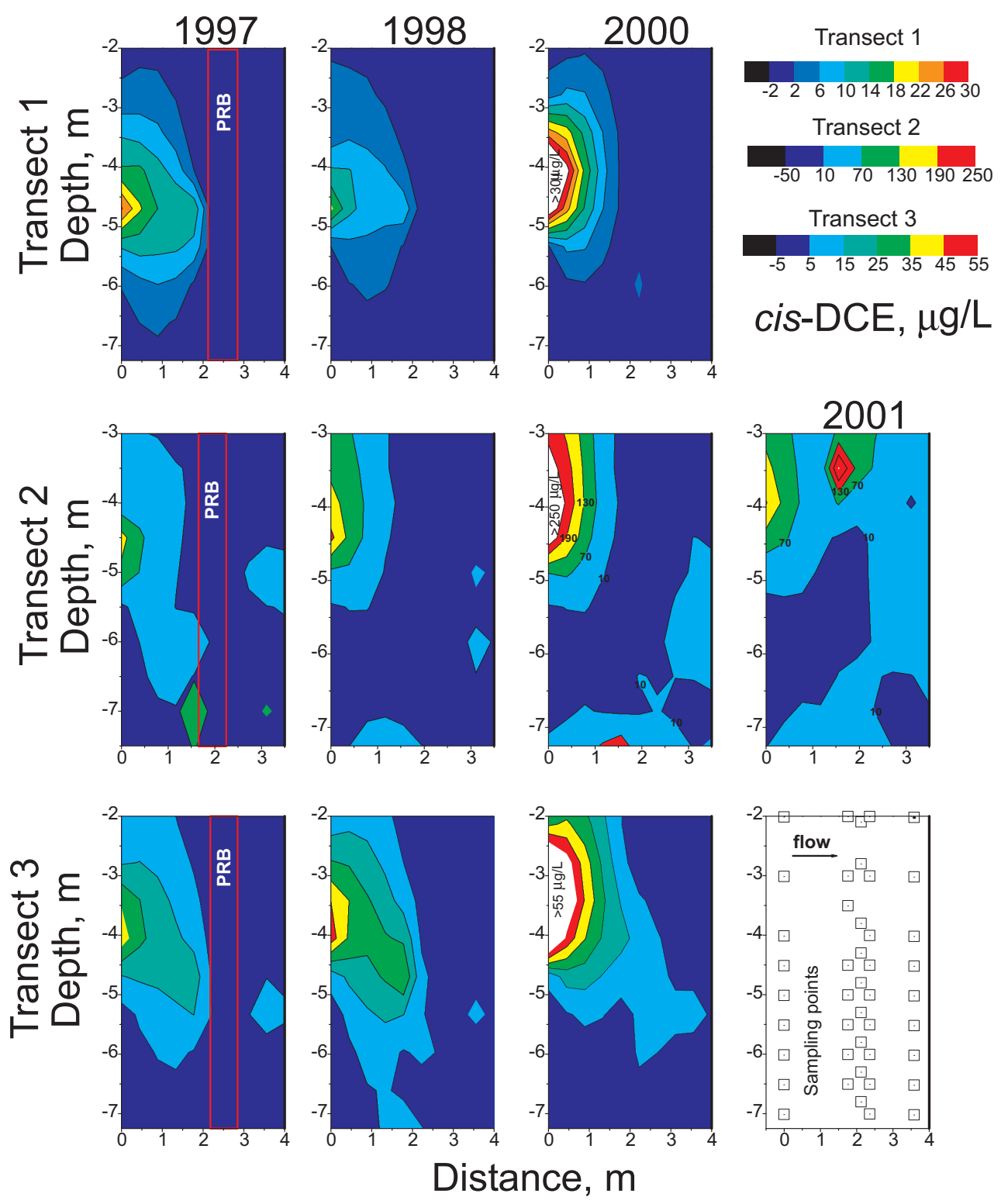


Figure 3.5 Cross-sectional profiles showing *cis*-DCE concentrations ($\mu\text{g/L}$) in transects 1, 2, and 3, Elizabeth City PRB.

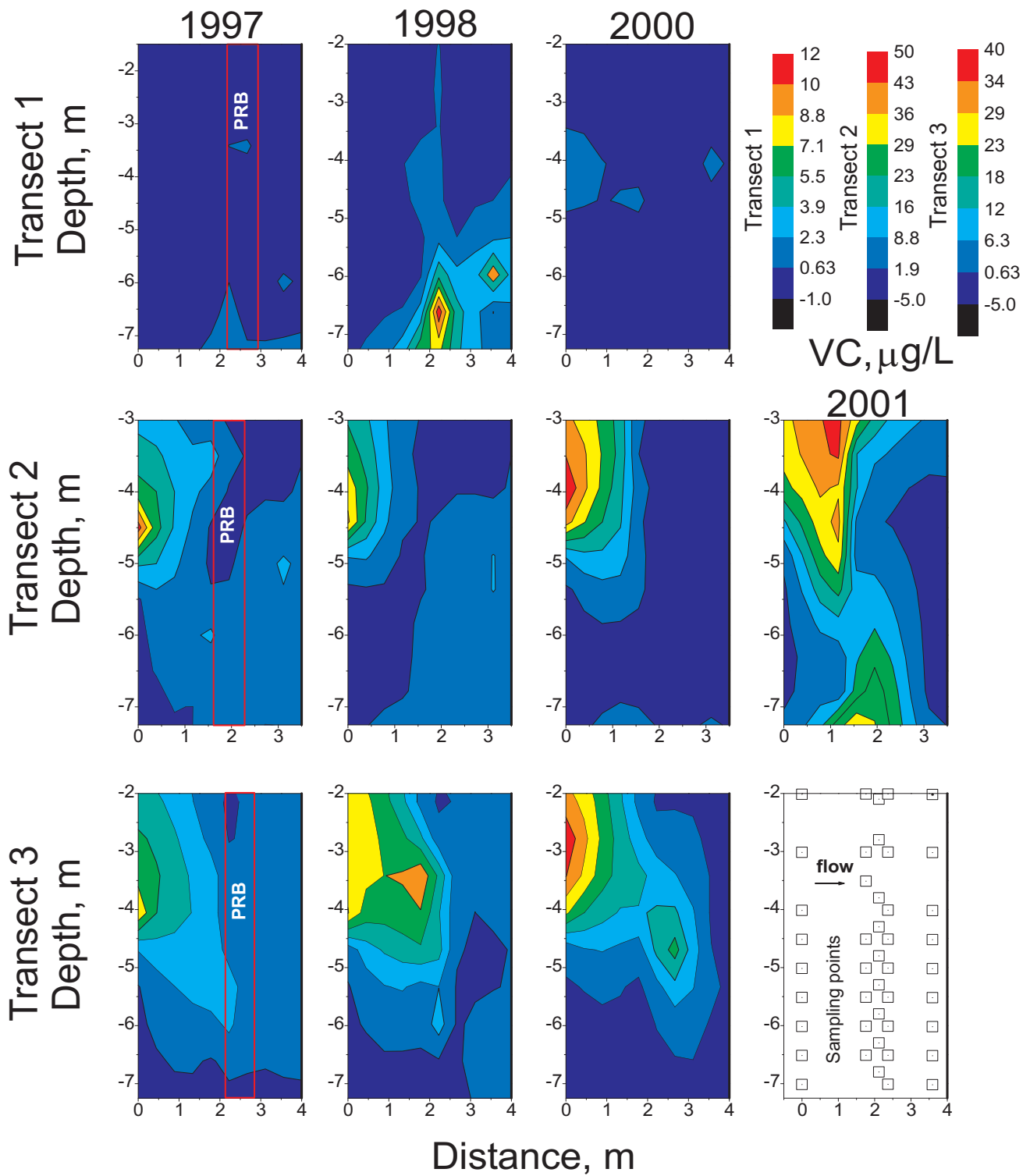


Figure 3.6 Cross-sectional profiles showing VC concentrations ($\mu\text{g/L}$) in transects 1, 2, and 3, Elizabeth City PRB.

Table 3.3. Geochemical Parameters in Upgradient, Iron Wall, and Downgradient Locations, Elizabeth City PRB

Location	Eh (mV)	pH	Specific Conductance (μ S/cm)
Upgradient	218 (\pm 311)	6.02 (\pm 0.24)	390 (\pm 177)
Iron wall	-258 (\pm 212)	9.53 (\pm 0.72)	186 (\pm 105)
Downgradient	-2 (\pm 190)	7.71 (\pm 1.14)	192 (\pm 110)

Notes: Average value and 1 s.d. reported for upgradient (ML11, ML21, and ML31), iron wall (ML14, ML24, and ML34), and downgradient (ML15, ML25, and ML35) well locations.

largely unchanged in time and space. Similarly, temporal and spatial distribution of pH within the iron media and in downgradient regions has remained consistent since 1997 (Figure 3.7). Transects 1 and 3 also show fairly consistent patterns in pH. Notable is a relatively narrow zone near the influent side of the PRB where increases of 3 to 4 pH units are observed; a sharp gradient in pH has been observed in each sampling event since 1997.

Iron corrosion is expected to result in moderately high pH and low Eh conditions. The contouring results shown in Figures 3.7 and 3.8 suggest, however, that pH and Eh values are *not* directly coupled (Wilkin, 2002). Values of Eh in the iron are gradually increasing with time (Figure 3.8), whereas pH has been consistent with time. For example, in transect 2, the cross-sectional area represented by Eh values below -100 mV has progressively decreased from 1997 to 2001 (Figure 3.8). There still exists after five years a sharp gradient in redox between the relatively oxidizing upgradient aquifer and the moderately to highly reducing reactive zone. The redox potential of upgradient waters is as high as $+500$ mV and values less than 0 mV are typical within the reactive media. After the first five years of operation, the redox gradient continues to support efficient removal of hexavalent chromium and chlorinated compounds. Nevertheless, a trend of decreasing reductive capacity with time is evident.

Corrosion of iron metal results in a moderately alkaline pH and low Eh geochemical environment that drives abiotic mineral precipitation and supports a variety of microbial metabolic pathways. The net effect of mineral precipitation is broadly captured in measurements of specific conductance (SC) that reflect an overall decrease in the concentration of total dissolved solids through the reactive barrier. In transect 2, the highest concentrations of ground-water solutes are observed at a depth of about 4 to 6 m below ground surface (Figure 3.9). This depth interval also corresponds to a maximum in SC and a zone within the PRB in which core analyses show enrichments in solid-phase concentrations of inorganic carbon, sulfur, and microbial biomass. Over the initial five-year period, variability in SC over a factor of about 2 has been observed in upgradient regions at the Elizabeth City site. Variability of specific conductance in upgradient regions is also reflected in the temporal and spatial distribution of SC values within the reactive media and in downgradient regions (Figure 3.9). The consistent trend of decreasing SC values through the reactive media suggests that mineral precipitation processes are operating over the lifetime of the reactive media, i.e., that the zero-valent iron has remained reactive over the first five years of operation. This sustained reactivity is likely due to the presence of the steep pH and/or Eh gradient as described above. The region where a minimum in Eh (most reducing) is observed corresponds to the depth of the SC maximum in upgradient ground water. This observation suggests that the concentration of ground-water solutes, or more likely the concentration of terminal electron acceptors such as sulfate and microbial activity, is perhaps what leads to the Eh minima rather than only anaerobic iron corrosion reactions. Furthermore, the subtle changes in Eh within the reactive media also seem to be time-dependent and reflect temporal changes in upgradient Eh and SC.

3.1.3 Dissolved Cations and Anions

The dominant cations in ground water at the Elizabeth City site are sodium, potassium, calcium, and magnesium. On a molar basis, sodium is the dominant cation followed by $\text{Ca} > \text{Mg} > \text{K}$. From 1997 to 2001, upgradient ground water contained up to 5.2 mM Na, 1.1 mM Ca, 0.8 mM Mg, and 0.2 mM K. Ground water most concentrated in dissolved solutes was consistently found at 4 to 6 meters below ground surface in each of the multilevel well bundles (Figure 3.9). Inspection of cross-sectional profiles in Figures 3.10-3.12 indicates that the zero-valent iron effectively removes calcium, magnesium, and to some extent, sodium, from ground water at the Elizabeth City site.

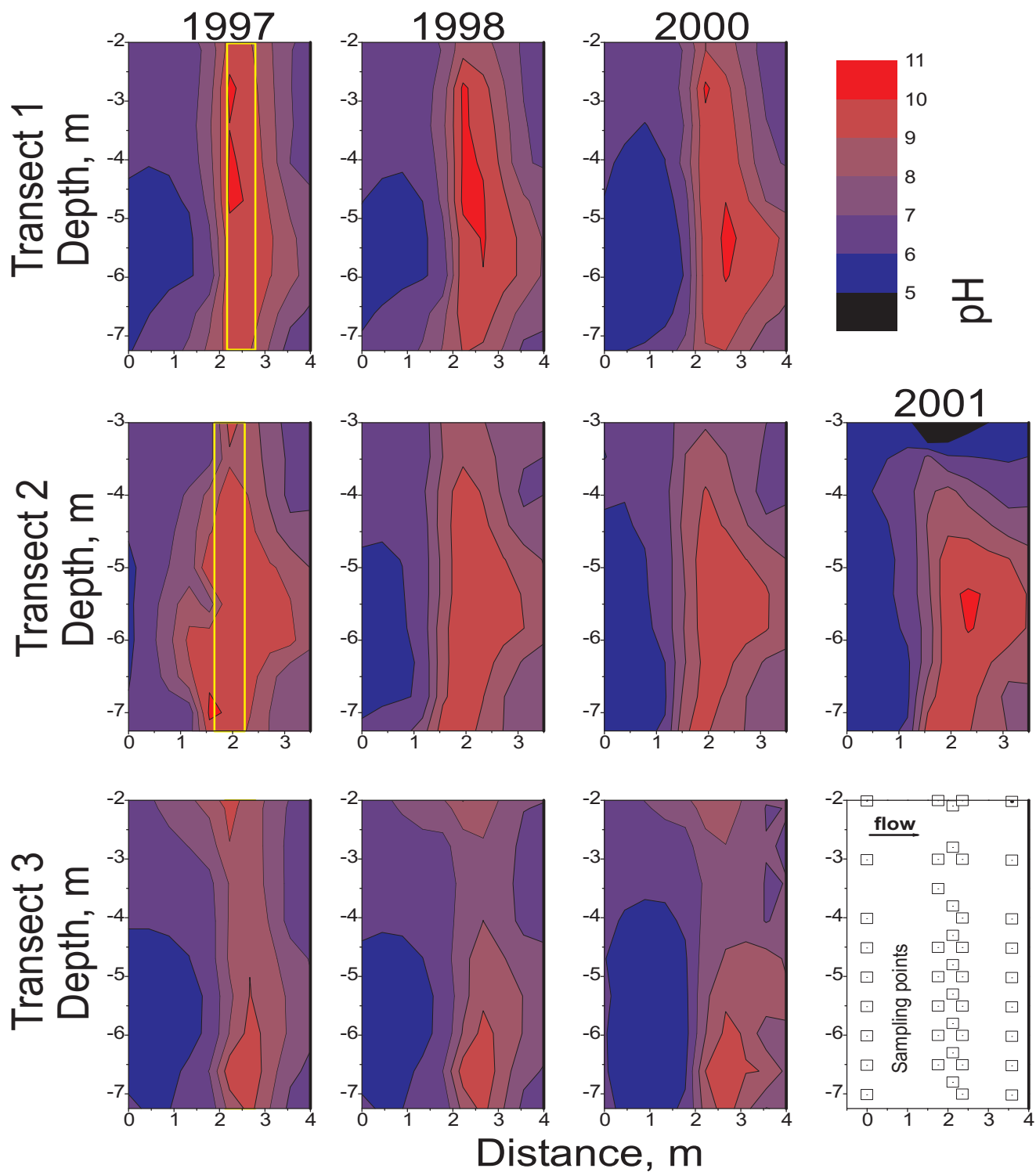


Figure 3.7 Cross-sectional profiles showing pH distributions in transects 1, 2, and 3, Elizabeth City PRB.

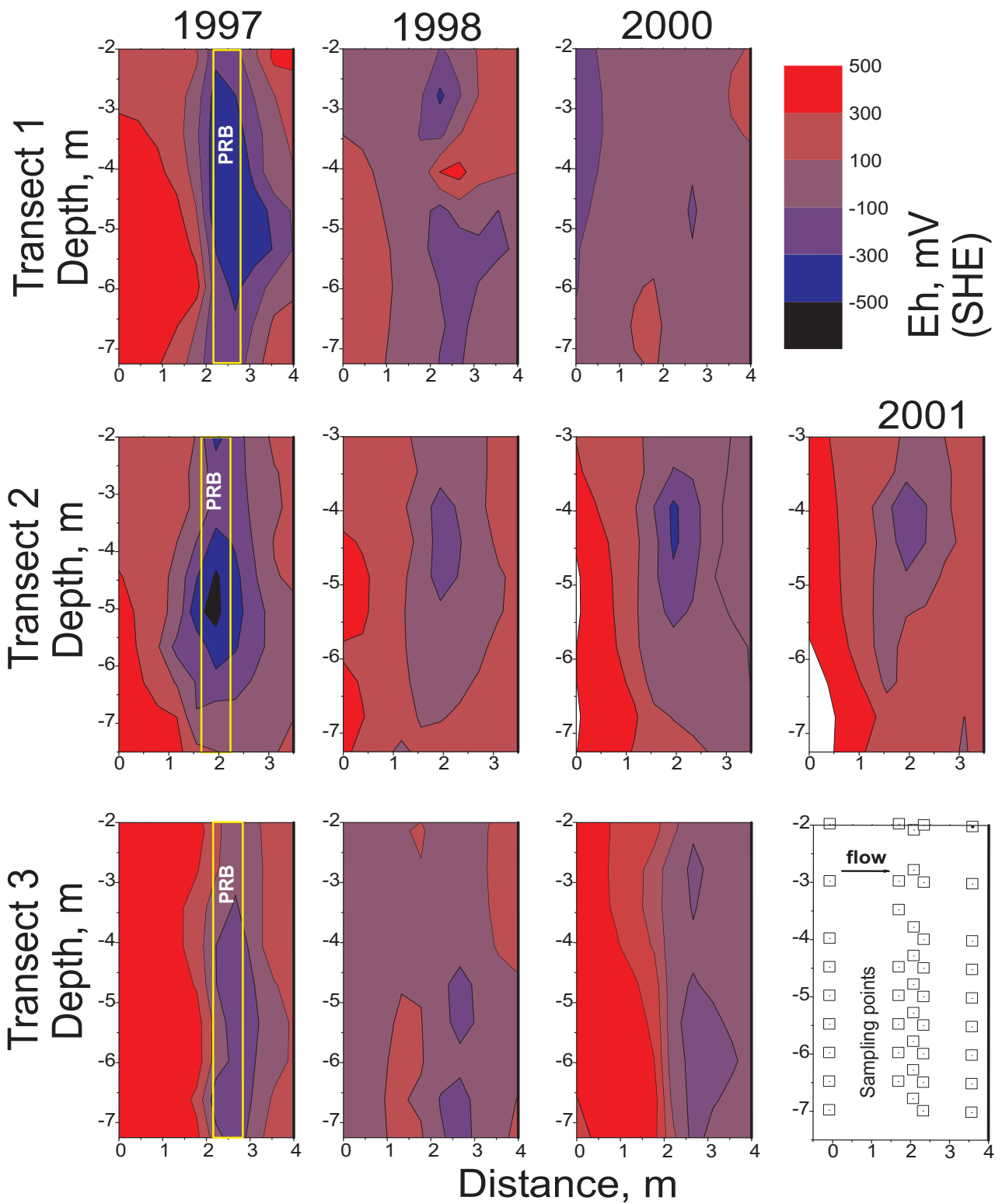


Figure 3.8 Cross-sectional profiles showing Eh distributions (mV) in transects 1, 2, and 3, Elizabeth City PRB.

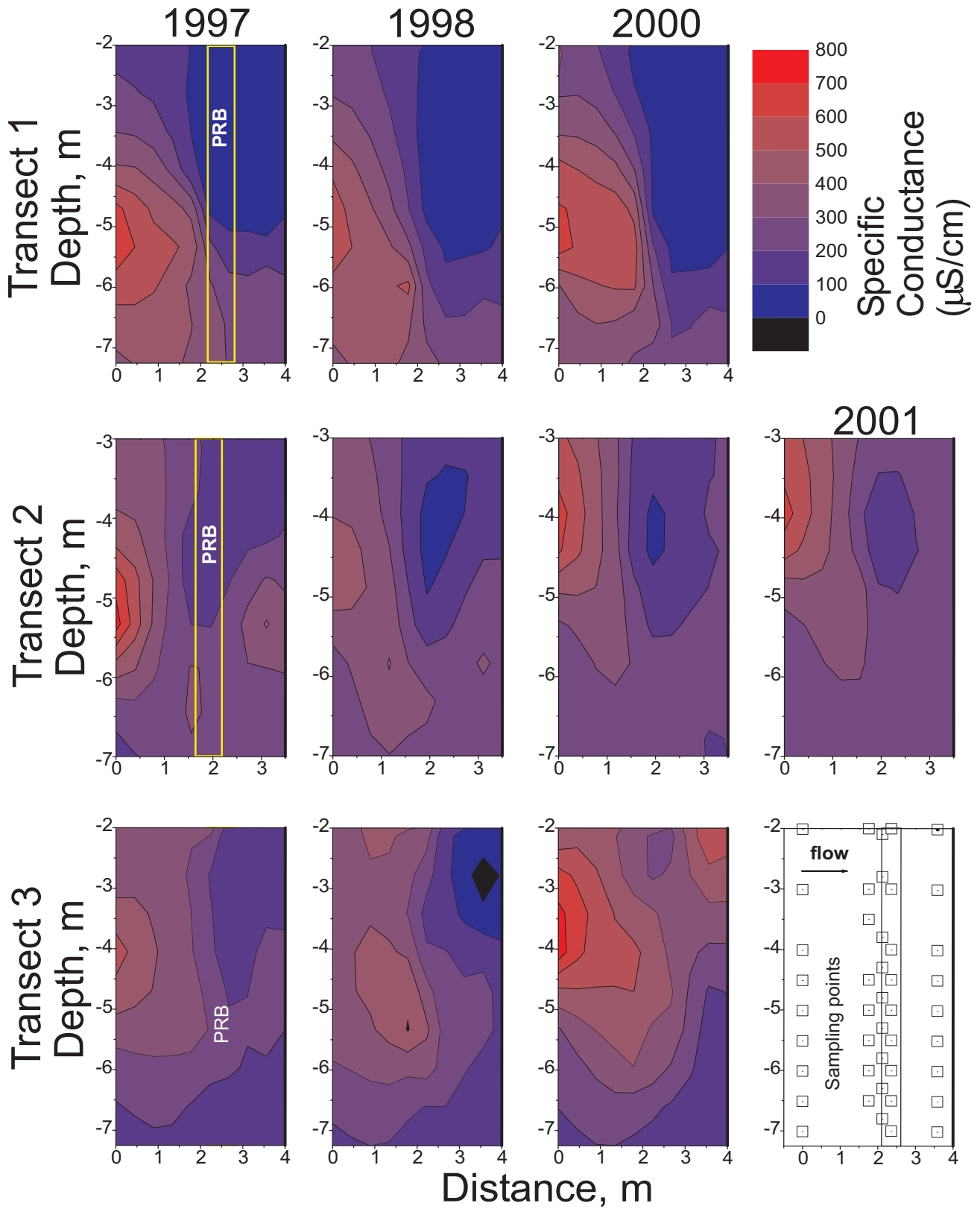


Figure 3.9 Cross-sectional profiles showing specific conductance distributions ($\mu\text{S}/\text{cm}$) in transects 1, 2, and 3, Elizabeth City PRB.

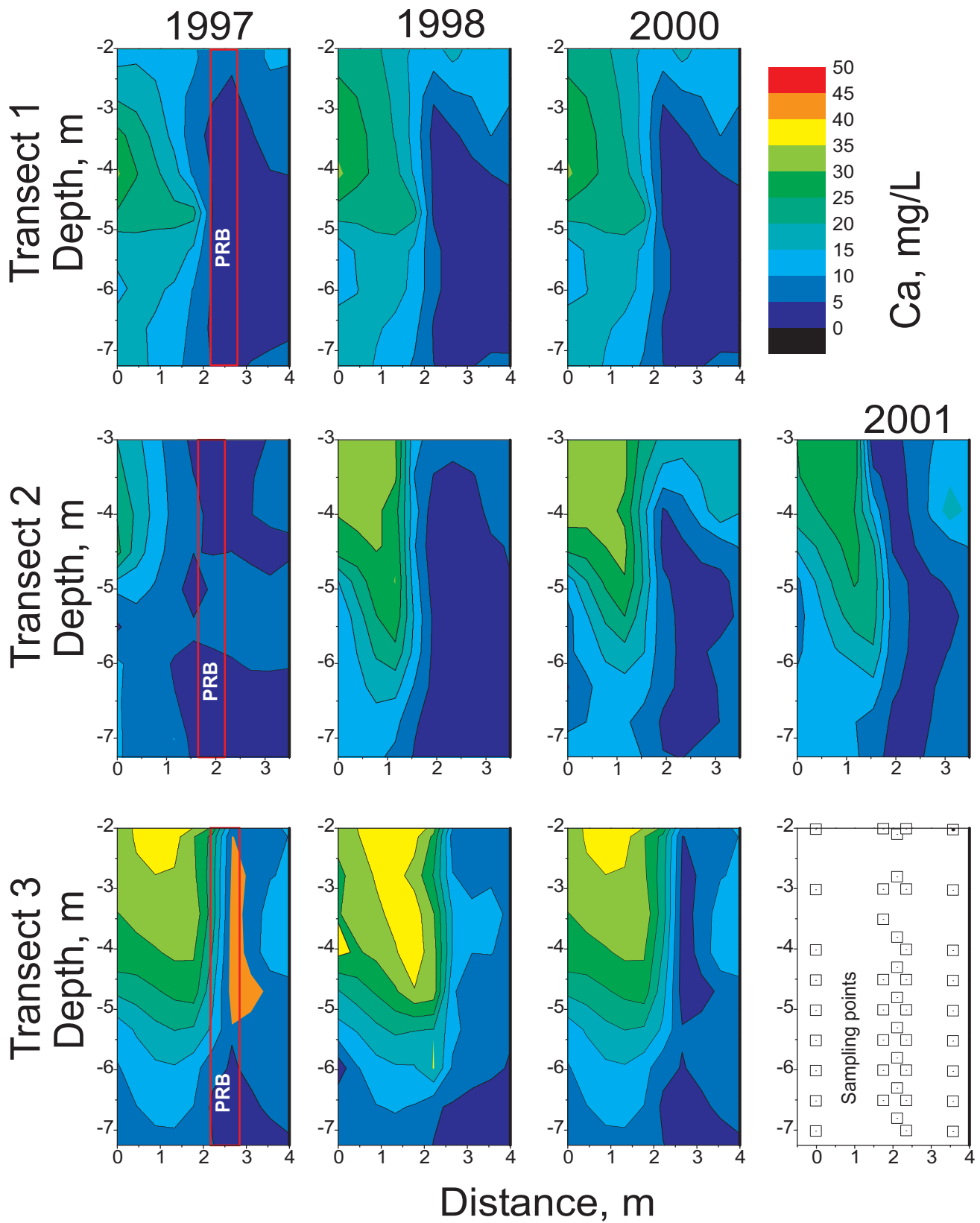


Figure 3.10 Cross-sectional profiles showing calcium concentrations (mg/L) in transects 1, 2, and 3, Elizabeth City PRB.

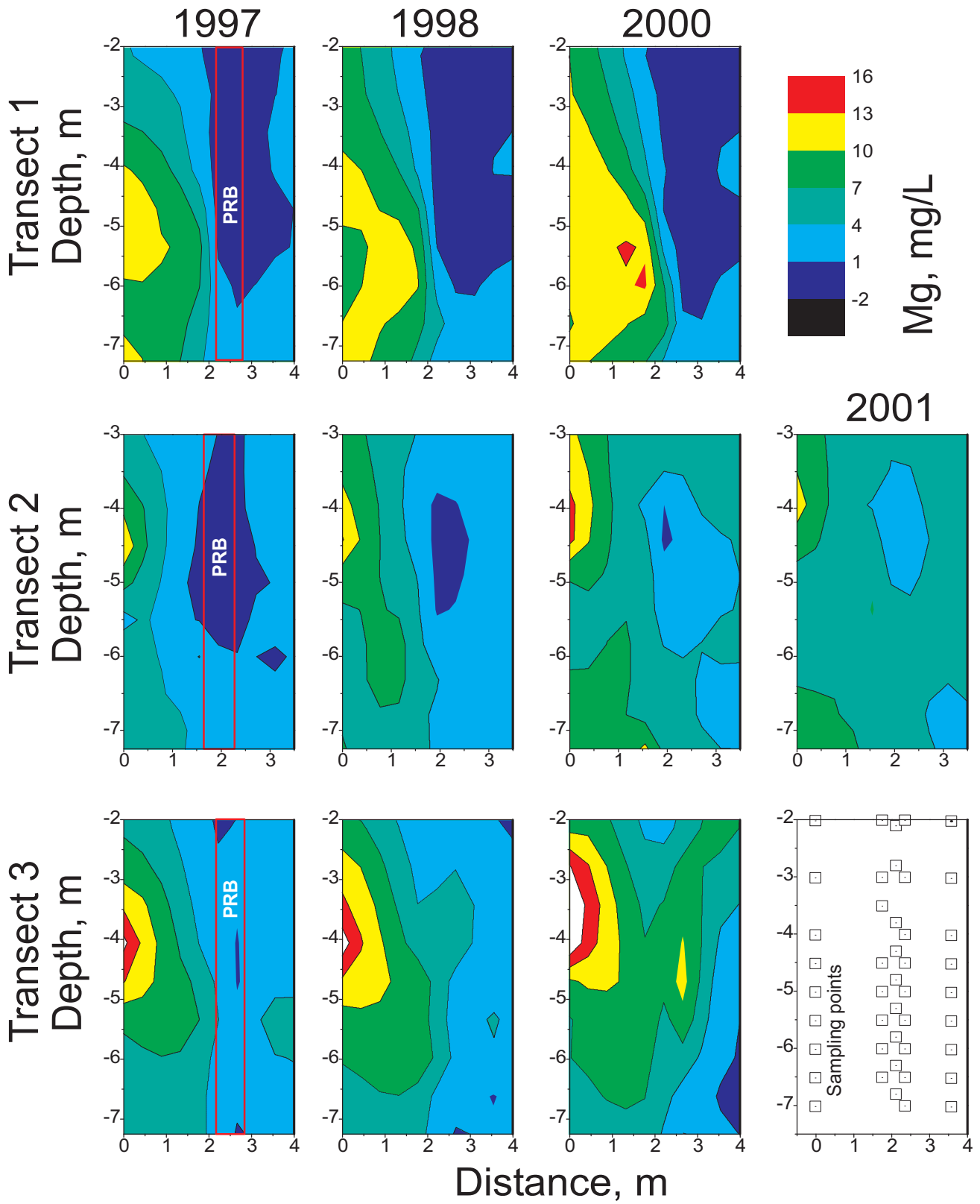


Figure 3.11 Cross-sectional profiles showing magnesium concentrations (mg/L) in transects 1, 2, and 3, Elizabeth City PRB

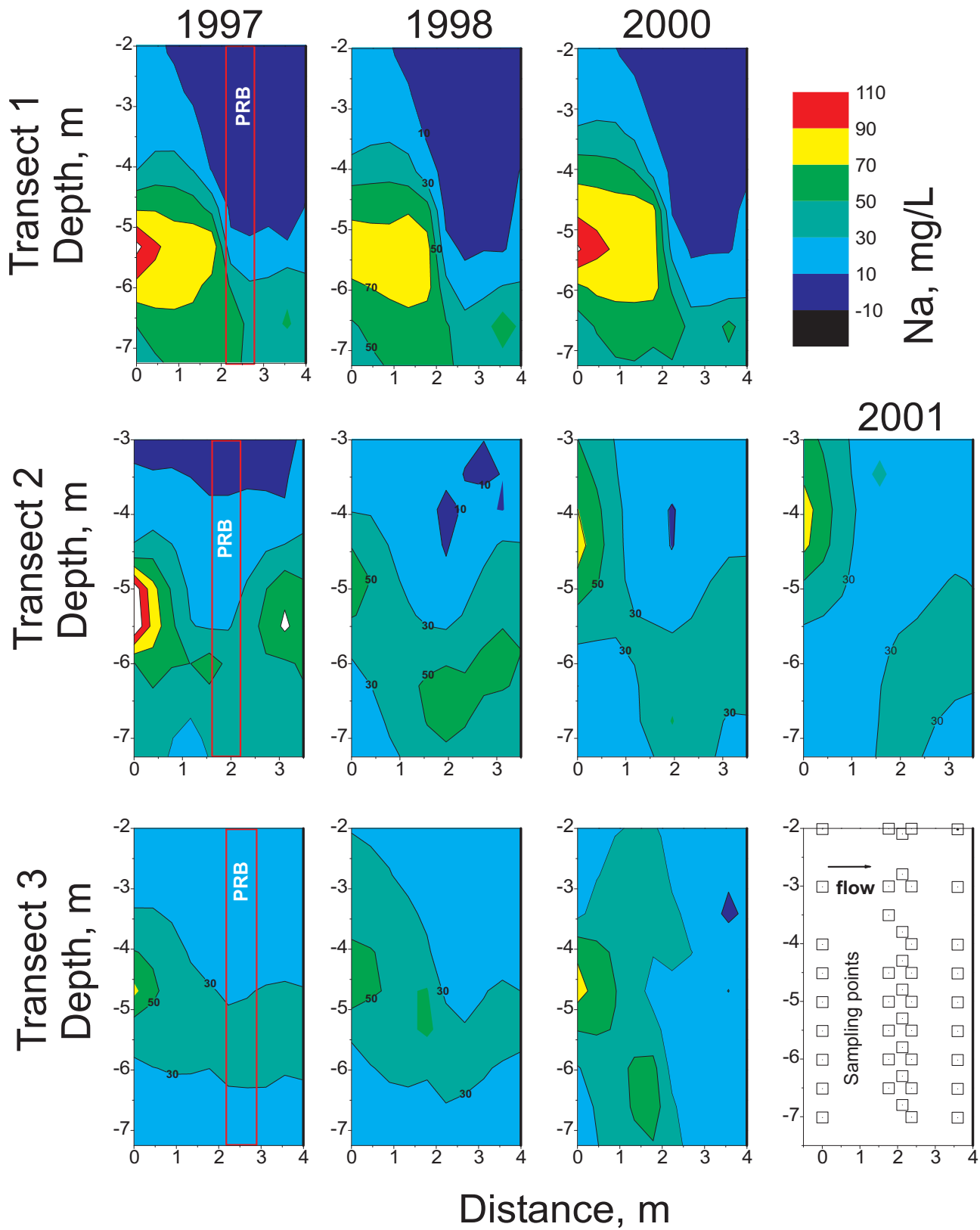


Figure 3.12 Cross-sectional profiles showing sodium concentrations (mg/L) in transects 1, 2, and 3, Elizabeth City PRB.

Concentrations of potassium appear to be largely unaffected by the reactive media (Figure 3.13). In transect 2, calcium concentrations range from about 5 to 30 mg/L in upgradient ground water and are typically less than 5 mg/L in downgradient ground water. Depth-dependent removal efficiencies of the major cations are presented in Table 3.4. At discrete depth intervals, up to 71% Ca, 73% Mg, and 60% Na are removed as ground water passes through the reactive media. Calcium and magnesium are consistently removed through time, although percent removal values are lower in 2001 compared to the average value from 1997 to 2001 (Table 3.4). This trend may suggest decreasing reactivity over time with respect to removal of divalent cations. Sodium shows removal at some intervals and relative gains in concentrations at deeper levels (Figure 3.12; Table 3.4). The 2-dimensional trends in sodium and chloride concentrations suggest that there may be some component of vertical redistribution of solutes within the PRB.

Anions present in ground water at the Elizabeth City site include chloride, sulfate, bicarbonate, and nitrate. On a molar basis, chloride and bicarbonate are the dominant anions followed by sulfate. Nitrate is commonly detected in upgradient ground water but always at concentrations below about 5 mg/L. In downgradient multilevel well bundles, nitrate is typically below the analytical detection limit (0.10 mg/L). In transect 2, sulfate concentrations typically range from about 25 to 90 mg/L in upgradient ground water, but then decrease to less than 1 mg/L in most downgradient multi-level wells. Inspection of the cross-sectional profiles in Figures 3.14-3.17 indicates that anionic species, especially sulfate and bicarbonate, are effectively removed by zero-valent iron. Depth-dependent removal efficiencies of the major anions are presented in Table 3.5. Typically >90% of influent sulfate is removed as ground water passes through the reactive media. The high removal efficiency of sulfate does not appear to be decreasing with time (Table 3.5). Nitrate is also effectively removed by the PRB (Table 3.5), although the anomalous trends apparent in 2000 are not understood. Chloride removal occurs at depths above 5 m but reactions in the PRB appear to be sources of chloride at depths below 5 m. The release of chloride is likely related to the degradation of TCE at depths below 5 m.

Silica in upgradient ground water is present at concentrations up to about 16 mg/L, dominantly as the uncharged form H_2SiO_4^0 (aq). Silica concentrations in the reactive media are typically <1 mg/L and levels then rebound in downgradient wells to values from about 1 to 8 mg/L (Figure 3.18). Similar behavior for dissolved silica was also reported at the Moffet Field and Lowry Air Force Base PRBs (Gavaskar et al., 2002).

Over the first five years of operation, the Elizabeth City PRB has consistently removed C, S, Ca, Mg, Si, and N from ground water. Over this time period there appears to be a slight to no discernible loss in the capacity or efficiency of removal of these inorganic components. These elements are removed from ground water by mineral precipitation or by adsorption, processes examined in more detail in later sections of this report.

3.2 Core Sampling at Elizabeth City

Core samples from the PRB were collected on an annual basis at Elizabeth City to assess the extent of corrosion and mineral buildup on the iron surfaces. Core collection methods and analysis procedures are described in Volume 2 of this EPA Report series. In all cases, 5 cm inner diameter cores were collected using a Geoprobe™. Core barrels were driven using a pneumatic hammer to the desired sampling location and continuous, up to 110 cm, sections of iron, iron + soil, or soil were retrieved. Angle cores (30° relative to vertical) and vertical cores were collected in order to assess the spatial distribution of mineral/biomass buildup in the reactive media. Prior to pushing the core barrel, an electrical conductivity profile was collected to verify the exact position of the iron/aquifer interface. Details of core collection procedures are described in Volume 2 of this EPA Report series. In all cases, core recovery was 50 to 92% of the expected value. Core materials from the Elizabeth City PRB were jet black in color without any obvious signs of cementation or oxidation. Immediately after collection, the cores were frozen and shipped back to the Ground Water and Ecosystems Restoration Division in Ada, OK for sub-sampling and analysis. The frozen cores were partially thawed and then placed in an anaerobic chamber with a maintained H_2 - N_2 atmosphere. Each core was logged and partitioned into 5 to 10 cm segments. Each segment was homogenized by stirring in the glove box and then split into 4 sub-samples: (1) inorganic carbon analyses, (2) sulfur analyses/X-ray diffraction (XRD), (3) Scanning electron microscopy (SEM)/X-ray photoelectron spectroscopy (XPS) analyses, and, (4) microbial assays (phospholipid fatty acids, PLFA). All sub-samples were retained in airtight vials to prevent any air oxidation of redox-sensitive constituents. Details of analytical methods and QA/QC procedures used to characterize the core materials are presented in Volume 2 of this EPA Report series.

Locations of coring events at Elizabeth City are shown in Figure 3.19, and information on core recovery, core length, and depth of core penetration is presented in Table 3.6. Cores collected from the upgradient aquifer/iron region generally penetrated the PRB at depths of 4.5 to 6.5 m below ground surface. As such, the cores were retrieved from portions of the PRB where the highest concentrations of chromium and total dissolved solutes entered the reactive media (see, e.g., Figure 3.3).

3.2.1 Carbon Analysis

Based on long-term trends in ground-water concentrations of bicarbonate and sulfate, significant accumulations of inorganic carbon and sulfur precipitates might be expected in the PRB at Elizabeth City. In order to confirm this

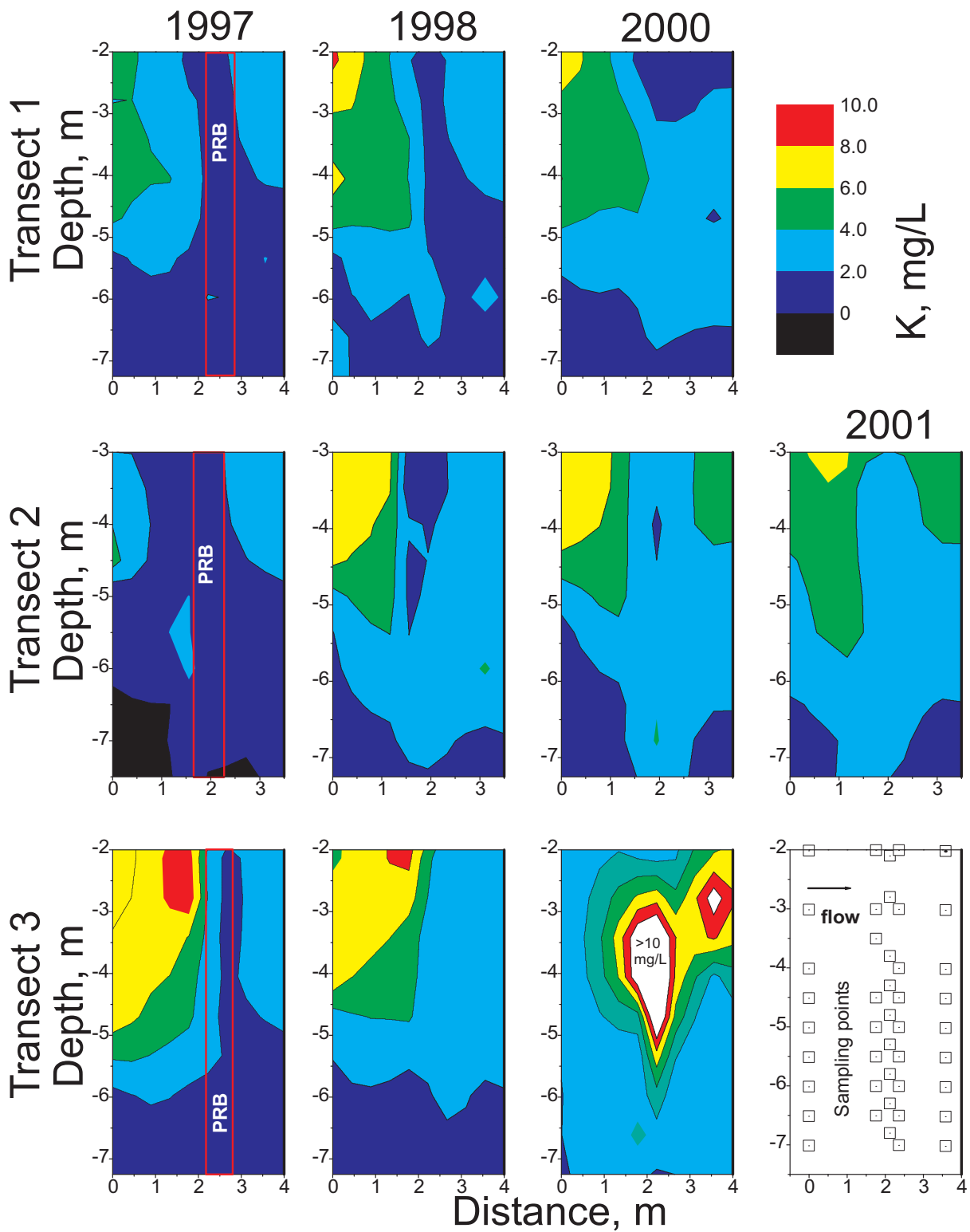


Figure 3.13 Cross-sectional profiles showing potassium concentrations (mg/L) in transects 1, 2, and 3, Elizabeth City PRB.

Table 3.4. Changes in Concentration of Metals in Ground Water at Transect 2 (Elizabeth City) as a Function of Time and Depth

Depth, m	Average values from 1997 to 2001			Values from 2001		
	ML21 Upgradient	ML25 Downgradient	% Change	ML21 Upgradient	ML25 Downgradient	% Change
	Ca, mg/L					
4	26.6	8.1	69.5	18.8	12.4	34.0
5	8.6	4.8	44.2	7.4	4.3	41.9
6	10.3	4.5	56.3	10.1	5.9	41.6
7	13.7	4.0	70.8	12.7	6.2	51.2
	Mg, mg/L					
4	12.0	3.2	73.3	10.0	5.2	48.0
5	6.3	3.5	44.4	5.9	5.1	13.6
6	6.5	2.6	60.0	6.8	4.3	36.8
7	8.1	2.3	71.6	7.9	3.5	55.7
	Na, mg/L					
4	52.6	20.9	60.3	78.8	19.8	74.9
5	66.3	47.1	29.0	35.6	34.5	3.1
6	27.6	42.1	-52.5	20.7	33.5	-61.8
7	23.0	34.1	-48.3	23.2	24.4	-5.2
	K, mg/L					
4	4.8	3.5	27.1	4.4	3.9	11.4
5	1.7	2.4	-41.2	3.6	3.1	13.9
6	1.3	2.3	-76.9	1.8	2.1	16.7
7	1.1	0.7	36.4	1.3	1.1	15.4

% change calculated using:

$$\frac{[(\text{upgradient concentration} - \text{downgradient concentration}) / (\text{upgradient concentration})] \times 100}{}$$

expectation and to document the concentration distribution of inorganic precipitates within the reactive media, solid phase analyses of carbon and sulfur were performed. Results of these analyses on Elizabeth City cores are listed in Table A1 (Appendix 1). Inorganic carbon results are given in weight percent C based upon carbon that is released from a sample after acidification with hot 5% perchloric acid. This acid digestion procedure releases inorganic carbon present in minerals such as calcite (trigonal CaCO_3), aragonite (orthorhombic CaCO_3), siderite (FeCO_3), magnesite (MgCO_3), rhodochrosite (MnCO_3), ferrous carbonate hydroxide ($\text{Fe}_2(\text{OH})_2\text{CO}_3$), and carbonate green rust ($\text{Fe}_6(\text{OH})_{12}\text{CO}_3 \cdot x\text{H}_2\text{O}$). The mineral composition of authigenic precipitates formed within the reactive barrier is more fully explored in the sections below on X-ray diffraction analysis and SEM analysis. The bulk carbon concentrations are used to access the space- and time-dependent quantity of inorganic carbon that has deposited in the reactive media, an understanding of which is necessary for estimating the extent of pore infilling through time.

Results of all carbon analyses on Elizabeth City core materials ($n = 170$) are presented in Table A1. The inorganic, acid-extractable carbon concentration in unreacted Peerless iron was found to be $15 \mu\text{g/g}$; therefore, concentrations of inorganic carbon in core materials above this value are the result of mineral precipitation processes that have taken place within the reactive media as a result of continued ground-water exposure. Concentrations of inorganic carbon within $>90\%$ iron samples range from <1 to $5870 \mu\text{g/g}$. In all cases, the highest concentrations were determined in samples collected adjacent to the upgradient aquifer/iron interface, and the lowest concentrations were detected near the downgradient edge of the reactive media. Accumulation of inorganic carbon precipitates does not occur at the same rate throughout the reactive media, rather carbon accumulation is highly spatially variable and is largely restricted to the upgradient portion of the reactive media (Wilkin et al., 2003).

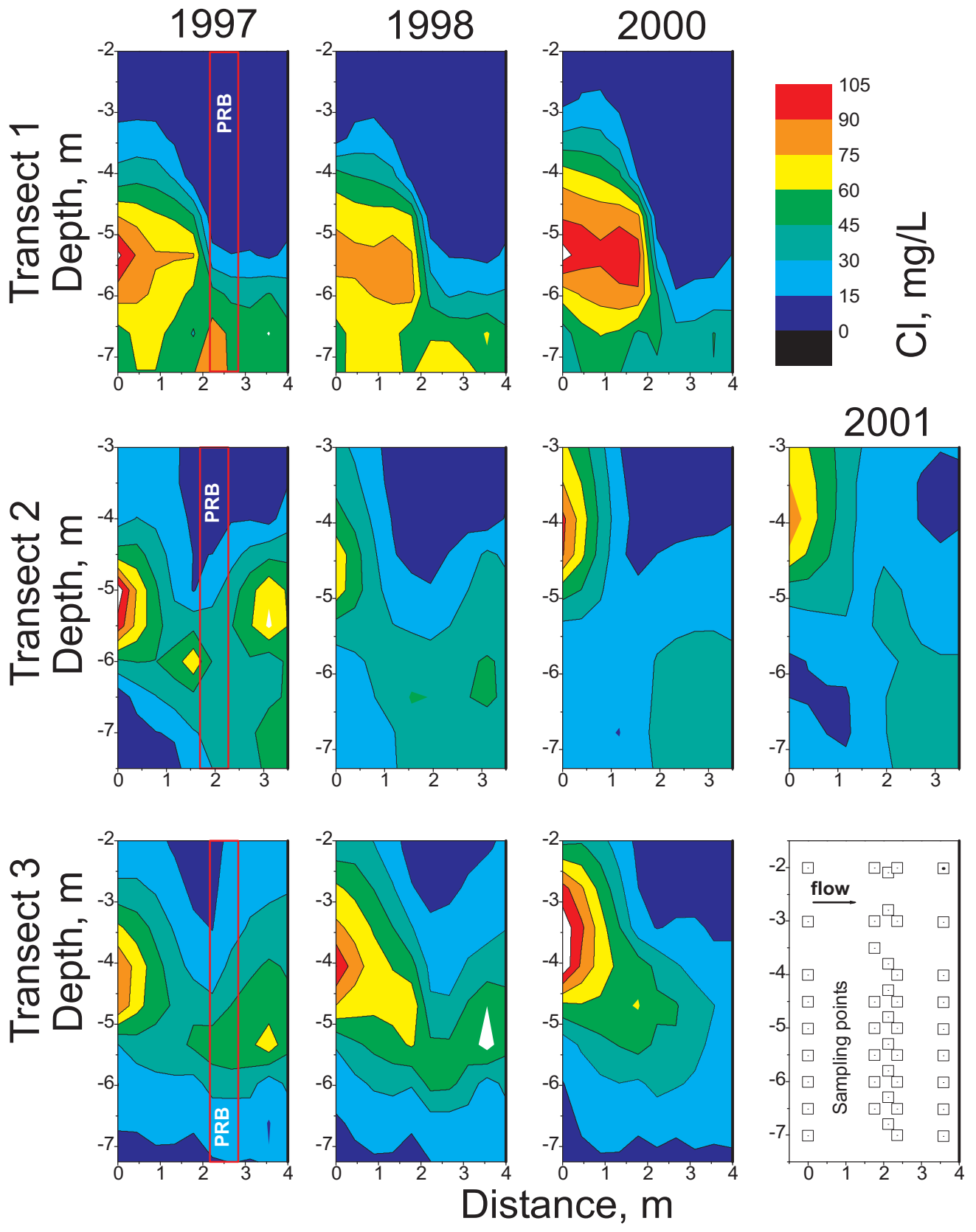


Figure 3.14 Cross-sectional profiles showing chloride concentrations (mg/L) in transects 1, 2, and 3, Elizabeth City PRB.

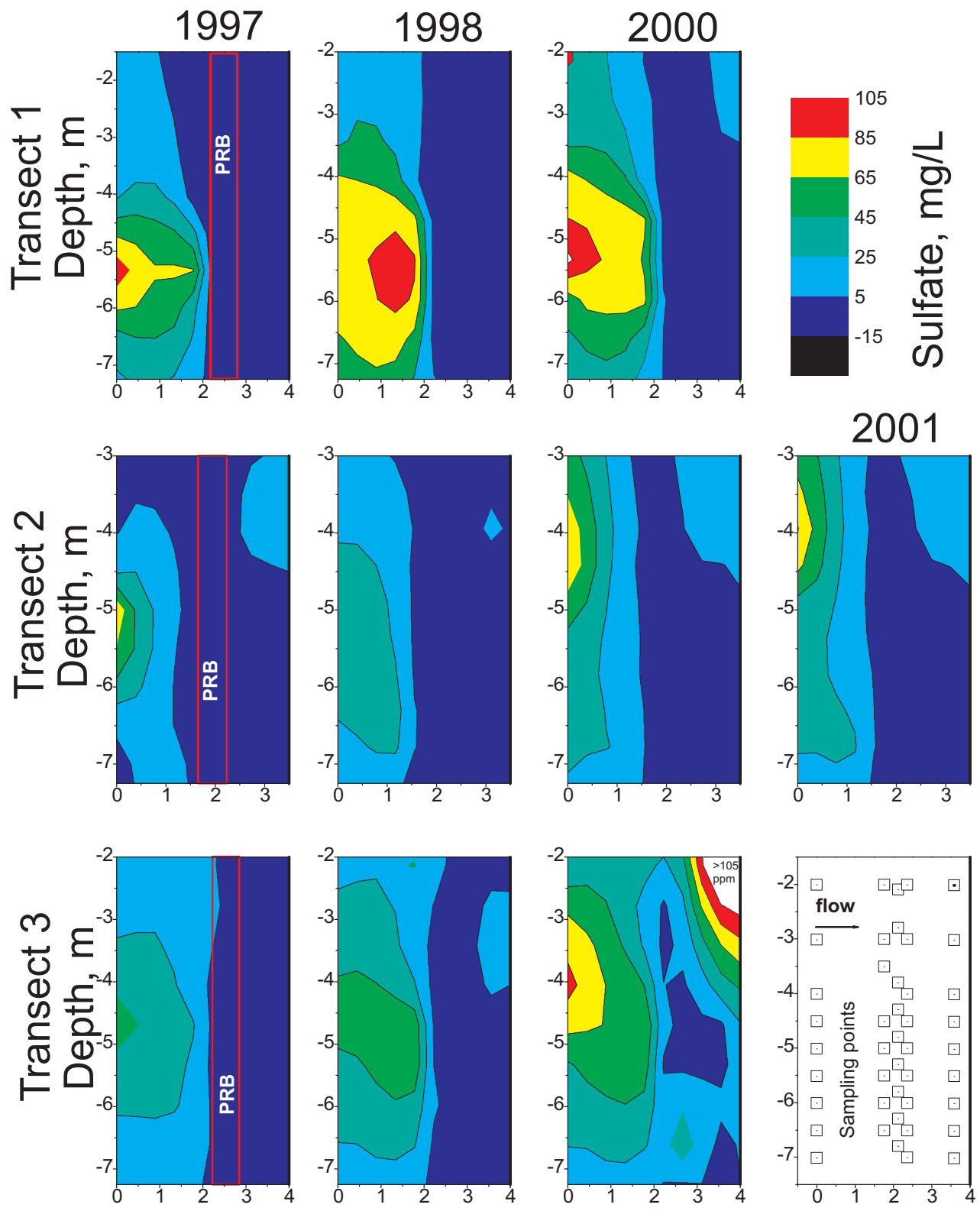


Figure 3.15 Cross-sectional profiles showing sulfate concentrations (mg/L) in transects 1, 2, and 3, Elizabeth City PRB.

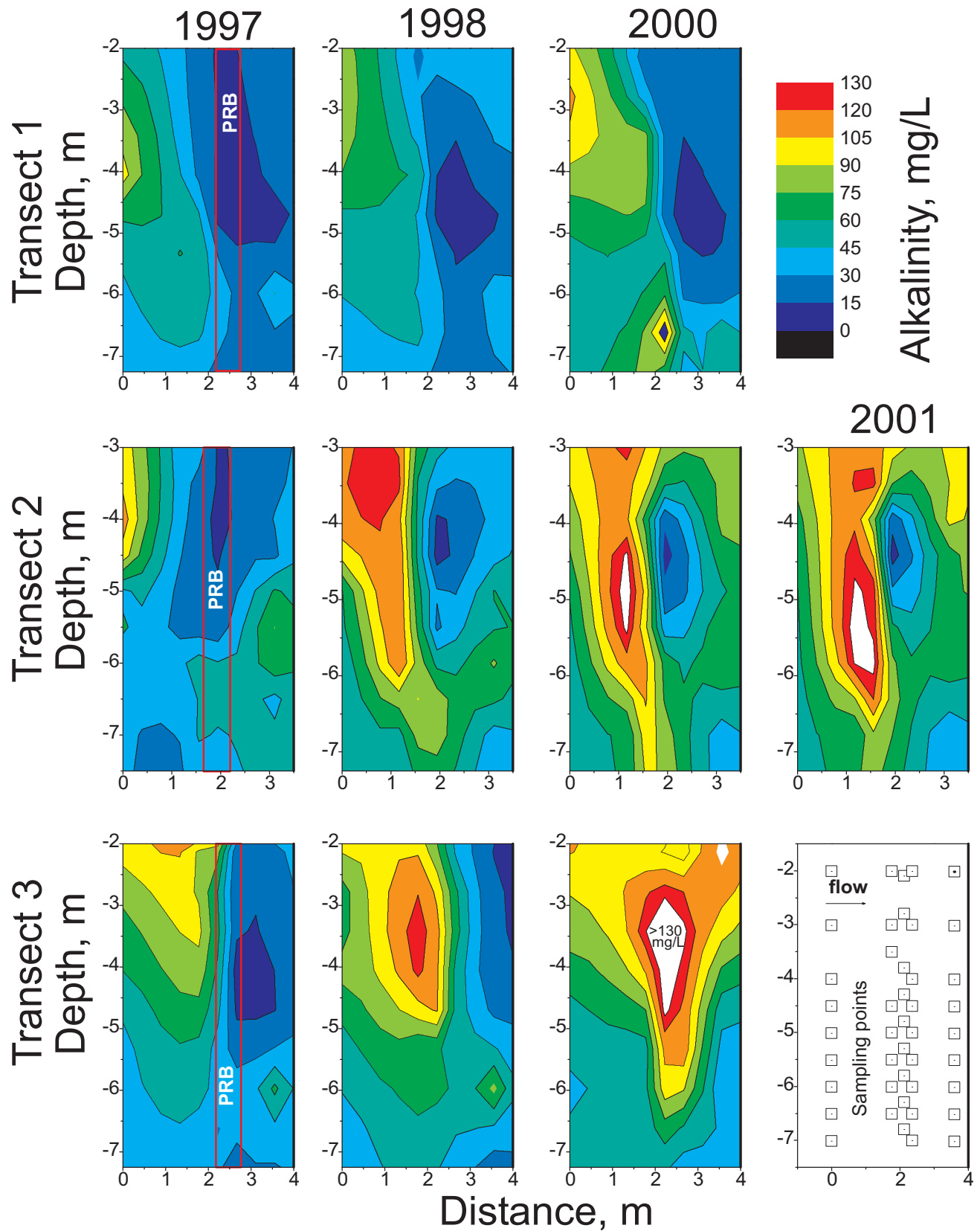


Figure 3.16 Cross-sectional profiles showing alkalinity distributions (mg/L) in transects 1, 2, and 3, Elizabeth City PRB.

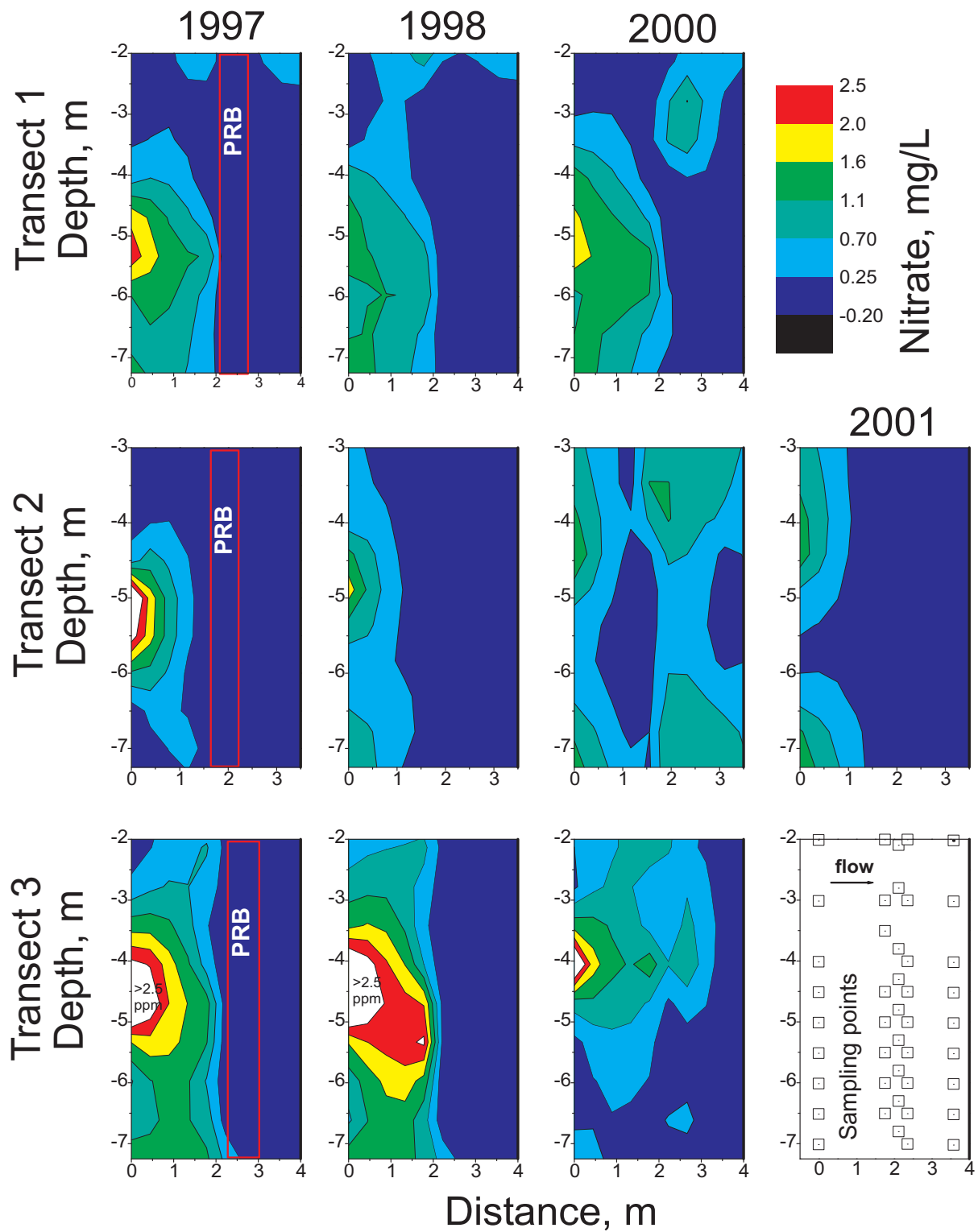


Figure 3.17 Cross-sectional profiles showing nitrate concentrations (mg/L) in transects 1, 2, and 3, Elizabeth City PRB.

Table 3.5. Changes in Concentration of Anions in Ground Water at Transect 2 (Elizabeth City) as a Function of Time and Depth

Depth, m	Average values from 1997 to 2001			Values from 2001		
	ML21 Upgradient chloride, mg/L	ML25 Downgradient	% Change	ML21 Upgradient	ML25 Downgradient	% Change
4	66.3	19.5	70.6	79.7	13.9	82.6
5	53.5	39.5	26.2	22.5	25.7	-14.2
6	17.1	39.2	-129.2	13.8	38.7	-180.4
7	21.4	38.3	-78.9	27.1	40.5	-49.4
	sulfate, mg/L					
4	47.9	7.4	84.6	79.7	10.1	87.3
5	47.8	0.32	99.3	32.2	<0.1	>99.7
6	27.4	0.48	97.8	27.9	<0.1	>99.6
7	16.2	0.48	97.0	23.4	<0.1	>99.6
	alkalinity, mg/L					
4	85	56	34.1	65	79	-21.5
5	54	64	-18.5	57	72	-26.3
6	50	58	-16.0	54	56	-3.7
7	55	33	40.0	54	28	48.1
	nitrate, mg/L					
4	4.7	0.08	98.3	1.4	<0.1	>92.9
5	1.4	0.08	94.3	0.3	<0.1	>66.7
6	0.5	0.5	0	0.4	<0.1	>75.0
7	1.2	0.4	36.1	1.6	<0.1	>93.8

% change calculated using:

$$\frac{(\text{upgradient concentration} - \text{downgradient concentration})}{(\text{upgradient concentration})} \times 100$$

A cross-sectional profile showing the concentration distribution of inorganic carbon in the solid-phase is shown in Figure 3.20. The concentration profile was constructed based upon three angle cores collected in May 2001 that intercepted the upgradient edge of the PRB at depths from about 4.8 to 6.2 m below ground surface. The sampling transect was located approximately 3 m west of multilevel well transect 1 (see Figure 3.19). At the time of sampling, the highest concentrations of inorganic carbon were found at a depth of about 5 m below ground surface and 5-10 cm inside of the reactive media/aquifer interface. The greatest amount of carbon accumulation is localized in a rather narrow depth interval that corresponds to the depth where a maximum in total dissolved solids and bicarbonate enters the reactive media (compare Figure 3.20 with Figures 3.9 and 3.16). Not surprisingly, “hotspots” of mineral precipitation within the reactive media are tied to areas where influent ground water is enriched in dissolved solutes.

The time-dependent accumulation of mineral precipitates is difficult to evaluate, in part, because the core sampling location, relative to ground-water solute inputs, is obviously important in governing accumulation rates. Unless core sampling is carried out at the exact same location through time, it may be difficult to evaluate time-resolved data sets. Figure 3.21 shows inorganic carbon concentrations in angle cores collected in 1997, 1998, 1999, 2000, and 2001. Each of these cores was collected from the same general vicinity so that the trends observed are considered to be comparable. Shown in Figure 3.21 is an overall regular increase in inorganic carbon concentrations with time. The trends clearly indicate that a front of precipitation is progressively passing through the reactive media with time. This observation is critically important because it suggests that complete, rapid pore-infilling does not occur in the region immediately adjacent to the upgradient aquifer/iron interface. Rather, mineral precipitation occurs in a larger volume of the reactive media than is present immediately adjacent to the upgradient interface.

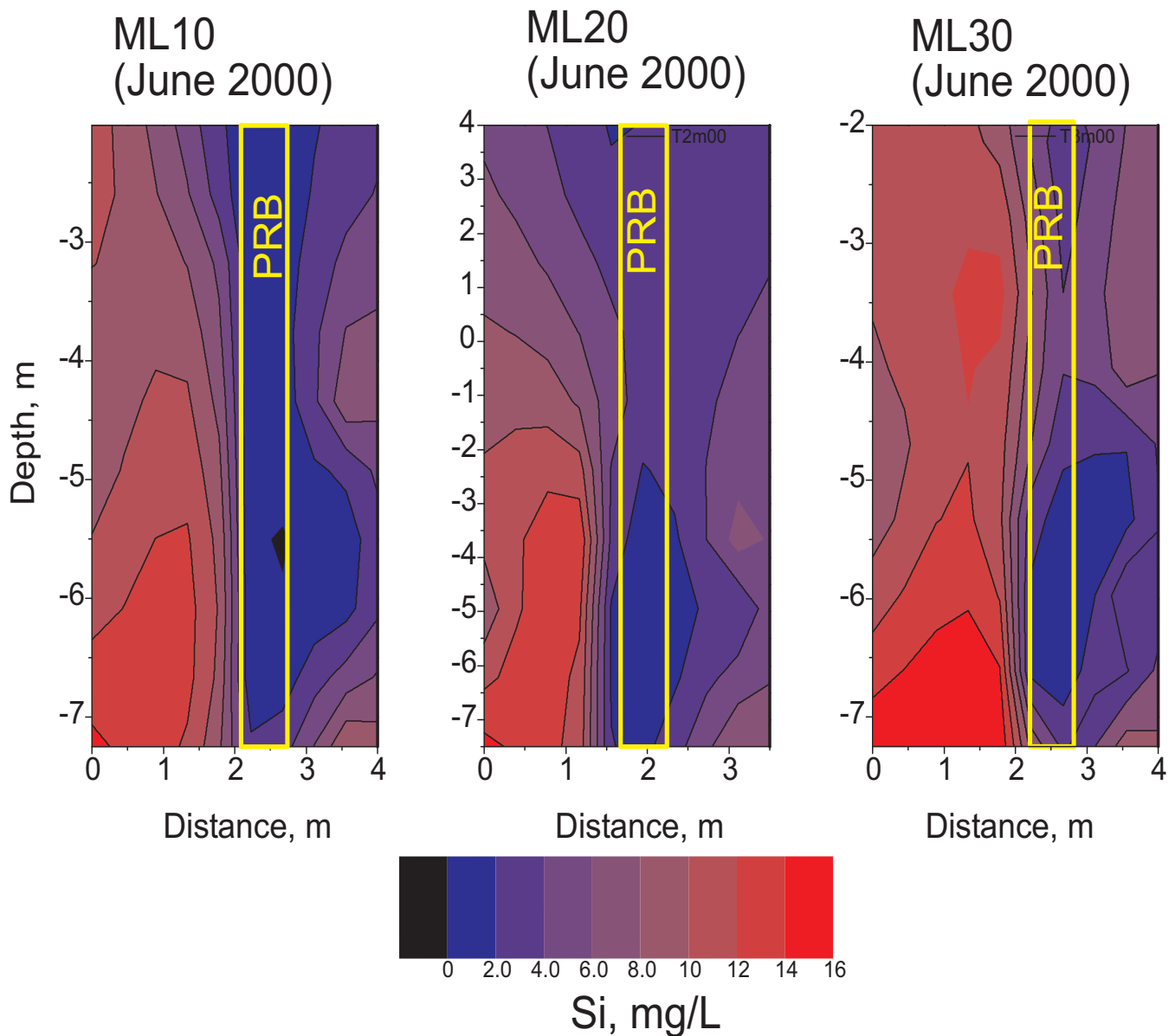


Figure 3.18 Cross-sectional profiles showing silica concentrations (mg/L) in transect 2, Elizabeth City PRB.

3.2.2 Sulfur Analysis

Total sulfur measurements were made with a UIC sulfur coulometer system. Iron samples were covered with V_2O_5 and combusted in the presence of oxygen at 1050 °C. Evolved gases are passed through a column of reduced Cu to quantitatively convert all sulfur to SO_2 , which is then carried to the coulometer cell where it is absorbed and coulometrically titrated. Results of total sulfur analyses on Elizabeth City cores are listed in Table A1. Un-reacted Peerless iron contains about 5 $\mu\text{g/g}$ of sulfur using this combustion method. In addition to total sulfur measurements, the concentrations of acid-volatile sulfide (AVS) and chromium-reducible sulfur (CRS) were determined by chemical extraction with hot, 6 M HCl and 1 M CrCl_2 in 0.5 M HCl, respectively (Zhabina and Volkov, 1978). These acid extraction methods determine the quantities of metal monosulfide precipitates (AVS) and iron disulfide precipitates (i.e., pyrite; CRS). Metal monosulfide precipitates, such as disordered mackinawite (Fe_{1+x}S) and mackinawite (Fe_{1+x}S), dissolve in dilute hydrochloric acid and subsequently release hydrogen sulfide gas which can be measured. Iron disulfide minerals, pyrite (cubic FeS_2) and marcasite (orthorhombic FeS_2), and elemental sulfur are not dissolved in dilute hydrochloric acid but are solubilized by using the more aggressive CrCl_2 -HCl solution. The hydrogen sulfide gas released in this extraction step (CRS) can again be quantified and related back to the concentration of disulfide-sulfur present in the core materials.

Groundwater flow

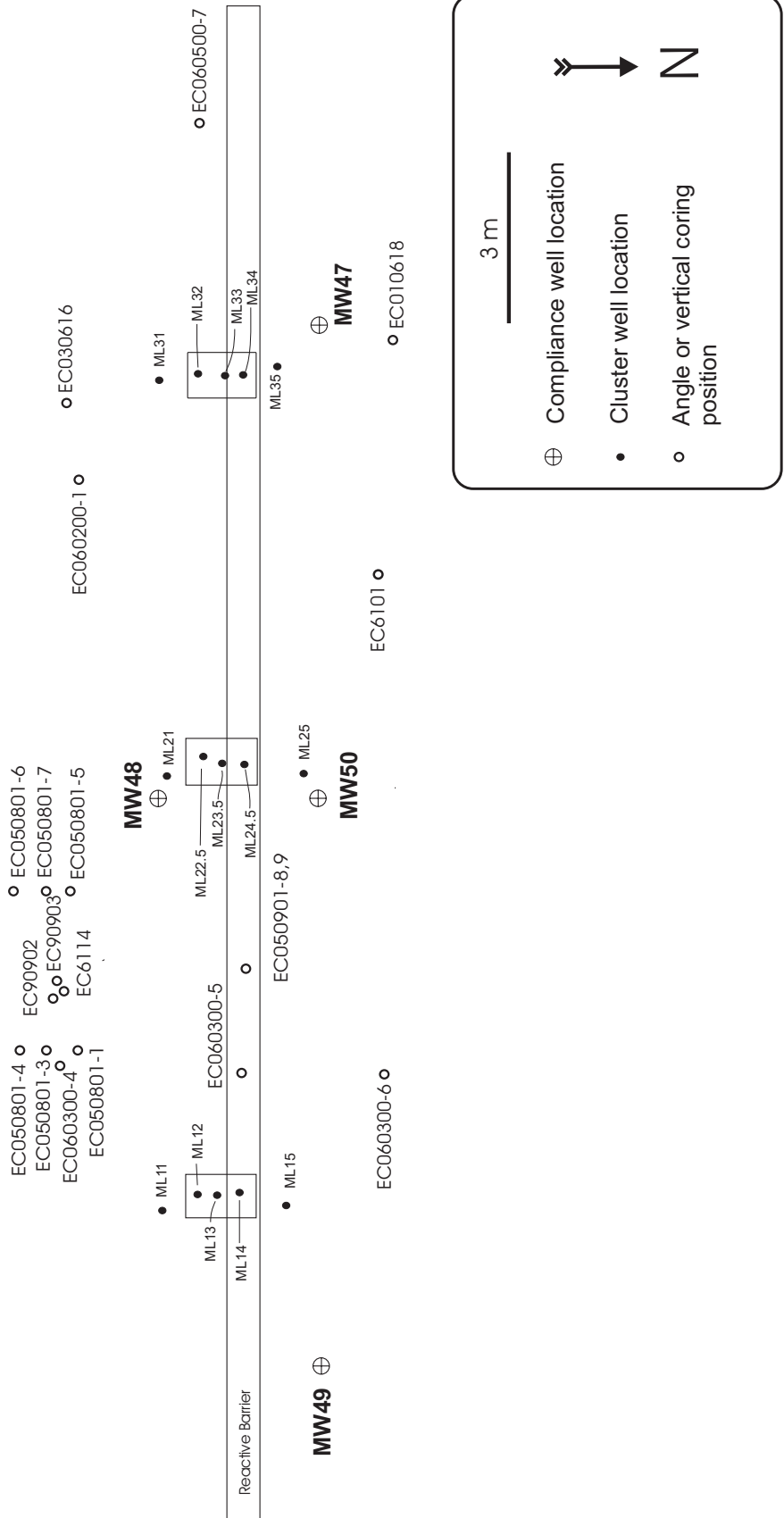


Figure 3.19. Coring locations and monitoring well locations at the Elizabeth City Permeable Reactive Barrier site (plan view).

Table 3.6 Cores Collected for Analysis at the Elizabeth City PRB

Sample ID	Location	Date	Angle	Core length	Recovery	Depth to Fe
EC050801-1	Upgradient	May-01	30	107	88	4.4
EC050801-3	Upgradient	May-01	30	99	81	5.3
EC050801-4	Upgradient	May-01	30	109	90	5.8
EC050801-5	Upgradient	May-01	30	94	77	4.9
EC050801-6	Upgradient	May-01	30	102	83	6.3
EC050801-7	Upgradient	May-01	30	109	90	5.6
EC050901-8	Vertical	May-01	90	102	83	2.2
EC050901-9	Vertical	May-01	90	112	92	2.2
EC060200-1	Upgradient	June-00	30	61	50	4.8
EC060300-4	Upgradient	June-00	30	76	63	4.8
EC060300-5	Vertical	June-00	90	84	69	2.2
EC060300-6	Downgradient	June-00	30	94	77	4.0
EC060500-7	Vertical	June-00	90	69	56	2.3
EC010618	Downgradient	June-99	30	61	50	5.2
EC030616	Upgradient	June-99	30	61	50	5.5
EC90902	Upgradient	September-98	30	61	50	4.8
EC90903	Upgradient	September-98	30	61	50	5.0
EC6101	Upgradient	June-98	30	69	56	4.8
EC6114	Upgradient	June-98	30	66	54	5.0

Notes: * Core EC6101 captures the upgradient iron/aquifer interface but was collected by pushing the core barrel from the downgradient side of the reactive barrier. Depth to iron is the depth below ground surface in meters where zero-valent iron was intercepted.

Inorganic Carbon

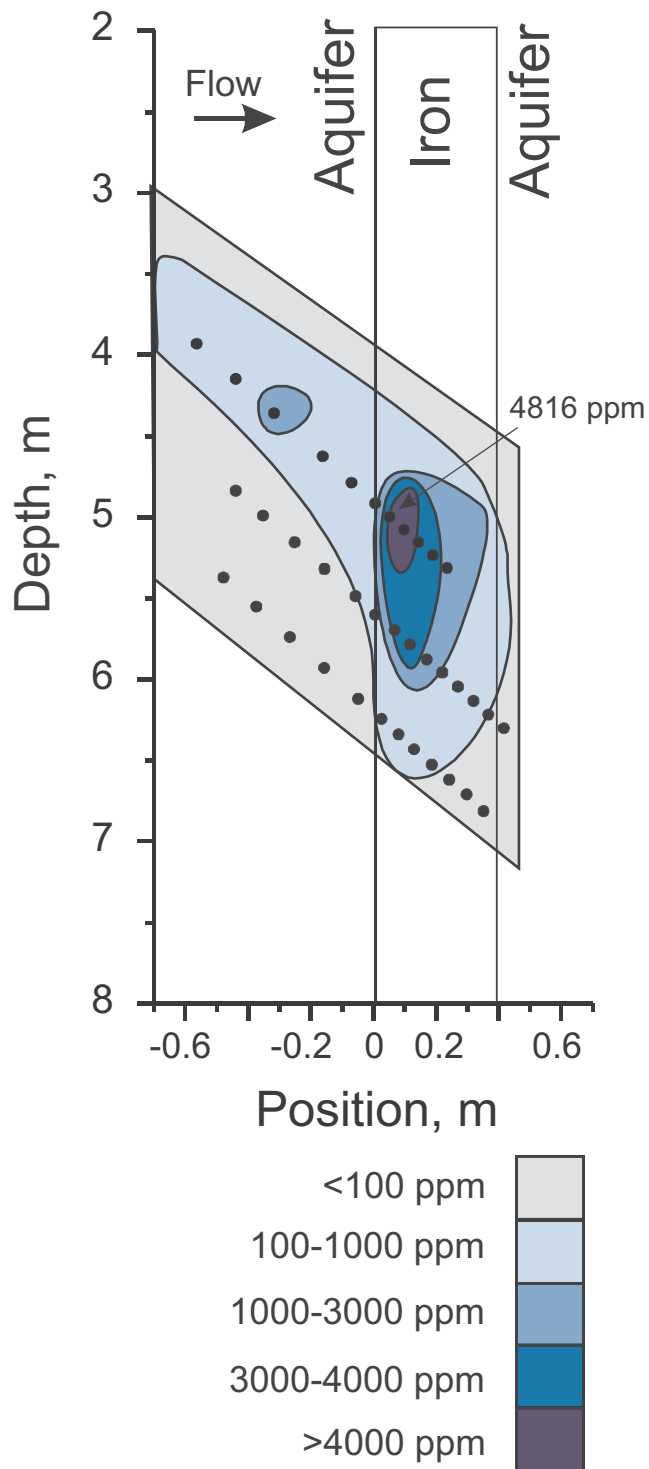


Figure 3.20 Cross-sectional profile showing concentration distribution of inorganic carbon in the solid phase ($\mu\text{g/g}=\text{ppm}$), Elizabeth City PRB (June 2002).

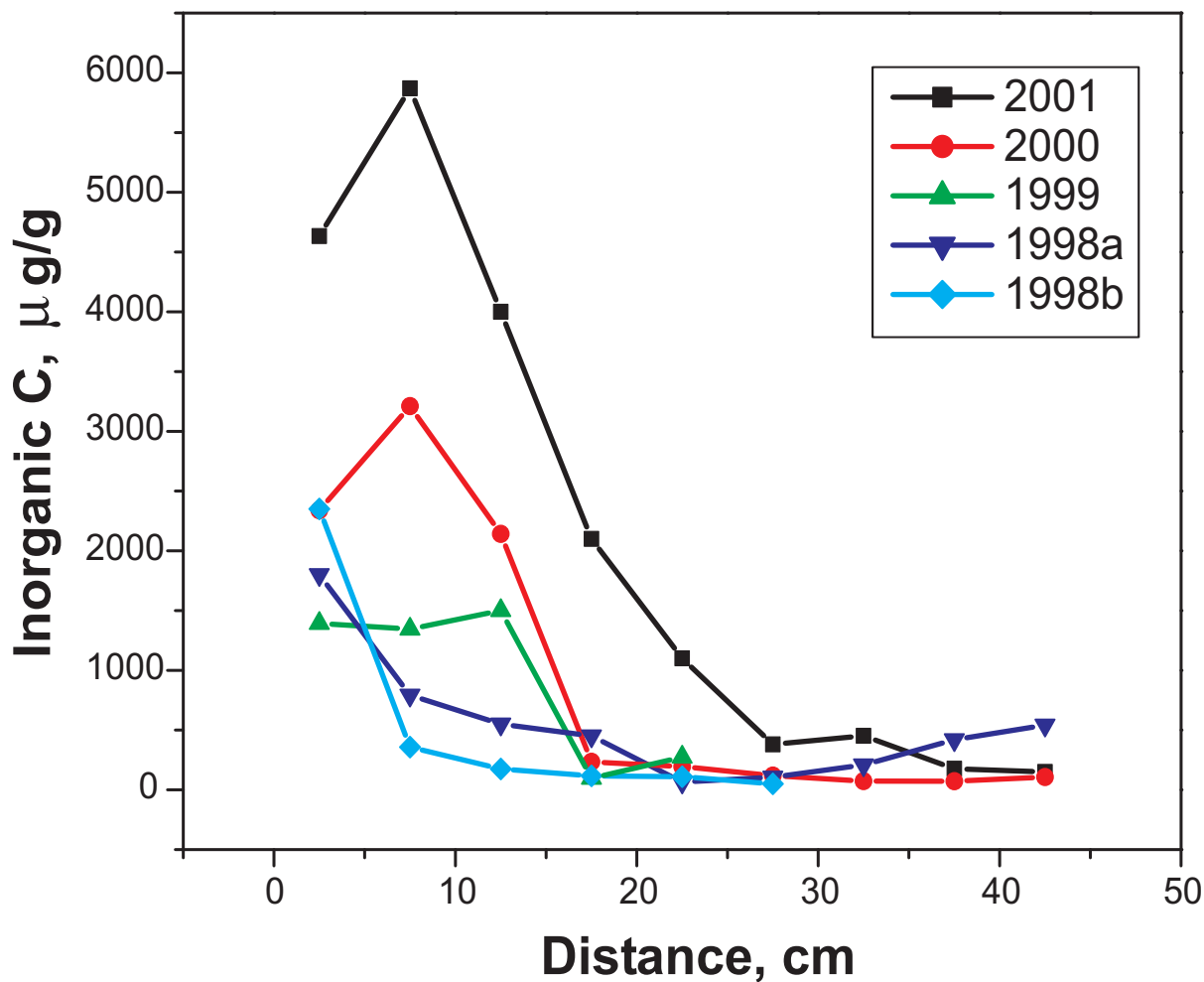


Figure 3.21 Concentrations of inorganic carbon ($\mu\text{g/g}$) in core materials through time (Elizabeth City PRB).

Concentrations of total sulfur in the iron media range from about 1 to 3880 $\mu\text{g/g}$. The concentration distribution of sulfur broadly compares with that of inorganic carbon (Figure 3.22). The highest sulfur concentrations are found near the upgradient interface in regions proximal to where maximum ground-water concentrations of sulfate enter the reactive zone (see Figure 3.15). The lowest concentrations of sulfur in the solid-phase are found near the downgradient edge of the PRB.

Sulfur may be present in the core materials as sulfide (disordered mackinawite, mackinawite, greigite), disulfide (pyrite or marcasite), elemental sulfur, or as sulfate (e.g., sulfate green rust). Total sulfur concentrations will reflect the sum of all of these sulfur forms. In order to more accurately determine sulfur partitioning and mineralogy, sequential extraction procedures were carried out (Wilkin et al., 2003). Results presented in Table A2 indicate that over 90% of the total sulfur is present as sulfide. The remaining sulfur would appear to be made up of iron disulfides (pyrite) and perhaps more acid-resistant forms of iron monosulfide such as greigite (Fe_3S_4). Both of these phases have been detected in minute quantities using high-resolution transmission electron microscopy (Furukawa et al., 2002). Sulfate green rust does not appear to be an important mineral form in the reactive media at Elizabeth City, which is consistent with geochemical modeling results. Based on the $\text{HCO}_3^-/\text{SO}_4^{2-}$ ratios of ground water at Elizabeth City the carbonate form of green rust is expected to dominate over the sulfate form (Wilkin et al., 2002). The solid-phase dominance of sulfide over sulfate in the reactive media and the complete loss of dissolved sulfate demonstrate that reduction of sulfate to sulfide has gone essentially to completion.

The masses of IC and S deposited within the iron barriers determined from solid-phase characterization agree reasonably well with estimated masses based on changes in concentrations of dissolved solutes and flow rates. Mass balance estimates are presented and discussed in Wilkin et al. (2002). Inorganic carbon mass balance agrees to within

Sulfur

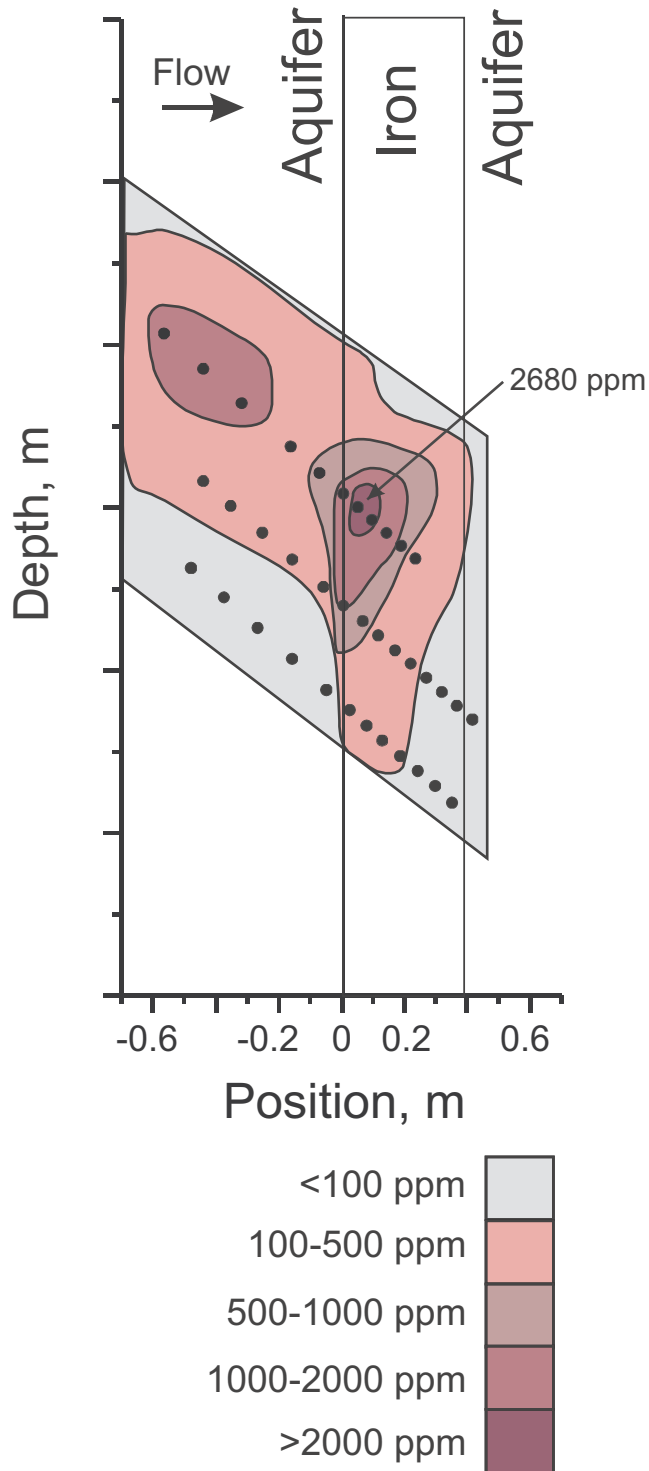


Figure 3.22 Cross-sectional profile showing concentration distribution of sulfur in the solid phase ($\mu\text{g/g}=\text{ppm}$), Elizabeth City PRB (June 2002).

a factor of 1.5x for the Elizabeth City PRB. More sulfur accumulation, however, would be expected in the Elizabeth City PRB, based on changes in sulfate concentrations than has been observed on the core materials. Several factors lead to uncertainty in mass balance calculations for PRBs. Estimates of mineral accumulation based on changes in ground-water chemistry critically depend on chemical and especially hydrogeologic measurements. Determination of dissolved constituents may be analyzed at a high level of accuracy and precision, <5%. Similarly, estimates of mass accumulation based on characterization of core materials depend on the accuracy of analytical measurements, in addition to estimates of emplaced iron density. However, estimates of ground water flow volumes moving through PRBs are prone to large uncertainties, and these dominate the total error of mass balance calculations (20-50%). Spatial variability in ground water flow velocity, concentration of solutes, concentration of solid phase products, and emplaced iron density all factor into the uncertainty analysis of mass balance calculations.

3.2.3 Cr Extractions

To understand the distribution of solid-phase chromium, dilute hydrochloric acid (1 M) leaches were performed on upgradient aquifer and reactive iron material. Analysis of un-reacted Peerless iron indicated acid-extractible chromium concentrations of about 8.8 µg/g. Concentrations of acid-extractible chromium as high as 72 µg/g were measured in the reacted iron media after five years of exposure. Chromium is enriched in the solid-phase in subsurface regions near the upgradient iron/aquifer interface.

3.2.4 X-ray Diffraction Analysis

Powder X-ray diffraction scans for core samples collected in 2000 and 2001 are shown in Figure 3.23. Materials for analysis were prepared by sonicating iron core samples in acetone for 10 minutes, followed by filtration of the released particulates through 47 mm diameter, 0.2-micron filter paper (polycarbonate). The separated particles were mounted on a zero-background quartz plate and scanned with Cu K α radiation from 3° to 80° 2-theta using a Rigaku Miniflex Diffractometer. Diffraction analysis is used to determine the bulk mineralogical composition of the materials removed from the reactive media. The results can be used to qualitatively evaluate the abundance of various mineral phases; no attempts were made to obtain quantitative results, in part, because of uncertainties regarding the separation efficiency of mineral precipitates during the sonication step.

A summary of the XRD results is reported in Table 3.7. Magnetite (Fe₃O₄) was observed in every iron core sample. Quartz (SiO₂) was sometimes detected, particularly in samples proximal to the edges of the reactive media. Aquifer grains had either been transported into the reactive media at some point during or after construction of the PRB, or the core sampling may have resulted in some limited mixing of aquifer material with the reactive iron zone. Aragonite (CaCO₃) and calcite (CaCO₃) were detected as minor components in some of the iron core samples. In addition to magnetite, other iron minerals detected were green rust (GR1) and iron carbonate hydroxide. Neither siderite (FeCO₃) nor iron sulfides were detected by X-ray diffraction in any of the samples analyzed. However, using micro-analytical methods, Furukawa et al. (2002) detected quantities of mackinawite, greigite, and pyrite in sample EC060200-1-3, as well as ferrihydrite (Fe(OH)₃) and lepidocrocite (FeOOH). Bulk X-ray analysis apparently captures the dominant mineral phases present, but the technique was not sufficiently sensitive to identify the full range of materials that form in PRBs, particularly those phases that have a poor degree of crystallinity. The principal authigenic phases present in the Elizabeth City reactive media are iron carbonate hydroxide, mackinawite, and magnetite; minor mineral products are aragonite, calcite, lepidocrocite, and green rust (GR1).

Iron carbonate hydroxide was identified and described by Erdös and Altorfer (1976) as an iron corrosion product formed in carbonate solutions. The stoichiometry of the material is reported to be Fe₂(OH)₂CO₃ (powder diffraction file PDF 33-0650). The material is related to siderite, FeCO₃, and the carbonate form of green rust, Fe₆(OH)₁₂CO₃·x H₂O. Like siderite, iron is present only in the ferrous state in iron carbonate hydroxide, whereas in green rust, iron is present in both the ferrous and ferric states (McGill et al., 1976). Iron hydroxide carbonate may be a precursor to carbonate green rust and magnetite, these phases forming by partial oxidation. Iron carbonate hydroxide was also found to be a major corrosion product at the Denver Federal Center (see Section 4.2.3) and was detected at the Moffett Field PRB (Gavaskar et al., 2002) and the Oak Ridge Y-12 site (Liang et al., 2003).

Mixed valence iron minerals include magnetite and carbonate green-rust compounds. Green-rust compounds are iron corrosion products that are expected to form under more reducing conditions than do ferric oxyhydroxides. Green rust precipitation is favored under moderately alkaline conditions, and transformation of these compounds to magnetite is expected based upon experimental evidence and thermodynamic calculations (e.g., Bonin et al., 2000). Green-rusts are highly susceptible to oxidation in the presence of dissolved oxygen or air. Green rust structural units consist of alternating positively charged tri-octahedral metal hydroxide sheets and negatively charged interlayers of anions (Taylor, 1973). Two types of GR are distinguishable based upon X-ray analyses: GR1 in which the distance between hydroxide sheets is between about 0.75 and 0.80 nm (e.g., GRCO₃²⁻) and GR2 in which the distance between sheets is about 1.1 nm (e.g., GRSO₄²⁻). X-ray diffraction results are consistent with the presence of GR1 in core materials from Elizabeth City.

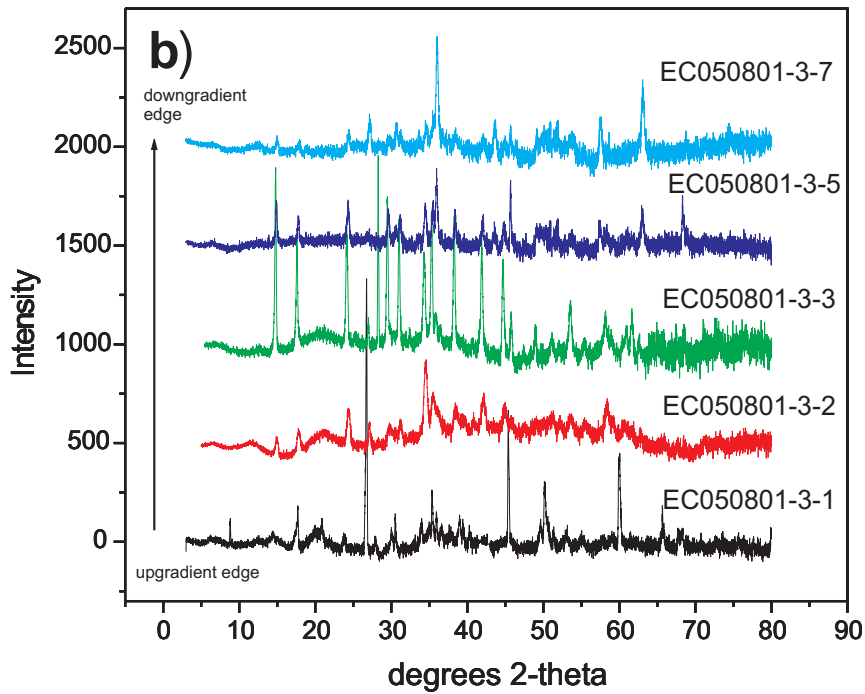
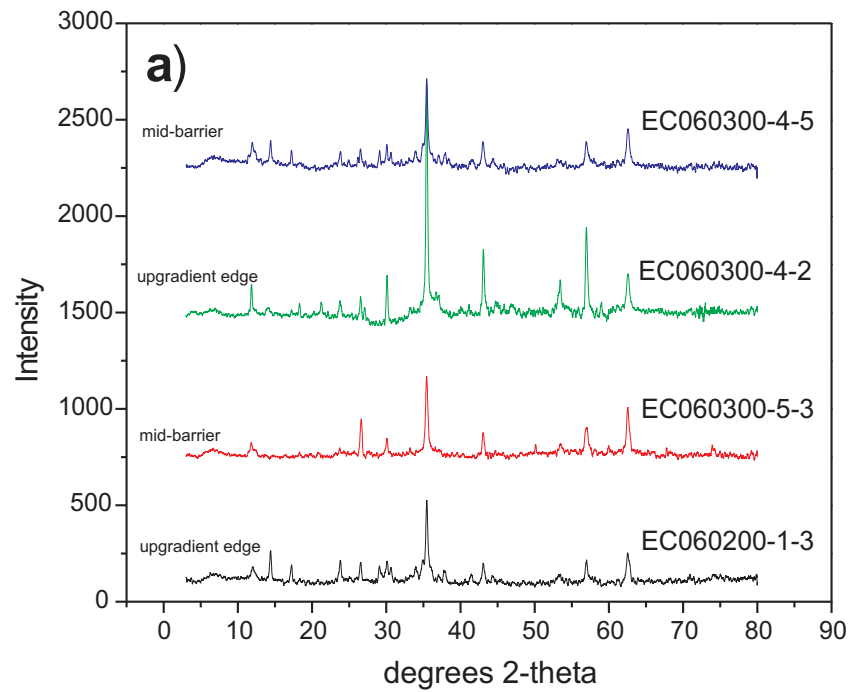


Figure 3.23 Powder X-ray diffraction data from fine-grained materials removed via sonication from cores collected at the Elizabeth City PRB: a) core EC060300-4; b) core EC050801-3.

Table 3.7. Results of Powder X-ray Diffraction Analysis of Core Materials from the Elizabeth City PRB

Sample	Major Component	Minor Component	Trace Component
EC060200-1-3	Magnetite, Iron carbonate hydroxide	Quartz, Calcite	
EC060300-5-3	Magnetite, Iron carbonate hydroxide	Quartz, Calcite	
EC060300-4-2	Magnetite, Iron carbonate hydroxide	Quartz, Aragonite, Calcite	Lepidocrocite, Mackinawite
EC060300-4-5	Magnetite, Iron carbonate hydroxide	Quartz, Calcite	
EC050801-3-1	Magnetite, Iron carbonate hydroxide	Quartz, Aragonite, Calcite, Green rust 1	
EC050801-3-2	Magnetite, Iron carbonate hydroxide	Quartz, Calcite	
EC050801-3-3	Magnetite, Iron carbonate hydroxide	Calcite	
EC050801-3-7	Magnetite, Iron carbonate hydroxide	Calcite	
EC050801-3-7	Magnetite, Iron carbonate hydroxide	Quartz, Calcite	Carbon

3.2.5 Scanning Electron Microscopy

Scanning electron microscopy (SEM) was used to evaluate the morphology and spatial relationships among mineral precipitates on the surfaces of zero-valent iron particles. In addition, energy dispersive X-ray spectroscopy (EDX) was conducted to determine on a semi-quantitative basis the composition of surface precipitates. Samples for SEM and EDX analysis were stored in an anaerobic glove box and then embedded in an epoxy resin. The sample mounts (1" diameter round mounts) were ground and polished using diamond abrasives and coated with a thin layer of carbon prior to being placed within the SEM sample chamber.

SEM photomicrographs are presented in Figure 3.24a-c for three samples from core EC060300-4 from the Elizabeth City site collected in June 2000. These three samples were retrieved from near the upgradient aquifer/iron interface region (EC060300-4-1, horizontal penetration ~ 2 cm; EC060300-4-3, horizontal penetration ~8 cm), and the downgradient edge of the reactive iron media (EC060300-4-7, horizontal penetration ~40 cm). The micrographs in Figure 3.24 are representative of particles contained in each of the samples and capture a range of magnifications from about 50x to 5000x.

Sample EC060300-4-1 was collected from a region near the upgradient interface and shows a fairly consistent accumulation of mineral precipitates on the surfaces of iron particles (Figure 3.24a). In this sample, the thickness of surface coatings on iron grains ranges from about 20 µm to 100 µm. This surface precipitate buildup occurred over the first four years of operation of the PRB. An average linear rate of precipitate accumulation of about 5 to 25 µm per year is indicated. The SEM images exhibit two types of precipitate morphology: platy/acicular aggregates and poorly crystalline clusters (Furukawa et al., 2002). Individual particles in the platy aggregates are on the order of 10 µm in length. Platy or acicular textures are oftentimes the result of rapid precipitation from highly oversaturated solutions.

a)

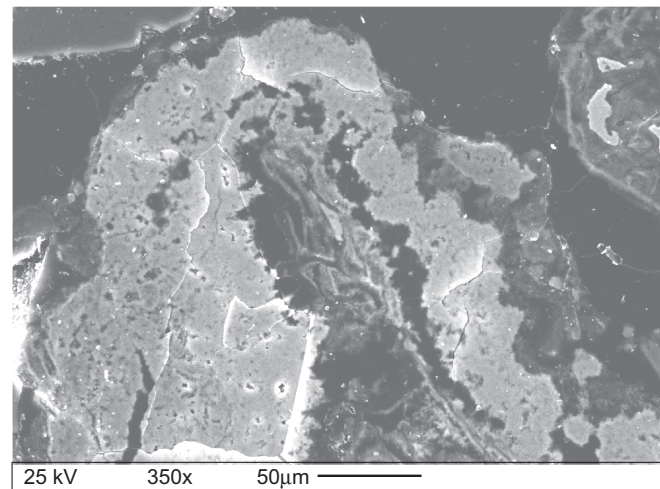
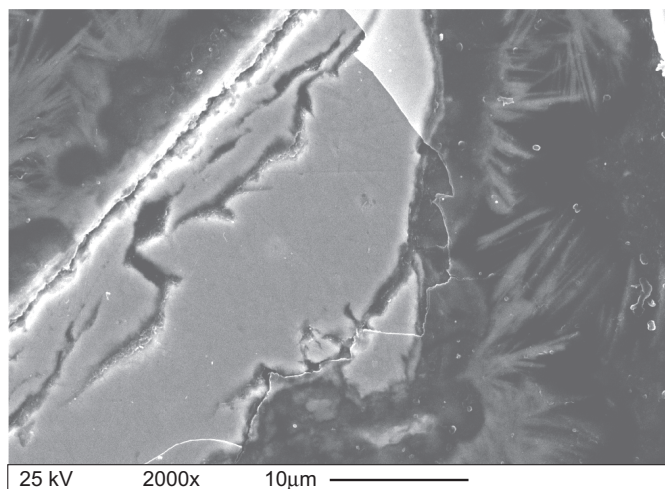
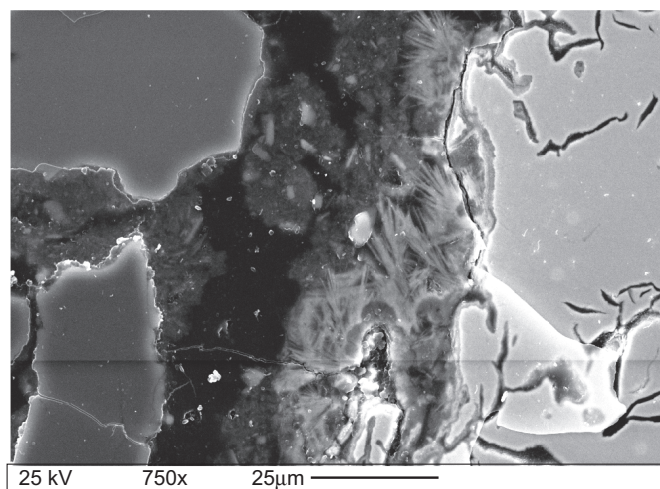
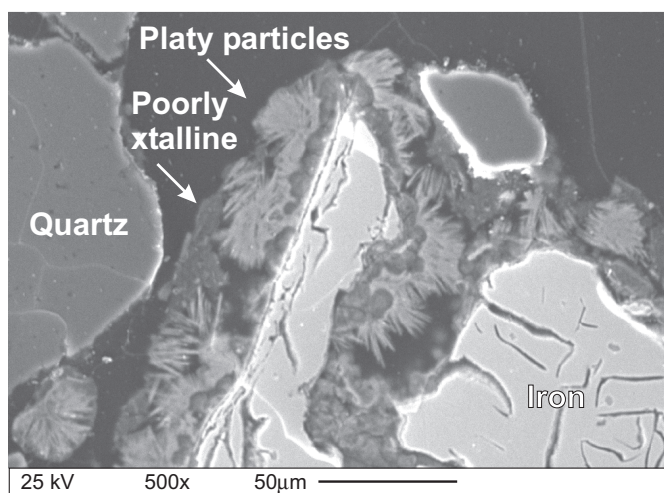
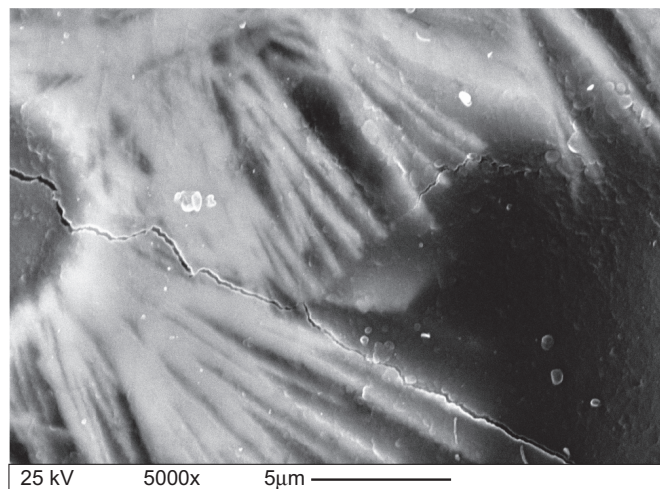
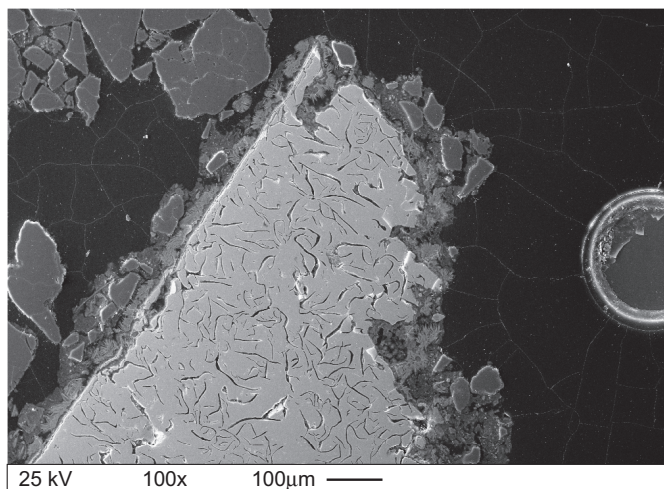


Figure 3.24 (continued) Scanning electron micrographs of samples from the Elizabeth City PRB: a) sample EC060300-4-1 located near the upgradient iron/aquifer interface; b) sample EC060300-4-3 located in the midbarrier; and, c) EC060300-4-7 located near the downgradient iron/aquifer interface.

b)

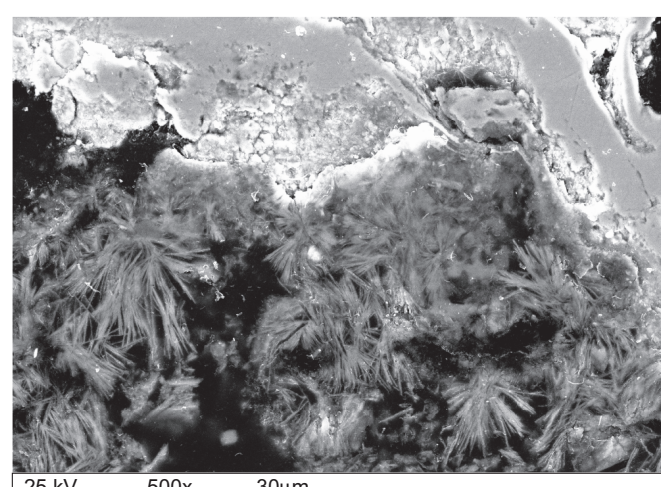
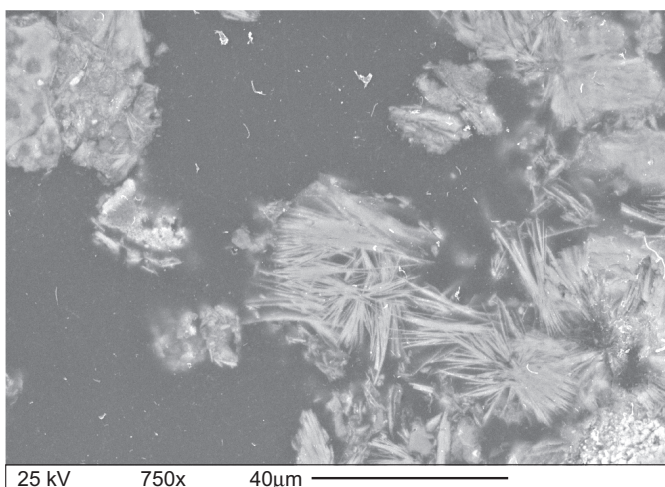
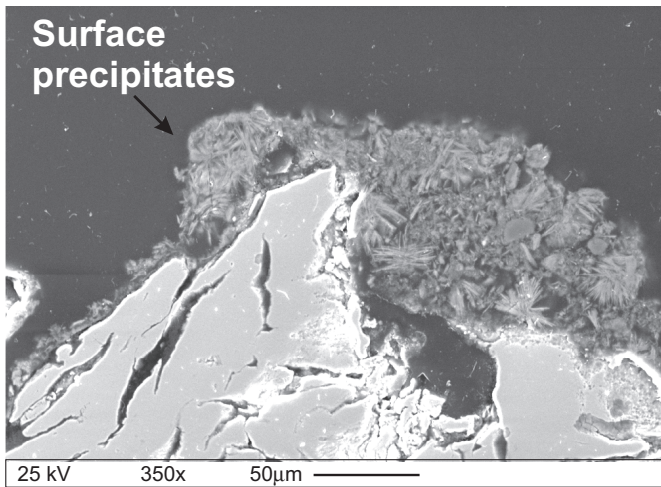
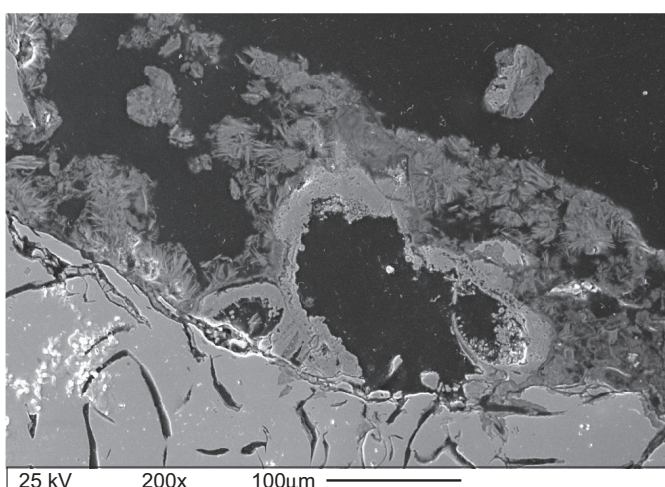
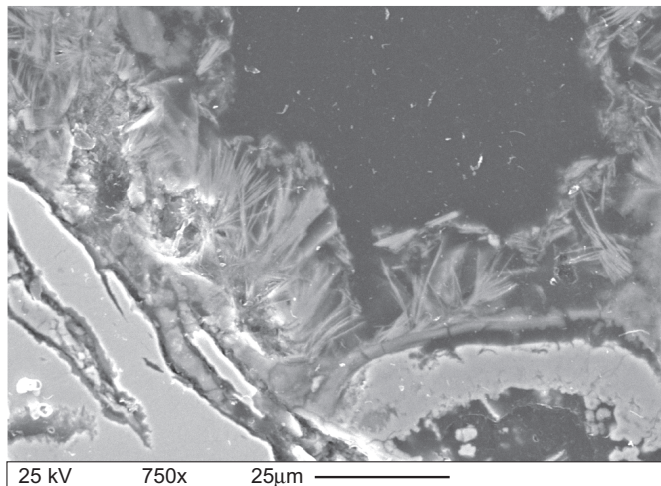
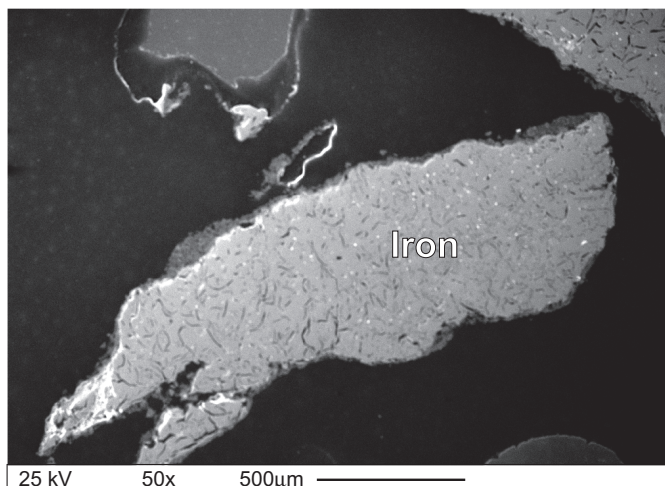


Figure 3.24 (continued) Scanning electron micrographs of samples from the Elizabeth City PRB: a) sample EC060300-4-1 located near the upgradient iron/aquifer interface; b) sample EC060300-4-3 located in the midbarrier; and, c) EC060300-4-7 located near the downgradient iron/aquifer interface.

c)

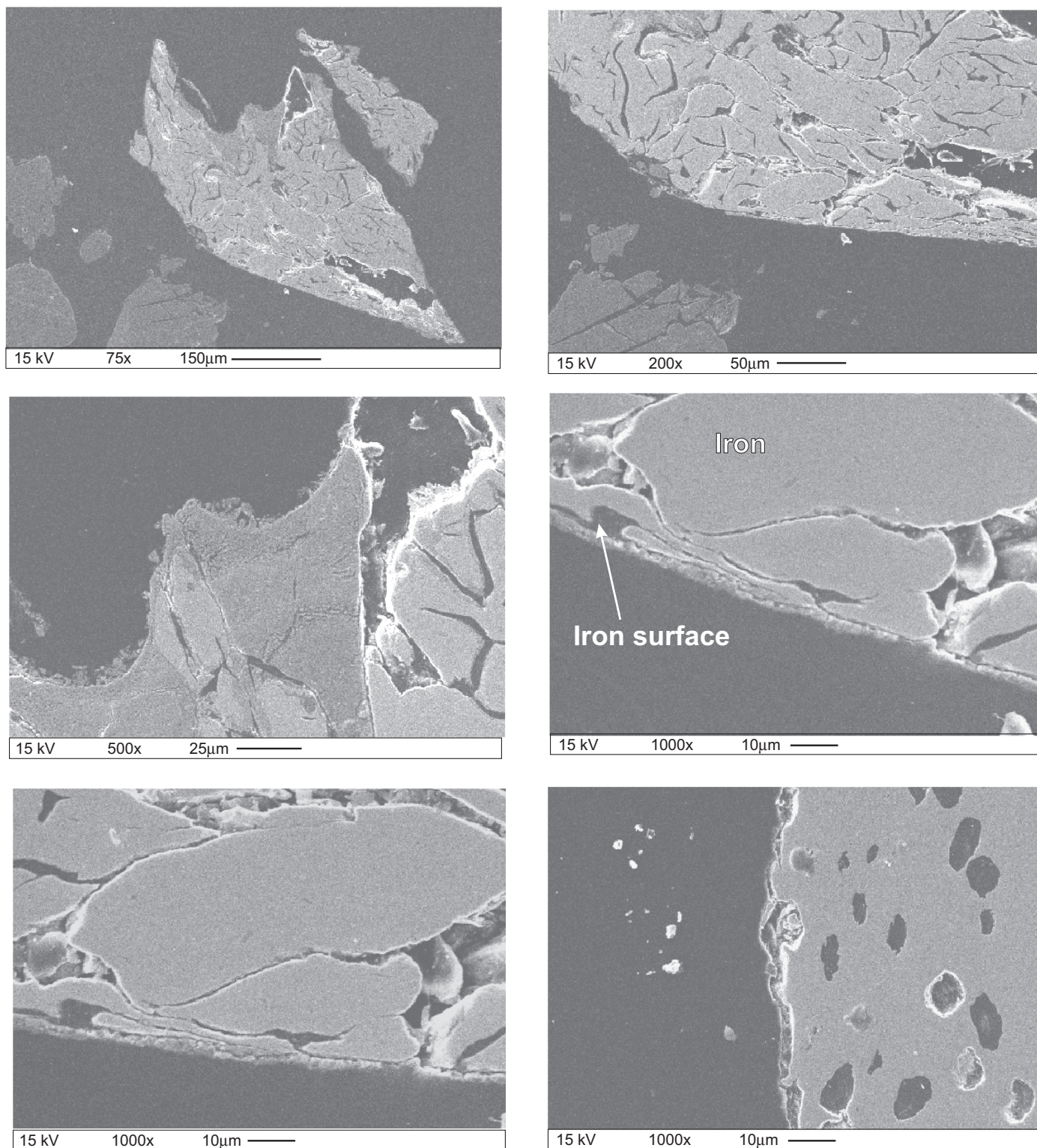


Figure 3.24 (continued) Scanning electron micrographs of samples from the Elizabeth City PRB: a) sample EC060300-4-1 located near the upgradient iron/aquifer interface; b) sample EC060300-4-3 located in the midbarrier; and, c) EC060300-4-7 located near the downgradient iron/aquifer interface.

Such conditions might be expected in the region where ground water passes from the aquifer into the reactive zone, i.e., where steep geochemical gradients are present (for example in pH and Eh). These observed morphologies are consistent with previous studies (e.g., Roh et al., 2000; Phillips et al., 2000). These previous studies found that acicular/platy aggregates in zero-valent iron PRBs were largely composed of green rust minerals, goethite, lepidocrocite, and calcium carbonates. The poorly crystalline clusters more typically were composed of mackinawite and poorly crystallized iron oxyhydroxides (Phillips et al., 2000). Poorly crystalline clusters are typically found immediately on the zero-valent iron surfaces, with the elongated particles apparently growing on the clusters. In other cases, however, the poorly crystalline clusters are found together with the elongated particles and not directly associated with the iron surfaces.

Sample EC060300-4-3 was collected near upgradient aquifer/PRB region but at a penetration depth further into the PRB compared to sample EC060300-4-1. Sample EC060300-4-3 shows the same particle morphologies as were noted in sample EC060300-4-1. However, the regularity of surface precipitates is less pronounced and the thickness of the surface precipitate layer is thinner, ranging from 0 to about 50 μm . In this sample, an average linear rate of precipitate accumulation of about 0 to 13 μm per year is indicated (Figure 3.24b). In sample EC060300-4-7, collected near the downgradient aquifer/iron interface, the surface precipitate thickness is very thin if present at all (Figure 3.24c). In most cases a 1- to 4- μm layer was observed on the iron grains in this sample collected near the downgradient edge of the reactive media. This observation suggests that after four years of ground-water exposure, iron particles free from precipitate coverage are still present at the Elizabeth City site. The PRB should still remain reactive, which is consistent with the previously described trends in geochemical parameters and contaminant concentrations.

Energy dispersive analyses of iron grains from the Elizabeth City PRB indicate the presence of iron (~97 wt%), silicon (~2.5%), and occasionally Mn (<0.7 wt%) and Cr (<0.6 wt%). Peerless iron is also known to contain concentrations of carbon and other trace elements, including S, P, Ni, V, Mo, Ti, and Cu. Because the samples were coated with carbon, this element could not be semi-quantitatively determined; other trace elements are present at concentrations below the operational detection limit of the EDX method. Oxygen was not detected on freshly polished surfaces of zero-valent iron. However, the coatings of surface precipitates are enriched in oxygen and comparatively depleted in iron relative to the composition of fresh zero-valent iron (Figure 3.25). Typically the most oxygen-enriched regions are those farthest away from the zero-valent iron surface. Particles with a platy morphology were found to contain iron (68.9 ± 8.2 wt%, $n=25$), oxygen (28.3 ± 7.5 wt%, $n=25$), silicon (2.4 ± 4.2 wt%, $n=25$), sulfur (0.2 ± 0.6 wt%, $n=25$), and manganese (0.5 ± 0.5 wt%, $n=25$) (Figure 3.26). Chromium was never detected in spot analyses of the platy particles, and calcium was detected in only 6 of 25 analyses, always at levels below 1 wt%. The poorly crystalline clusters are similar to the platy particles with respect to iron concentrations (64.5 ± 8.0 wt%, $n=30$) and are broadly comparable in terms of the element distributions of Si, S, Mn, and Ca. Chromium was detected in 10 of 30 of the spot analyses of the poorly crystalline clusters in concentrations up to about 2 wt%.

Chromium was detected by EDX spot or small area analysis in 72 separate measurements. Concentrations of chromium ranged from 0.1 wt% to 1.8 wt%. The micro-scale measurements are much greater than bulk-scale Cr concentrations determined by acid leaching large (~1–5 gm) quantities of material. Pearson correlation coefficients presented in Table 3.8 indicate significant correlation of chromium abundance with S and Mn. The high degree of correlation with Mn suggests that Cr uptake is in some way tied to Mn behavior; either they are present together in some discrete phase or as a co-precipitate. This observation is somewhat surprising as most laboratory studies have concluded that Cr is removed from solution through the formation of a solid solution or by adsorption of Cr(III) onto iron oxyhydroxide surfaces (Powell et al., 1995; Blowes et al., 1997; Pratt et al., 1997).

XPS scans show that iron particle surfaces from Elizabeth City contain C, O, Fe, Si, S, Mg, Ca, Mn, and N. The XPS data indicate a surface layer dominated by iron oxyhydroxides, an intermediate layer of iron oxide, and finally, zero-valent iron at the greatest sputtering depths. Surface carbon is present predominately as carbonate with some detected hydrocarbon (binding energy 284.6 eV). The oxidation state of sulfur is predominantly present as sulfide (-2) but with minor amounts of sulfate (+6). Surface enrichment in the elements Ca, Mg, S, and Si are consistent with observed decreases in ground-water concentrations of these elements. Chromium was sometimes detected by XPS in iron samples from Elizabeth City.

3.2.6 Microbial Characterization

From 1999 to 2001, 117 samples were collected from the Elizabeth City site for phospholipid fatty acid (PLFA) extract characterization. Samples were collected from regions within the reactive iron media and from adjacent regions of the upgradient and downgradient aquifer. Samples for PLFA analysis were frozen immediately after collection from the subsurface and shipped frozen to Microbial Insights (Rockford, Tennessee). The complete PLFA data set from the Elizabeth City site is shown in Table B1 (Appendix B) and summarized in Table 3.9.

Biomass contents spanned several orders of magnitude from <1 to 2614 picomoles per gram (dry weight basis), or from about 2.5×10^3 to 5.23×10^7 cells per gram of dry material. The biomass is dominated by Prokaryote PLFA. The highest biomass concentrations were found near the upgradient aquifer/iron interface region, in the same region of the reactive

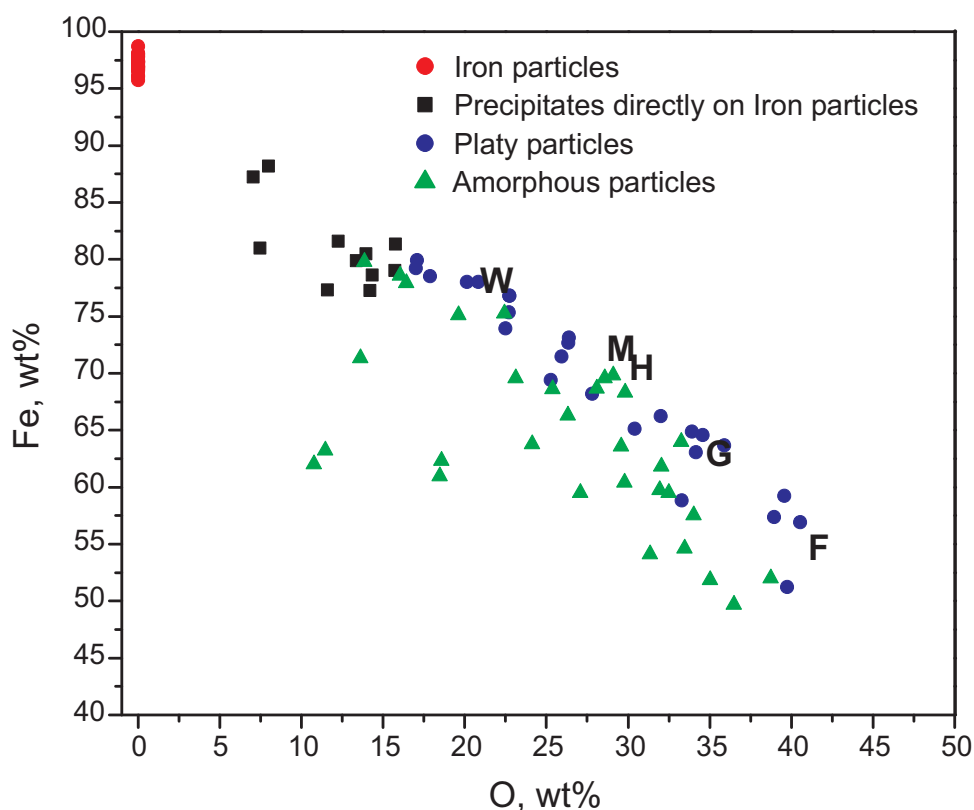


Figure 3.25 Iron concentration versus oxygen concentration in iron grains and surface precipitates (SEM-EDX); Fe-O compositions noted for wustite (W, FeO), magnetite (M, Fe₃O₄), hematite (H, Fe₂O₃), goethite (G, FeOOH), and ferrihydrite (F, Fe(OH)₃).

Table 3.8. Pearson’s Correlation Matrix of Element Concentrations Determined by SEM-EDX Analysis

	O	Si	S	Cl	Mn	Fe	Cr	Ca
O	1							
Si	0.712	1						
S	0.031	-0.126	1					
Cl	0.242	0.281	0.177	1				
Mn	-0.127	-0.082	0.346	0.458	1			
Fe	-0.747	-0.532	-0.658	-0.392	-0.237	1		
Cr	0.057	0.014	0.254	0.292	0.655	-0.269	1	
Ca	0.597	0.471	-0.119	0.029	-0.187	-0.351	-0.162	1

media where enrichments in inorganic precipitates are observed (Figure 3.27 and 3.28). Downgradient regions tend to be comparatively depleted in microbial biomass (Figure 3.28). The lower counts associated with the mid-barrier and downgradient samples suggest that the environment at these locations is more challenging to bacterial growth and survival. Examining the geochemical conditions associated with these locations supports this hypothesis. Figures 3.5 and 3.15, for example, indicate a decrease in biologically available electron acceptors such as cis-DCE and sulfate in mid-wall and downgradient locations. The higher pH and lower availability of electron acceptors would also tend to create a more severe environment for bacterial growth.

The highest biomass contents detected were found in samples collected in 2001, four years after installation of the iron wall (sample EC050801-5-2). However, nearly equivalent values were detected in samples collected in 1999 (sample EC90903), only two years after installation. These data suggest non-constant microbial growth rates, or they may

Table 3.9. Summary of PLFA Data from the Elizabeth City PRB

	Fe(0) Upgradient Elizabeth City	Fe(0) Downgradient Elizabeth City	Aquifer Elizabeth City
Number of samples	27	33	46
Average PLFA concentration (pmoles/g)	611	26	33
PLFA range	6-2614	<1-260	<1-348
PLFA Structural Groups average % (range %)			
Monoenoic Found in Gram-negative bacteria	36.9 (14.0-73.5)	35.9 (<1-74.8)	28.9 (<1-63.0)
Terminally Branched Saturated Found in many Gram-positive bacteria, and in some Gram- negative bacteria	19.1 (5.3-42.1)	4.1 (<1-28.3)	4.5 (<1-19.2)
Branched Monoenoic Common in obligate anaerobes, such as sulfate- reducing and iron-reducing bacteria	11.5 (<1-30.3)	3.1 (<1-37.8)	3.9 (<1-29.8)
Mid-Chain Branched Saturated Common in actinomycetes and sulfate-reducing bacteria	7.8 (<1-38.9)	0.6 (<1-7.9)	2.4 (<1-17.1)
Normal Saturated Ubiquitous in prokaryotes and eukaryotes	22.6 (5.2-74.5)	50.4 (<1-100)	59.1 (15.6-100)
Polyenoic Found in fungi, protozoa, algae, higher plants, and animals	2.0 (<1-49.6)	2.9 (<1-53.7)	1.3 (<1-9.5)

suggest that comparisons of microbial biomass concentrations must be made in the context of the sample location relative to the ground-water plume (i.e., the input of electron acceptors). The enrichments in microbial biomass at 5 to 6 meters below ground surface correspond to the depth where the highest concentrations of terminal electron accepting species enter the reactive media via ground-water transport (Figure 3.27).

PLFA profiles from the Elizabeth City site are enriched in fatty acid biomarkers indicative of anaerobic sulfate- or iron-reducing bacteria (Dowling et al., 1986; Edlund et al., 1986; Tunlid and White, 1991; Parkes et al., 1993). The high proportions of terminally branched and branched monoenoic PLFA specifically indicate anaerobic metabolism. Terminally branched PLFA are typical of Gram-positive bacteria, but can also be present in the cell membranes of some anaerobic Gram-negative bacteria. However, because high proportions are present of branched monoenoic PLFA

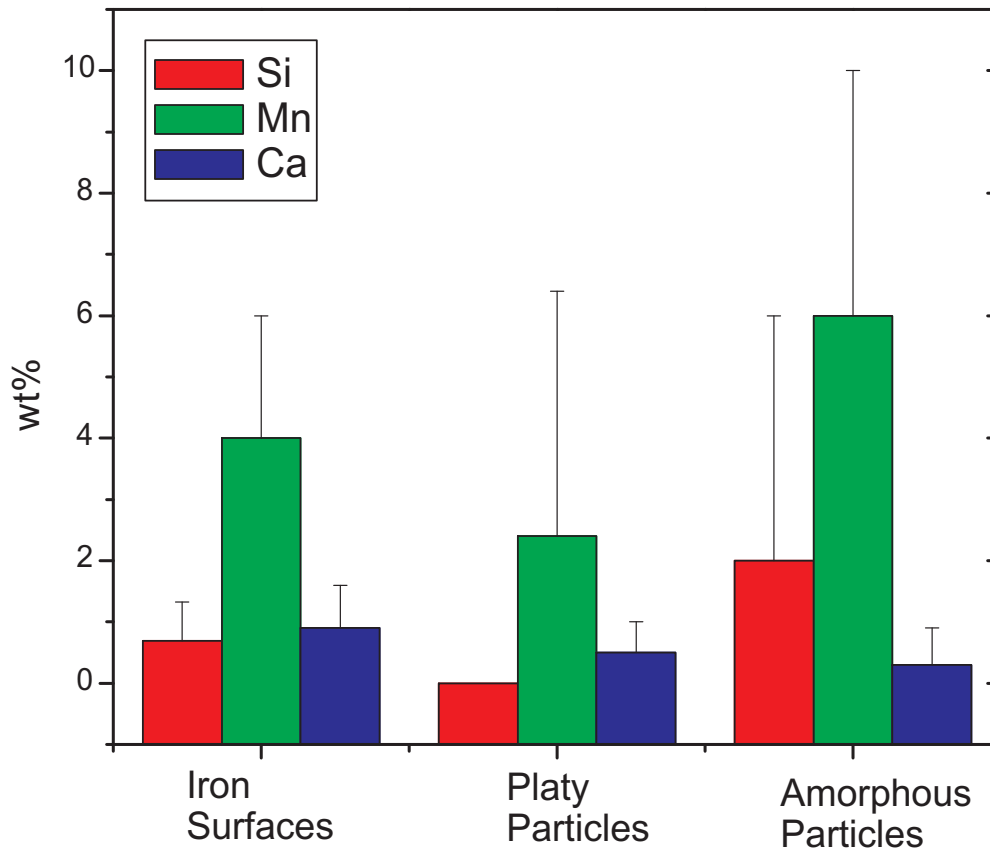


Figure 3.26 Element concentrations in surface precipitates from the Elizabeth City PRB; iron surfaces=precipitates directly in contact with iron grains.

indicative of anaerobic metal reducing bacteria, the terminally branched PLFA are likely to be mainly from sulfate or iron reducing bacteria. Where biomass is most concentrated (i.e., near the upgradient aquifer/iron interface), the distribution of PLFA overall appears to be distinct from the PLFA distribution observed in the native aquifer materials (Figure 3.29). Near the upgradient aquifer/iron interface, the proportion is greater of branched monoenoic PLFA and PLFA indicative of sulfate-reducing bacteria compared to the PLFA signature of native aquifer materials (Figure 3.29). Where biomass is least concentrated (i.e., near the downgradient aquifer/iron interface), the distribution of PLFA overall appears to match the PLFA distribution observed in the native aquifer materials (Figure 3.29).

3.3 Summary of Results from the Elizabeth City Site

Results of the long-term performance evaluation at the Elizabeth City site indicate that the reactive barrier there continues to remove contaminants from ground water after five years of operation. The PRB at Elizabeth City is expected to retain an effective level of reactivity and hydraulic performance for at least another five year time period. The salient results of the Elizabeth City site study are summarized below:

- Removal of contaminants, Cr, TCE, cis-DCE, and VC, continues after five years of PRB operation. In all cases, chromium concentrations have been reduced to below the MCL, and in the majority of sampling events, Cr was undetected in monitoring wells located downgradient from the PRB. Concentrations of volatile organic compounds have been significantly reduced, but TCE concentrations above the MCL have been observed in some downgradient wells.
- After five years, ground water in the PRB is moderately alkaline (pH>9) and moderately reducing (Eh<-100 mV). Time trends in pH suggest quasi-steady-state conditions. Time trends in Eh, however, suggest that the PRB is gradually losing the capacity to produce reducing conditions due to progressive exposure to ground water. Time trends in specific conductance values indicate that influent solutes continue to be

PLFA

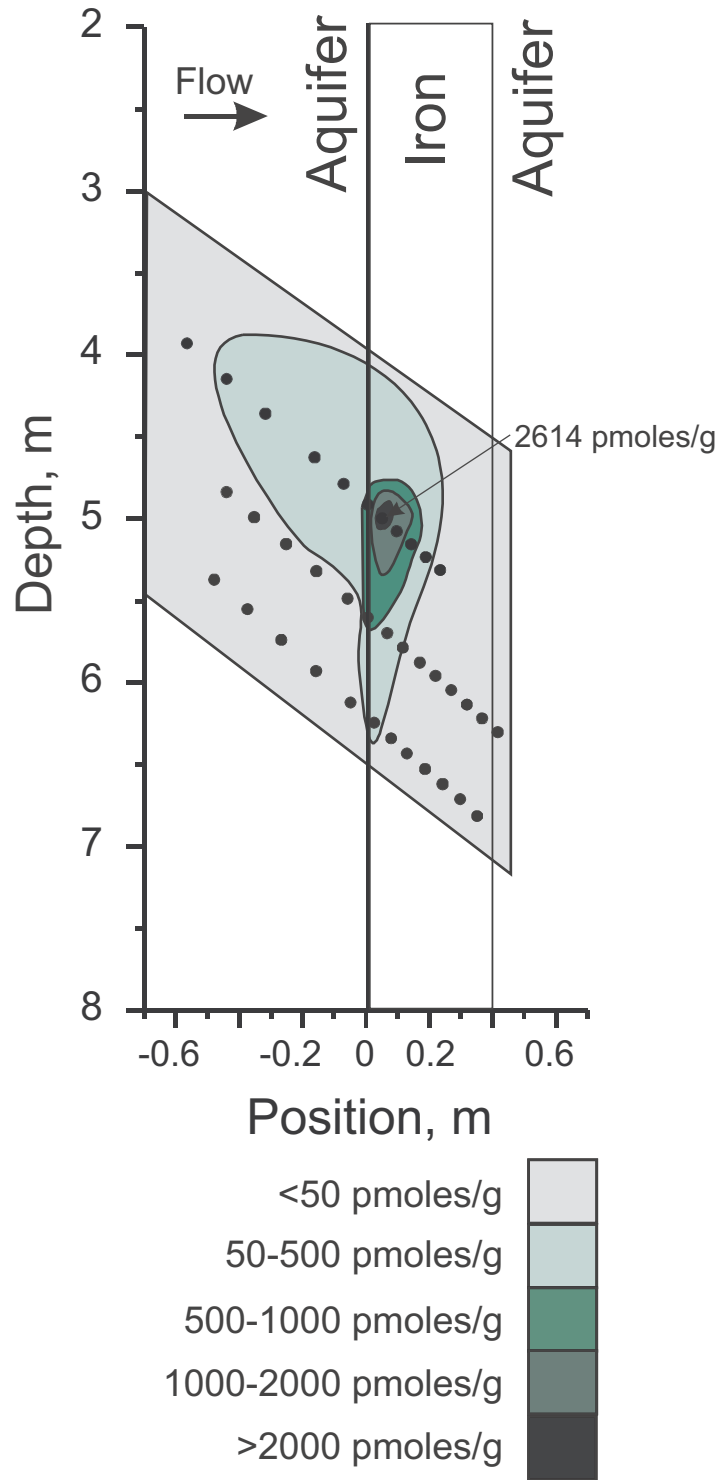


Figure 3.27 Cross-sectional profile showing concentration distribution of biomass (from PLFA data) in picomoles per gram, Elizabeth City PRB (June 2002).

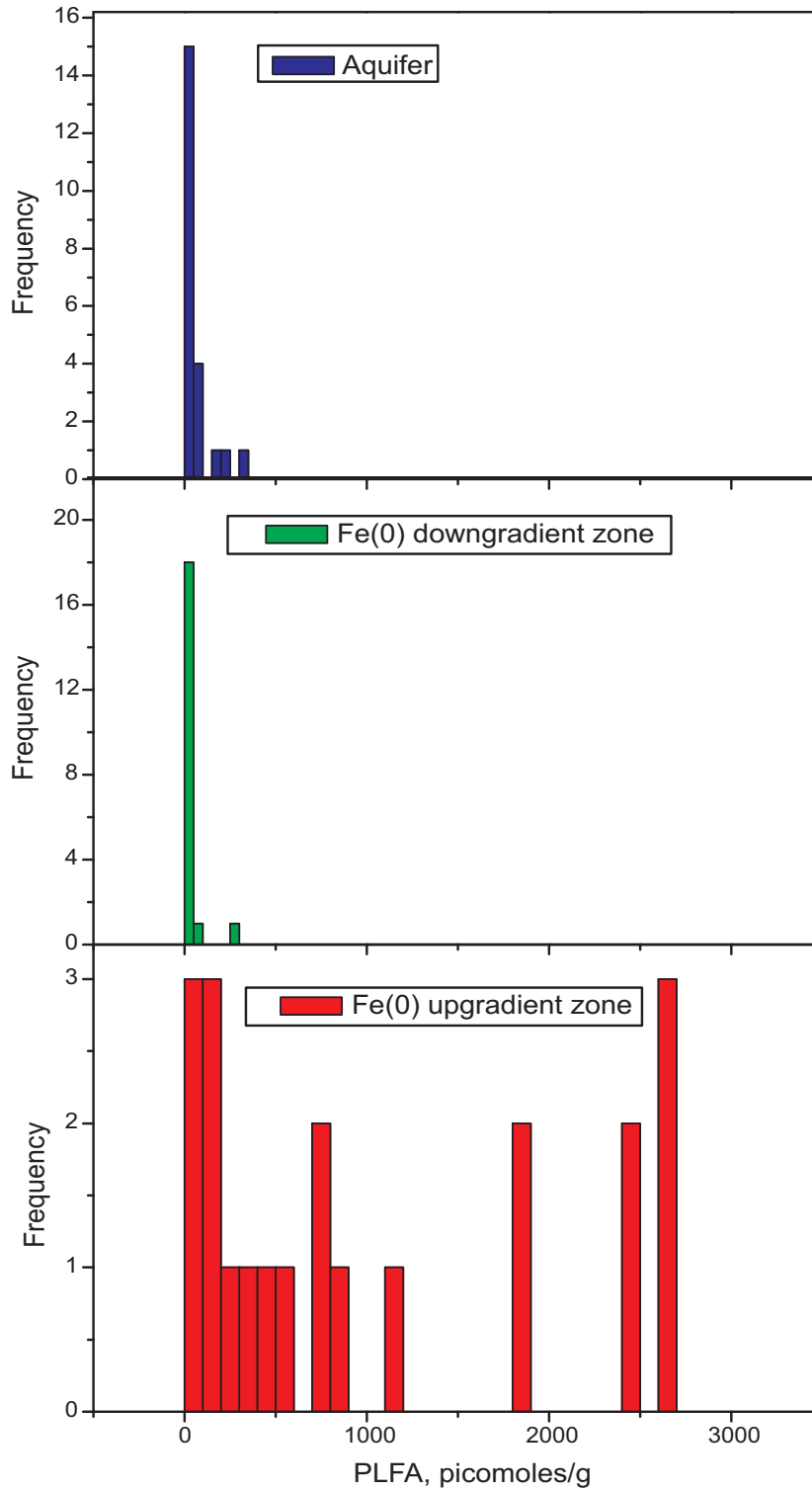


Figure 3.28 Histograms of microbial biomass concentrations (from Elizabeth City PLFA data) in picomoles per gram in aquifer materials, iron from near the downgradient aquifer/iron interface, and iron from near the upgradient aquifer/iron interface.

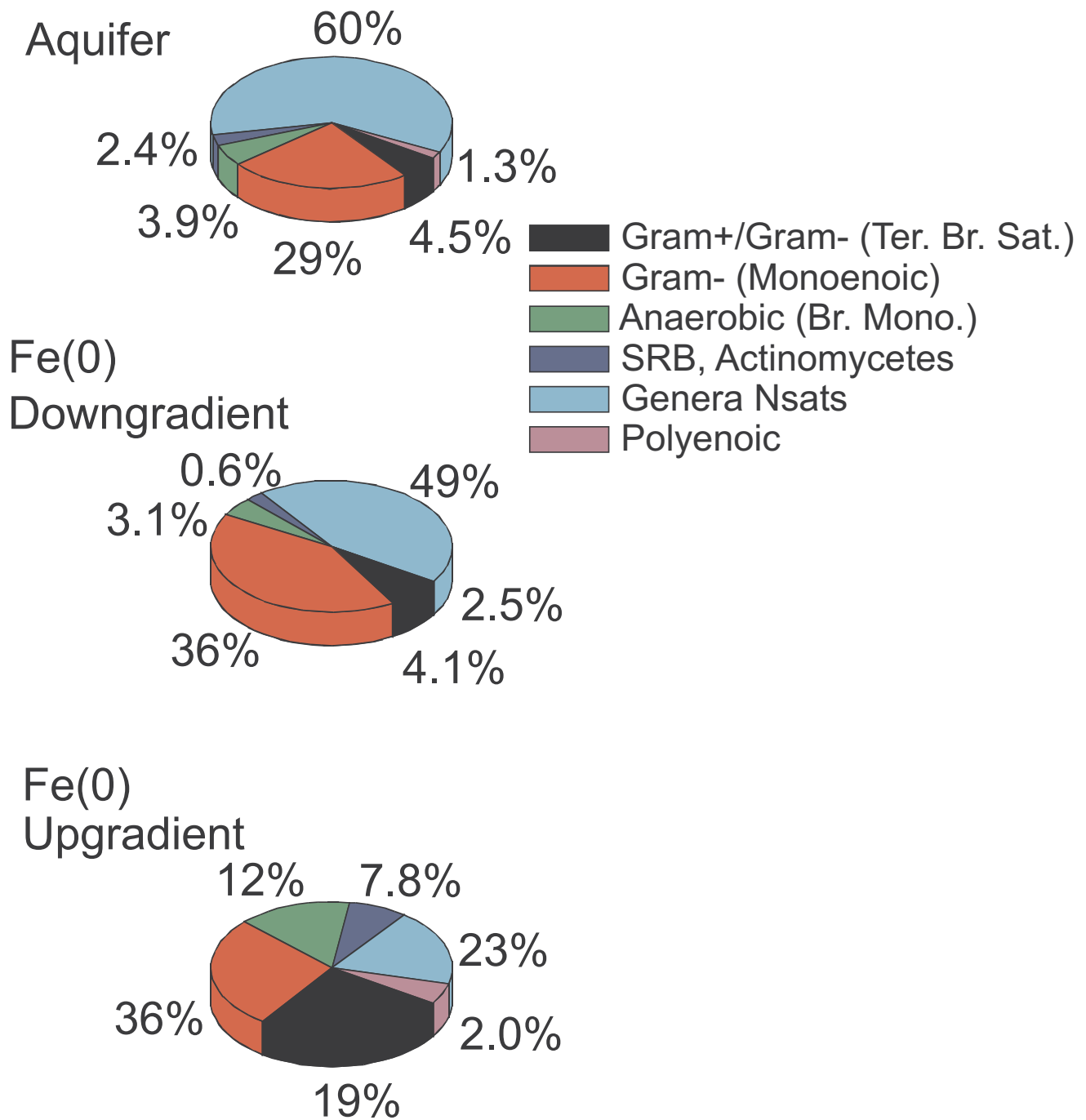


Figure 3.29 Pie graphs showing structural distribution of PLFA compounds (average values) at the Elizabeth City site.

removed within the reactive medium and partitioned into the solid phase after five years of PRB operation. The geochemistry of ground water downgradient of the PRB is impacted by the PRB, in that higher pH and lower Eh conditions are observed in wells located within 2 m of the downgradient iron/aquifer interface.

- The Elizabeth City PRB has consistently removed inorganic carbon, sulfate, calcium, magnesium, silicon, and nitrogen from influent ground water. These components have either been precipitated out in the PRB, adsorbed to iron granules or secondary precipitates within the PRB, or have been chemically transformed by biotic or abiotic processes.
- Mineralogical characterization of soil core materials indicates the formation of calcite/aragonite, iron carbonate hydroxide, magnetite, lepidocrocite, mackinawite, and carbonate green rust in the PRB at Elizabeth City. Inorganic carbon is present in several calcium- and iron-containing minerals. Sulfur is dominantly present in the iron sulfide mackinawite. Mineral precipitation mainly occurs near the upgradient edge of the PRB, although there is an indication that a precipitation front is progressively moving through the PRB. Iron core collected near the downgradient edge of the PRB contains very little if any mineral precipitate mass. After five years of operation, less than 10% of the available pore space has been lost due to mineralization near the upgradient edge. Near the downgradient edge, <1% of the available pore space has been lost.
- Microscopic characterization of core materials indicates that mineral accumulation is occurring mainly on the surfaces of iron granules. After five years, coverage of iron granules near the upgradient edge is regular and approximately 20 to 100 μm thick. Near the downgradient edge, coverage of the iron grains is less consistent and where present mineral coatings are generally <5 μm thick. Although the available reactive surface area of Fe^0 has been reduced through time, some of the secondary mineral precipitates identified (magnetite, green rust, mackinawite) also support contaminant transformation and uptake, thus potentially compensating for the loss in iron metal reactivity due to surface precipitation.
- Microbial characterization results, based on PLFA profiles, from the Elizabeth City PRB and adjacent aquifer materials showed a diverse microbiological community dominated by Gram-negative bacteria. Iron core samples from near the upgradient edge of the PRB are typically enriched in microbial biomass (up to 5.23×10^7 cells/g) and contained elevated proportions of biomarkers indicative of metal-reducing and sulfate-reducing bacteria. Aquifer materials (up to 6.96×10^6 cells/g) and iron from near the downgradient PRB edge (5.20×10^6 cells/g) were comparatively depleted in total biomass and in biomarkers indicative of metal-reducing and sulfate-reducing bacteria.

4.0 Denver Federal Center PRB Monitoring Results

4.1 Ground-water Monitoring

Ground-water monitoring wells in and around gates 1, 2, and 3 at the Denver Federal Center (DFC) were sampled on an annual basis starting in May of 1999, approximately 2.5 years after the funnel-and-gate system was installed. Up to 20 monitoring wells were sampled to obtain contaminant and geochemical profiles in upgradient, iron media, and downgradient positions. The Federal Highway Administration provided a more extensive ground-water data set, covering the entire history of the DFC PRB (FHWA, 2002 pers. commun.; Pacific Western Technologies, 2000). These secondary data were collected under an approved QA/QC program (USGS, 1999). The locations of the monitoring wells in relation to the reactive iron media in gates 1-3 at the DFC are shown in Figures 4.1-4.3.

Methods of ground-water and soil core sampling, preservation and analysis, in addition to Quality Assurance/Quality Control procedures used in this five-year investigation of PRB performance, are described and discussed in Volume 2 of this EPA Report series.

4.1.1 Gate 1 Contaminant Behavior

Time-dependent concentrations of volatile organic compounds (1,1-DCE, 1,1,1-TCA, TCE, and 1,1-DCA) in monitoring wells located in upgradient, iron wall, and downgradient positions near gate 1 are shown in Figure 4.4. Data plotted in Figures 4.4, 4.5, and 4.7 were provided by FHWA. It should be noted that not all monitoring data collected at the DFC are discussed in this report. The data presented correspond to wells that overlap between EPA's performance study and monitoring efforts conducted by FHWA and GSA. The concentrations of 1,1-DCE and 1,1,1-TCA have gradually decreased with time in upgradient well GSA-21 (Figures 4.4a). This trend in contaminant concentrations suggests that natural attenuation processes are taking place in regions of the plume upgradient from the southern most extension of the funnel-and-gate system at the DFC. Concentrations of TCE and 1,1-DCA in ground water entering gate 1 at the DFC have remained fairly constant since January 1998 at 23 ± 7 $\mu\text{g/L}$ and 7 ± 2 $\mu\text{g/L}$, respectively. Concentrations of vinyl chloride and cis-DCE have not been detected in upgradient monitoring points in the vicinity of gate 1.

Within the iron media of gate 1 (well C1-I2), concentrations of TCE and 1,1,1-TCA have remained at or below nominal quantification limits (Figure 4.4b). Concentrations of 1,1-DCE were not detected until November 1999. At that time, concentrations of 1,1-DCE began to increase at a time-averaged rate of about 5 $\mu\text{g/L}$ per year. Similarly, concentrations of 1,1-DCA were not detected until November 1999. However, since that time 1,1-DCA has remained at a fairly constant value of 7 ± 0.8 $\mu\text{g/L}$. Concentrations of vinyl chloride and cis-DCE have not been detected in monitoring wells located within the reactive media of gate 1. Although lower contaminant concentrations are present, parallel trends in contaminant levels are observed in well C1-I2, located approximately 3 m to the south of well C1-I1 along the mid-point axis of the reactive media in gate 1 (see Figure 4.1).

Based on laboratory studies to evaluate contaminant removal rates in the presence of zero-valent iron, degradation rates of chlorinated ethenes and ethanes decrease in the order 1,1,1-TCA>TCE>1,1-DCE>cis-DCE>VC (see Johnson et al., 1996). In general, with each successive dehalogenation the degradation reaction proceeds more slowly (Matheson and Tratnyek, 1994; but also see Arnold and Roberts, 2000). In a performance scenario where zero-valent iron progressively loses reactivity over time relative to an initial reactivity defined by laboratory batch or column studies, it might be expected that less reactive contaminants such as VC, cis-DCE, and 1,1-DCE would appear or "break through" prior to more rapidly degraded compounds such as TCE and 1,1,1-TCA. These trends are in fact observed in gate 1 at the DFC. It should be noted that monitoring points C1-I1 and C1-I2 are located at the approximate mid-point of the reactive media so that contaminants should continue to degrade in the downgradient direction.

Ground-water seepage velocities in gate 1 have been measured using heat-flow sensors and range from about 0.40 to 0.82 m/d (McMahon et al., 1999; Pacific Western Technologies, 2000). Based on this range of flow rates, an average saturated thickness of 4.5 m, and a saturated gate throughput area of 55 m², gate 1 has removed approximately 0.8-1.6 kg of TCE, 2-4 kg of 1,1,1-TCA, and 3.2-6.4 kg of 1,1-DCE over the first five-year period of operation. By February 1998, a clean front was observed in downgradient well GSA-20. At that time, concentrations of 1,1-DCE and 1,1, DCA increased to above detectable limits and have remained at detectable levels to the present time. The reasons for the increase in the concentrations of these compounds is not certain but would appear to relate to a loss of reactivity or change in residence time of contaminants in the reactive media.

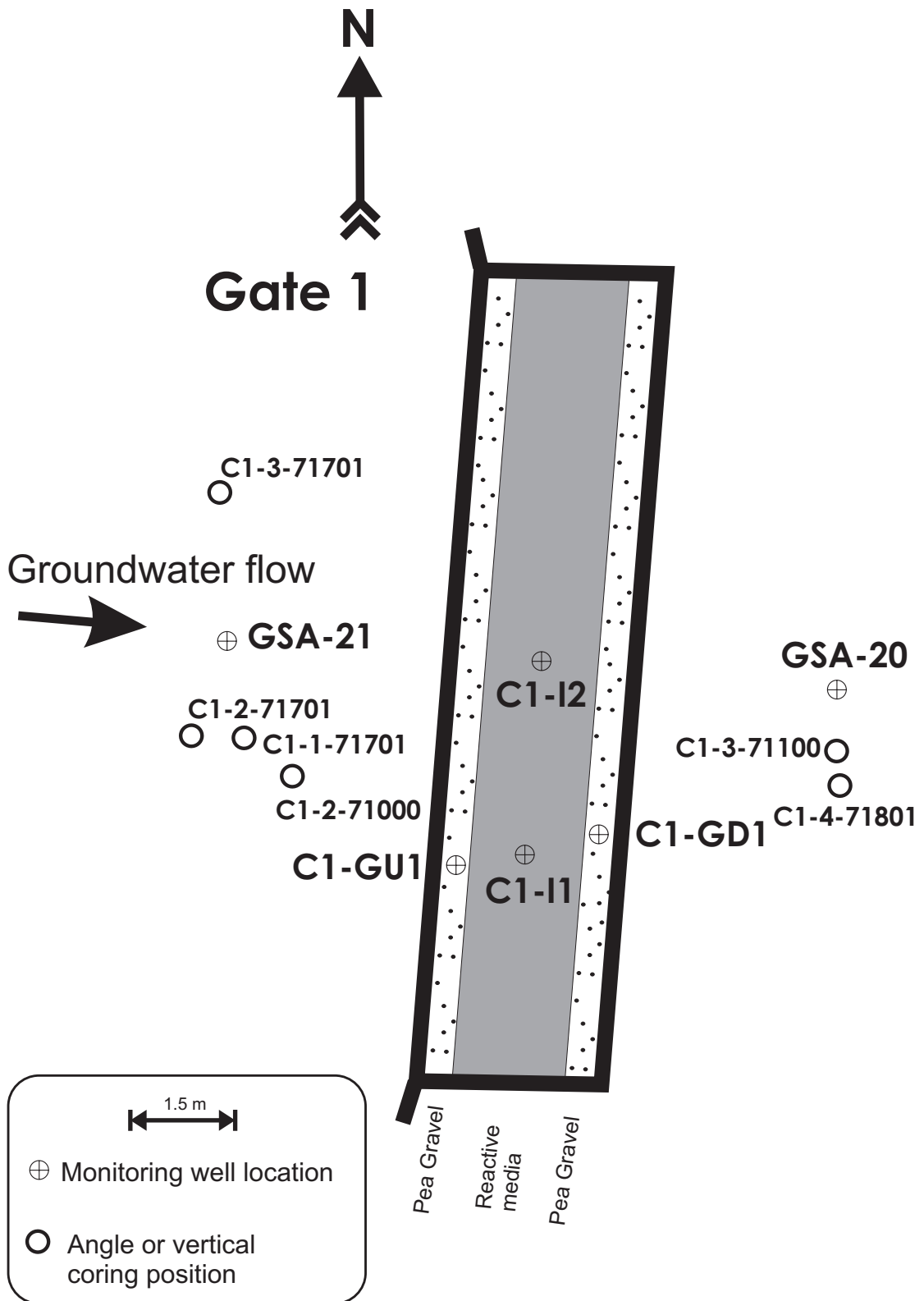


Figure 4.1. Coring locations and monitoring well locations at the Denver Federal Center, gate 1 (plan view).

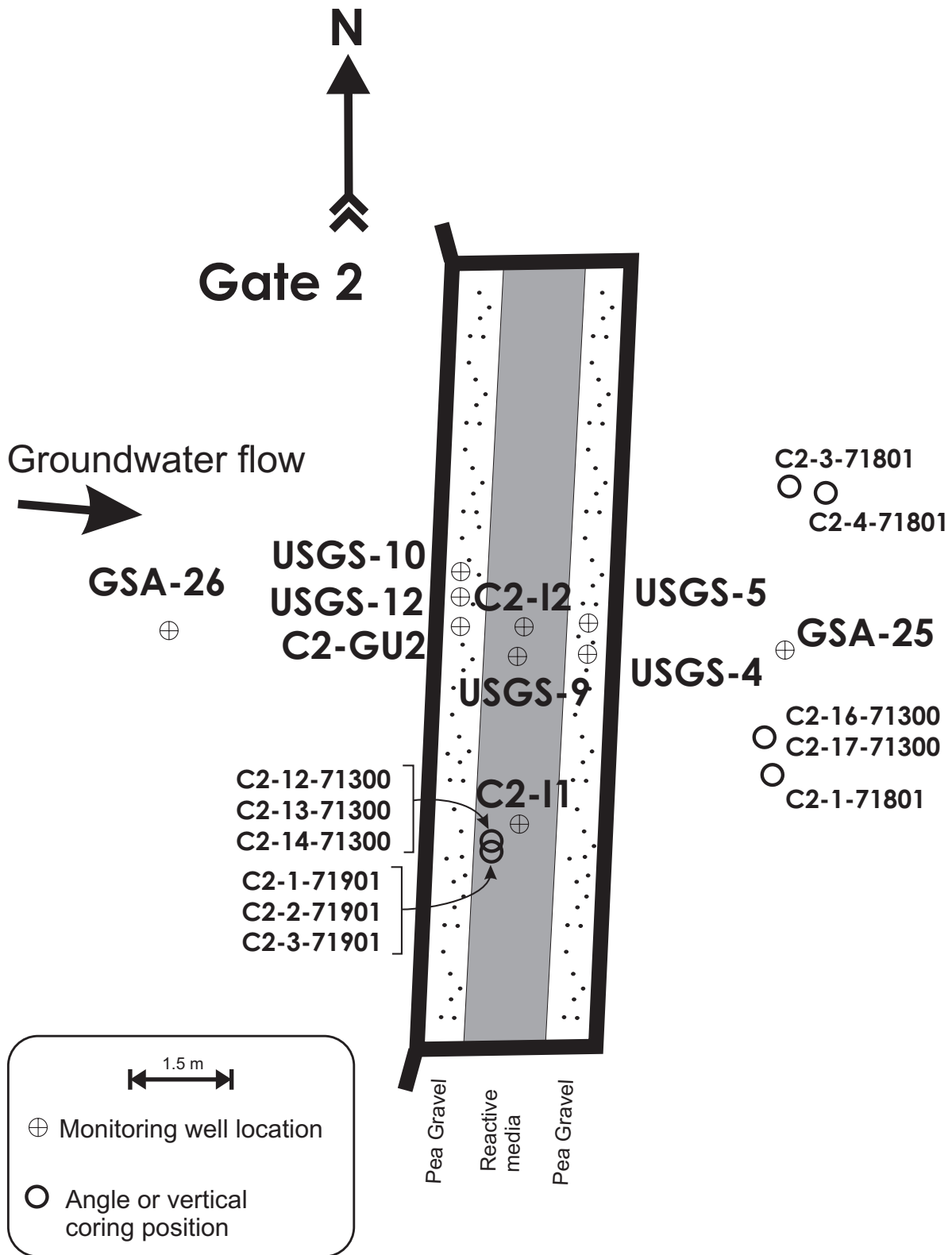


Figure 4.2. Coring locations and monitoring well locations at the Denver Federal Center, gate 2 (plan view).

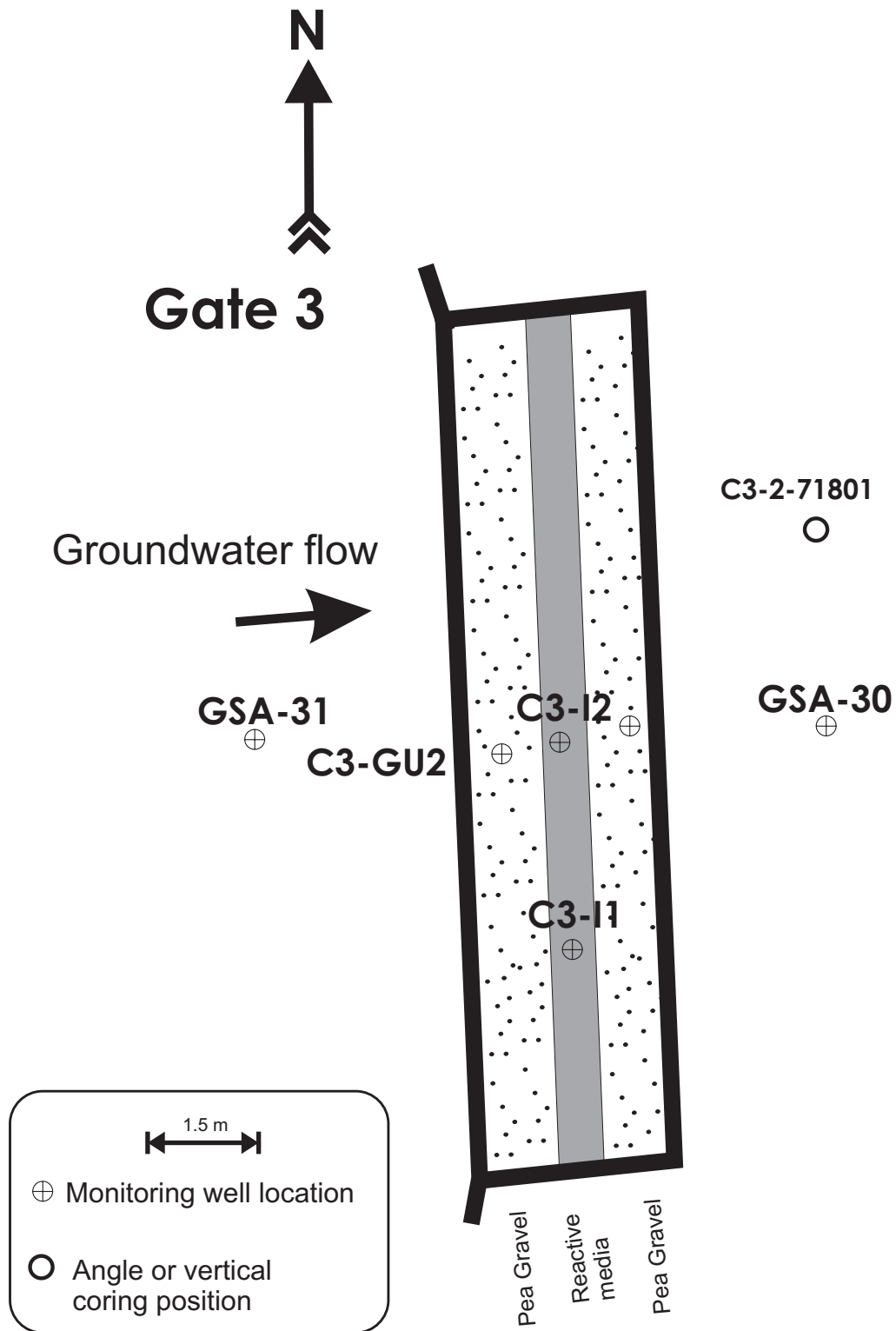
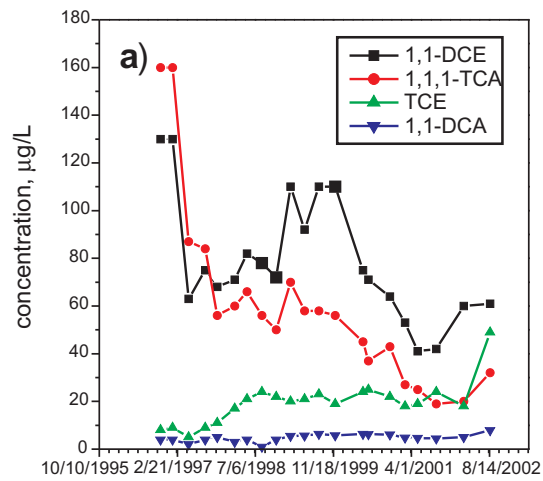
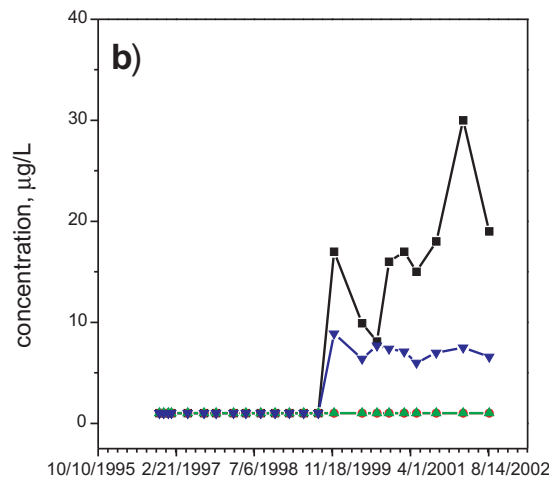


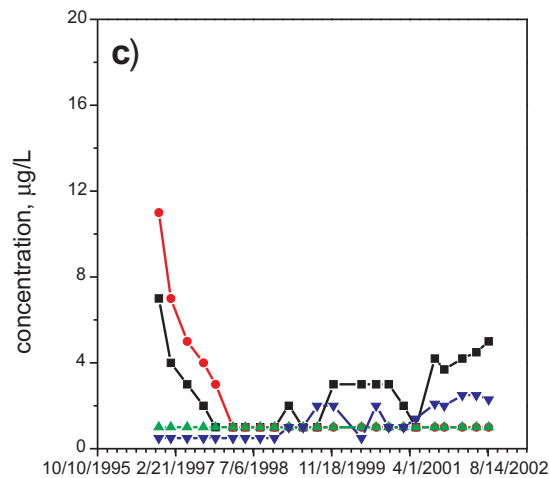
Figure 4.3. Coring locations and monitoring well locations at the Denver Federal Center, gate 3 (plan view).



GSA-21
Gate 1
Upgradient



C1-11
Gate 1
Fe(0)



GSA-20
Gate 1
Downgradient

Figure 4.4 Concentrations of contaminants through time in monitoring wells from the Denver Federal Center, gate 1 (data from FHWA): a) well GSA-21 (upgradient); b) well C1-11 (iron wall); c) well GSA-20 (downgradient). Symbol key shown in Figure 4.4a applies to each graph; note change in concentration plotting range to show trends through time.

4.1.2 Gate 2 Contaminant Behavior

Gate 2 is located approximately 120 meters north of gate 1. Of the four treatment cells at the DFC, the highest concentrations of total volatile organic compounds are found in the vicinity nearby gate 2. Since November 1996, concentrations of 1,1-DCE and 1,1,1-TCA have gradually decreased in the upgradient well, GSA-26, to values of about 110 µg/L and 50 µg/L, respectively (Figure 4.5a). In this same well, concentrations of TCE, 1,1-DCA, and cis-1,2-DCE have been steady since November 1996 at 72 ± 12 µg/L, 8 ± 1 µg/L, and 1 ± 0.5 µg/L, respectively (Figure 4.5a). The highest TCE concentrations observed, in either upgradient or downgradient monitoring locations, are in downgradient well GSA-25 (Figure 4.5c). A maximum TCE concentration of 600 µg/L was measured in ground water collected from GSA-25 in January 1997. From January 1997 to November 1998, TCE concentrations rapidly dropped in GSA-25, and since November 1998, TCE and all other volatile organic compounds have remained at relatively constant concentrations (Figure 4.5c).

Because TCE concentrations are comparatively low in wells located within the iron media of gate 2 and in the pea gravel immediately downgradient of gate 2, the TCE observed in downgradient well GSA-25 is thought to be derived from residual bedrock contamination from a proximal release of TCE (Pacific Western Technologies, 2000). Yet, concentrations of 1,1-DCE have been consistently present in wells both within iron media of gate 2 and in downgradient pea gravel wells (Figure 4.5b). The increase beginning in November 1998 of 1,1-DCE levels both in downgradient well GSA-25 and in the iron well C2-I2 corresponds to the installation of a distribution trench placed on the downgradient side of gate 2. The trench was installed with the goals of increasing the flow through gate 2 and lowering the hydraulic head differential across the gate. Although the timing of trench construction matches the point at which 1,1-DCE concentrations increase, the mechanism linking these events is uncertain. Alternatively, the increasing 1,1-DCE levels could be from incomplete degradation within the iron media due either to loss of iron reactivity or to changing flow regimes within gate 2 (decrease in residence time). Iron reactivity tests and mineral precipitate/microbial biomass characterization studies on the iron media in gate 2 are discussed in following sections of this report. Equally equivocal is the trend of decreasing concentrations in C2-I2 beginning in September 2001 (Figure 4.5b), which would be an unexpected outcome if channeling was occurring or if the iron media had lost reactivity.

A previous study proposed that ground-water mounding upgradient of gate 2 was likely driving flow underneath of the funnel-and-gate system near gate 2 (McMahon et al., 1999). Multi-level sampling using low-volume diffusion samplers in well GSA-25 shows that TCE concentrations in this well are highly depth dependent with the greatest concentrations detected near the bottom of the screened interval (Figure 4.6). These concentration trends cannot be used to reliably confirm or refute underflow of contaminants beneath the gate. The necessary hydraulic data are not available to make this assessment. However, examination of [TCE]/[1,1-DCE] ratios suggests that ground water upgradient of gate 2 (1,1-DCE-rich) is distinct from and not likely to be a source of ground water present in downgradient well GSA-25.

4.1.3 Gate 3 Contaminant Behavior

The concentrations of volatile organic compounds in monitoring wells around gate 3 of the DFC are shown in Figure 4.7. In general, the concentrations of individual contaminants are at levels below 5 µg/L in well C3-I2 located within the treatment cell, with the exceptions of late-summer sampling events in August 2000, September 2001, and August 2002. In gate 3, temporal trends in contaminant distributions are clearly intermittent. Concentrations of cis-DCE, 1,1-DCE, VC, and 1,1-DCA in upgradient well GSA-31, for example, spiked in August of 2000. At the same time, elevated contaminant concentrations are found in well C3-I2 located within the reactive media. However, co-temporal spikes are not observed in downgradient well GSA-30. As in gate 2, contaminants detected in downgradient monitoring points are thought to be derived from residual bedrock contamination (Pacific Western Technologies, 2000). Correlations have been noted between high concentrations of volatile organic compounds and low ground water levels, but the mechanism linking these observations is unclear.

4.1.4 Geochemical Parameters

At the Denver Federal Center, trends in pH have followed consistent patterns from May 1999 to July 2001. Gates 1 through 3 show comparable trends in pH from upgradient to downgradient sampling locations (Figure 4.8). Trends in contaminant degradation behavior among the reactive cells do not clearly correlate with pH, i.e., pH values in gate 2 are similar to pH values measured in gate 1 and gate 3. One notable feature is the continued decrease in pH of about 0.1 pH units per year in ground water from the iron media in gates 1, 2, and 3. This trend is marginally significant with respect to the precision and accuracy of the pH measurements but might be related to an overall decrease in residence time of ground water in the reactive media, related to pore-infilling by mineral precipitates and microbial biomass.

The specific conductance (SC) of ground water at the Denver Federal Center shows variable patterns (Figure 4.9). In gate 1, SC values in the reactive iron media decrease by an average of about 31% relative to upgradient ground water; in gate 3 SC values in the reactive media decrease by about 28% relative to upgradient ground water. As described previously, decreases in SC are expected as ground water passes through zero-valent iron reaction zones due to mineral precipitation. On the other hand, trends in SC in gate 2 are anomalous. In 1999 and 2000, SC values in the iron

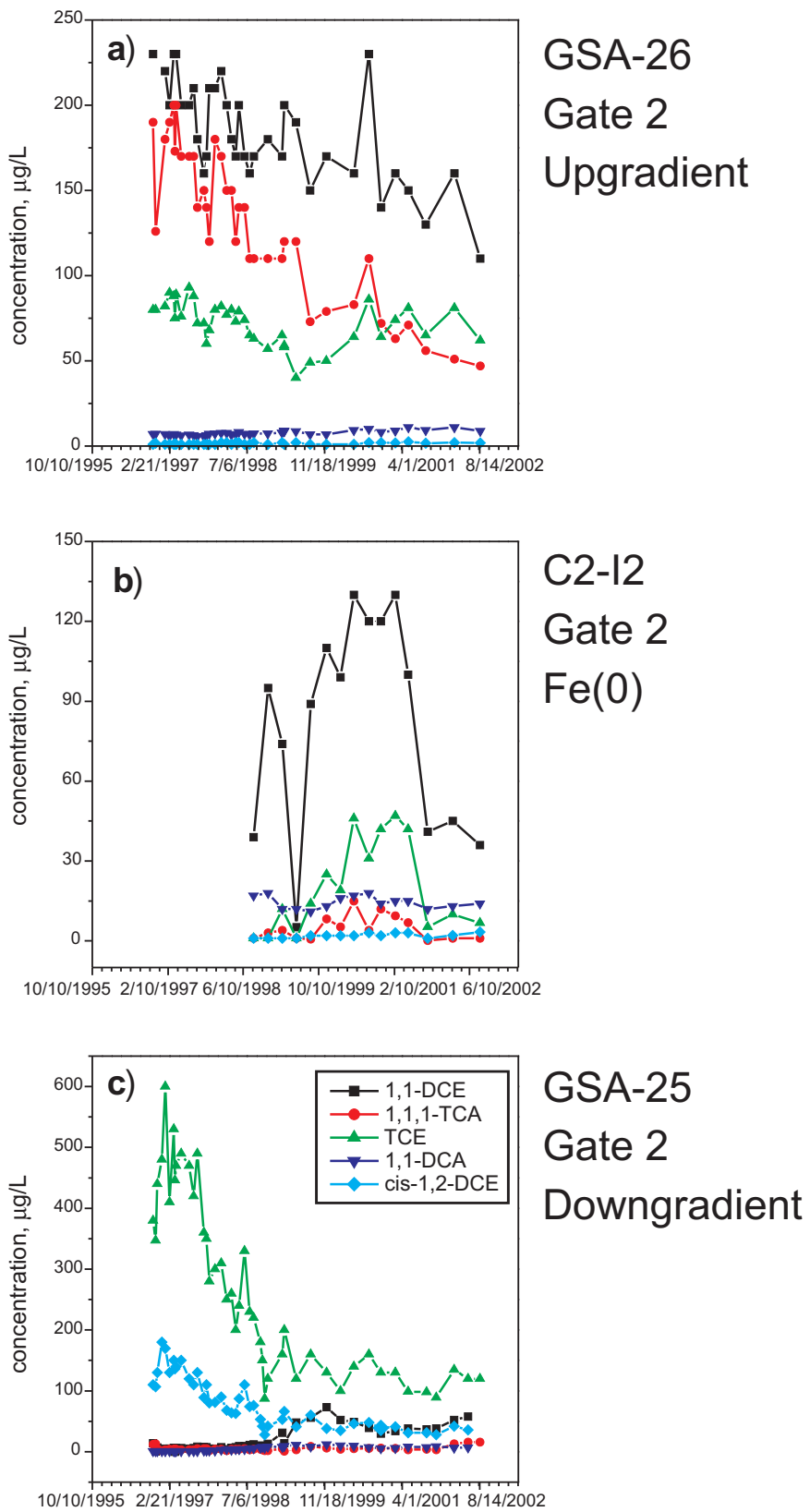


Figure 4.5 Concentrations of contaminants through time in monitoring wells from the Denver Federal Center, gate 2 (data from FHWA): a) well GSA-26 (upgradient); b) well C2-I2 (iron wall); c) well GSA-25 (downgradient). Symbol key shown in Figure 4.5c applies to each graph; note change in concentration plotting range to show trends through time.

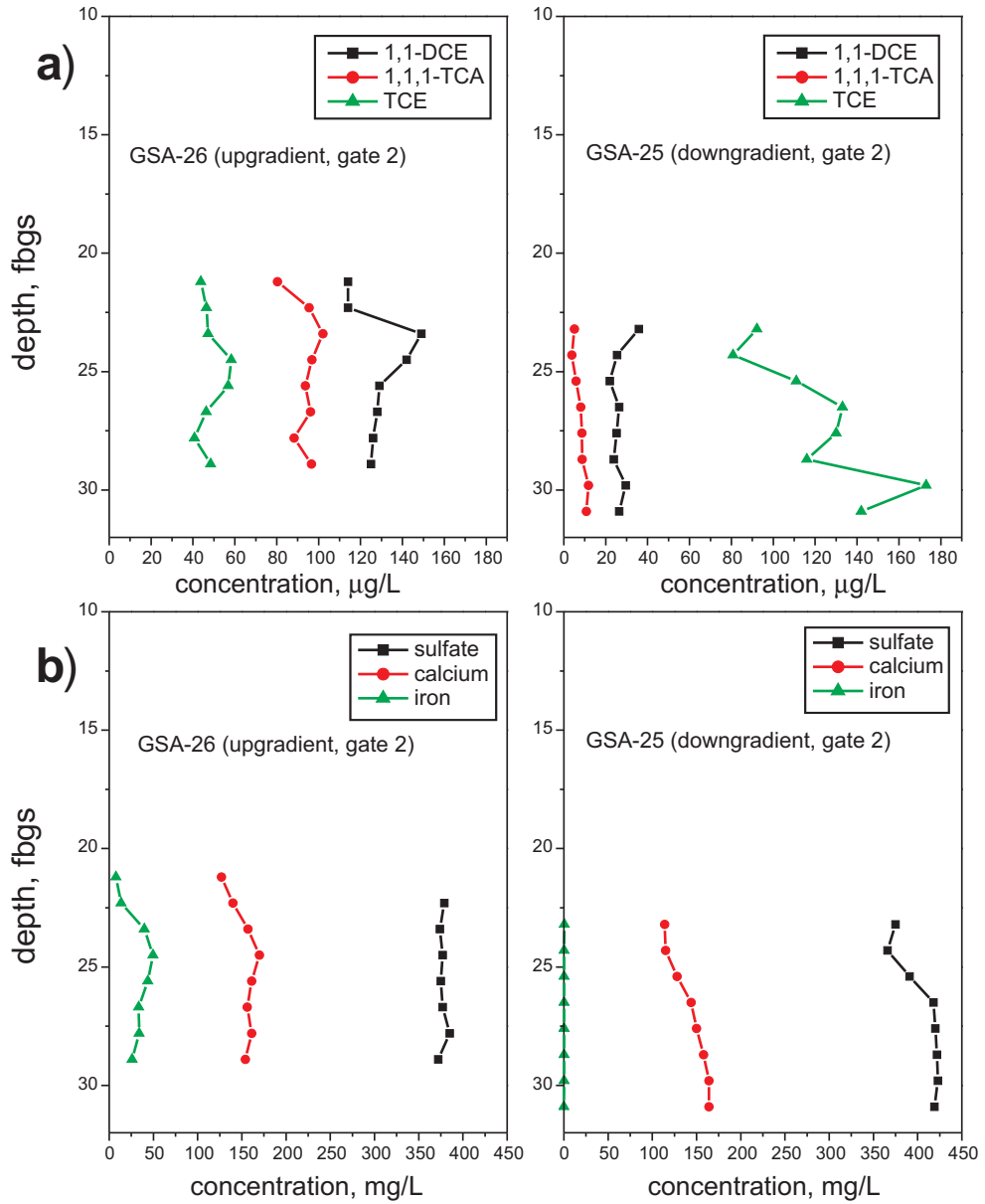


Figure 4.6 Depth-resolved concentrations of a) contaminants ($\mu\text{g/L}$) and b) sulfate, calcium, and iron (mg/L) in wells GSA-26 and GSA-25 from the Denver Federal Center (gate 2). Data collected in May 1999.

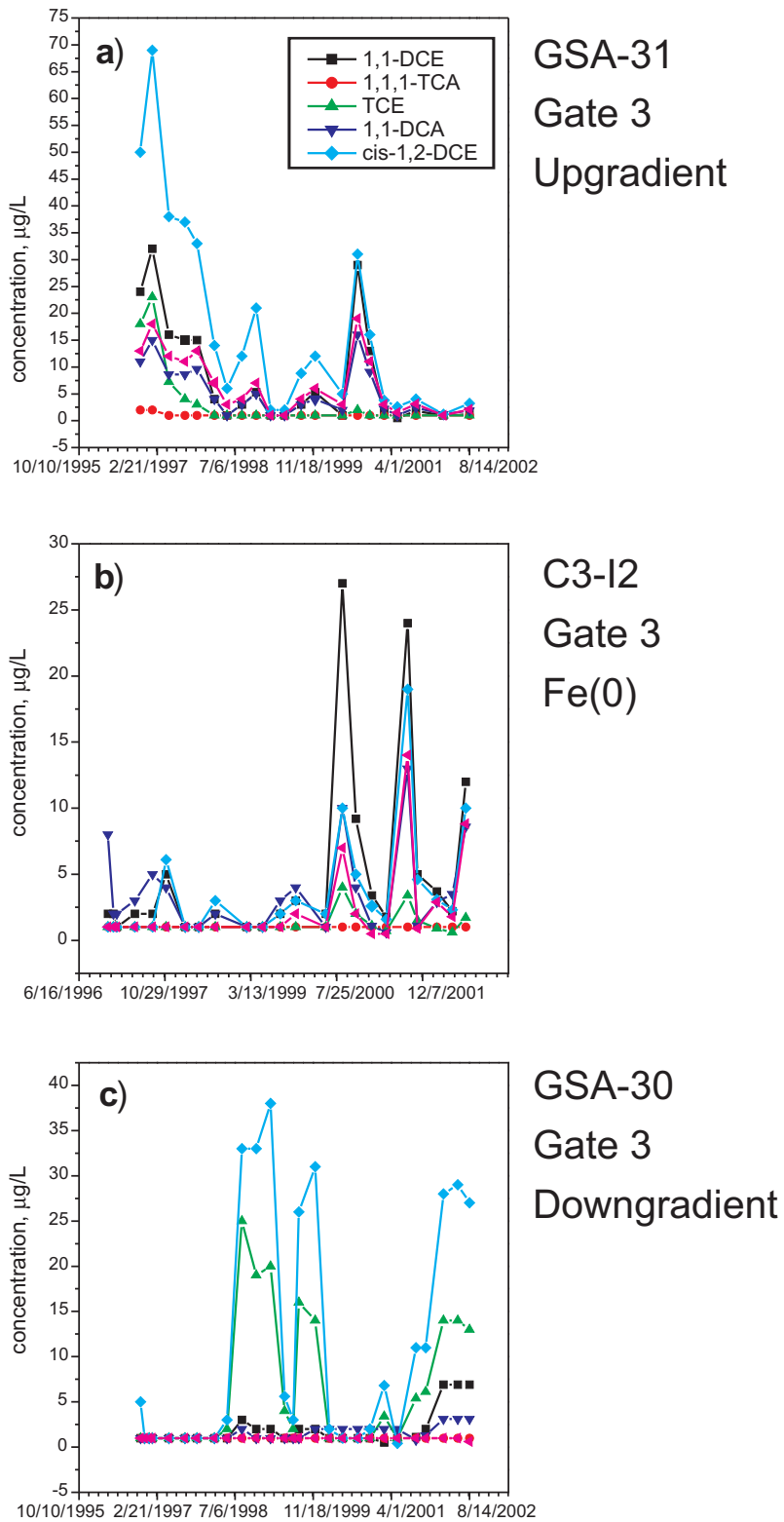


Figure 4.7 Concentrations of contaminants through time in monitoring wells from the Denver Federal Center, gate 3 (data from FHWA): a) well GSA-31 (upgradient); b) well C3-I2 (iron wall); c) well GSA-30 (downgradient). Symbol key shown in Figure 4.7a applies to each graph; note change in concentration plotting range to show trends through time.

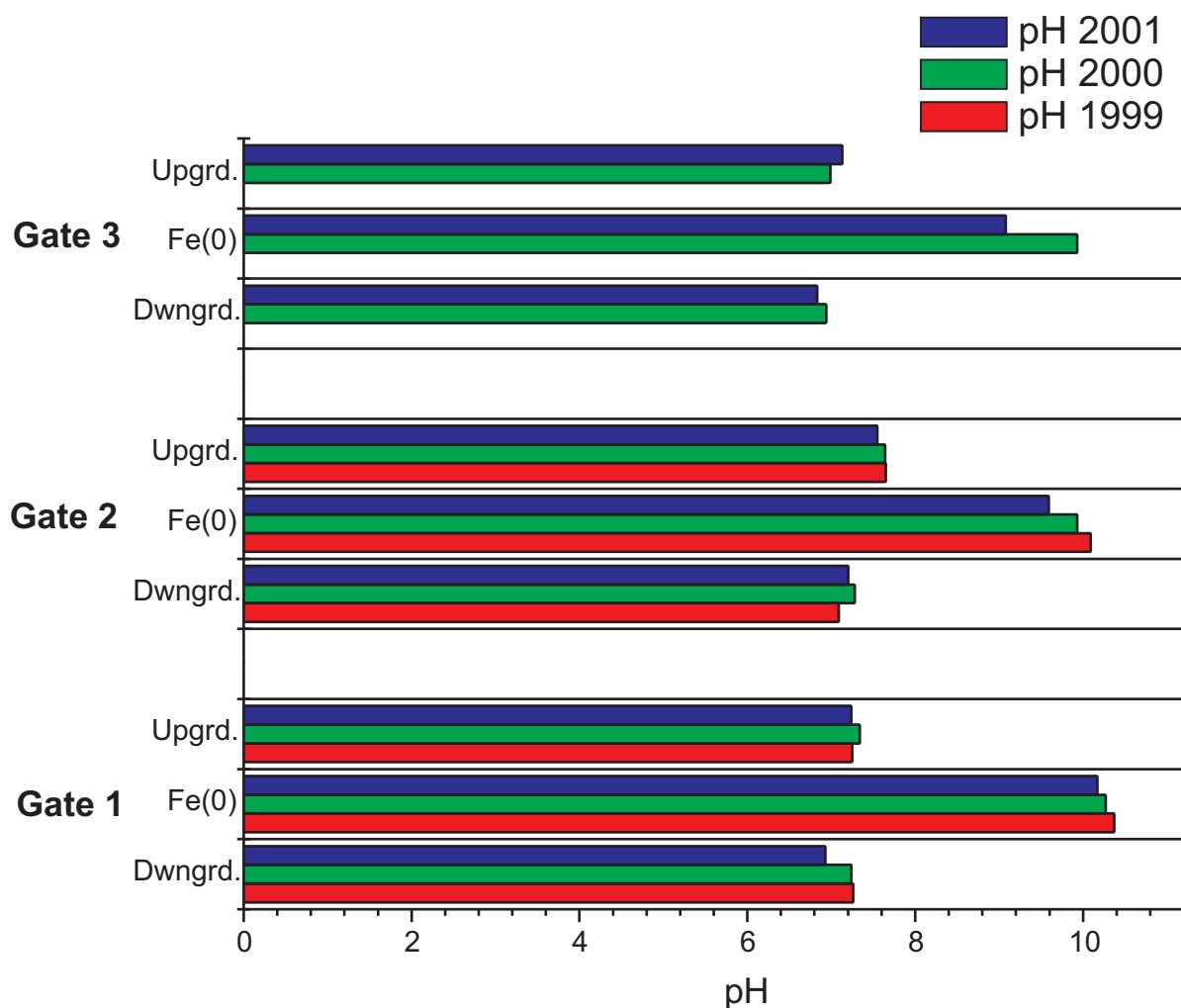


Figure 4.8 Average pH values through time in wells from upgradient, iron wall, and downgradient positions relative to gate 1, gate 2, and gate 3 at the Denver Federal Center.

media were actually greater than the values obtained from upgradient ground water. In 2001, the trend reversed to what is considered to be normal behavior, i.e., SC values were low within the reactive media (Figure 4.9). The high values of SC in Cell 2 in 1999 and 2000 indicate that the iron media in gate 2 was a source of dissolved solutes rather than a sink. Such anomalous trends in SC may be indicative of decreased performance or at least of non-typical reactive behavior. In gate 3, downgradient ground water has a significantly higher SC than ground water upgradient and within the treatment cell. This result suggests that the ground-water chemistry and contaminant distributions in ground-water from well GSA-30 are not greatly influenced by water emerging from the reactive cell (gate 3).

At the Denver Federal Center, ground-water upgradient from the funnel-and-gate system is progressively more reducing moving northward from gate 1 to gate 3. Fairly typical trends in Eh values are observed in gate 1 (Figure 4.10). Eh values in ground water collected from upgradient and downgradient compliance wells range from about -75 mV to +150 mV. In the reactive iron media of gate 1, Eh values are negative (-175 to -250 mV), and in downgradient locations, Eh values generally rebound to positive values. Somewhat lower and more variable Eh values are apparent in gate 2, reinforcing the overall anomalous behavior in this iron wall (Figure 4.10).

4.1.5 Hydrogen Gas Concentrations

The concentration of dissolved hydrogen gas is another key indicator of redox conditions that may be useful in PRB monitoring programs. Figure 4.11 shows trends in dissolved hydrogen concentrations in gate 1 at the DFC. Comparatively high concentrations of hydrogen are observed within the reactive media of gates 1-3. High dissolved hydrogen concentrations are an expected consequence of iron corrosion. Hydrogen concentrations are the greatest in

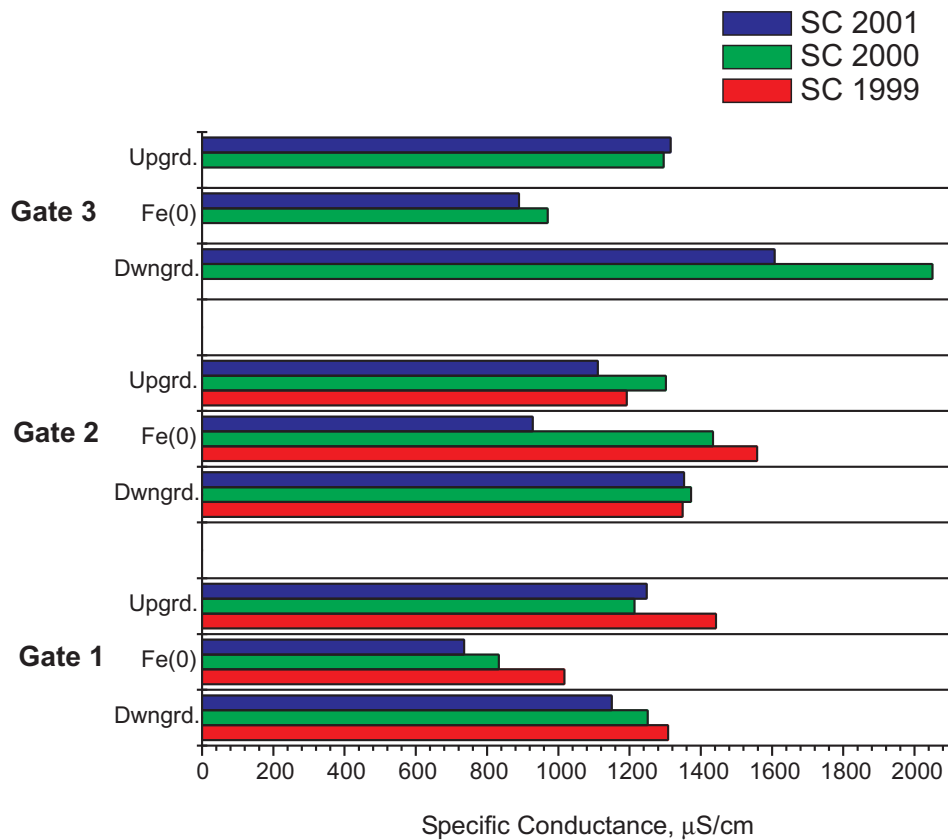


Figure 4.9 Average specific conductance values ($\mu\text{S}/\text{cm}$) through time in wells from upgradient, iron media, and downgradient positions relative to gate 1, gate 2, and gate 3 at the Denver Federal Center.

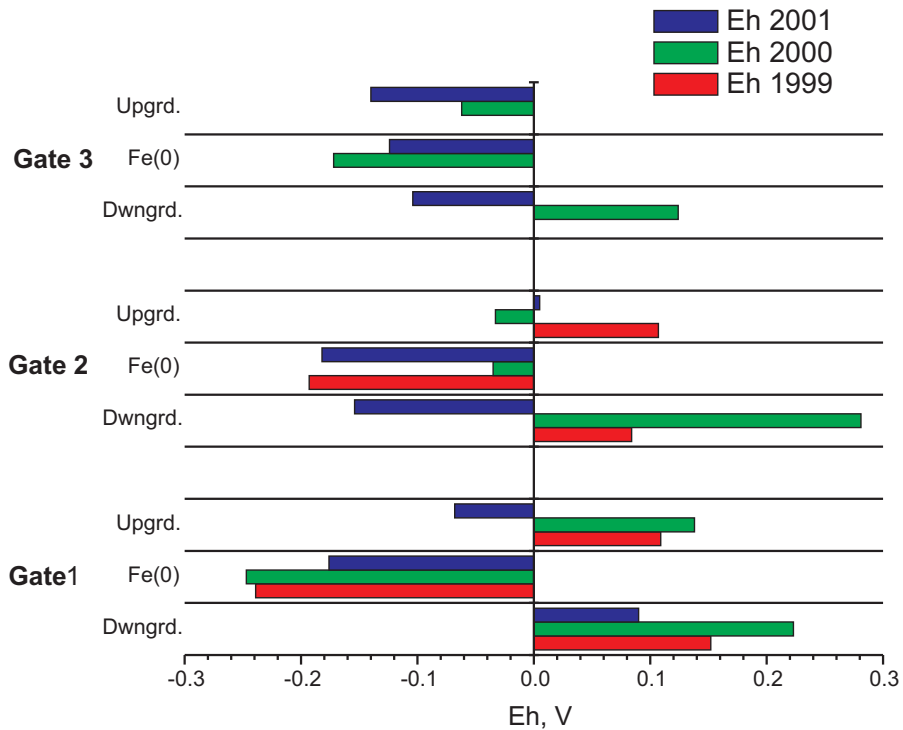


Figure 4.10 Average Eh (V) values through time in wells from upgradient, iron media, and downgradient positions relative to gate 1, gate 2, and gate 3 at the Denver Federal Center.

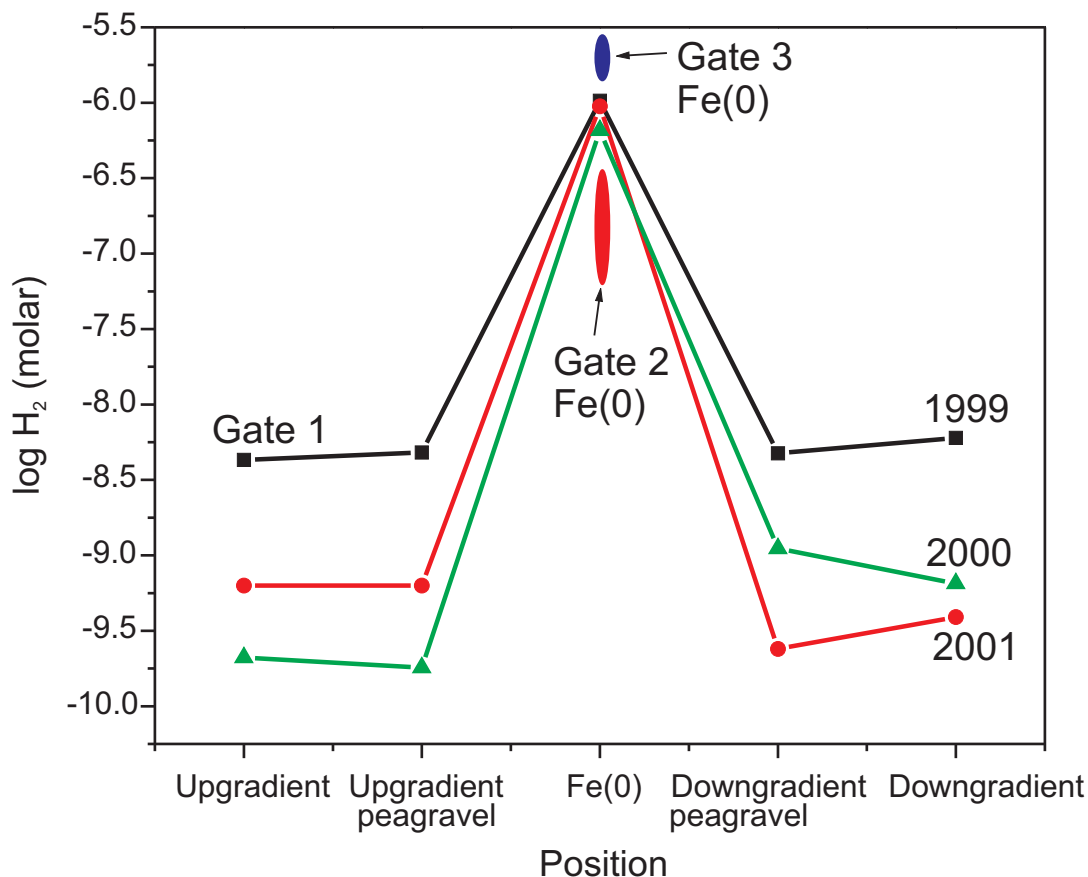


Figure 4.11 Concentrations of dissolved hydrogen (log molar) as a function of sampling position and time in gate 1 at the Denver Federal Center. Also shown are the concentration ranges of dissolved hydrogen measured in the iron media in gate 2 and gate 3.

the reactive media of gate 3 and the least in gate 2. In gate 1, measured concentrations of hydrogen in the iron media and downgradient positions have progressively decreased from 1999 to 2001. The lowest hydrogen levels were observed in gate 2, which is consistent with the lower redox potentials indicated by platinum electrode measurements in this iron cell. The decreased reducing potential in gate 2 indicated by Eh and H_2 measurements seems to correspond with the lower degree of contaminant removal in this reactive cell. Dissolved H_2 concentrations observed within the reactive iron media correspond to equilibrium hydrogen gas partial pressures of about 0.05 to 1 mbar. In all cases, H_2 concentrations within the iron zones are greater than those typically encountered in methanogenic aquifers (5 to 30 nM, see Chapelle et al., 1996).

4.1.6 Dissolved Cations and Anions

The cation compositions of ground water upgradient from gates 1, 2, and 3 are broadly comparable. On a molar basis, sodium is the most abundant cation, followed by calcium, magnesium, and potassium. Cation concentrations in ground water from upgradient wells (GSA-21, GSA-26, GSA-31) range from 5.7-7.9 mM Na, 2.7-2.9 mM Ca, 0.8-1.8 mM Mg, and about 0.01 mM K. Ground water upgradient of gate 1 is slightly more enriched in Na, but depleted in Ca and Mg compared to ground water from regions upgradient of gate 3 (Figures 4.12-4.14). In the reactive cells, concentrations of calcium and magnesium are greatly reduced compared to upgradient wells, whereas concentrations of sodium are largely unchanged relative to upgradient regions. Potassium concentrations increase slightly in the upgradient pea gravel probably due to the dissolution of potassium-bearing aluminosilicates that are present in the pea gravel material. From 1999 to 2001, average reductions in the concentrations of calcium and magnesium between upgradient and mid-wall positions were greater than 95% and 75%, respectively, in gate 1. Similarly, average reductions in the concentrations of calcium and magnesium between upgradient and mid-wall positions were greater than 95% and 50%, respectively, in gate 2 between 1999 and 2001.

DFC Gate 1

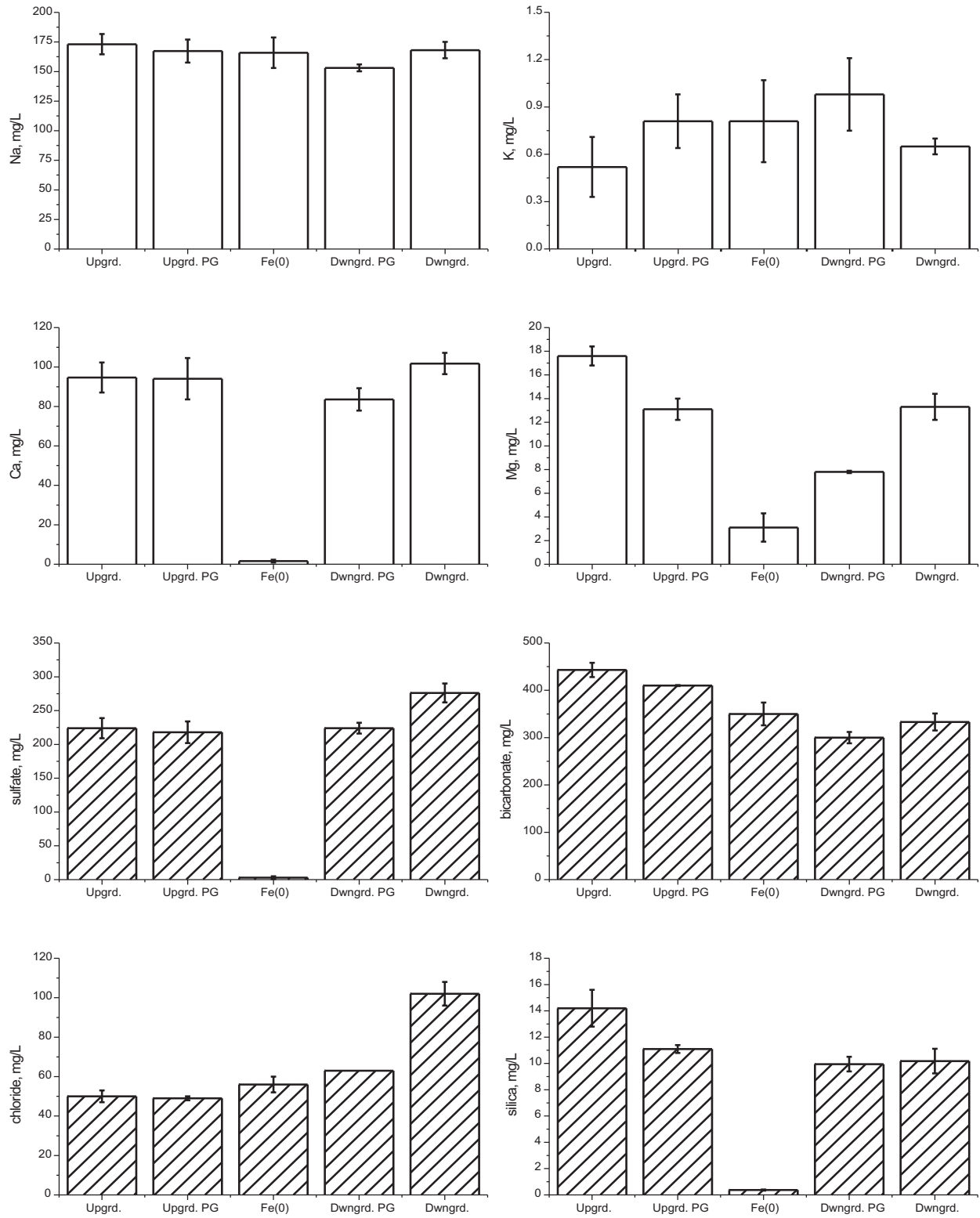


Figure 4.12 Average (± 1 s.d.) concentrations of Na, K, Ca, Mg, sulfate, bicarbonate, chloride, and silica (mg/L) as a function of sampling position in gate 1 at the Denver Federal Center.

DFC Gate 2

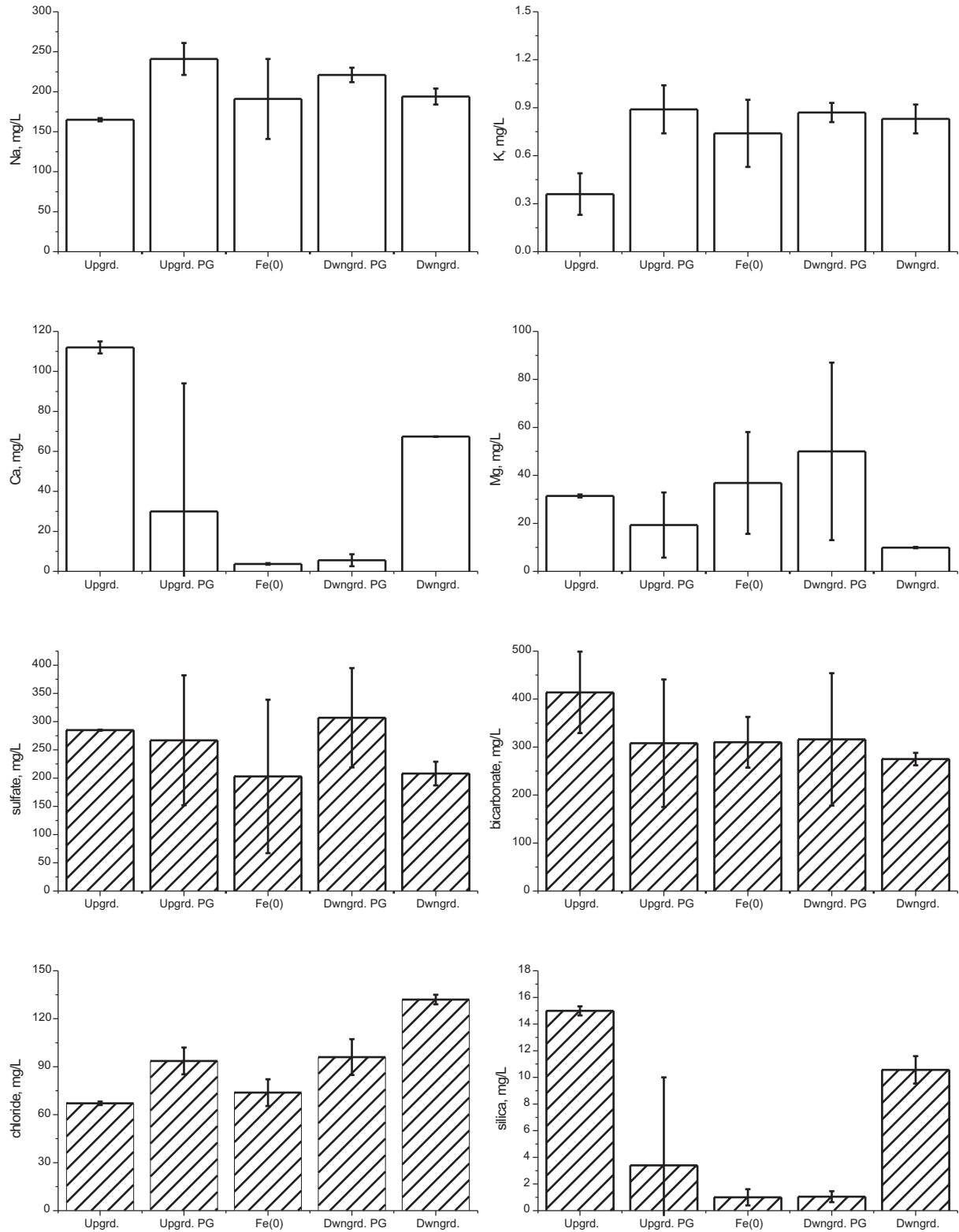


Figure 4.13 Average (± 1 s.d.) concentrations of Na, K, Ca, Mg, sulfate, bicarbonate, chloride, and silica (mg/L) as a function of sampling position in gate 2 at the Denver Federal Center.

DFC Gate 3

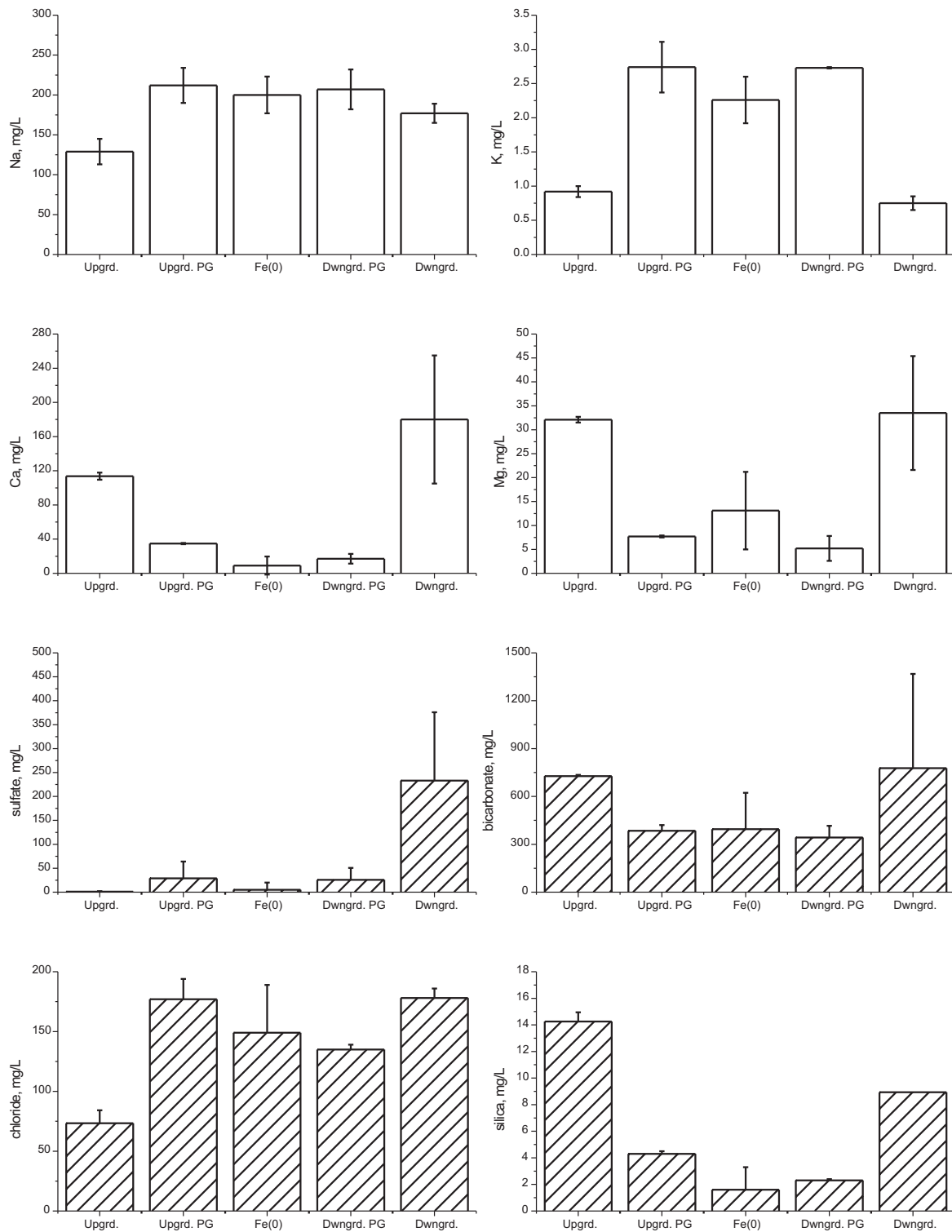


Figure 4.14 Average (± 1 s.d.) concentrations of Na, K, Ca, Mg, sulfate, bicarbonate, chloride, and silica (mg/L) as a function of sampling position in gate 3 at the Denver Federal Center.

In downgradient wells (GSA-20, GSA-25, and GSA-30), concentrations of sodium, calcium, magnesium, and potassium were broadly comparable to those measured in upgradient-monitoring locations (Figures 4.12-4.14). Calcium concentrations are slightly depleted (30% reduction) in downgradient well GSA-25 (gate 2) compared to Ca concentrations in upgradient well GSA-26. In well GSA-30, located downgradient from gate 3, concentrations of sodium and calcium are greater than those in upgradient well GSA-31. As noted previously, specific conductance values are also greater in well GSA-31 compared to well GSA-30 indicating that gate 3 only partially impacts the chemistry of downgradient ground water. Iron concentrations in downgradient monitoring points have always been below 0.5 mg/L (<0.01 mM). Interestingly, influent ground water to gate 3 is elevated in ferrous iron (>15 mg/L), perhaps due to an influence of anoxic bottom waters in Downing Reservoir. Dissolved iron concentrations, however, are expected to decrease within the reactive media due to the corrosion-induced pH increase, consequent development of oversaturated conditions with respect to iron hydroxide precipitates, and iron partitioning into the solid phase.

In contrast to the cationic compositions of ground water collected from upgradient wells at the DFC that show only a moderate amount of variability, anionic compositions are more variable. In gates 1-3, the predominant anion on molar basis is bicarbonate, which ranges in concentration from about 5.9 mM (gate 2) to 11.9 mM (gate 3). Sulfate concentrations are fairly consistent in upgradient wells from gate 1 (2.5 mM) and gate 2 (2.9 mM), but sulfate was not detected in ground water upgradient of gate 3 (<0.01 mM). Chloride concentrations are fairly uniform, ranging from 1.5 mM upgradient of gate 1 to 2.1 mM upgradient of gate 3. Concentrations of nitrate entering the funnel-and-gate system at the DFC are low to below detection limits (<0.03 mM). Alkalinity concentrations are between 26% and 55% lower in the reactive cells than in upgradient sampling wells. Sulfate concentrations are often below detection limits within the reactive cells; however, higher concentrations of sulfate (relative to upgradient points) were observed in wells located within the reactive media of gate 2 in 1999 and 2000 (up to 154% higher). This trend in sulfate concentrations in gate 2 is highly unusual compared to other PRB systems and suggests that some re-oxidation of sulfide precipitates was occurring, perhaps due to infiltration of oxidizing ground water. In 2001, however, the trend in sulfate concentrations in gate 2 reversed, i.e., lower concentrations were detected within the reactive media, but not to the >95% depletion levels typical in gate 1 or at the Elizabeth City PRB as previously described. Nitrate was never detected in mid-wall monitoring wells or in downgradient wells.

Chloride concentrations are significantly higher in downgradient wells compared to upgradient wells. Up to about two times as much chloride is found in downgradient wells GSA-20, GSA-25, and GSA-30 as compared to upgradient wells GSA-21, GSA-26, GSA-31 (Figures 4.12-4.14). Similarly, sulfate concentrations are greater in the downgradient regions of gate 1 and gate 3, whereas concentrations of bicarbonate are lower. In general, the geochemical trends at the DFC are fairly atypical of other PRB sites investigated in the Tri-Agency initiative. Well transects across the various reactive cells do not appear to show geochemical connectivity between upgradient and downgradient regions. As was observed in the contaminant distributions, the geochemistry of downgradient ground water is only partially represented by the chemistries of ground water emerging from the various treatment cells.

4.2 Core Sampling at the Denver Federal Center

Core samples were collected at the DFC from gate 1, gate 2, and gate 3 in July 2000 and 2001. Similar core collection methods to those used at the Elizabeth City site were adopted at the DFC. Core collection methods and analysis procedures are described in Volume 2 of this EPA Report series. In all cases 5 cm inner diameter cores were collected using direct-push methods (Geoprobe™). Angled cores (30° relative to vertical) and vertical cores were collected in order to assess the spatial distribution of mineral/biomass buildup in the reactive media. Prior to pushing the core barrel, an electrical conductivity profile was collected to verify the exact position of the iron/pea gravel interface.

Core materials from the DFC PRB were jet black in color. Cores collected in July 2000 showed no obvious signs of cementation. Several cores collected in July 2001, however, contained sub-spherical welded nodules of iron grains up to about 3 cm in diameter (Figure 4.15). Iron grains from the upgradient interface of DFC gate 2 were noticeably enriched in a black-colored, gel-like material (mixture of biomass and fine-grained mineral precipitates). This core consistency was not observed at other DFC gates or at the Elizabeth City PRB (Figure 4.16).

Immediately after collection, the cores were frozen and shipped back to the Ground Water and Ecosystems Restoration Division in Ada, OK for sub-sampling and analysis. The frozen cores were partially thawed and then placed in an anaerobic chamber maintained with a H₂-N₂ atmosphere. Each core was logged and partitioned into 5 to 10 cm segments. Each segment was homogenized by stirring in the glove box and then split into 4 sub-samples: (1) inorganic carbon analyses, (2) sulfur analyses/X-ray diffraction (XRD), (3) Scanning electron microscopy (SEM)/X-ray photoelectron spectroscopy (XPS) analyses, and, (4) microbial assays (phospholipid fatty acids, PLFA). All sub-samples were retained in airtight vials to prevent any air oxidation of redox-sensitive constituents. Details of analytical methods used to characterize the core materials are presented in Volume 2 of this EPA Report series.

Locations of coring events at the DFC are shown in Figures 4.1-4.3 and information about core recovery, core length, and depth of core penetration is presented in Table 4.1. Cores collected from the upgradient aquifer/iron region generally penetrated the PRB at depths of 4.5 to 6.5 m below ground surface.



Figure 4.15 Picture showing cemented nodules recovered from a gate 1 core collected at the Denver Federal Center (core C1-1-71701).



Figure 4.16 Picture showing the appearance of a core collected at the Denver Federal Center, from gate 2 near the upgradient pea gravel/iron interface.

Table 4.1. Cores collected for analysis at the Denver Federal Center PRB

Sample ID	Location	Date	Angle	Core length cm	Recovery %	Depth to Fe m bgs
C1-1-71701	Upgradient	July-01	30	102	83	5.3
C1-2-71701	Upgradient	July-01	30	79	65	6.3
C1-3-71701	Upgradient	July-01	30	81	67	5.3
C1-4-71801	Downgradient	July-01	30	112	92	5.3
C2-1-71801	Upgradient	July-01	30	117	96	5.8
C2-3-71801	Upgradient	July-01	30	97	79	5.8
C2-4-71801	Upgradient	July-01	30	97	79	6.1
C2-1-71901	Vertical	July-01	90	114	94	4.2
C2-2-71901	Vertical	July-01	90	107	88	4.2
C2-3-71901	Vertical	July-01	90	91	69	4.2
C3-2-71801	Upgradient	July-01	30	81	67	5.5
C1-2-71000	Upgradient	July-00	30	82	73	4.8
C1-3-71100	Downgradient	July-00	30	81	69	5.3
C2-17-71300	Upgradient	July-00	30	43	71	5.8
C2-16-71300	Downgradient	July-00	30	28	46	4.3
C2-12-71300	Vertical	July-00	90	102	83	4.2
C2-13-71300	Vertical	July-00	90	91	75	4.2
C2-14-71300	Vertical	July-00	90	71	62	4.2

Notes: All gate 2 and gate 3 cores (C2, C3) were collected by pushing the core barrel from the downgradient side of the reactive barrier. Depth to iron is the depth below ground surface in meters at which zero-valent iron was intercepted. The percent recovery was calculated as (length compacted core/push length)x100.

4.2.1 Carbon Analysis

Results of all carbon analyses of DFC core materials ($n = 251$) are presented in Table A3 (Appendix A). Concentrations of inorganic carbon within >95% iron samples range from about 10 to 11,600 $\mu\text{g/g}$. In all cases the highest concentrations were found in samples collected adjacent to the upgradient or downgradient pea gravel/iron interfaces and the lowest concentrations were detected near the center regions of the iron gates.

The concentration distribution of inorganic carbon in cores collected from DFC gate 1 is shown in Figure 4.17. The maximum concentration near the upgradient edge of gate 1 was observed in core C1-1-71701 (8700 $\mu\text{g/g}$) in material that contained a mixture of Fe^0 and pea gravel (Figure 4.17). A concretion was recovered in this core at the location corresponding to the maximum carbonate concentration (Figure 4.17). Inorganic carbon concentrations fell below 300 $\mu\text{g/g}$ in gate 1 at horizontal penetration depths >25 cm. Core materials were not collected from the mid-barrier regions, but the trends shown in Figure 4.17 suggest that carbonate accumulation near the center of the iron wall is negligible. Surprisingly, elevated inorganic carbon concentrations were observed in two cores collected at the downgradient pea gravel/ Fe^0 interface region (Figure 4.17). Concentrations in core C1-4-71801 were even higher than those detected near the upgradient region of the reactive media. Concretions up to 2-cm in diameter were recovered in samples that contained between about 8,000 and 11,600 $\mu\text{g/g}$ inorganic carbon.

Gate 2 shows trends in inorganic carbon concentrations that are similar to those observed in gate 1. Concentrations as high as 7,700 $\mu\text{g/g}$ were detected in core C2-3-71801; concretions were also identified in this core (Figure 4.18). Vertical cores were collected in gate 2 (C2-1-71901, C2-2-71901, and C2-3-71901) to examine the depth-dependent distribution of carbon and sulfur accumulation in the reactive media. The vertical sampling position was located approximately 15 cm downgradient of the upgradient pea gravel- Fe^0 interface (Figure 4.2). Results show that there is a depth interval between about 5.5 m and 8.0 m below ground surface where very little inorganic carbon accumulation is occurring (Figure 4.19); significant amounts of carbonate precipitation has occurred only near the bottom and the top of the reactive zone. The implication of this trend, which is also mirrored in the concentration profiles of sulfur and microbial biomass, is that little ground water is entering gate 2 over the depth interval from about 5.5 m to 8 m below ground surface. Flow would appear to be occurring near the very top and the bottom of the reactive cell. This result could help explain the anomalous behavior of this gate with respect to contaminant removal performance.

4.2.2 Sulfur Analysis

Results of sulfur analyses of DFC core materials strongly correlate with the inorganic carbon results (Figures 4.20-4.21). Concentrations of sulfur in core materials from the DFC range from about 100 $\mu\text{g/g}$ to 7,500 $\mu\text{g/g}$ (Table A3). Chemical extractions indicate that over 90% of the total sulfur present in the core materials is as sulfide, in acid-volatile sulfide materials such as poorly crystalline to crystalline mackinawite (Table A2; Wilkin et al., 2003). The remaining sulfur is likely present as iron disulfides (pyrite) and perhaps as sulfate associated with iron corrosion products (Furukawa et al., 2002). Figure 4.22 shows the good correlation between concentrations of carbon and sulfur in the solid phase in cores collected from the Elizabeth City and Denver Federal Center PRBs. The average S/C ratio in core materials from the DFC is about 0.42, which is slightly greater than the S/C ratio observed in Elizabeth City core materials (S/C=0.33). The difference is apparently related to a higher average ground-water S/C ratio at the Denver Federal Center site compared to the Elizabeth City site.

4.2.3 X-ray Diffraction Analysis

Powder X-ray diffraction scans for samples from DFC core C2-3-71801, collected in 2001, are shown in Figure 4.23. Materials for analysis were obtained by sonicating iron core samples in acetone for 10 minutes followed by collection of the released particulates on a 0.2-micron filter paper (polycarbonate). The separated particles were then mounted on a zero-background quartz plate and scanned with Cu K_α radiation from 3° to 80° 2-theta using a Rigaku Miniflex Diffractometer.

A summary of the XRD analysis results is reported in Table 4.2. Qualitative abundances of the mineral phases identified are reported based upon observed peak intensities (Table 4.2). Magnetite (Fe_3O_4) and iron carbonate hydroxide were observed in every iron core sample. Graphite and quartz were detected in one of the samples (C2-3-71801-3). Aragonite (CaCO_3) was not detected in the diffraction analysis, although the presence of calcite was confirmed using XRD, SEM and optical microscopy. Using micro-analytical diffraction methods, Furukawa et al. (2002) also detected quantities of mackinawite, greigite, ferrihydrite, and goethite in core materials collected from the DFC.

4.2.4 Scanning Electron Microscopy

SEM photomicrographs for three samples from the DFC collected in July 2000 are shown in Figure 4.24. These samples were retrieved from near the upgradient pea gravel/iron interface region from gate 2 (C2-17-71300-2, horizontal penetration ~4 cm; Figure 4.24a, C2-17-71300-7, horizontal penetration ~16 cm; Figure 4.24b) and gate 1 (C1-2-71000-3, horizontal penetration ~6 cm; Figure 4.24c). The SEM micrographs in Figure 4.24 are representative of particles contained in each of the samples and capture a range of magnifications from about 50x to 2000x.

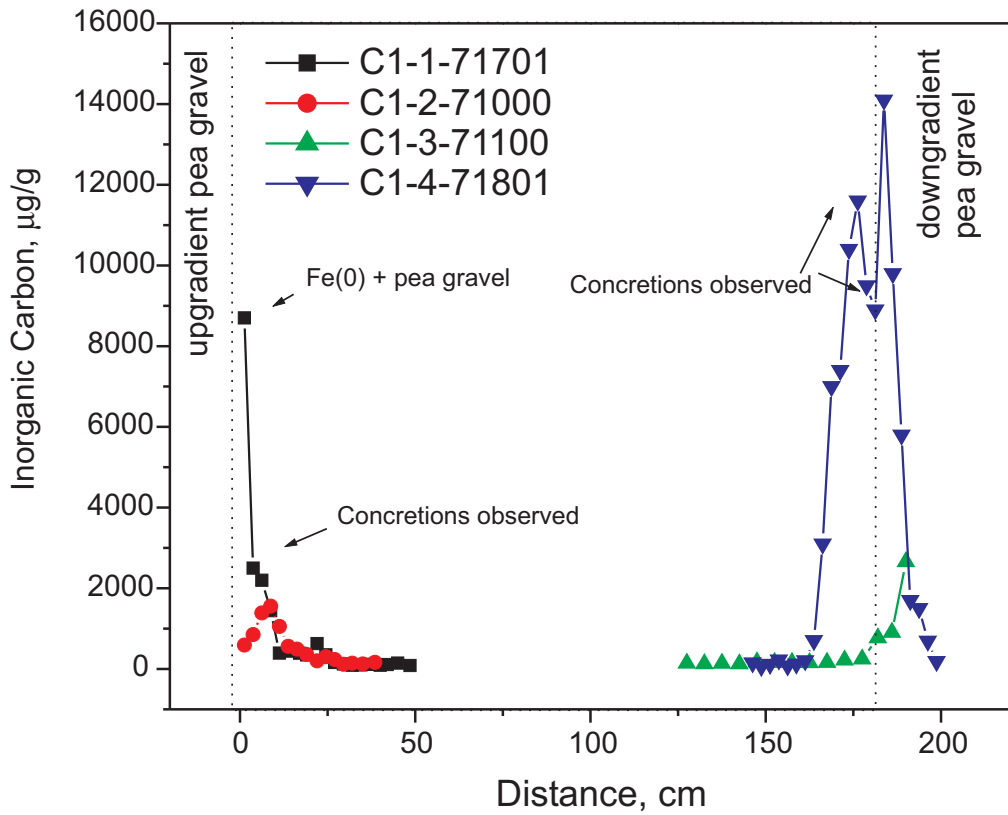


Figure 4.17 Concentration distribution of solid phase inorganic carbon in angle cores collected from gate 1 at the Denver Federal Center.

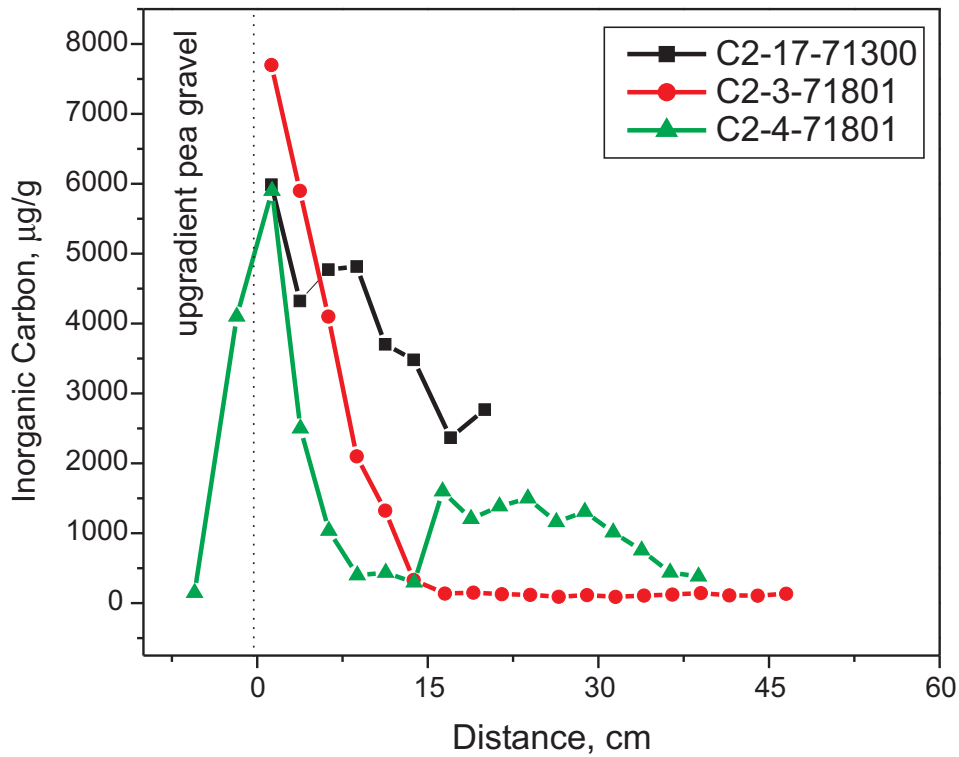


Figure 4.18 Concentration distribution of solid phase inorganic carbon in angle cores collected from gate 2 at the Denver Federal Center.

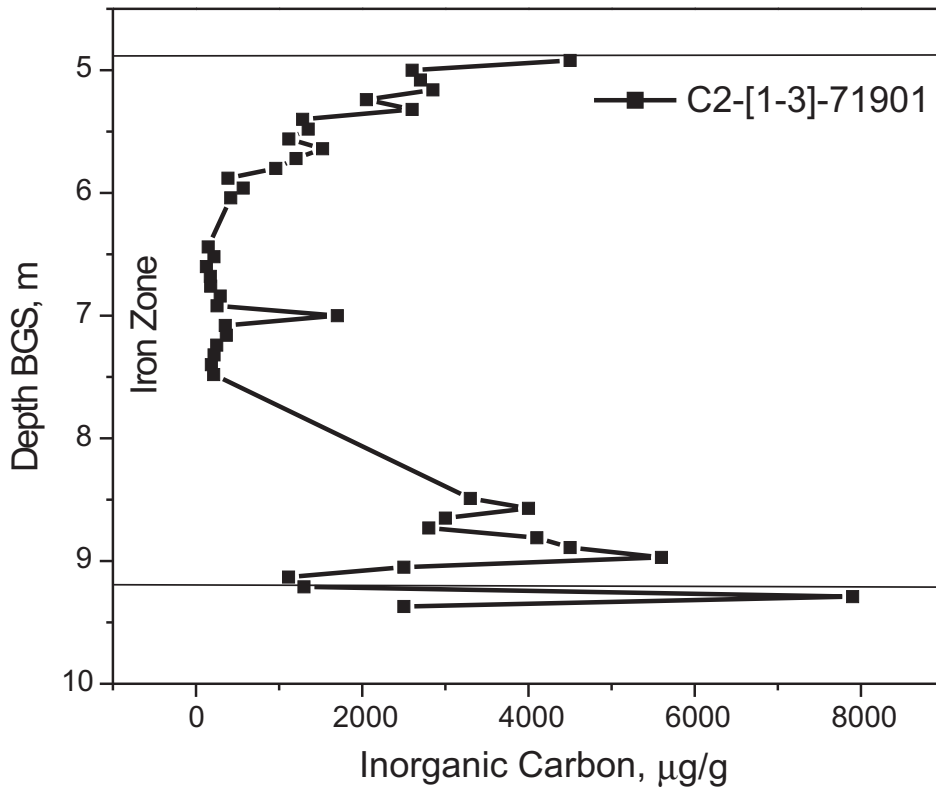


Figure 4.19 Concentration distribution of solid phase inorganic carbon in a vertical core collected from gate 2 at the Denver Federal Center.

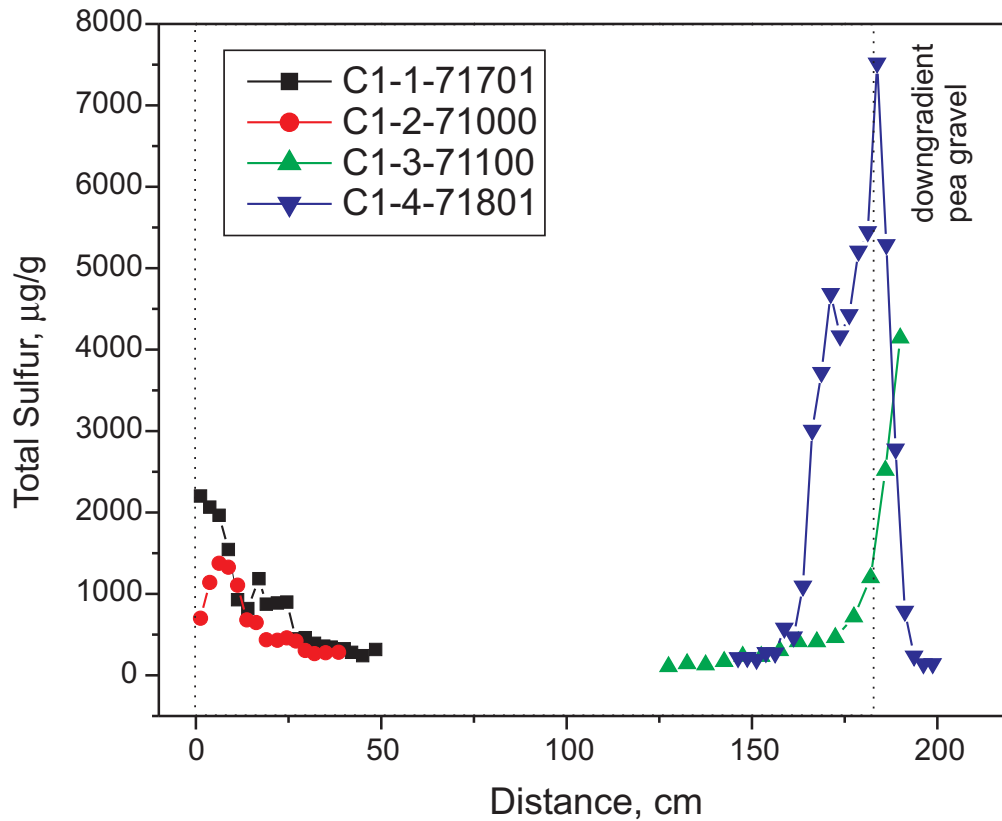


Figure 4.20 Concentration distribution of solid phase sulfur in angle cores collected from gate 1 at the Denver Federal Center.

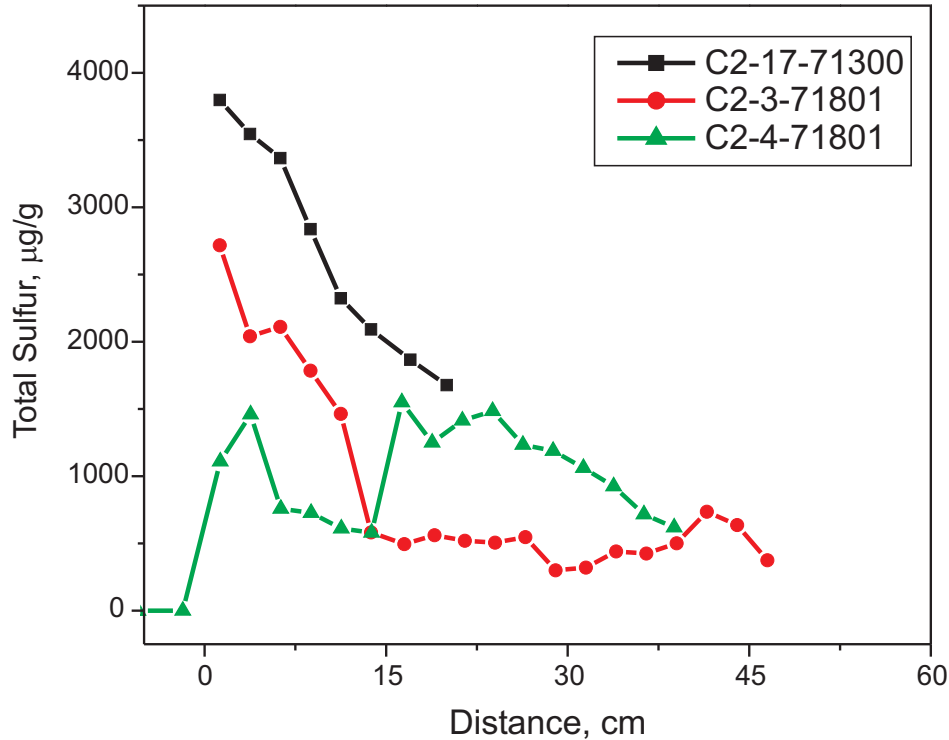


Figure 4.21 Concentration distribution of solid phase sulfur in angle cores collected from gate 2 at the Denver Federal Center.

Sample C2-17-71300-2, collected from a region near the upgradient interface in gate 2, shows a fairly regular accumulation of mineral precipitates on the iron surfaces (Figure 4.24a). The thickness of the surface coating ranges from about 10 μm to 100 μm . This precipitate accumulation took place over the initial four years of operation of the PRB, or at a rate of about 3 to 25 μm per year, similar to the average linear rate of precipitate accumulation observed at the Elizabeth City site. As noted before, ground-water chemistry is different between these two sites as is the total mass of mineral precipitate accumulation. Rates of inorganic carbon and sulfur accumulation are between 2 and 10 times greater within the DFC reactive media as compared to the Elizabeth City reactive media (Wilkin et al., 2003). The similar average thickness of mineral precipitates found on iron grains near the upgradient edge at the two sites suggests that mineral precipitation at the DFC must occur over a wider range of penetration depths, i.e., with time a mineral precipitate front moves through the reactive barrier.

The DFC samples contain a significant proportion of free grains, grains not directly bound to the iron surfaces (Figure 4.24a). In all cases, these large free grains (up to 300 μm in diameter) are composed of calcium carbonate. At greater horizontal penetration depths in gate 2, surface coatings were thinner, 10 to 50 μm , but the abundance of free calcium carbonate grains persisted (Figure 4.24b). It cannot be determined conclusively whether the free grains actually grew within pore spaces, or whether they were at one point attached to the iron surfaces, but were subsequently detached, for example, during vibratory coring or during sample handling. In gate 2, surface coverage and particle morphologies are similar to those observed in gate 1 (Figure 4.24c). The micrographs clearly reveal an abundance of calcium carbonate grains associated with the iron surfaces.

Energy dispersive X-ray analyses of iron grains from the DFC (Table 4.3) indicate the presence of iron (~97 wt%), silicon (~2.3%), and to some extent Mn (<1.1 wt%) and Cr (<1.2 wt%). Oxygen was not detected on freshly polished surfaces of zero-valent iron. The compositions of Ca- and O-rich grains (presumably calcium carbonate) associated with iron surfaces are identical to those found as free grains (Table 4.3). These particles appear to be enriched in calcium compared to ideal CaCO_3 (40.0 wt% Ca), and this is probably related to quantitative inaccuracies of the EDX method. Surface precipitates, i.e., materials that are generally fine-grained and coat the iron surfaces, are enriched in oxygen and depleted in iron, respectively, compared to the composition of fresh zero-valent iron (Table 4.3). In addition to iron and

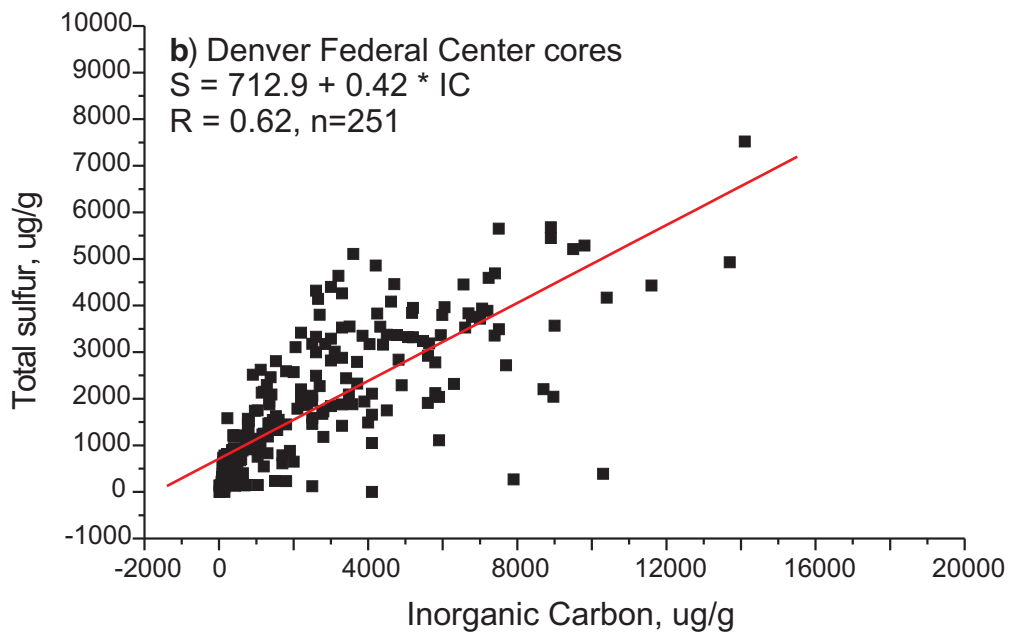
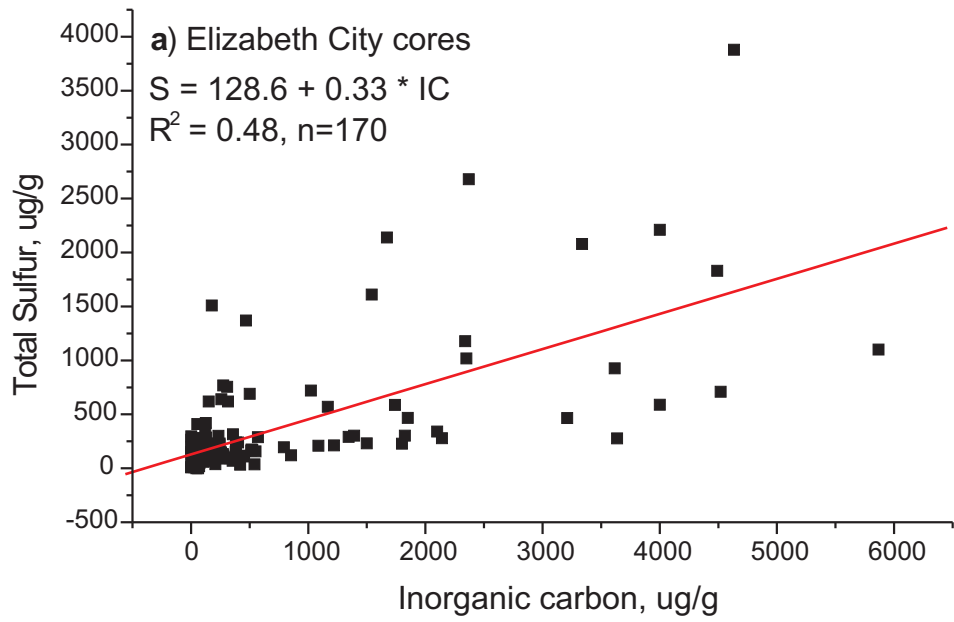


Figure 4.22 Inorganic carbon concentrations versus total sulfur: a) Elizabeth City core materials; b) Denver Federal Center core materials.

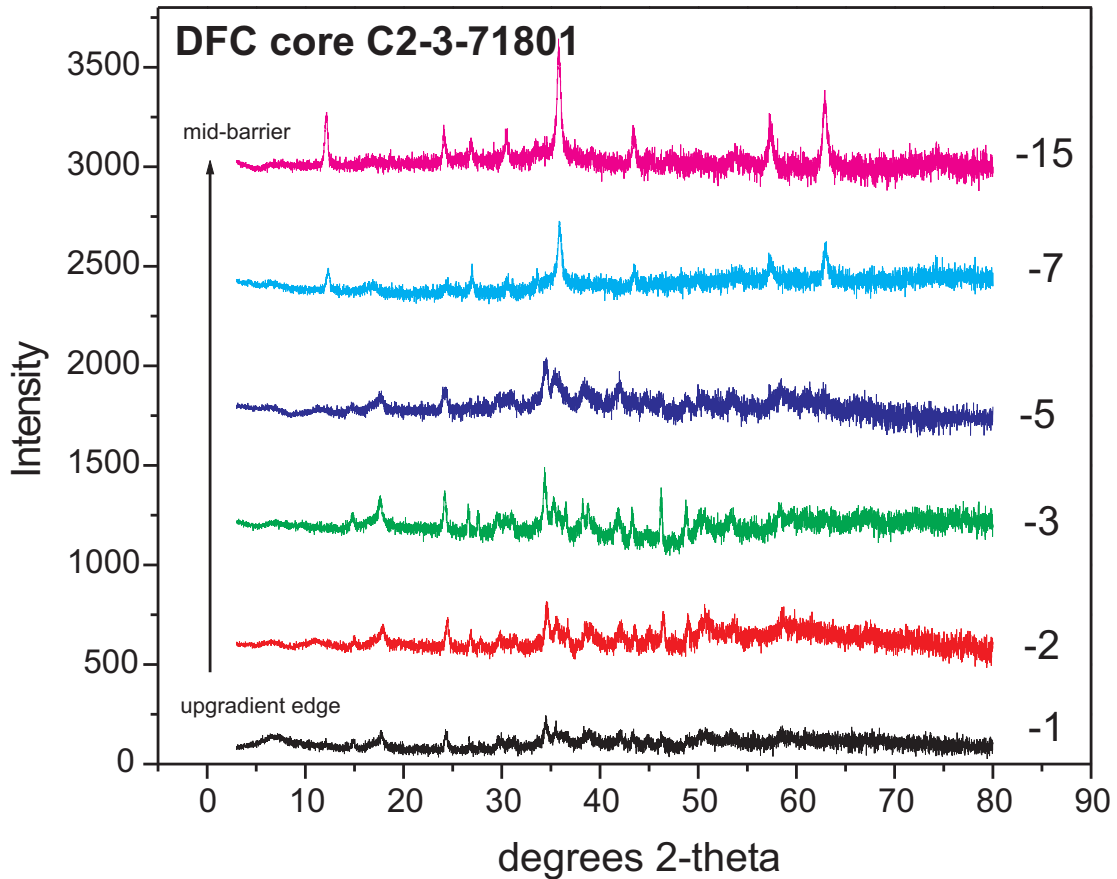


Figure 4.23 Powder X-ray diffraction data from fine-grained materials removed via sonication from cores collected at the Denver Federal Center PRB (core C2-3-71801).

Table 4.2. Results of Powder X-ray Diffraction Analysis of Core Materials from the Denver Federal Center PRB

Sample	Major Component	Minor Component	Trace Component
C2-3-71801-1	Magnetite, Iron carbonate hydroxide	Green rust 1, Calcite	
C2-3-71801-2	Magnetite, Iron carbonate hydroxide	Mackinawite, Calcite	Goethite
C2-3-71801-3	Magnetite, Iron carbonate hydroxide	Mackinawite, Calcite	Quartz, Graphite
C2-3-71801-5	Magnetite, Iron carbonate hydroxide	Mackinawite, Calcite	
C2-3-71801-7	Magnetite, Iron carbonate hydroxide	Mackinawite, Calcite	
C2-3-71801-15	Magnetite, Iron carbonate hydroxide	Calcite	

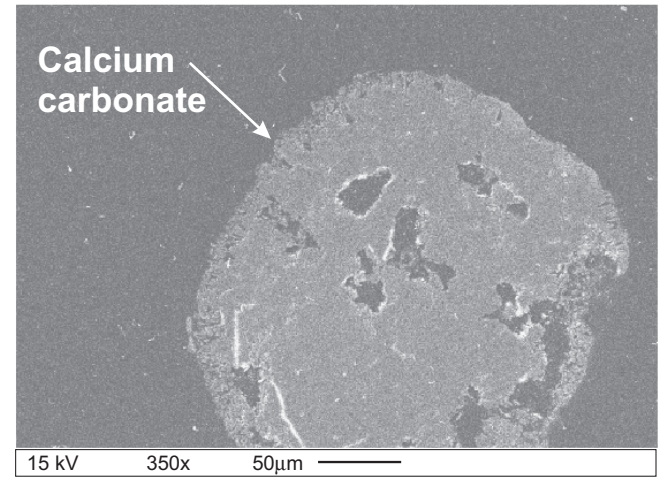
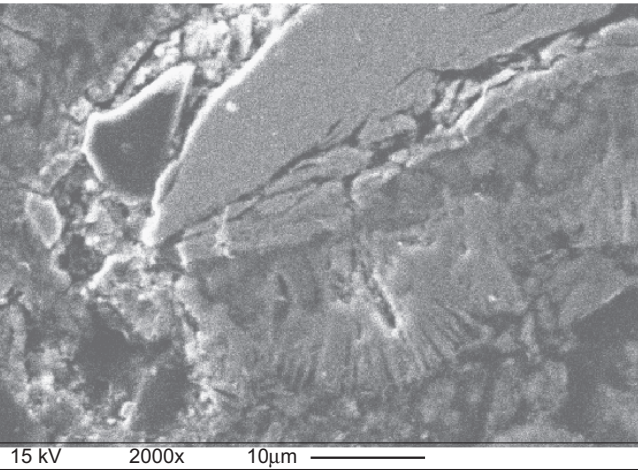
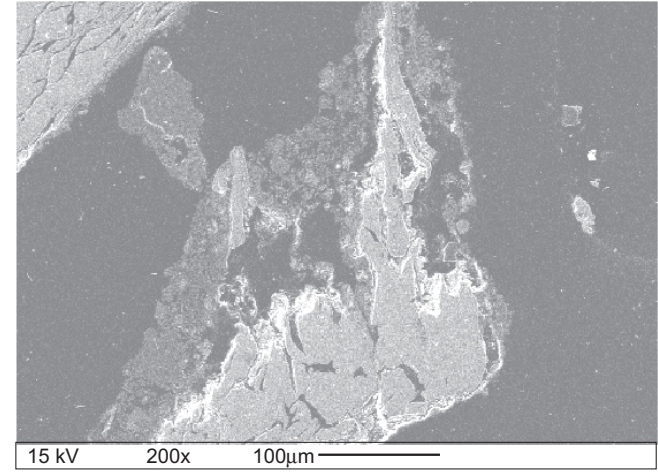
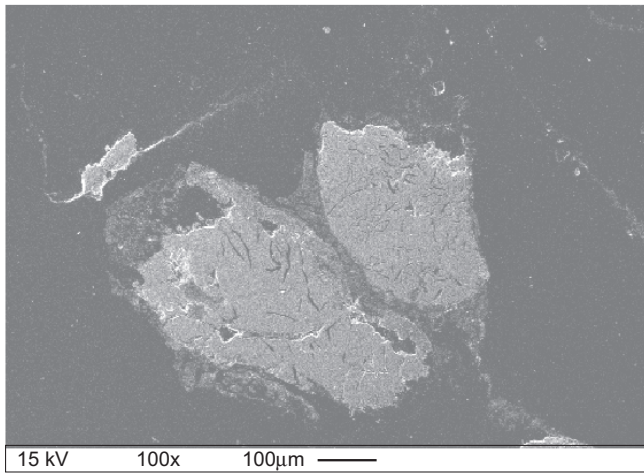
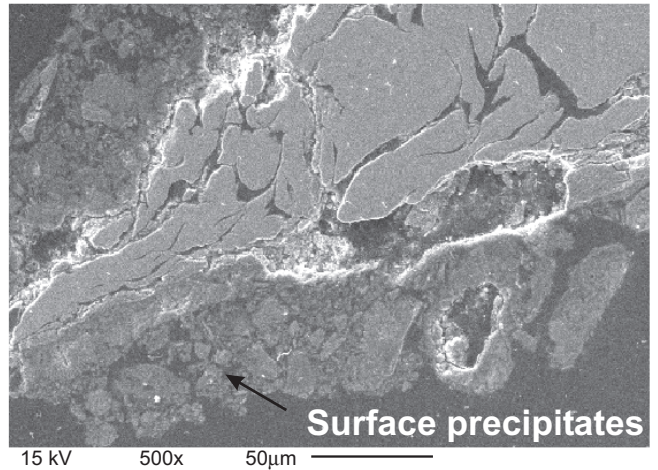
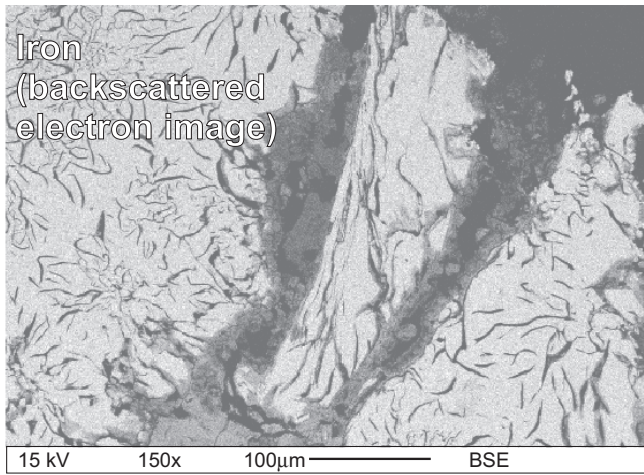


Figure 4.24 Scanning electron micrographs of samples from the Denver Federal Center PRB: a) sample C2-17-71300-2 located near the upgradient edge of gate 2; b) sample C2-17-71300-7 located in a midbarrier region of gate 2; and, c) sample C1-2-71000-3 located near the upgradient edge of gate 1.

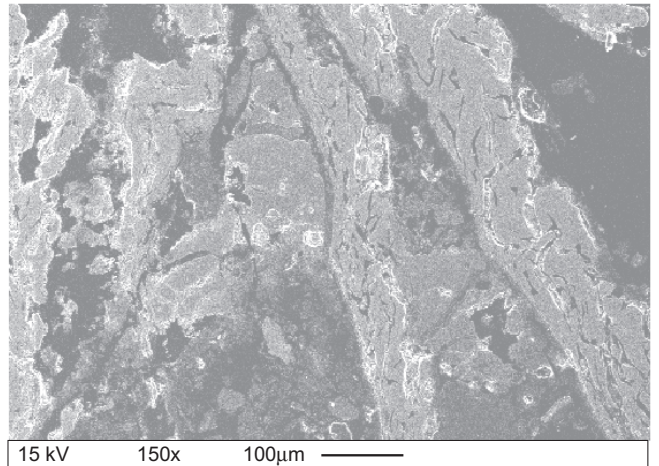
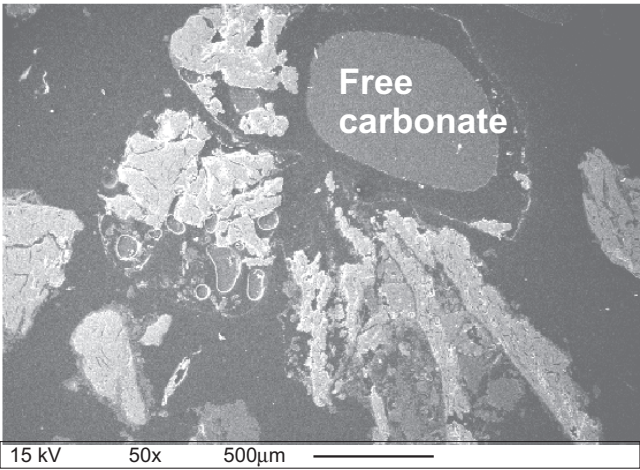
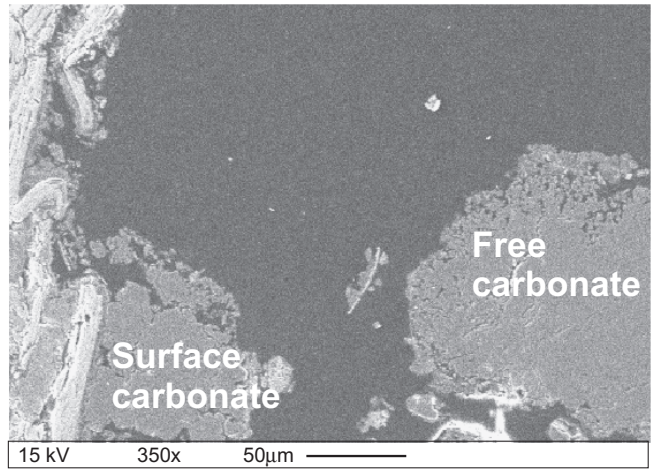
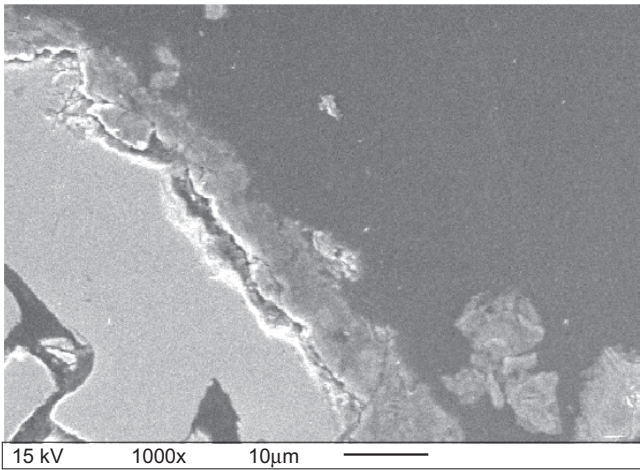
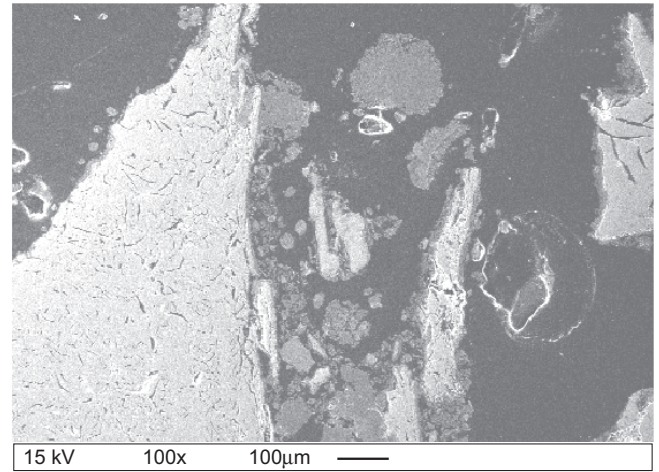
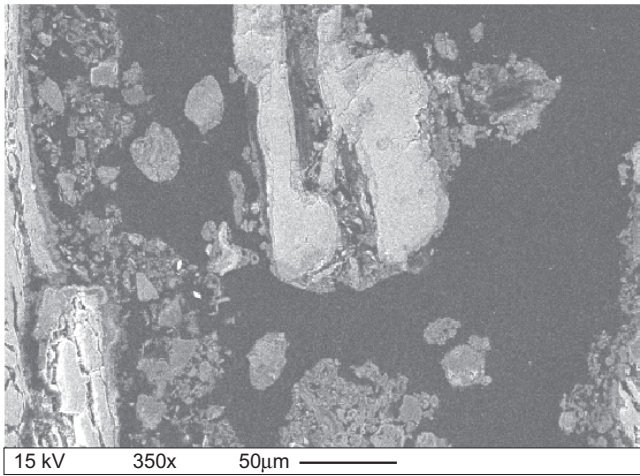


Figure 4.24 (continued) Scanning electron micrographs of samples from the Denver Federal Center PRB: a) sample C2-17-71300-2 located near the upgradient edge of gate 2; b) sample C2-17-71300-7 located in a midbarrier region of gate 2; and, c) sample C1-2-71000-3 located near the upgradient edge of gate 1.

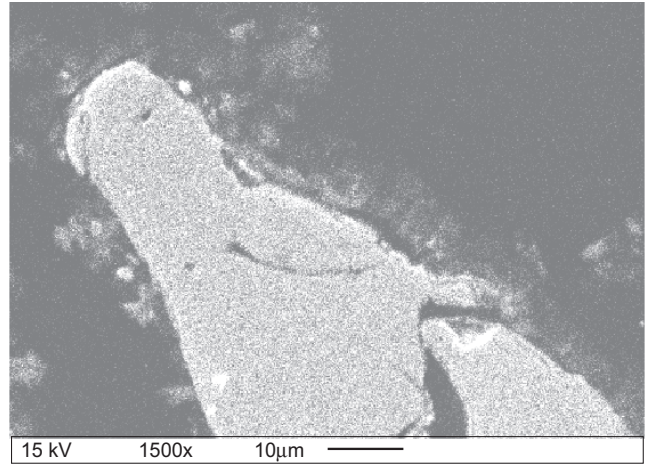
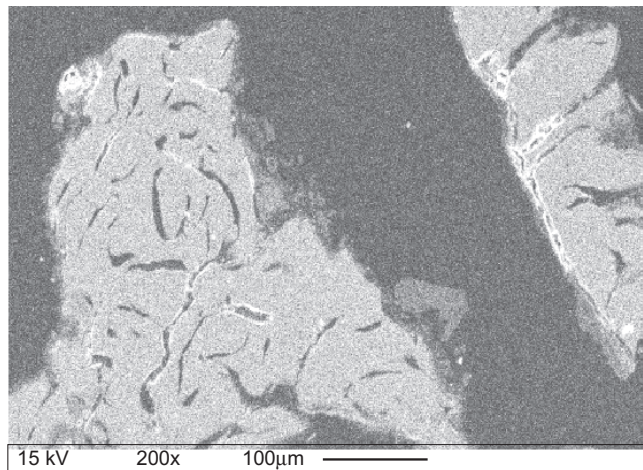
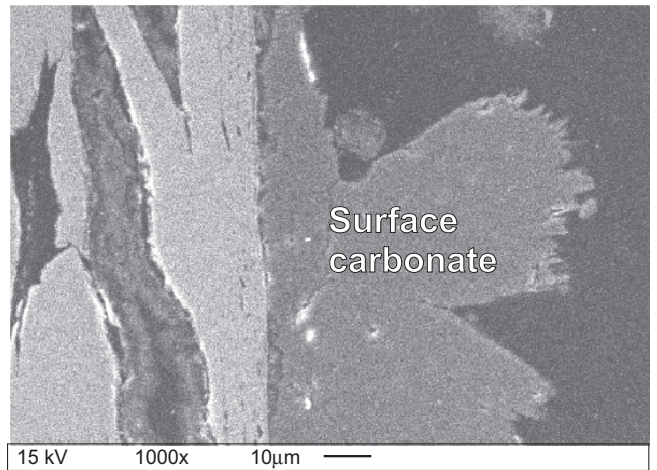
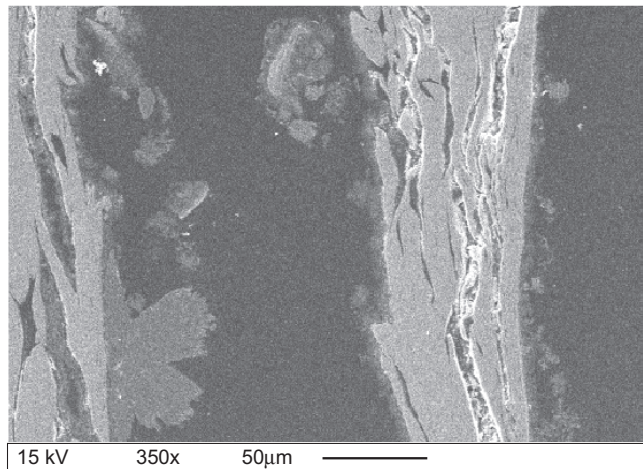
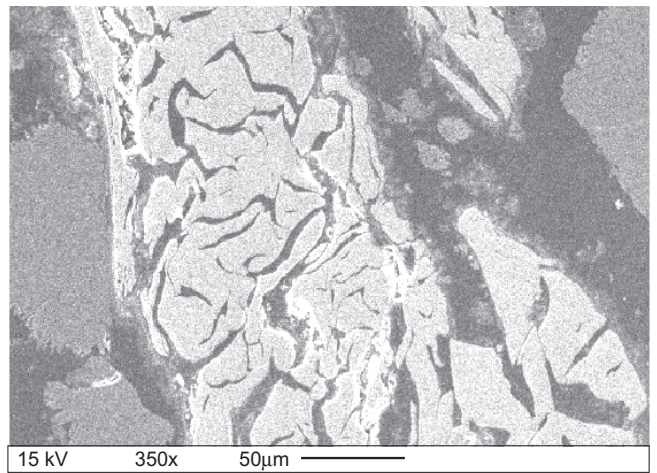
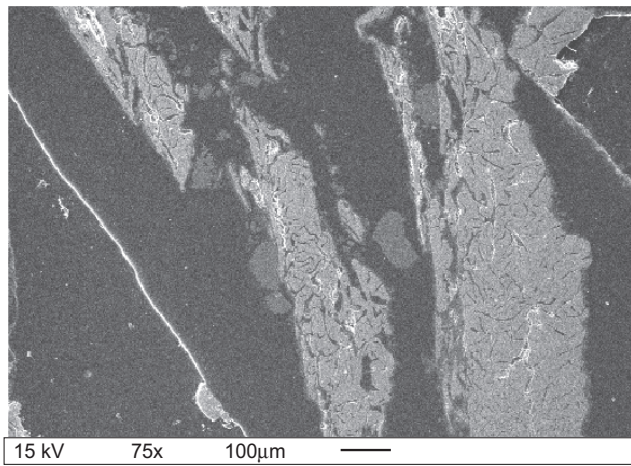


Figure 4.24 (continued) Scanning electron micrographs of samples from the Denver Federal Center PRB: a) sample C2-17-71300-2 located near the upgradient edge of gate 2; b) sample C2-17-71300-7 located in a midbarrier region of gate 2; and, c) sample C1-2-71000-3 located near the upgradient edge of gate 1.

Table 4.3. Results of SEM-EDX Analysis of Core Materials from the Denver Federal Center PRB

	Fe (wt%)	O (wt%)	S (wt%)	Mn (wt%)	Cr (wt%)	Ca (wt%)	Mg (wt%)	Si (wt%)
Iron (n=25)	97.4 (±0.7)	not detected	not detected	0.15 (±0.14)	0.3	not detected	not detected	2.30 (±0.4)
Ca-rich precipitates, on iron surfaces (n=23)	0.2	54.7 (±3.5)	not detected	not detected	not detected	44.5 (±3.4)	not detected	not detected
Ca-rich precipitates, free (n=11)	not detected	54.8 (±1.5)	not detected	not detected	not detected	44.6 (±1.9)	not detected	not detected
Surface precipitates (n=57)	58.3 (±10.5)	31.6 (±5.5)	3.9 (±3.0)	0.34 (±0.7)	0.04	1.2 (±5.2)	0.11 (±0.3)	3.89 (±3.0)

oxygen, the surface precipitates also contain silicon (3.4 ± 1.9 wt%, n=58), sulfur (3.89 ± 3.0 wt%, n=58), manganese (0.34 ± 0.70 wt%, n=58), chromium (0.04 ± 0.2 wt%, n=58), calcium (1.2 ± 5.2 wt%, n=58), and magnesium (0.11 ± 0.30 wt%, n=25). The presence of Ca, Mg, and Si in the surface coatings is consistent with their removal from ground water. Other than CaCO_3 , the identity of mineral species could not be confirmed by using EDX measurements.

4.2.5 Microbial Characterization

Eighty-one samples from 2000 to 2001 were collected at the DFC for phospholipid fatty acid (PLFA) extract characterization. Samples were collected mainly from within the reactive iron media near the upgradient iron/pea gravel interface and near the downgradient iron/pea gravel interface. Samples for PLFA analysis were shipped frozen on dry ice to Microbial Insights (Rockford, Tennessee). The complete PLFA data set for samples from the DFC is shown in Table B2 (Appendix B) and summarized in Table 4.4.

In samples collected at the DFC, biomass contents spanned several orders of magnitude from 15 to 4924 picomoles per gram (dry weight basis), or from about 3.85×10^5 to 9.85×10^7 cells per gram. The highest biomass contents observed in this study were in gate 2 of the DFC, where maximum PLFA concentrations were about 1.5 to 3 times the maximum concentrations observed in DFC gate 1 or in the Elizabeth City PRB.

In gate 1 and gate 2, the highest biomass concentrations were found near the upgradient pea gravel/iron interface region, in the same portion of the reactive media where enrichments in inorganic precipitates are observed (Figure 4.25). This same trend was observed at the Elizabeth City PRB and appears to be repeated at other PRB sites (Gu et al., 2002). Downgradient regions are comparatively depleted in microbial biomass. The lower counts associated with the mid-barrier and downgradient samples suggest that the environment at these locations is more challenging to bacterial growth and survival. Vertically resolved biomass concentrations and total sulfur concentrations from gate 2 are plotted in Figure 4.26. The results parallel those previously shown for inorganic carbon (Figure 4.19). The depth interval between about 5.5 and 8.0 m below ground surface is characterized by low accumulation of sulfur and microbial biomass suggesting stagnant conditions in this portion of gate 2.

PLFA profiles from DFC are typically dominated by fatty acid biomarkers indicative of anaerobic sulfate- or iron-reducing bacteria (Figure 4.27). High proportions of terminally branched and branched monoenoic PLFA specifically indicate anaerobic metabolism. Terminally branched PLFA are typical of Gram-positive bacteria, but can also be present in the cell membranes of some anaerobic Gram-negative bacteria. Because high proportions are present of branched

Table 4.4. Summary of PLFA Data from the Denver Federal Center PRB

	Fe(0) Upgradient DFC - Gate 1	Fe(0) Downgradient DFC – Gate 1	Fe(0) Upgradient DFC - Gate 2	Fe(0) Downgradient DFC - Gate 2
Number of samples	9	9	38	6
Average PLFA concentration (pmoles/g)	841	49	1440	98
PLFA range	95-1904	15-127	50-4924	24-332
PLFA Structural Groups average % (range %)				
Monoenoic Found in Gram-negative bacteria	59.6 (10.1-71.2)	77.4 (9.2-87.8)	52.2 (31.6-85.3)	69.6 (54.9-77.7)
Terminally Branched Saturated Found in many Gram- positive bacteria, and in some Gram-negative bacteria	7.0 (2.7-11.4)	2.1 (<1-6.9)	14.2 (3.4-26.4)	6.8 (3.1-26.4)
Branched Monoenoic Common in obligate anaerobes, such as sulfate-reducing and iron-reducing bacteria	8.3 (2.0-11.1)	3.7 (<1-8.9)	10.1 (<1-16.5)	2.6 (<1-8.4)
Mid-Chain Branched Saturated Common in actinomycetes and sulfate-reducing bacteria	4.2 (1.7-6.2)	1.3 (<1-4.7)	6.1 (<1-22.2)	2.4 (<1-10.6)
Normal Saturated Ubiquitous in prokaryotes and eukaryotes	18.5 (4.6-23.2)	12.2 (3.8-17.3)	15.4 (8.9-30.6)	11.2 (8.6-13.2)
Polyenoic Found in fungi, protozoa, algae, higher plants, and animals	2.4 (0.2-6.7)	3.3 (<1-9.4)	2.0 (<1-8.2)	7.4 (1.7-18.4)

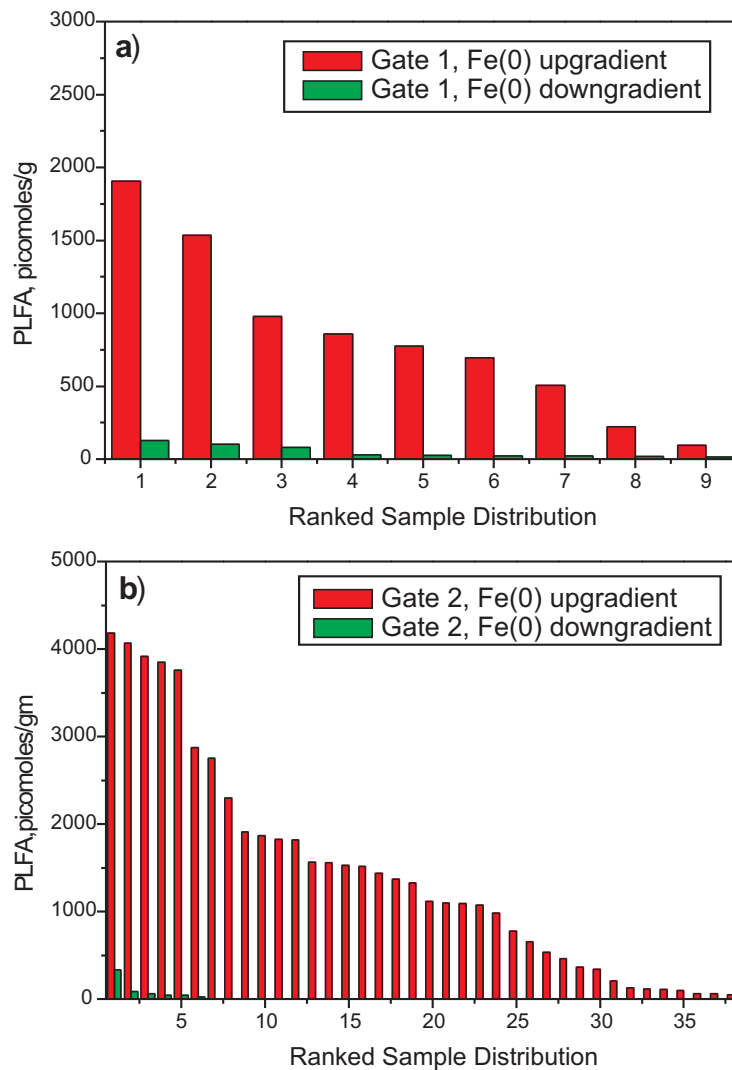


Figure 4.25 Ranked concentration distribution of microbial biomass (from Denver Federal Center PLFA data) in iron from near the upgradient pea gravel/iron interface and iron from near the downgradient pea gravel/iron interface: a) gate 1; b) gate 2.

monoenoic PLFA indicative of anaerobic metal reducing bacteria, the terminally branched PLFA are likely to be mainly from sulfate- or iron-reducing bacteria. Where biomass is most concentrated (i.e., near the upgradient pea gravel/iron interface), the distribution of PLFA overall appears to be distinct from the PLFA distribution observed in regions further downgradient (Figure 4.27). Near the upgradient pea gravel/iron interface, the proportion is greater of branched monoenoic PLFA and PLFA indicative of sulfate-reducing bacteria compared to the PLFA signature of materials collected at the downgradient pea gravel/iron interface (Figure 4.27).

4.3 Summary of Results from the Denver Federal Center Site

The Denver Federal Center permeable reactive barrier is a funnel-and-gate system with four reactive gates, each separated by up to about 120 m of metal sheet pile. In this study, ground-water sampling, core collection, and solid phase characterization studies were carried out in gates 1, 2, and 3. After five years of operation, gate 1 and gate 3 have been effective in significantly decreasing concentrations of TCE, 1,1,1-TCA, 1,1-DCE, and cis-DCE from influent ground water. A noticeable clean ground-water front is identifiable in the downgradient aquifer near gate 1. The performance of gate 2 has been more difficult to assess, in part, because of an apparent source of residual bedrock TCE contamination

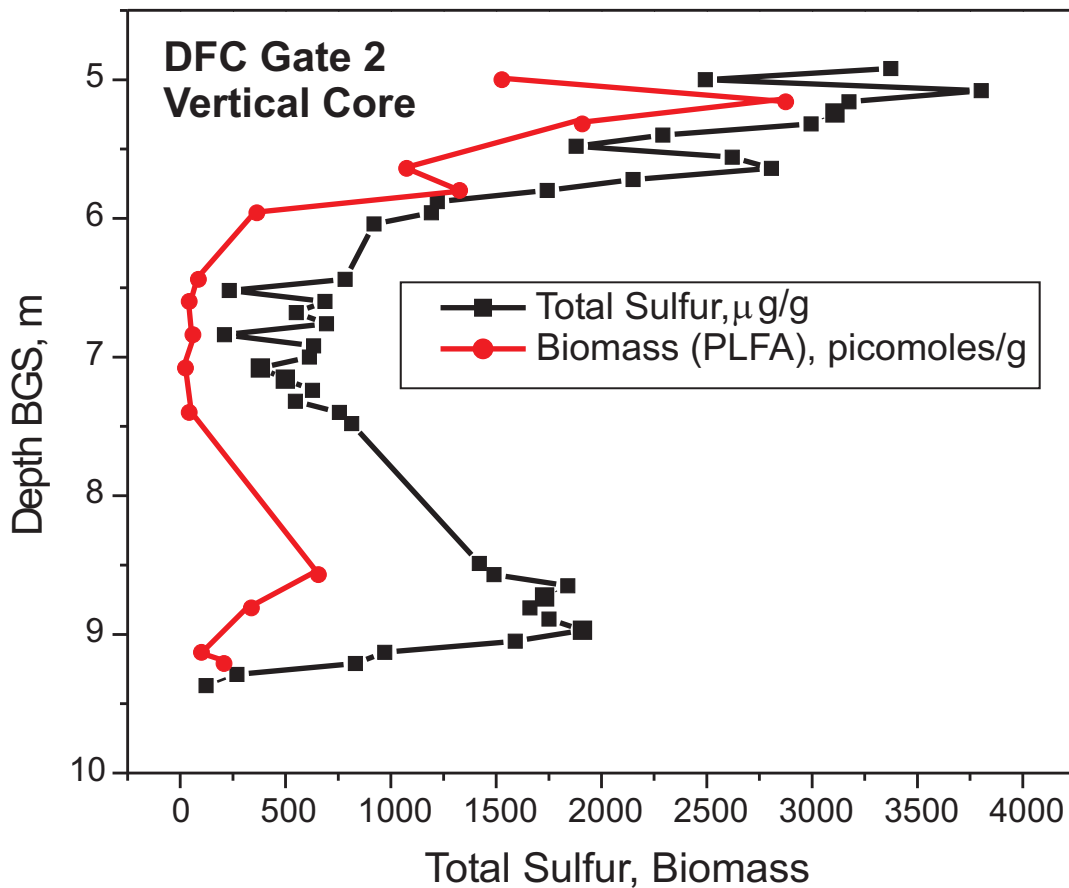
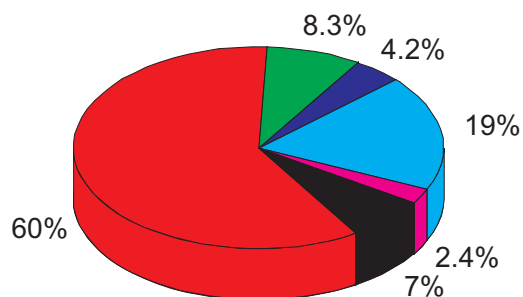


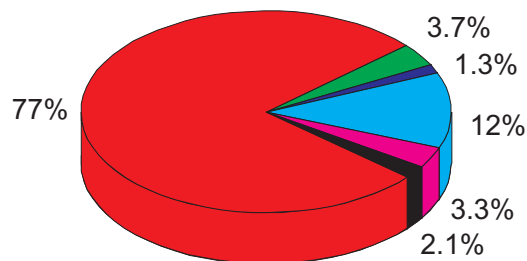
Figure 4.26 Concentration distribution of solid phase sulfur and microbial biomass (from PLFA data) in a vertical core collected from gate 2 at the Denver Federal Center (vertical cores C2-1-71901, C2-2-71901, and C2-3-71901).

located just downgradient of gate 2 and because of the large hydraulic head differential across the gate. Concentrations of volatile organic compounds in gate 2, especially 1,1-DCE, have shown increases with time. Results of the Denver Federal Center site study are summarized below:

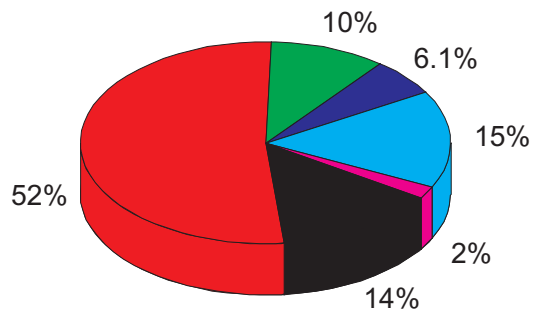
- Trends in pH in gates 1, 2, and 3 were fairly consistent from May 1999 to July 2001. There is some indication that pH in the iron zone is slowly increasing with time, perhaps due to increasing residence time. Measurements of Eh and hydrogen gas concentrations indicate consistent reducing conditions in gates 1 and 3. Gate 2 shows evidence of having decreased reducing potential, based on increased Eh and decreasing hydrogen gas concentrations.
- The reactive gates at the Denver Federal Center have removed most of the dissolved calcium, magnesium, sulfate, and silicon in the water flowing through the PRB. Levels of alkalinity and total dissolved solids were reduced. Ground water from the DFC is comparatively (~3x) more enriched in concentrations of total dissolved solids compared to ground water from the Elizabeth City site. Consequently, more mineral precipitate mass has accumulated over five years in the DFC gates compared to the Elizabeth City PRB. After five years, core sampling revealed the presence of cemented iron nodules in some of the cores collected at the DFC.
- Mineralogical characterization of soil cores indicates the formation in the iron gates of calcite, iron carbonate hydroxide, magnetite, mackinawite, carbonate green rust, and goethite. Overall, this assemblage of mineral precipitates is very similar to that observed at the Elizabeth City site and at other PRB installations. Mineral



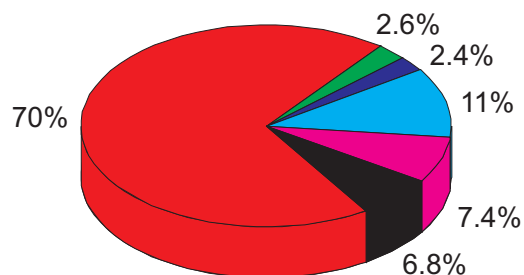
Gate 1 upgradient



Gate 1 downgradient



Gate 2 upgradient



Gate 2 downgradient

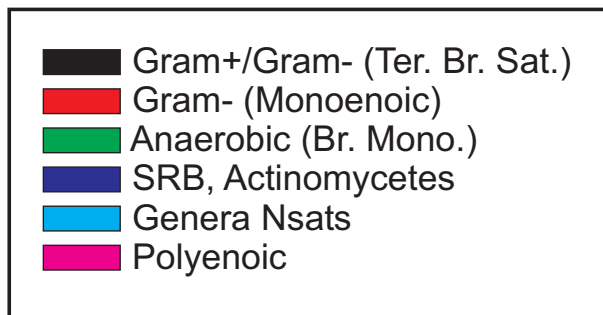


Figure 4.27 Pie graphs showing average structural distribution of PLFA compounds in Iron core materials from the Denver Federal Center.

precipitates are enriched in gate 1 and gate 2 at both the upgradient and downgradient edges of the reactive medium. After five years of operation, up to 50% of the available pore space has been lost due to infilling of mineral precipitates near the leading edges of the iron treatment zones. The high infilling rate has led to partial cementation of the iron zone. Because of the high influent TDS concentrations and rates of mineralization, hydraulic performance of the system is expected to degrade over the next five years.

- Vertical coring in gate 2 reveals a zone from 5.5 to 8 m below ground surface with little mineral or microbial biomass accumulation, suggesting a substantial zone of reduced flow through the PRB. This reduced flow zone may be related to the low permeability zone or smear zone that developed during construction of the gate.
- Microbiological results, based on PLFA analyses, indicate enriched biomass in gate 2 of the Denver Federal Center (up to 9.85×10^7 cell/g). Biomass concentrations in gate 2 were a factor of about 2x greater compared to gates 1 and 3, and the Elizabeth City PRB. The higher biomass concentrations may be linked to low-flow conditions in the gate and high sulfate concentrations. Concentrations of iron sulfide precipitates are also comparatively high in gate 2 of the DFC (up to 5650 $\mu\text{g/g}$). Gram-negative bacteria dominate the microbial community. Present in the iron samples are elevated proportions of biomarkers indicative of metal-reducing and sulfate-reducing bacteria.



5.0 Factors Affecting Longevity and Performance

Permeable Reactive Barriers are principally designed to remove contaminants from ground water, yet it has been shown that zero-valent iron reactive barriers are long-term sinks for other dissolved components in ground water. In particular, inorganic carbon, sulfate, calcium, magnesium, nitrate, and silica are either entirely or partially removed from influent waters to PRBs. Removal processes for inorganic constituents include mineral precipitation, adsorption, and biochemical transformation. Mineral precipitation, in particular, can lead to changes in porosity and permeability, or both, in addition to affecting the reactivity of zero-valent iron media by forming coatings on the reactive grains. In this way, geochemical reaction processes can have an effect on the hydraulic and reactive performance of PRB systems. A major research effort, therefore, has gone into 1) identifying the nature of element removal processes in PRBs, 2) linking these processes to site geochemistry and hydrogeology, and 3) linking these processes to declining remedial performance. Considerable progress has been made on the first question relating to identifying element removal process. Observations from numerous PRB installations and laboratory studies are used below to develop a framework for understanding how ground-water chemistry may be evaluated for the purpose of predicting longevity and barrier performance through time. This framework will be useful in constructing remedial designs and in developing performance-monitoring programs.

Iron metal dissolution, microbial sulfate reduction, microbial nitrate reduction, adsorption, gas production, and mineral precipitation (oxides, hydroxides, carbonates, and sulfides) are processes that have been recognized as important geochemical and biogeochemical processes in zero-valent iron walls. The lifetime of an iron wall will essentially be determined by the extent that these processes impact the reactive barriers' ability to remove contaminants from ground water. These processes are discussed in the following sections.

5.1 Fe⁰ Dissolution

The corrosion of zero-valent iron in aqueous environments has been widely studied (e.g., Davies and Burstein, 1980; Reardon, 1995; Blengino et al., 1995; Gui and Devine, 1994; Odziemkowski et al., 1998). In water, zero-valent iron may be oxidized to ferrous- or ferric-iron, leading to dissolution and volume loss of the metal. Under oxic conditions, dissolved oxygen acts as the electron acceptor and can lead to an increase in pH and the production of ferrous-iron and/or ferric-iron:



Ferric-iron is not expected to remain soluble and will precipitate, for example, as ferric hydroxide:



As oxygen is consumed, iron corrosion reactions result in the production of hydrogen.



Both aerobic and anaerobic iron corrosion reactions lead to an increase in pH. Aerobic corrosion is a more rapid process, as evidenced by the rapid loss of dissolved oxygen in iron-water systems. As iron corrosion proceeds, iron mineral precipitates form on or near the surface of corroding iron grains, which increases the thickness of an iron oxide passivation layer already present at the metal surface (e.g., Ritter et al., 2002). Under anaerobic conditions, hydrogen gas produced through reaction (5.4) may also temporarily passivate the iron surface. In general, low pH and the presence of oxidants result in more rapid iron corrosion rates. However, many species abundant in ground water can affect the rate and pathway of iron corrosion. For example, chloride, carbonate, and sulfate can all affect the corrosion rate of iron metal.

The major consequences of iron dissolution that follow from reactions (5.1)-(5.4) are the production of OH⁻ (pH increase), decrease in oxidation-reduction potential (Eh decrease), increase in hydrogen concentration, release of ferrous iron, and possible precipitation of sparingly soluble iron precipitates. Laboratory and field studies have shown that pH values in iron walls are typically >9 and <11. Eh values measured in zero-valent iron systems are oftentimes below -0.50 V.

Measured Eh values in PRBs are likely governed by redox reactions involving Fe(0), Fe(II), and Fe(III). For example, reactions that might bracket measured Eh values in iron walls are:



and,



The Eh-pH equation for the ferrihydrite-zero-valent iron couple ($E^0=0.053$ V) is:

$$\text{Eh} = E^0 + \alpha RT / nF \log[\text{H}^+]^3 \quad (5.7)$$

where R is the gas constant, T is temperature, F is Faraday's constant, and n is the number of electrons in the balanced half-cell reaction. Using a ΔG_f^0 for Fe(OH)_3 of -696.3 kJ/mol (Langmuir, 1997) and ΔG_f^0 for $\text{H}_2\text{O(l)}$ of -237.18 kJ/mol, we calculate $E^0 = -\Delta G_f^0/nF = 0.053\text{V}$, so that equation (5.7) reduces to:

$$\text{Eh} = 0.053 - 0.0592 \text{ pH} \quad (5.8)$$

Similarly, the Eh-pH equation for the ferrihydrite-ferrous iron couple is

$$\text{Eh} = 0.975 + 0.0592 \log [\text{H}^+]^3 [\text{Fe}^{2+}]^{-1} \quad (5.9)$$

Assuming ideal behavior and $\text{Fe}^{2+} = 0.001$ mg/L, equation (5.9) reduces to:

$$\text{Eh} = 1.43 - 0.178 \text{ pH} \quad (5.10)$$

Figure 5.1 shows equilibrium trends in Eh and pH for the $\text{Fe}^0\text{-Fe(OH)}_3$ couple (eqn. 5.8), the $\text{Fe}^0\text{-Fe}_3\text{O}_4$ couple, and the $\text{Fe}^{2+}\text{-Fe(OH)}_3$ couple (eqn. 5.10) compared to field measurements of ground-water pH and Eh from Elizabeth City monitoring wells located within the zero-valent iron media. The scattering of measured data points generally falls in between the two equilibrium trends plotted on Figure 5.1. This observation suggests that the measured Eh values in Fe^0 PRBs are not equilibrium potentials resulting from one redox pair, but are likely the result of mixed potentials from multiple redox reactions. These redox reactions are generally bracketed by the $\text{Fe}^0\text{-Fe(OH)}_3$ couple and the $\text{Fe}^{2+}\text{-Fe(OH)}_3$ couple.

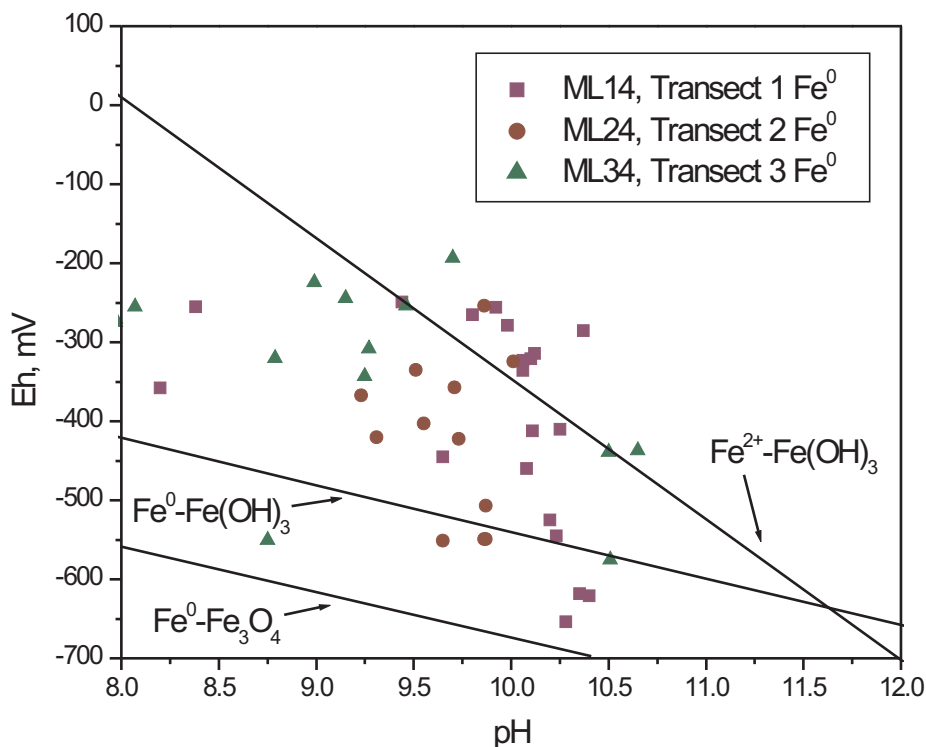


Figure 5.1 Redox -pH diagram showing composition of ground water from the Elizabeth City iron wall compared to equilibrium trends for the $\text{Fe}^0\text{-Fe(OH)}_3$, $\text{Fe}^0\text{-Fe}_3\text{O}_4$, and $\text{Fe}^{2+}\text{-Fe(OH)}_3$ couples ($\text{Fe}_T=0.001$ mg/L).

Eh-pH diagrams showing equilibrium relations in the system Fe-H₂O-C-S are shown in Figures 5.2-5.7. These Eh-pH diagrams were constructed using the EQ3/6 thermodynamic database (Wolery, 1979), modified to include data for green rust (Drissi et al., 1995; Bourrié et al., 1999; Refait et al., 2003), iron sulfides (Benning et al., 2000), and iron metal. The diagrams show both predominance areas for aqueous species (dashed lines) and solid phases (bold lines). All diagrams were drawn with the activity of iron equal to 10⁻⁵. Figures 5.2-5.4 were constructed with no suppressed minerals, i.e., they represent the equilibrium description of the systems based on the inclusion of all possible iron phases and aqueous species in the EQ3/6 database. In some cases, suppressing phases that are not expected to form based upon kinetic reasoning is useful in constructing and interpreting Eh-pH diagrams. Figures 5.5-5.7 were constructed with selected phases suppressed as described below.

Equilibrium relations in the system Fe-H₂O at 25 °C are shown in Figure 5.2. Within the stability field of liquid water, iron metal dissolution (corrosion) is expected below pH 8. Note this pH boundary depends on the specified iron activity. At lower iron activities, the solution-solid boundary will shift to the left so that the Fe²⁺ field will shrink in size. Above pH 8, iron metal is expected to corrode and be replaced by FeO and magnetite. At higher redox potentials and over a wide pH range, hematite (Fe₂O₃) is a stable mineral. Figure 5.3 shows equilibrium relations in the system Fe-H₂O-C (ΣC = 10⁻²) at 25 °C. With carbon in the system, stability fields appear for siderite and carbonate green rust. At the specified conditions for Figure 5.2, green rust is a stable phase and not metastable as is sometimes assumed, i.e., no mineral phases were suppressed in order for green rust to appear on the equilibrium diagram. When sulfur is exchanged for carbon, a broad stability field for pyrite (FeS₂) appears at low redox potentials (Figure 5.4).

Note that although there is a strong thermodynamic driving force for forming pyrite, kinetic factors may limit the formation of pyrite in PRBs. Solid-phase characterization studies indicate that mackinawite (Fe_{1+x}S) is the dominant iron sulfide in Fe⁰ PRBs with only trace quantities of greigite and pyrite detected (Wilkin et al., 2003; Furukawa et al., 2002). Because pyrite is not a major corrosion product in iron walls, suppression of pyrite from the Eh-pH diagram is reasonable (Figure 5.5). As pyrite is removed from the thermodynamic database, other iron sulfides: pyrrhotite, greigite, troilite, and mackinawite, appear as the stable solid phase at low redox potentials. Figure 5.6 was constructed with all sulfides suppressed. In this case, magnetite and FeO reappear at pH>8 and low redox potentials, as does a narrow window of sulfate green rust stability.

Hematite is typically not identified as a corrosion product in iron walls, although Fe(III)-bearing corrosion products are common. Suppression of hematite from the thermodynamic database leads to the appearance of goethite (Figure 5.6) in the Fe-H₂O-C system. Further suppression of goethite, magnetite, FeO, and siderite leads to broad fields of carbonate green rust and ferrihydrite. There is in fact very little kinetic hindrance for the precipitation of these phases (Figure 5.7). Note that the carbonate green rust field expands as the more insoluble phases hematite and goethite are replaced by ferrihydrite.

5.2 Anion Composition

The anionic composition of ground water is a critical factor in governing the rate of Fe⁰ corrosion and in directing the types of mineral precipitates that form within Fe⁰ reactive walls. Table 5.1 lists the authigenic minerals that have been identified in Fe⁰ barriers; these include an assortment of oxides, sulfides, and carbonates. The tendency of ferrous iron to form complexes with the common anions present in ground water increases in the order Cl⁻>HCO₃⁻>SO₄²⁻>>OH⁻. Therefore, it might be reasonably expected that iron metal corrosion rates will be the fastest in chloride-rich ground water and slowest in bicarbonate- or sulfate-rich ground water. Ground-water chemistry at the Elizabeth City and Denver Federal Center PRB sites is perhaps typical of many contaminated sites where PRBs might be used in that they contain a mixture of chloride, bicarbonate, and sulfate (Figure 5.8). If mineral precipitates form as surface coatings on the reactive iron grains (see Figures 3.24 and 4.24), the effectiveness of iron to degrade halogenated hydrocarbons may be reduced. In addition, mineral precipitation may result in porosity and permeability reductions (Reardon, 1995). On the other hand, some mineral coatings may be advantageous for the removal of both organic (e.g., Butler and Hayes, 2000; Lee and Batchelor, 2002a,b) and inorganic contaminants (e.g., Furukawa et al., 2002), as long as the hydraulic integrity of the system is retained to prevent ground water bypass of the reactive media.

The amount of mineral precipitation expected in Fe⁰ barriers is linked to the site-specific distribution of anionic species and to the concentration of total dissolved solids (TDS) in influent waters. High TDS concentrations in influent waters to Fe⁰ barriers will in most cases result in high mineral accumulation rates. Figure 5.9 shows the range in TDS values reported from several PRB systems examined in the Tri-Agency research initiative. Note that TDS values are comparatively low at the Elizabeth City PRB, and this correlates with comparatively low rates of mineral accumulation at this site.

5.2.1 Bicarbonate Reactions

Inorganic carbon can have an effect on the longevity of zero-valent iron PRBs in two different ways: 1) by accelerating the corrosion rate of Fe⁰ and the production of dissolved iron and H₂, and 2) by forming metal carbonate precipitates

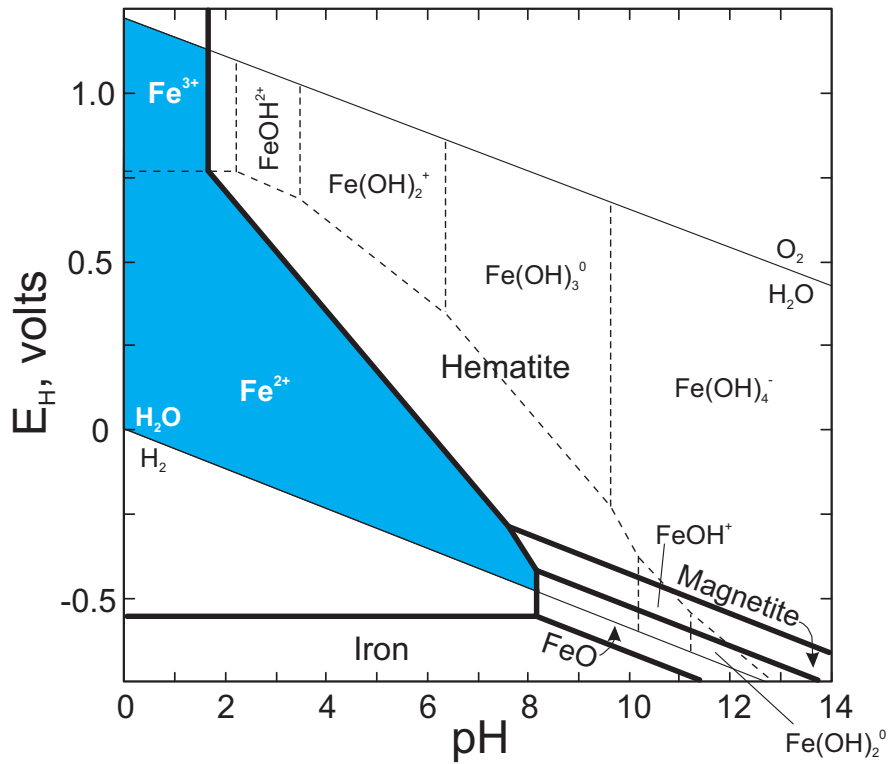


Figure 5.2 Redox-pH diagram for the Fe-H₂O system at 25 °C, showing speciation of soluble iron (dashed lines) and stability fields of iron-bearing minerals (solid lines). Diagram is drawn assuming iron species activities of 10⁻⁵ (blue shaded area shows field for iron in solution).

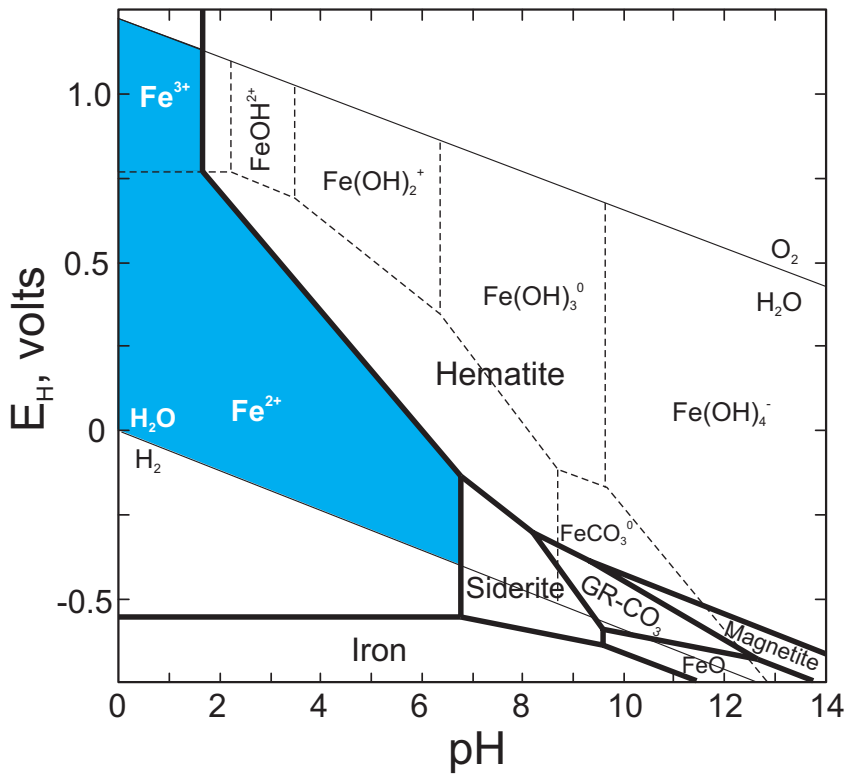


Figure 5.3 Redox-pH diagram for the Fe-CO₂-H₂O system at 25 °C, showing speciation of soluble iron (dashed lines) and stability fields of iron-bearing minerals (solid lines). Diagram is drawn assuming iron species activities of 10⁻⁵ and carbon species activities of 10⁻² (blue shaded area shows field for iron in solution).

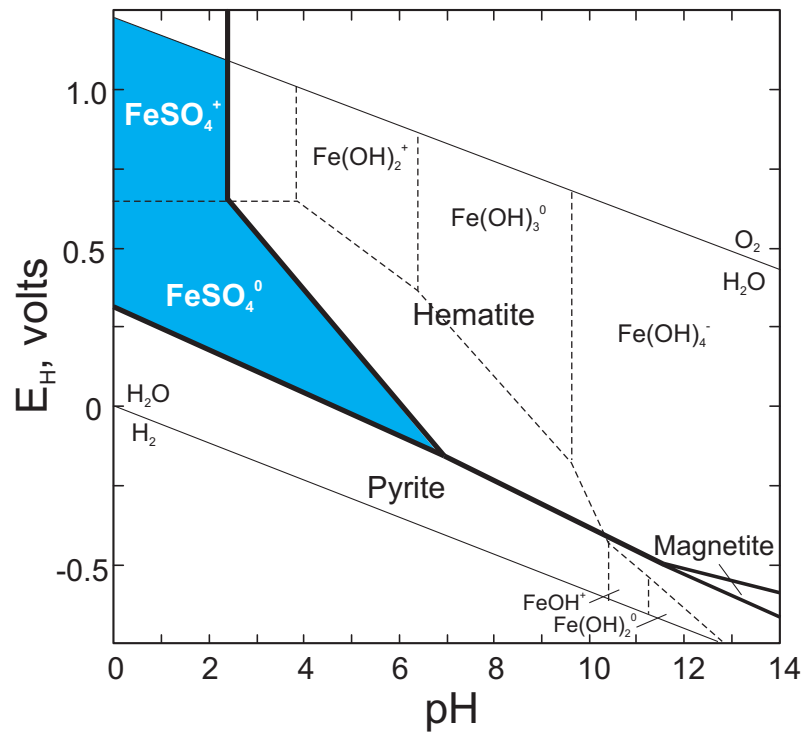


Figure 5.4 Redox-pH diagram for the Fe-S-CO₂-H₂O system at 25 °C, showing speciation of soluble iron (dashed lines) and stability fields of iron-bearing minerals (solid lines). Diagram is drawn assuming iron species activities of 10⁻⁵, carbon species activities of 10⁻², and sulfur species activities of 10⁻³ (blue shaded area shows field for iron in solution).

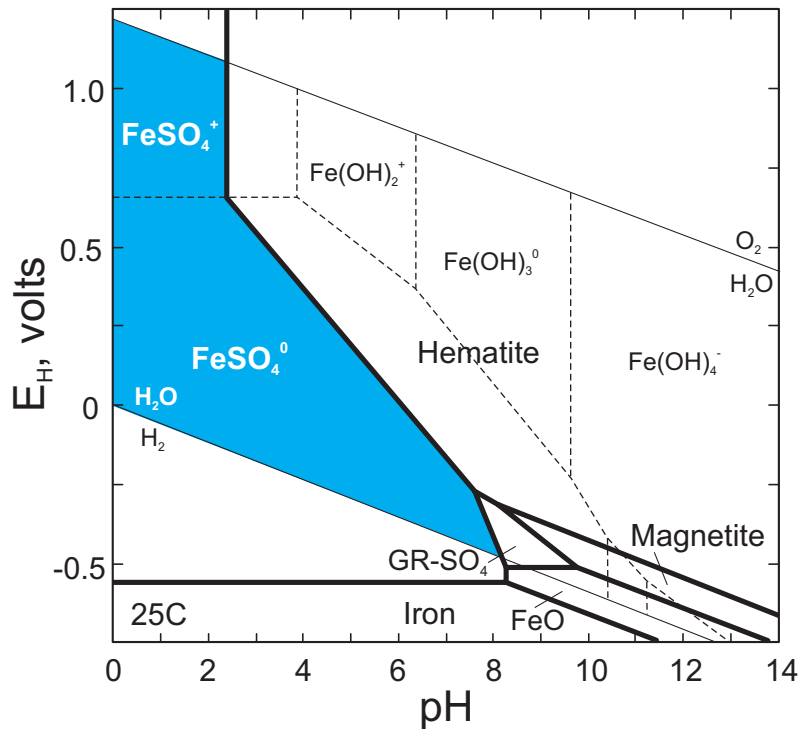


Figure 5.5 Redox-pH diagram for the Fe-S-CO₂-H₂O system at 25 °C, showing speciation of soluble iron (dashed lines) and stability fields of iron-bearing minerals (solid lines). Diagram is drawn assuming iron species activities of 10⁻⁵, carbon species activities of 10⁻², and sulfur species activities of 10⁻³ (blue shaded area shows field for iron in solution). Diagram drawn by suppressing all sulfide minerals.

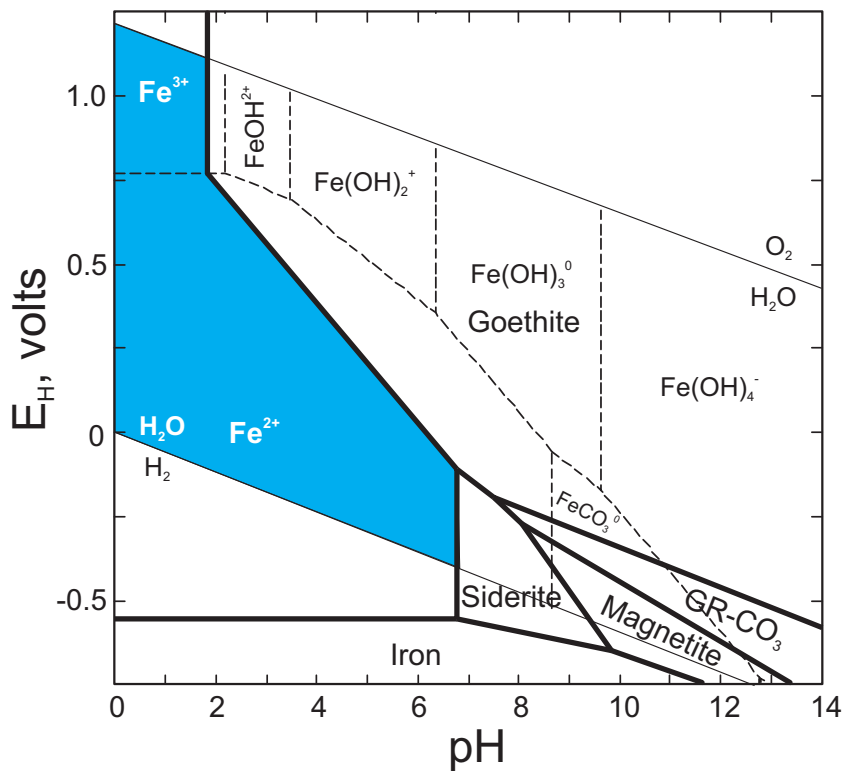


Figure 5.6 Redox-pH diagram for the Fe-CO₂-H₂O system at 25 °C, showing speciation of soluble iron (dashed lines) and stability fields of iron-bearing minerals (solid lines). Diagram is drawn assuming iron species activities of 10⁻⁵ and carbon species activities of 10⁻². Diagram drawn by suppressing hematite and FeO(s).

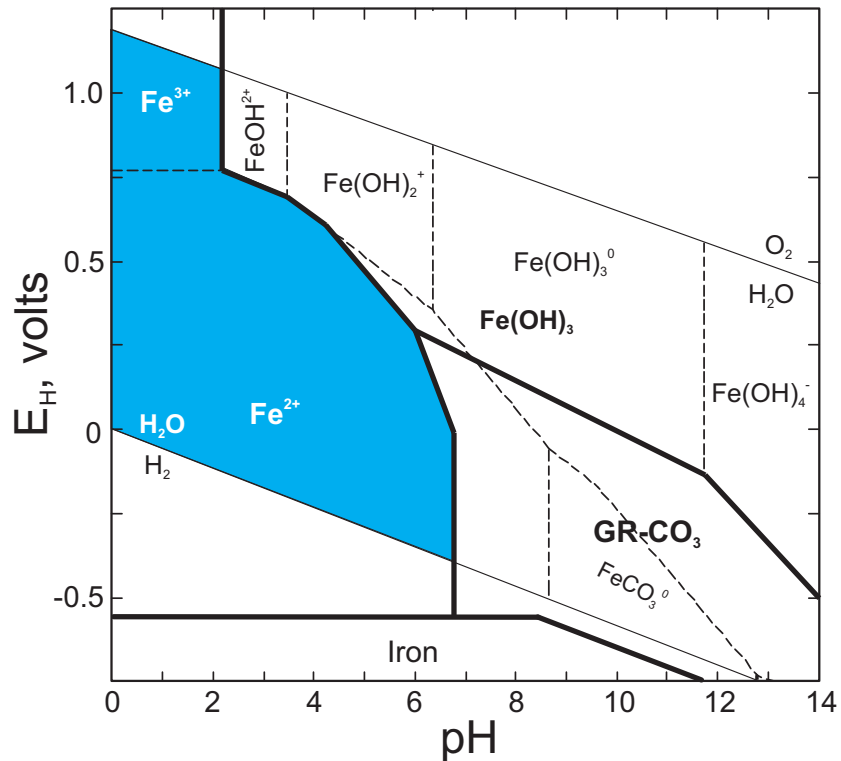


Figure 5.7 Redox-pH diagram for the Fe-CO₂-H₂O system at 25 °C, showing speciation of soluble iron (dashed lines) and stability fields of iron-bearing minerals (solid lines). Diagram is drawn assuming iron species activities of 10⁻⁵ and carbon species activities of 10⁻². Diagram drawn by suppressing hematite, goethite, magnetite, FeO(s), and siderite.

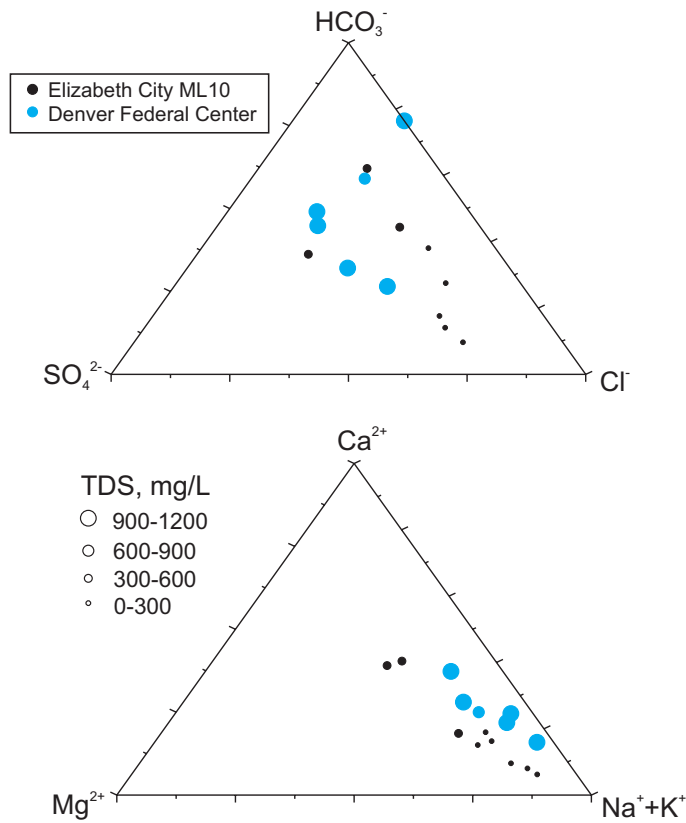
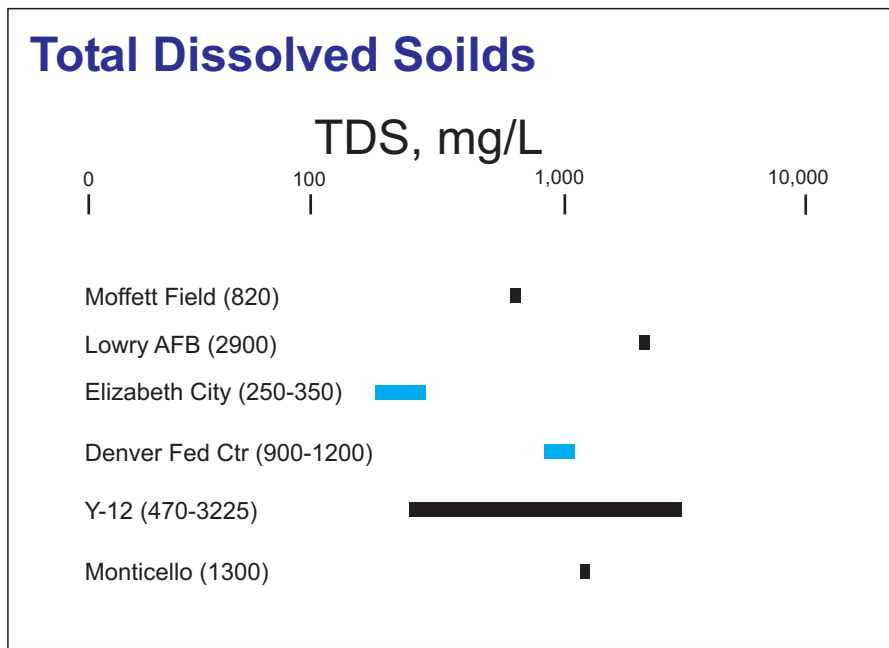


Figure 5.8 Upgradient ground-water compositions (molar ratios) and TDS values for the Elizabeth City and Denver Federal Center PRB sites.



Data source: Tri-Agency PRB Initiative, Combined Report

Figure 5.9 Comparison of total dissolved solids concentrations at PRB sites studied in the Tri-Agency initiative.

which may coat iron metal surfaces, block reactive sites, fill pore space, and through time, impact hydraulic performance. Abundant field and laboratory evidence indicates that inorganic carbon is removed from ground water during transit through zero-valent iron PRBs (Vogan et al., 1999; Phillips et al., 2000; Roh et al., 2000). The decrease in dissolved inorganic carbon is also accompanied by decreases in the concentrations of calcium and magnesium. Aragonite, calcite, siderite, ferrous carbonate hydroxide, and the carbonate form of green rust have all been identified in Fe⁰ reactive barriers (Table 5.1).

Iron corrosion generally leads to a pH increase and a consequent increase in the [CO₃²⁻/HCO₃⁻] ratio in solution. Generally, influent ground water to iron barriers is saturated to undersaturated with respect to various carbonate minerals. Increases in pH and the [CO₃²⁻/HCO₃⁻] ratio will impact reaction affinity and favor precipitation of carbonates such as aragonite and siderite. At the Elizabeth City PRB, ground water upgradient of multilevel well transect 2 is undersaturated with respect to both aragonite and calcite (Figure 5.10), based upon the reaction:



Ground-water compositions from within the iron wall clusters near the saturation point of both aragonite and/or calcite, and this observation is in agreement with: 1) the measurement of inorganic carbonate in the solid phase, and 2) the identification of aragonite by powder X-ray diffraction in core materials. Ground water downgradient of the iron wall is saturated to undersaturated with respect to CaCO₃ (Figure 5.10). A similar analysis shows that upgradient ground water is undersaturated with respect to magnesite and siderite, and that ground water within the Fe⁰ media is near-saturated to undersaturated with respect to these minerals. Even though ground-water compositions cluster near the saturation point for Mg and Fe carbonates, we were unable to detect magnesite or siderite in core materials collected from Elizabeth City. Conclusions about the identity of phases accumulating in reactive barriers that are based solely on the analysis of mineral saturation states can be misleading. Both magnesite and siderite are known to exhibit very slow dissolution/precipitation kinetics (e.g., Langmuir, 1997). Solid-phase characterization studies indicate that iron hydroxy carbonate is, in fact, the dominant mineral carbonate at Elizabeth City, and calcium carbonate and iron hydroxy carbonate dominate mineral carbonate forms at the Denver Federal Center. There are presently no thermodynamic data for iron hydroxy carbonate that can be used, for example, to estimate solution saturation indices.

The factors that govern the distribution and form of carbonate precipitates are still unclear. Iron hydroxy carbonate appears to be a common precipitate documented in both lab and field studies (e.g., this study, Gavaskar et al., 2002; Kamolpornwijit et al., 2002). The formation of Ca vs. Fe carbonates could in part be controlled by the Ca concentration of influent water to PRBs. For example, following the exchange reaction:



Table 5.1. Mineral Precipitates Identified in Iron Walls

Mineral precipitate type	Minerals identified in zero-valent iron PRBs
Oxides and Hydroxides	Ferrihydrite, Fe(OH) ₃ Lepidocrocite, γ-FeOOH Goethite, α-FeOOH Hematite, Fe ₂ O ₃ Maghemite, Fe ₂ O ₃ Green rust 1, Fe ₆ (OH) ₁₂ CO ₃ ·xH ₂ O Magnetite, Fe ₃ O ₄
Carbonates	Calcite, CaCO ₃ Aragonite, CaCO ₃ Iron carbonate hydroxide, Fe ₂ (OH) ₂ CO ₃ Siderite, FeCO ₃
Sulfides	Mackinawite, Fe _{1+x} S Greigite, Fe ₃ S ₄ Pyrite, FeS ₂

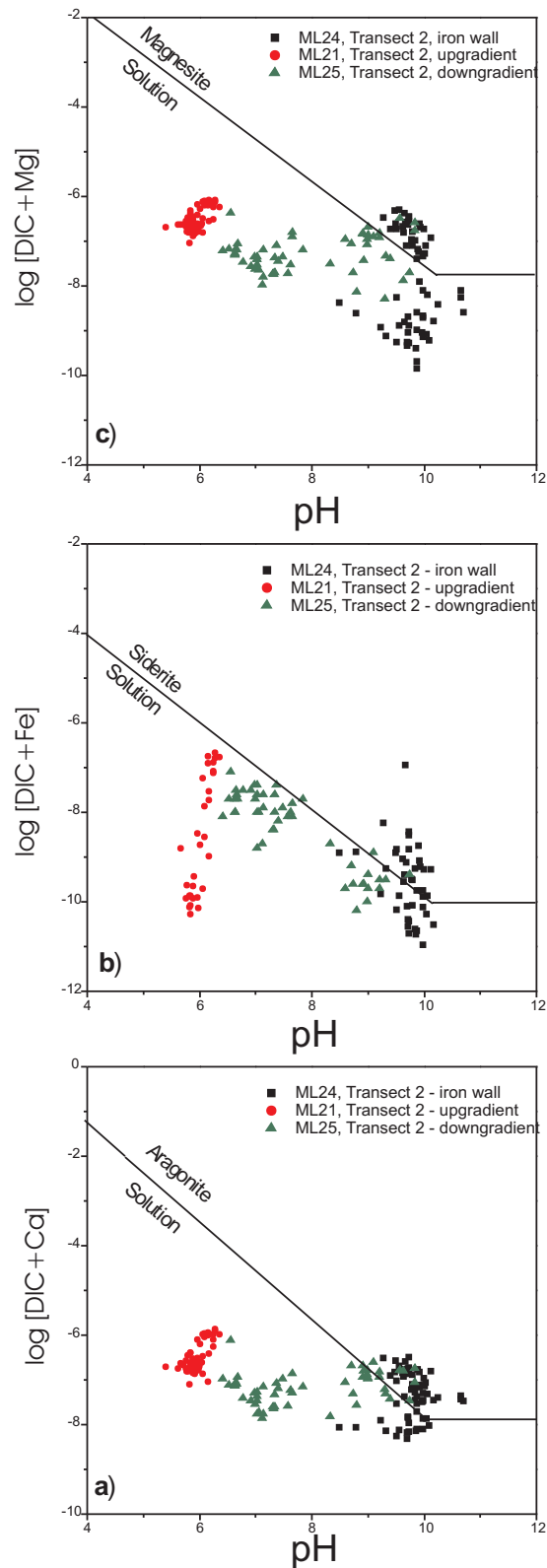


Figure 5.10 Solubility diagram showing the stability field of a) aragonite, b) siderite, and c) magnesite as a function of pH and log activities of dissolved inorganic carbon, Ca^{2+} , Fe^{2+} , and Mg^{2+} . Also plotted are ground-water compositions from upgradient, iron wall, and downgradient sampling locations (Elizabeth City PRB).

with $\log K_{[5.12]} = 2.2$ and ideal behavior in the solid phase, solution concentration ratios of $[\text{Ca}^{2+}]/[\text{Fe}^{2+}] > 158$ should favor the formation of calcite over siderite. In batch laboratory tests devoid of calcium, siderite is often found to be the primary carbonate phase as might be expected (e.g., Agrawal et al., 2002). As the concentration of Ca increases, calcium carbonates are likely to become more important than siderite. Both aragonite and calcite are observed in iron walls. The formation of aragonite over calcite may be linked to the $[\text{Mg}^{2+}/\text{Ca}^{2+}]$ ratio in solution in addition to the absolute Mg^{2+} concentration. In experiments designed to explore the growth of calcite and aragonite in seawater, Berner (1975) showed that calcite growth was sensitive to the Mg^{2+} in solution. In a seawater matrix, the growth rate of calcite was depressed at Mg^{2+} concentrations >70 ppm and aragonite growth was favored from supersaturated solutions. It is also possible that other ground-water solutes have an effect on directing the nucleation and growth of aragonite over calcite and subsequent transformation.

Agrawal et al. (2002) recently examined the effect of carbonate precipitation on the reaction between Fe^0 and 1,1,1-trichloroethane (TCA) in model experiments. Time-dependent trends in degradation half-lives suggest an initial increase followed by a decrease. The exposure of iron surfaces to bicarbonate solution apparently results in an initial period of inhibited corrosion due to the presence of a film of iron oxide, followed by bicarbonate-enhanced iron corrosion, and eventually passivation occurs as a result of carbonate precipitation (siderite and carbonate green rust). These three regimes yield different contaminant degradation kinetics and perhaps different degradation mechanisms.

5.2.2 Sulfate Reactions

Decreases in sulfate concentrations in Fe^0 barriers are attributed to the microbial activity of sulfate-reducing bacteria. At both the Elizabeth City and DFC PRBs, sulfate concentrations are near completely removed as ground water moves through the reactive media. Accompanying the reduction of sulfate concentrations is the accumulation in the solid-phase of mackinawite (Fe_{1+x}S) and microbial biomass with a phospholipid fatty extract signature consistent with the presence of sulfate-reducing bacteria. Abiotic reduction of sulfate to sulfite, thiosulfate, elemental sulfur, or hydrogen sulfide are known to be a sluggish processes at temperatures below 100°C (Trudinger et al., 1985). The slow kinetics of the abiotic process is related to the eight-electron transfer required to reduce sulfate to sulfide.

In many subsurface systems, microbial reduction of sulfate is accompanied by oxidation of reduced organic carbon, e.g.,



In Fe^0 barriers the amount of reduced organic carbon present would appear to be limiting and insufficient to account for the amount of sulfate removed from solution and the quantity of iron sulfide precipitates observed in the solid phase. Sulfate-reducing bacteria, such as *Desulfovibrio desulfuricans*, can also utilize hydrogen as a substrate for the reduction of sulfate, e.g.,



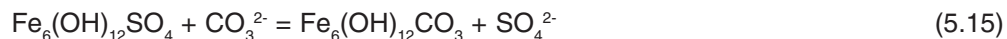
In gate 2 of the DFC, we detected high concentrations of iron sulfide within the iron wall and comparatively low concentrations of hydrogen. These observations are consistent with sulfate-reduction being an important sink for hydrogen in Fe^0 barriers. A potential negative consequence of the presence of bacteria is biofouling. Proliferation of bacteria could reduce the hydraulic conductivity of the barrier (Roh et al., 2000; Wilkin et al., 2003). On the other hand, iron sulfide can be effective in enhancing the degradation of TCE and other halogenated aliphatic compounds (e.g., Butler and Hayes, 2000, 2001) and sulfur impurities in iron metal may also influence reactivity (e.g., Hassan, 2000). The formation of iron sulfides in Fe^0 barriers, therefore, may be beneficial to their continued operation. In addition, compost-based reactive barriers have been used to remove metal contaminants from ground water (Waybrant et al., 1998, 2002; Benner et al., 1997). This treatment strategy is analogous to the use of anaerobic solid-substrate bioreactors for removing metals from solution (e.g., Dvorak et al., 1992; Drury, 1999). These systems rely on carbon-based media as a substrate for sulfate reduction, sulfide production, and precipitation of insoluble metal sulfides. Sulfate-reduction could also serve to increase the removal of metals in Fe^0 barriers through direct precipitation of metal sulfides, co-precipitation with FeS , and/or adsorption onto iron sulfide surfaces.

Complete reduction of sulfate to bisulfide could lead to high levels of aqueous sulfide species in the absence of any removal process. At near-neutral pH, iron monosulfides are insoluble so that all sulfide produced is likely to be precipitated and removed from solution. At the DFC, we observed total dissolved sulfide concentrations of <1 ppm; concentrations of sulfide in the solid-phase were as high as about 0.5 wt% S.

Field evidence suggests that microbial sulfate reduction is most effective in decreasing sulfate concentrations in low-flow regimes. Iron barriers that experience higher flow-rates tend to show less effective removal of sulfate (e.g., Morrison et al., 2001; Kamolpornwijit et al., 2003).

Several studies have suggested that another possible sink for sulfate in Fe^0 barriers is the formation of sulfate green rust. Geochemical modeling studies of iron corrosion described in Wilkin et al. (2002) suggest that the carbonate form of

green rust is favored over the sulfate form at the Elizabeth City and DFC sites. X-ray diffraction results from these sites are consistent with the formation of the carbonate form of green rust; sulfate green rust has not been detected. These observations can be understood by considering the following exchange equilibrium based upon the anhydrous GR components:



so that,

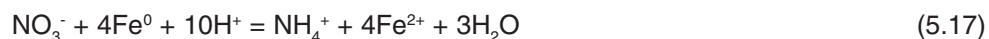
$$K_{[5.15]} = [\text{SO}_4^{2-} / \text{CO}_3^{2-}] / [\text{Fe}_6(\text{OH})_{12}\text{CO}_3 / \text{Fe}_6(\text{OH})_{12}\text{SO}_4] \quad (5.16)$$

Assuming ideal mixing relations in the solids and taking thermodynamic data from Bourrié et al. (1999) for the anhydrous carbonate and sulfate forms of green rust, we estimate $K_{[5.15]} = 10^{3.1}$. Consequently, sulfate green rust (GR2) is expected to be a primary iron corrosion product only when sulfate-rich and bicarbonate-poor waters interact with zero-valent iron. High-sulfate conditions are most likely to be present in areas impacted by the oxidative weathering of metal sulfide deposits.

5.2.3 Nitrate Reactions

Field-deployed zero-valent iron systems effectively remove nitrate from ground water (e.g., Gillham et al., 1994; McMahon et al., 1999; Liang et al., 2002). In this study, nitrate removal was consistently observed at the Elizabeth City and Denver Federal Center PRBs over the initial five-year period of operation (Blowes et al., 1999b, Puls et al., 1999a, Wilkin et al., 2002; this report). Laboratory investigations suggest that nitrate can inhibit the reduction of TCE and other chlorinated ethenes through competition for reducing equivalents (e.g., Schlicker et al., 2000), however, as of yet, this behavior has not been documented in the field.

At the Y-12 Pathway 2 PRB (Oak Ridge, TN), influent water contains nitrate at concentrations approaching 1,000 mg/L; nitrate concentrations in effluent waters and in wells adjacent to the zero-valent iron zone are near or below analytical detection limits (Liang et al., 2002). Unlike sulfate reduction that only proceeds via microbial respiration, reduction of nitrate may proceed by either abiotic or biotic pathways (Siantar et al., 1996; Huang et al., 1998; Till et al., 1998; Gandhi et al., 2002). Abiotic reduction is a pH-dependent process that results in the formation of ammonium and possibly nitrite as an intermediate product. Rates of nitrate reduction in sterile systems are fast at $\text{pH} \leq 4$ (Huang et al., 1998), but apparently reduction rates can be significant even at circumneutral pH (Siantar et al., 1996; Alowitz and Scherer, 2002, but also see Huang et al., 1998). The overall reaction may follow:



Huang et al. (1998) propose that electrons necessary for nitrate reduction are supplied directly from Fe^0 or indirectly through an iron corrosion product (H_2).

Data presented in Gandhi et al. (2002) suggest that the effective removal of nitrate observed in field PRB systems is likely the result of significant biotic contributions. In biologically mediated systems, reduced organic carbon is frequently the electron donor for the redox transformation (Postma et al., 1991). In zero-valent systems, biotic reduction of nitrate occurs by denitrifying bacteria that likely use cathodic H_2 as an electron donor to respire NO_3^- (e.g., Till et al., 1998; Gandhi et al., 2002). Nitrogen gas is the principal product of biotic nitrate reduction rather than ammonia (Till et al., 1998). A significant result of nitrate reduction from both abiotic and biotic mechanisms is increased iron corrosion, leading to secondary mineral precipitation (Kamolpornwijit et al., 2003).

5.2.4 Reactions with Silica

Field evidence indicates that dissolved silica is removed by Fe^0 barriers (Gavaskar et al., 2002; Wilkin et al., 2003). Ground-water concentrations of silica typically range between saturation values with respect to quartz and amorphous silica (3 to 54 mg/L Si). Within iron walls, concentrations of Si typically fall below 1 mg/L. Using high-resolution microscopy, Furukawa et al. (2002) observed silica predominantly associated with iron corrosion products. The role that silica might play in passivated iron surfaces is not clear. However, recent long-term column studies suggest that silica, carbonate, and natural organic matter co-solutes reduce the reactivity of Fe^0 (Vikesland et al., 2002).

Forms of SiO_2 are not likely precipitating in iron walls because of their slow precipitation kinetics and because increasing pH increases rather than decreases SiO_2 solubility. One possibility is that silica is associated with magnesium in the clay mineral sepiolite, $\text{Mg}_4(\text{OH})_2\text{Si}_6\text{O}_{15} \cdot \text{H}_2\text{O}$. Sepiolite typically occurs as finely fibrous aggregates, but is less frequently encountered in natural systems compared to the layered clay minerals. Sepiolite has a chain-like crystal structure of continuous Si_2O_5 sheets with ribbons of Mg octahedra leaving channels that can incorporate water or organic molecules. Figure 5.11 shows saturation indices of magnesium-bearing phases, sepiolite and brucite ($\text{Mg}(\text{OH})_2$), as a function of pH for Elizabeth City ground water. With increasing pH, ground water approaches or clusters near the saturation points of both sepiolite and brucite. Both phases, therefore, represent possible sinks for magnesium in iron walls ($\text{pH} > 9$), and in addition, sepiolite is a possible sink for silica. Appreciable buildup of these phases might only be expected in PRB

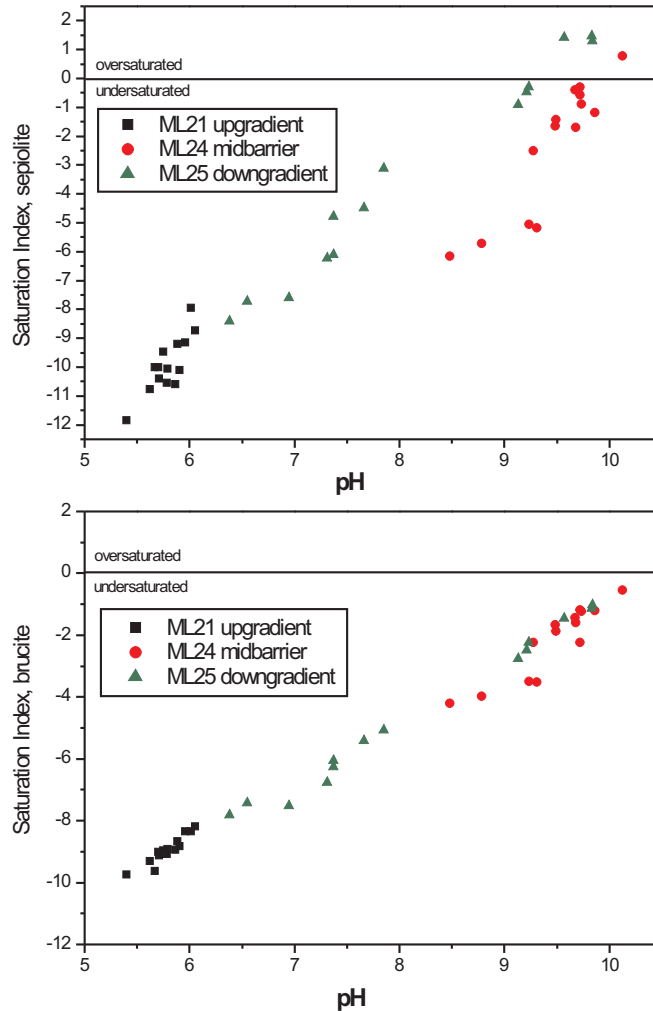


Figure 5.11 Saturation indices of magnesium-bearing phases (brucite, $\text{Mg}(\text{OH})_2$; sepiolite, $\text{Mg}_4(\text{OH})_2\text{Si}_6\text{O}_{15}\cdot\text{H}_2\text{O}$) as a function of pH in ground water from upgradient, iron wall, and downgradient sampling locations (Elizabeth City PRB).

systems with greater influent magnesium concentrations than are encountered at the Elizabeth City or Denver Federal Center sites.

5.2.5 Reactions with Oxygen

Concentrations of dissolved oxygen in influent ground water to Fe^0 barriers are rapidly consumed. Low concentrations and the presence of dissolved ferrous iron complicate the accurate quantitation of dissolved oxygen in ground water samples collected around iron walls. Oxygen is incorporated into a complex mixture of mineral oxides formed near the surface of Fe^0 particles. The oxide film that develops on iron surfaces could be composed of magnetite, green rust, maghemite ($\gamma\text{-Fe}_2\text{O}_3$), hematite, goethite, lepidocrocite, or ferrihydrite. The oxide layer at the metal surface is expected to evolve from a predominantly Fe(III) phase where oxygen-containing solutions enter the Fe^0 zone to a mixed-valent or pure Fe(II) phase under highly-reducing conditions expected in mid-barrier regions (e.g., Scherer et al., 1999; Odziemkowski et al., 1998). High concentrations of dissolved oxygen entering Fe^0 barriers are especially problematic due to rapid oxidation reactions, cementation by Fe(III) materials, and plugging (e.g., Liang et al., 2000).

5.3 Mineral Precipitation

Mineral precipitates in zero-valent iron PRBs can be classified by formation processes into three groups: 1) those that result from changes in chemical conditions (i.e., change in pH, e.g., calcite); 2) those that are a consequence of microbial activity (i.e., sulfate reduction, e.g., mackinawite); and 3) those that are the result of iron metal instability and corrosion (e.g., magnetite). As noted in many publications, the formation of mineral precipitates in PRBs can impact system performance through time. As minerals precipitate in iron walls they occupy volume and, therefore, reduce porosity and permeability of the reactive zone. In this way, the hydraulic performance of PRBs (e.g., residence time, capture zone) could degrade through time as the effective porosity of the iron wall approaches or exceeds that in the adjacent aquifer. For example, preferential mineral accumulation in regions of a PRB resulting from higher inputs of dissolved solutes may lead to increases in ground-water residence times. However, adjacent regions of the reactive barrier may experience greater throughput and decreased residence times, potentially leading to contaminant breakthrough (Figure 5.12).

A second effect of mineral precipitation relates to the reactivity of materials placed in PRBs. As mineral precipitates accumulate on iron surfaces (see Figures 3.24 and 4.24) it is expected that electron transfer processes, critical for the degradation of chlorinated organic compounds, become less efficient. The formation of mineral precipitates has been viewed generally as a process that limits the long-term performance of reactive barriers for ground-water cleanup. Yet some corrosion products that deposit on the surfaces of iron particles may also contribute to the overall treatment effectiveness of reactive barriers (e.g., Butler and Hayes, 1998, 1999, 2000; Lee and Batchelor, 2002; Furukawa et al., 2002). For example, iron sulfides, magnetite, and green rust minerals can chemically transform chlorinated organic compounds.

5.3.1 Pore Volume Reduction

The infilling of pore space by mineral precipitates can be assessed by theoretical modeling efforts and through direct field measurements. The development of models of mineral precipitation in PRBs is of great interest because these models can be used as predictive tools during remedial investigations at contaminated sites (e.g., Blowes and Mayer, 1999; Mayer et al., 2001; Yabusaki et al., 2001; Liang et al., 2003). Field measurements are critical in verifying model predictions at specific sites. Based upon the results of this and other studies, volume loss in zero-valent iron systems results primarily from the formation of mineral precipitates containing carbon, sulfur, and iron.

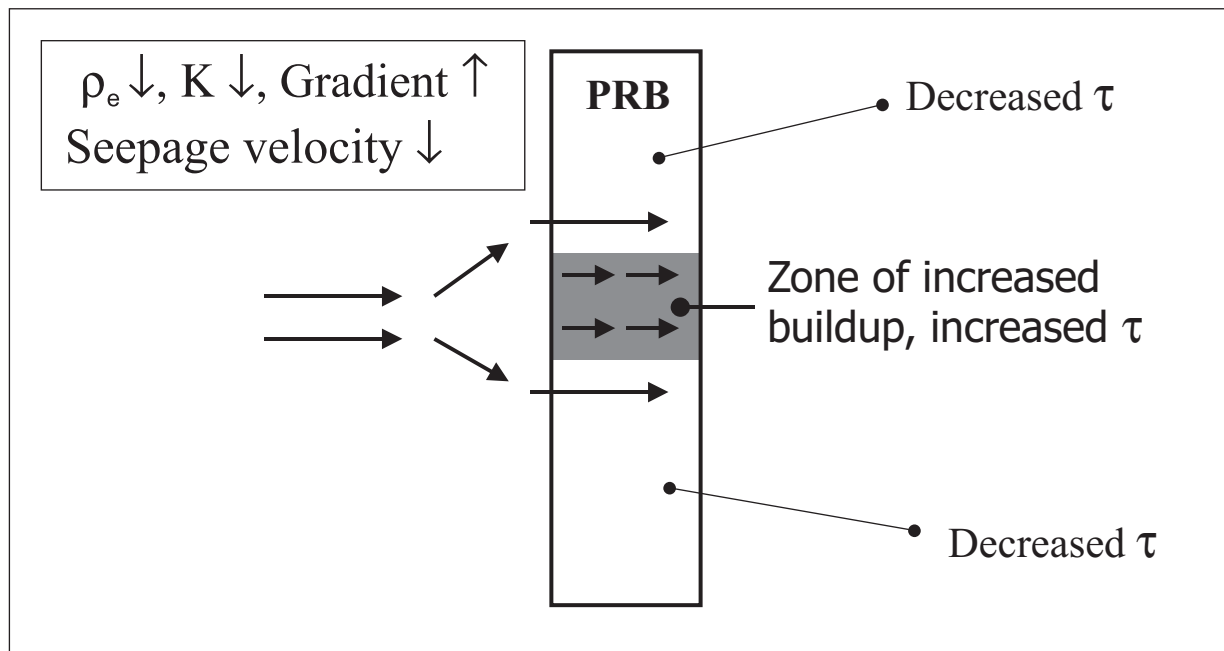


Figure 5.12 Conceptual model of the impact of mineral and biomass accumulation to PRB hydraulic performance (ρ_e =effective porosity; K =hydraulic conductivity; τ =residence time).

After five years of mineral accumulation, concentrations of inorganic carbon in core materials from the Elizabeth City and Denver Federal Center PRBs range from <1 to about 14,100 $\mu\text{g/g}$. This concentration range can be directly related to a fractional porosity reduction, i.e., the reduction in the fraction of the total volume occupied by pore space. In Figure 5.13, fractional porosity reduction resulting from formation of carbonate minerals is plotted as a function of the concentration of inorganic carbon. An inorganic carbon concentration of 15,000 $\mu\text{g/g}$ would result in a decrease of the fractional porosity by 0.13 to >0.5, depending on how the carbon is distributed in the solid phase (i.e., siderite or carbonate green rust, respectively). The least amount of pore infilling occurs when carbon is partitioned into minerals with low molar volumes, such as siderite, aragonite, and calcite (Table 5.2). Greater porosity loss is a consequence of the formation of carbonate green rust and iron hydroxy carbonate, materials with comparatively high molar volumes (Figure 5.13; Table 5.2). After the first five years of operation at Elizabeth City, the maximum loss of fractional pore space near the upgradient iron/aquifer interface due to the formation of inorganic carbon precipitates is estimated to be about 0.07. At the Denver Federal Center, the maximum loss of fractional pore space due to the formation of inorganic carbon precipitates is estimated to be about 0.17 after the first five years of operation.

The main sulfur-bearing mineral in zero-valent iron PRBs is mackinawite (FeS) as seen in this study and at other sites (e.g., Phillips et al., 2000; Roh et al., 2000). The low molar volume of mackinawite results in little loss of porosity (<0.05) even at the highest concentrations of total sulfur observed in this study (7,520 $\mu\text{g/g}$; Figure 5.14). If through time mackinawite were to completely transform to pyrite, the loss of pore space would be even lower due to the low molar volume of pyrite (Table 5.2). Sulfur partitioned into sulfate green rust would result in much more significant porosity reductions (Figure 5.14).

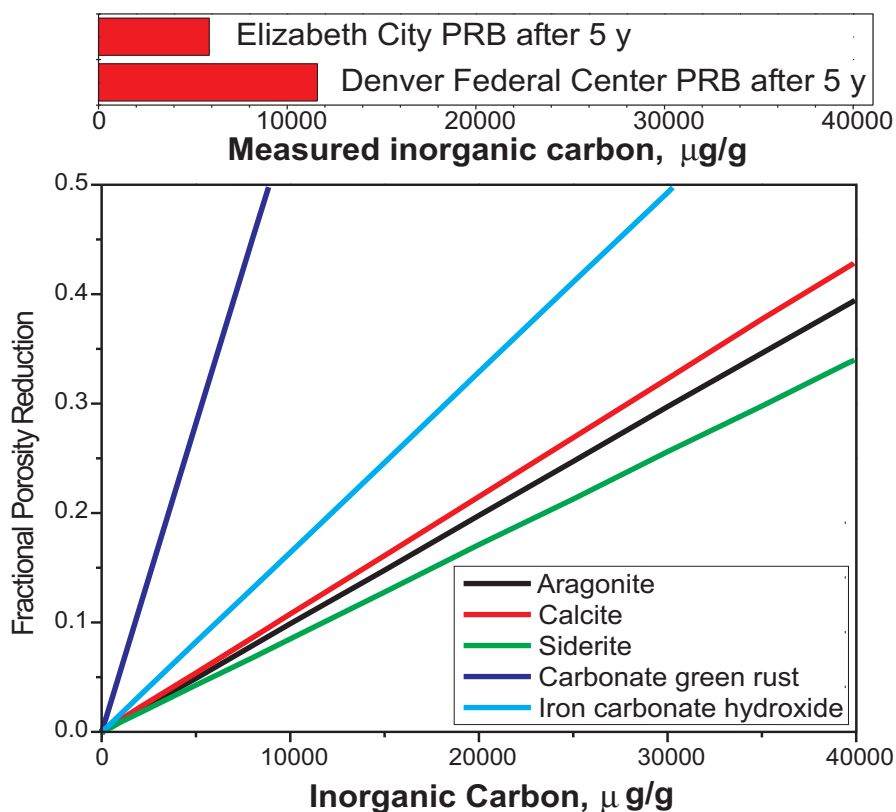


Figure 5.13 Fractional porosity reduction as a function of inorganic carbon concentration in the solid phase. The lines represent volume loss due to the accumulation of a carbon-bearing phase assuming that all carbon is present in that phase. Fractional porosity reduction is calculated assuming an initial porosity of 0.50 and iron density of 7.0 g/cm^3 . The range of observed inorganic carbon concentrations after 5 years at the Elizabeth City and the Denver Federal Center PRBs are shown.

Table 5.2. Molar Volume and Density of Mineral Precipitates

Phase	Formula	Molecular Weight (g/mole)	Density (g/cm ³)	Molar Volume (cm ³ /mole)
Calcite	CaCO ₃	100.09	2.71 ^a	36.93
Aragonite	CaCO ₃	100.09	2.95 ^a	33.93
Siderite	FeCO ₃	115.86	3.96 ^a	29.26
Green Rust – CO ₃	Fe ₆ (OH) ₁₂ CO ₃	599.17	3.5 ^b	171.19
Iron Hydroxy Carbonate	Fe ₂ (OH) ₂ CO ₃	205.72	3.65 ^c	56.36
Mackinawite	FeS	87.91	4.1 ^d	21.44
Pyrite	FeS ₂	119.98	5.02 ^a	23.90
Green Rust – SO ₄	Fe ₆ (OH) ₁₂ SO ₄	635.23	3.5 ^b	181.49
Iron	Fe	55.85	7.0 ^a	7.98
Magnetite	Fe ₃ O ₄	231.54	5.18 ^a	44.70
Hematite	Fe ₂ O ₃	159.69	5.26 ^a	30.36
Goethite	FeOOH	88.85	4.37 ^a	20.33
Ferrihydrite	Fe(OH) ₃	106.87	3.1 ^b	34.47

Molar volume = MW/density

^a Hurlbut and Klein (1977); ^b estimated; ^c Erdös and Altorfer (1976); ^d Vaughan and Craig (1978)

Corrosion reactions in which iron reacts to form iron oxides such as magnetite, hematite, goethite, or ferrihydrite also result in volume increases and porosity reductions. For example, the molar volume change of the reaction (ΔV_r) from Fe⁰ to magnetite can be computed from the reaction:



by using the molar volumes (V_m) of Fe⁰ and magnetite listed in Table 5.2. The molar volume change of reaction is given by:

$$\Delta V_r = 1/3(V_m \text{ magnetite}) - (V_m \text{ Fe}^0) = 6.9 \text{ cm}^3/\text{mol} \quad (5.19)$$

Given the assumption that iron is conserved in the solid phase, transformation reactions of iron metal to iron hydroxides, oxyhydroxides, and oxides all have positive molar volume changes. The fractional porosity reduction associated with various iron transformations are plotted in Figure 5.15 as a function of extent of reaction or extent of transformation. Although it is well documented that magnetite, for example, is a product formed in iron walls, the overall extent of the transformation has not been directly determined or estimated. Based upon microscopic examination, iron particles collected from the Elizabeth City and DFC PRBs (after five years) are dominantly composed of Fe⁰ and not iron oxidation products. An average rate of iron metal corrosion in ground water is estimated to be 0.6 mmol/kg d (Reardon, 1995). At this rate of corrosion, after five years the extent of reaction to magnetite is estimated to be 0.02. If ferrihydrite is the end product instead of magnetite, the extent of reaction is estimated to be 0.06. Consequently, the extent of reaction after 5 years is likely to be less than 0.3 and probably much less than 0.1. As shown in Figure 5.15, the volume loss accompanying the transformation to magnetite is not expected to exceed 0.1 after five years. It should be noted that where rapid oxidation occurs due to the influx of ground water with high levels of dissolved oxygen (>2 mg/L), reaction to form goethite or ferrihydrite has been documented. Figure 5.15 shows that even partial conversion of Fe⁰ to ferrihydrite can dramatically impact the porosity of zero-valent iron systems.

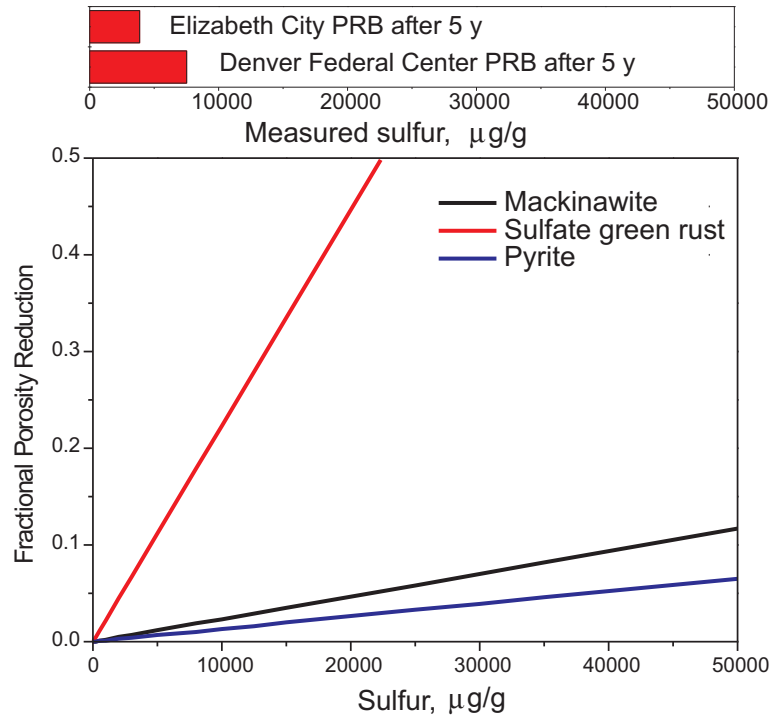


Figure 5.14 Fractional porosity reduction as a function of sulfur concentration in the solid phase. The lines represent volume loss due to the accumulation of a sulfur-bearing phase assuming that all sulfur is present in that phase. Fractional porosity reduction is calculated assuming an initial porosity of 0.50 and iron density of 7.0 g/cm^3 . The range of observed sulfur concentrations at the Elizabeth City and the Denver Federal Center PRBs are shown.

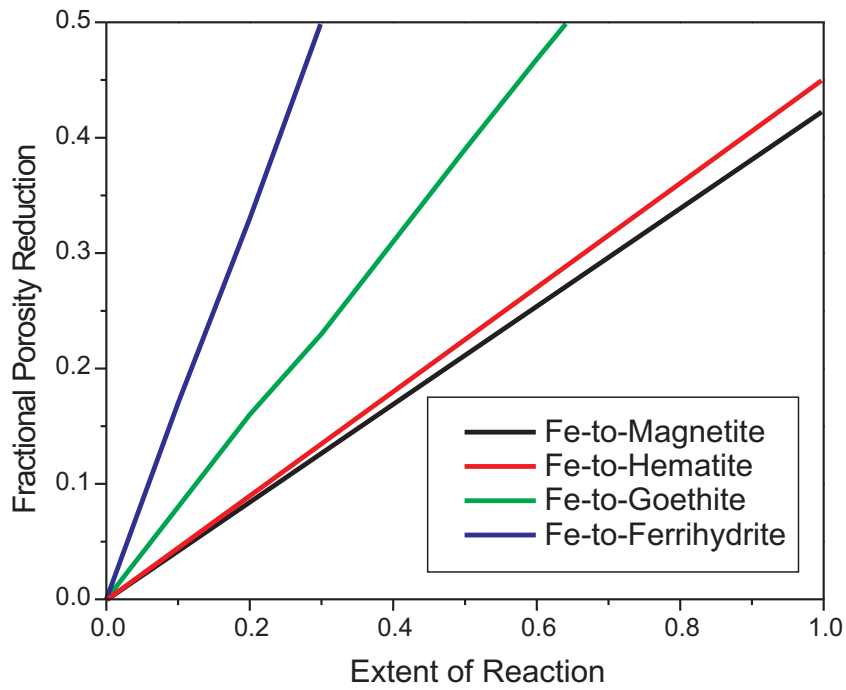


Figure 5.15 Fractional porosity reduction as a function of the positive molar volume change as iron metal reacts to form magnetite, hematite, goethite, and ferrihydrite.

5.3.2 Loss of Reactivity

The previous calculations examining porosity reductions in iron walls as a consequence of mineral precipitation relate primarily to potential impacts to the hydraulic performance of PRBs. However, these calculations provide no direct insight about how mineral precipitation affects or could interfere with contaminant removal processes. In order to examine changes in the reactivity of zero-valent iron as a function of exposure time, we conducted batch experiments using fresh iron (Peerless Iron) and materials that were collected from the Elizabeth City and Denver Federal Center PRBs after five years of exposure to ground water. In the batch tests, iron samples used were collected from upgradient and midbarrier locations as summarized in Table 5.3. The water composition used in the batch tests was prepared using reagent grade sodium bicarbonate, calcium sulfate, magnesium sulfate, magnesium chloride, potassium chloride, and hydrochloric acid to approximately match ground-water compositions encountered at the two PRB sites (Table 5.4). Solutions were deoxygenated by purging with high-purity nitrogen gas for one hour.

Stock solutions were prepared using high purity trichloroethylene (99+%, Aldrich), 1,1,1-trichloroethane (anhydrous, 99+%, Aldrich), and 1,1-dichloroethene (99%, Aldrich). Experiments to determine the kinetics of VOC degradation and Cr removal were carried out in 45-mL glass VOA vials, each containing 10 g of iron and filled with freshly prepared synthetic ground water. The VOA vials were sealed without headspace with Teflon-lined screwcaps. Next the reaction vessels were injected with a volume of the VOC stock solution and placed in a rotary shaker at 100 rpm at room temperature (23 ± 1 °C). Visual observations suggest that the gentle mixing did not result in any physical abrasion of the iron particles or corrosion products. Periodically vials were withdrawn for sample collection and measurement of pH, oxidation-reduction potential, sulfate, chloride, calcium, magnesium, iron, sodium, potassium, chromium, and VOCs. Control experiments (without iron) showed no loss of organohalides or metals over the relevant experimental timescales.

Results of the batch experiments show that field-exposed iron samples from both midbarrier and upgradient locations are able to remove contaminants from solution at rates comparable or, even better, to those observed in systems containing unreacted zero-valent iron (Figure 5.16; Table 5.5). The initial removal rate of chromium is actually greater for field-

Table 5.3. Samples Used in Batch Reactivity Tests

Sample	Location	Inorganic Carbon, $\mu\text{g/g}$	Sulfur, $\mu\text{g/g}$	PLFA, pm/g
Unreacted Peerless Iron	-8/+50 mesh size	<15	<5	ND
EC050801-3-1	Elizabeth City, upgradient	4633	3880	ND
EC050901-9-1	Elizabeth City, midbarrier	100	100	ND
C1-1-71701-19	Denver Federal Center, Gate 1, midbarrier	87	318	ND
C2-3-71801-4	Denver Federal Center, Gate 2, upgradient	2100	1785	455

Table 5.4. Composition of Water Used in Batch Reactivity Tests

Component	Synthetic Elizabeth City Ground Water (mg/L)	Synthetic Denver Federal Center Ground Water (mg/L)
Ca	10	110
Mg	7	32
Na	31	163
K	4	4
Cl	17	68
SO ₄	30	300
HCO ₃	82	433
pH	6.0	7.2

exposed iron compared to unreacted iron (Figure 5.16). The added component of mineral precipitates (carbonates and sulfides) and microbial biomass to zero-valent iron apparently increases the uptake rate of chromium, probably due to an increase in the number of available sorption sites. Increased chromium removal was also observed in experiments with field-exposed iron materials from the DFC (where chromium is not a ground-water contaminant).

Table 5.5 presents a summary of rate data for reactions of TCE and 1,1,1-TCA. Values of $\log k_{SA}$ in Table 5.5 are based on pseudo-first-order reaction kinetics. In general, $\log k_{SA}$ values for TCE are independent of whether the iron used was fresh or contained quantities of mineral precipitates and microbial biomass. The linearity of $\ln[\text{TCE}]$ vs. time plots decreases in the order unreacted iron > midbarrier iron > upgradient iron, as indicated by the standard regression coefficient. This trend suggests that removal processes are more complicated in materials containing authigenic components. Results for 1,1,1-TCA give $\log k_{SA}$ values that range from -3.1 to -4.0 . The effect that mineral precipitates play is still unclear as the slowest and fastest kinetics were observed, respectively, in systems containing upgradient iron from the DFC and Elizabeth City PRBs.

The batch experiments indicate that zero-valent iron retains reactivity and the ability to remove chlorinated ethenes, ethanes, and hexavalent chromium even after long-term exposure times to ground water. Interestingly, the ability of zero-valent iron to remove chromium from ground water appears to improve with time. The Elizabeth City PRB is expected to remain effective for chromium removal for another five-year period at a minimum. Observations of contaminant breakthrough in field PRBs may be more directly tied to decreases in hydraulic performance (i.e., system residence time, plume bypass) rather than loss of reactivity of zero-valent iron.

5.4 Microbial Activity

The oxidation or corrosion of zero-valent iron may be stimulated or inhibited by microorganisms. From a subsurface ecological perspective, metallic iron represents a significant energy reservoir. Due to the limited solubility of oxygen in ground water and the rapid reduction of molecular oxygen by Fe(0) and Fe(II), PRBs usually exist as anaerobic environments. Under anaerobic conditions molecular oxygen-driven chemical corrosion rates may be reduced, but biologically mediated anaerobic corrosion may occur at rates exceeding those seen under oxygenated conditions. In the absence of oxygen, protons may serve as electron acceptors and allow for the formation of oxidized iron species such as Fe(II).

The enhancement of anaerobic corrosion and the formation of dissolved Fe(II) and hydrogen gas is not necessarily detrimental to PRB performance. If the target contaminant such as Cr(VI) is reduced by Fe(II) as well as Fe(0), production of aqueous Fe(II) could increase the size of the reaction/treatment zone as compared to the surface contact area of Fe(0) alone. However, the utilization of dissolved hydrogen may result in bacterial growth and biofilm formation. The development of this biofilm in a PRB may be detrimental to performance through several mechanisms. Biofilm growth in a porous medium may reduce the total volume and the average size of the pores (e.g., Taylor et al., 1990a; Thullner et al., 2002). Changes in PRB hydraulic conductivity, the masking of active sites, the removal of active chemical species, mineral precipitation, production of gas bubbles, and the competition for reducing equivalents are processes mediated by bacteria that could negatively affect PRB performance. Conversely some microbial processes could enhance PRB performance. In some instances, bacteria may be more effective at contaminant transformation or may degrade compounds unaffected by PRBs. It is, therefore, evident that a clear understanding is needed of microbial/PRB interactions for the design and efficient operation of PRBs.

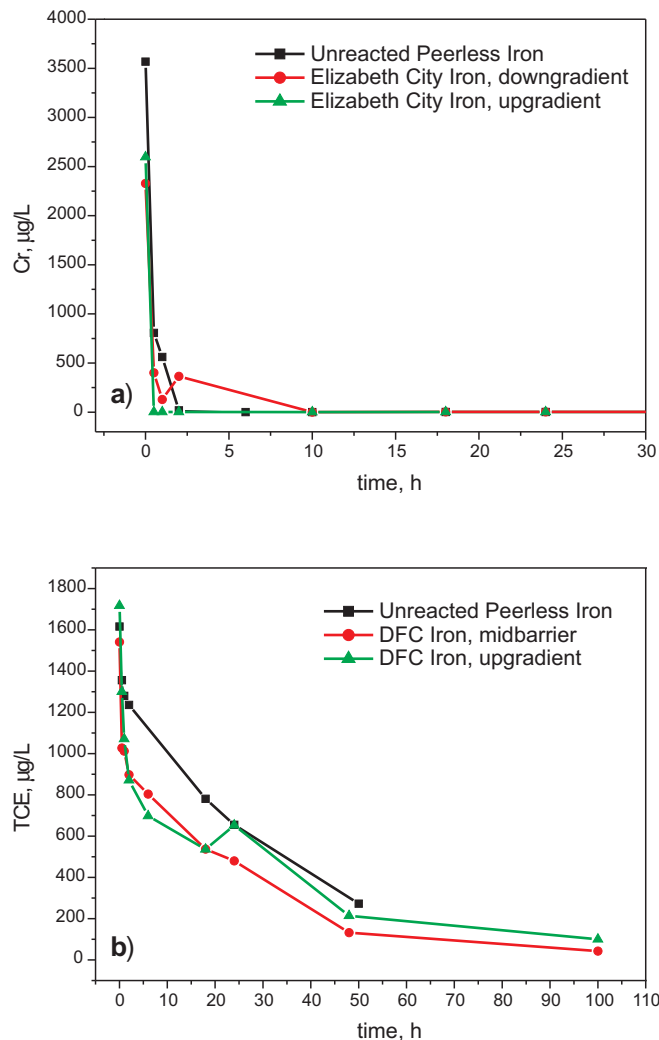


Figure 5.16 Concentration versus time in batch tests: a) chromium; b) TCE.

The possibility of exploiting microorganisms to enhance reductive treatment has been explored in laboratory studies (e.g., Till et al., 1998; Weathers et al., 1997; Gu et al., 1999; Oh et al., 2001; Gandhi et al., 2002). Scherer et al. (2000) provide a detailed review of laboratory investigations on combined microbial-Fe⁰ systems. Bacterial improvements are possible, for example, by iron-reducing bacteria that could reductively dissolve Fe(III) oxide layers, participate in forming reactive mineral species such as green rust, or directly degrade contaminants. Gandhi et al. (2002) conclude that bioaugmentation with specialized strains could enhance contaminant removal in some instances or increase the range of pollutants that could be treated in iron systems. Yet the effect of microorganisms on the long-term permeability and reactivity of PRB systems is not completely understood.

Studies that evaluate the microbiology of field Fe⁰ PRBs are few. Gu et al. (2002) investigated the microbial population and community structure at the Oak Ridge Y-12 Plant site. They found a diverse microbial community in the Fe⁰ media despite mildly alkaline conditions (pH up to 10). Concentrations of microbial biomass were from one to three orders magnitude greater within the Fe⁰ media compared to values found in adjacent aquifer materials. DNA analysis indicated the presence of sulfate-reducing and denitrifying bacteria in the iron wall. The activity of methanogenic bacteria was found to be relatively low, apparently due to competition by sulfate- and metal-reducing bacteria.

The results of this study at the Elizabeth City and Denver Federal Center PRBs are in broad agreement with those of Gu et al. (2002). At both sites elevated concentrations of microbial biomass were found within the iron wall as compared to adjacent aquifer materials (up to three orders of magnitude greater in biomass). The highest biomass accumulations were found near the upgradient aquifer/iron interface where electron donors enter the reactive treatment zone.

Table 5.5. Summary of Rate Data for Reactions of TCE and 1,1,1-TCA with Zero-valent Iron (Unreacted and Collected from Field PRBs)

System	TCE log k_{SA} (L/h·m ²)	R^2	1,1,1-TCA log k_{SA} (L/h·m ²)	R^2	n
Elizabeth City (GW) Unreacted Peerless Fe	-3.77	0.885	-3.86	0.949	10
Elizabeth City (GW) EC Iron midbarrier	-3.67	0.841	-3.66	0.935	7
Elizabeth City (GW) EC Iron upgradient	-3.72	0.781	-3.12	0.978	6
DFC (GW) Unreacted Peerless Fe	-3.83	0.988	-3.52	0.998	7
DFC (GW) DFC Iron midbarrier	-3.81	0.962	-3.82	0.990	9
DFC (GW) DFC Iron upgradient	-3.93	0.906	-4.06	0.884	8

Midbarrier and downgradient regions of the reactive barrier are, in most cases, free of microbial biomass. PLFA analysis suggests that a diverse assemblage of microorganisms colonize zero-valent iron systems at Elizabeth City and the Denver Federal Center. The formation of comparatively high-density, contaminant-reactive iron sulfides is one indirect consequence of microbiological activity (sulfate reducing bacteria).

The visual appearance and results of PLFA analyses from iron core materials collected from DFC gate 2 suggests that high levels of microbial biomass could significantly reduce permeability of PRBs. Previous laboratory investigations have documented this effect (e.g., Taylor and Jaffé, 1990b; Vandevivere and Baveye, 1992). Low-flow systems may be problematic in this regard. Although it is clear that microorganisms colonize zero-valent iron systems, an outstanding question remains as to whether microorganisms play a direct role in reducing contaminant concentrations. Additional research is needed to address this question.

A comparison of the average PLFA distribution among samples within reactive iron materials collected from Elizabeth City, DFC gate 1, DFC gate 2, and the Moffett Field PRB (data from Gavaskar et al., 2002) is shown in Figure 5.17. PLFA distributions in these four PRBs are broadly comparable. The Elizabeth City PRB is comparatively enriched in normal saturated (Nsats) structural groups that are ubiquitous in both prokaryotic and eukaryotic organisms. The broad similarity suggests that similar microbial populations colonize zero-valent iron systems. PLFA profiles in the reactive media tend to mirror profiles found in the aquifer materials sampled immediately upgradient to the reactive media; however, biomass concentrations are significantly greater within the iron zones. Indigenous microbial communities (especially anaerobes) appear to be stimulated by the placement of iron in the subsurface.

Microbial Biomass – PLFA Distribution

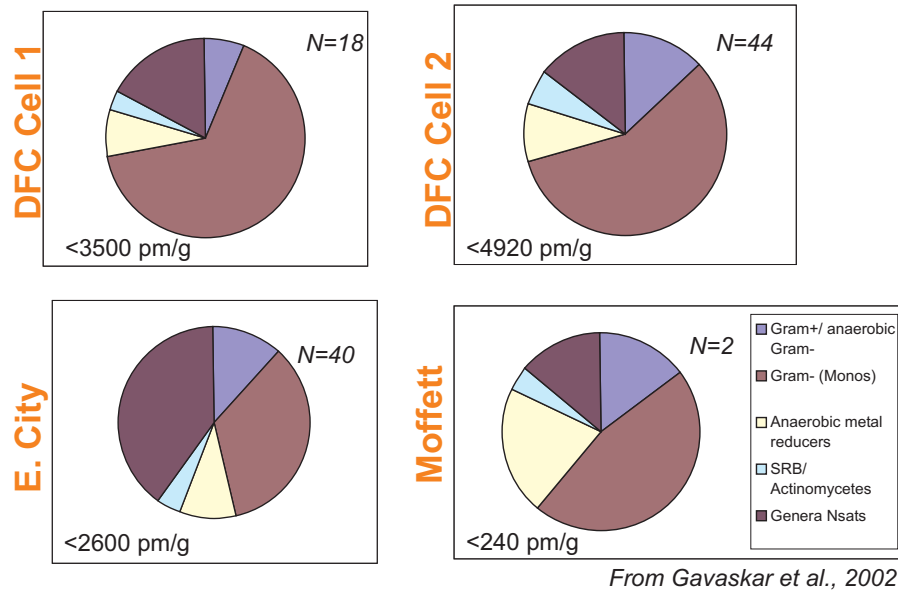


Figure 5.17 Comparison of PLFA distribution in four iron walls.

5.5 Hydrogeological Issues

The majority of recent research concerning PRBs has been directed at understanding geochemical processes involving different reactive materials as well as issues relating to predicting long-term performance. In comparison, fewer studies have explored issues of ground-water hydrology and flow behavior in PRBs. Clearly hydraulic and geochemical processes in PRBs are interrelated (see Tratnyek et al., 1997; Yabusaki et al., 2001; Mayer et al., 2001; Das, 2002). An understanding of the hydrologic properties of aquifers and reactive media, such as porosity, hydraulic conductivity distribution, hydraulic gradients, and flow velocities, heavily factor into the design and ultimately the success of PRB installations (Gavaskar et al., 1998). Two critical issues in system design that require an understanding of the spatial and temporal aspects of site hydrology are: 1) plume capture, i.e., ensuring that contaminated ground-water plumes are directed through the reactive material without bypass, underflow, or overflow; and, 2) residence time, i.e., ensuring that ground water remains in contact with the reactive media for an adequate period of time to allow for the removal or transformation of contaminant compounds.

Aquifer heterogeneity in chemical and physical properties is typically present to some degree at all sites. Such heterogeneities will result in variable contaminant flux across the influent area of the PRB and variable residence time requirements for contaminant treatment. Reliance on the use of bulk or averaged geochemical and hydraulic parameters may potentially result in inadequate system designs (Gavaskar et al., 2002). Several studies provide some insight into how aquifer heterogeneity can impact the performance of PRBs. Eykholt et al. (1999) concluded that seepage velocities within a homogeneous reactive media are principally controlled by heterogeneity in the downgradient aquifer. They showed that variability in hydraulic conductivity spanning two orders of magnitude resulted in variability in flow velocities and residence times within the barrier that span one order of magnitude. Studies by Tri-Agency partners (Kamolpornwijit et al., 2003; Moline et al., 2002) show that treatment of high nitrate and TDS ground water has led to increased mineral precipitation, which facilitated the development of heterogeneous flow, in addition to the initial heterogeneity present. This additional preferential flow over a year of PRB operation could cause ground-water bypass. In another modeling study, Benner et al. (2001) showed that localized or narrow high conductivity zones within the aquifer lead to greater preferential flow within the reactive media (see also Gupta and Fox, 1999). Benner et al. (2001) suggest that less variable flow will be attained using thicker, homogeneous barriers.

One of the most critical issues that must be addressed in the design of PRBs is the selection of the appropriate barrier width. The barrier width must provide sufficient contact time to insure that contaminants are degraded to target levels.

The barrier width must be selected based upon the range of ground-water flow velocities expected and the desired extent of contaminant removal for a given reactive material. Tratnyek et al. (1997) used laboratory derived kinetic data pertaining to the degradation of various chlorinated halogens by zero-valent iron and a one-dimensional transport model to estimate the minimum barrier width required for specified contaminant reductions as a function of ground-water flow velocity. This type of analysis is critical for providing a quantitative basis for system design to accompany laboratory feasibility testing.

Gavaskar et al. (1998) discuss the tools and methods that may be used to maximize the probability of success in hydraulic aspects of PRB performance. They emphasize the importance of thorough site characterization and ground-water flow modeling. A principal goal of site characterization is the development of a detailed understanding of site geology, hydrogeology, and contaminant distributions. Site characterization efforts should be to the level of capturing seasonal and spatial variability. Ground-water modeling efforts incorporate site characterization data to simulate water and contaminant transport. Modeling results will directly feed into a system design that ensures plume capture and adequate residence time for contaminant removal.

Hydraulic aspects of performance monitoring generally include water level surveys, hydraulic conductivity measurements, and determinations of seepage velocity. Water level surveys provide information on ground-water gradients and capture zones of PRBs. Water level surveys were regularly conducted at the Elizabeth City site on a quarterly basis. The results of water level surveys from June 1997, 1998, and 1999 are shown in Figure 5.18. Inspection of the water level map shows that the primary flow direction is across the PRB. In general, the hydraulic gradient in June varies from about 0.001 to 0.004, and this range further captures annual variability in the hydraulic gradient at this site. Based on hydraulic conductivities measured from slug tests and the hydraulic gradient obtained from water level measurements, a typical ground-water velocity of 0.5 ft/day and a typical residence time of four days are estimated.

McMahon et al. (1999) discussed the hydraulic performance of the Denver Federal Center PRB. Installation of the funnel-and-gate system at the DFC resulted in the mounding of ground water on the upgradient side of the sheet pile due to insufficient flow through the system. The buildup of ground-water levels on the upgradient side of the PRB raised concerns about the increased potential for ground-water bypass; flow under, over, or around the PRB. Follow-up studies suggest that underflow and overflow are not occurring, but that some bypass occurs around the southern side of gate 1 (Pacific Western Technologies, 2000). A downgradient distribution ditch was installed in late 1998, connecting gates 1 and 2, to decrease the ground-water mound. Although this attempt was unsuccessful in decreasing the head difference across the gates, the trench did greatly decrease the water levels within gates 1 and 2 (Pacific Western Technologies, 2000). Before and after installation of the distribution trench, the head differential across gate 2 has averaged approximately 7 ft. The lowering of water level in gates 1 and 2 suggested that only partial hydraulic connectivity existed at the upgradient aquifer/iron interface. Further studies by FHWA and the GSA were initiated to understand the hydraulic and performance issues at the DFC, including parts of the investigation described in this report.

It is believed that the head differential in gate 2 is a result of low permeability zone that was produced by backfilling pre-excavation trenches with muddy material. Pre-excavation was required in order to install the sheet pile. Alternatively, a smear zone of fine materials could have resulted as a consequence of the installation and removal of sheet piling installed for gate construction. In either case, flow velocity through gate 2 is reduced compared to that through gate 1. Characterization studies described in this report suggest that flow through gate 2 is reduced over a depth interval from about 5.5 to 8 m below ground surface. This reduced flow zone may be related to the low permeability zone or smear zone that developed during construction of the gate.

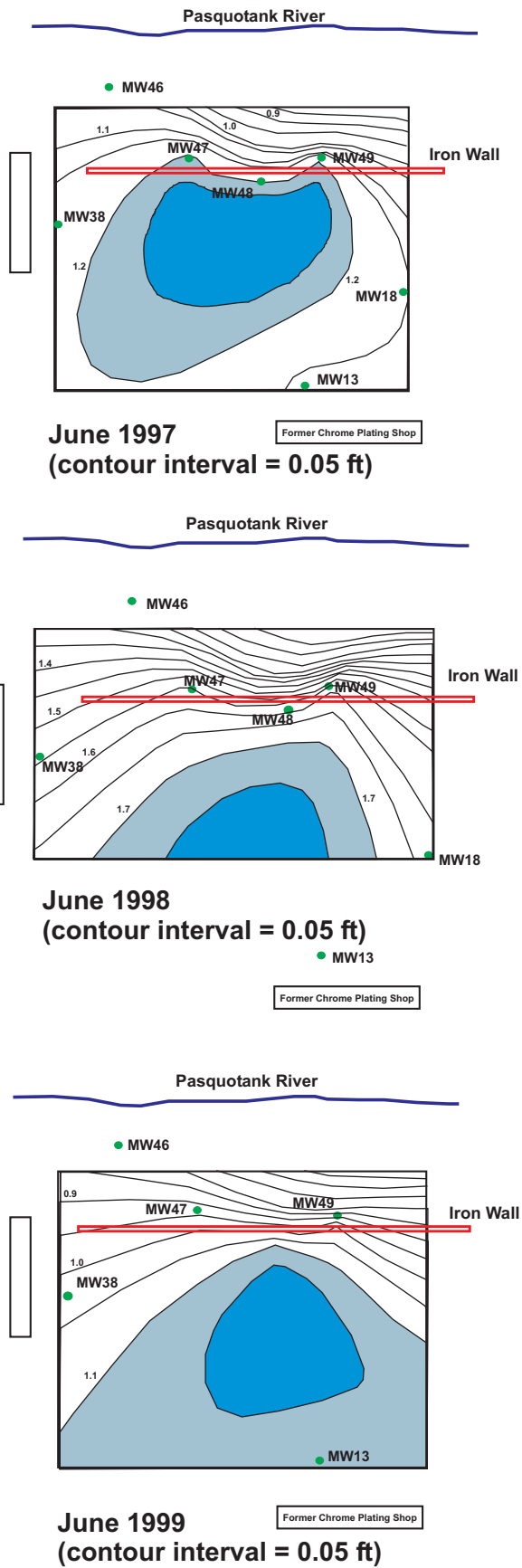


Figure 5.18 Water levels in Elizabeth City monitoring wells.



6.0 State of Permeable Reactive Barrier Technology and Lessons Learned from Long-Term Performance Monitoring

6.1 Permeable Reactive Barriers: An Accepted Remedial Option for Containment & Treatment of Contaminated Ground Water

The use of permeable reactive barriers for the restoration of contaminated ground water has evolved from innovative to accepted, standard practice, for the containment and treatment of a variety of contaminants in ground water. Like any remedial technology, the decision to use PRBs will be conditioned by the nature of the natural system, the target contaminants, and the treatment objectives. In the past 10 years, more than 100 sites have implemented this technology to treat chlorinated solvent compounds, fuel hydrocarbons, and various inorganic contaminants in ground water. As with any technology used to treat or extract contaminants in the subsurface, successful implementation will be contingent on effective site characterization, design, and construction. Our studies on long-term performance of the technology at a number of sites in the United States have shown the following with respect to ensuring (designing) and verifying (monitoring) that the PRB meets performance objectives:

- Adequate site characterization is necessary on the scale of the PRB. Site characterization approaches, typical of remedial feasibility investigations, are oftentimes not adequate. Additional localized characterization of the plume distribution in four dimensions (including time), understanding of local hydrogeology, and knowledge of the geochemistry of the site is required.
- Understanding of site hydrology has emerged as the most important factor for successful implementation. This is not surprising given the nature of the technology. The PRB must be located to intercept the plume. Once located in the subsurface, it cannot be moved, so an understanding of how the PRB will impact the prevailing flow patterns is important. It is imperative that the selected design allow for capture of the plume in its present configuration, as well as allow for variations in flow direction, depth, velocity, and concentrations of contaminants, which may vary over time.
- There is a need to develop contingency plans in case a system fails to meet design objectives. This requires specification of design criteria, performance objectives, and what constitutes a failure in order to clearly trigger the activation of contingency plans, i.e., alternative technologies or remedies to the installed PRB system.

Performance goals should target the adequacy of plume capture and contaminant treatment such that acceptable downgradient water quality is achieved in a reasonable time frame. Short-term objectives generally involve establishment of adequate residence time of the contaminant(s) in the reactive media to achieve treatment goals, while long-term objectives revolve around longevity or lifetime expectations for the system, which in turn, affect cost.

Specific criteria need to be established for all these concerns, and both parties (site owner and regulator) need to be clear on what triggers contingency plans. Maximum contaminant level (MCL) concentrations for contaminants in ground water are often used as criteria at points of compliance. This approach becomes complicated when contaminant levels already exceed goals at the point of compliance, and meeting these goals is contingent on desorption of residual contaminants or “flushing” over time. A time period needs to be specified in such a case that is reasonable given site characteristics and known contaminant behavior.

Performance goals are usually developed for the site as a whole and contingent upon plume and barrier location relative to compliance points and/or site boundaries. The performance goals can be numeric, regulatory-driven targets and may have system design features including remedial measures, such as natural attenuation, downgradient of the barrier location. The time horizon for sustaining performance goals will depend on site-specific factors related to chemical, physical and microbiological processes, but also such factors as the extent of source removal, source containment or expected lifetime of the source as a plume generator.

In many cases, contingency plans are required in the event that the PRB fails to meet performance criteria. Such plans may range from minor modifications of the PRB to use of an alternative technology. If the PRB fails to capture a portion of the plume, an extension to the PRB may be prescribed. If concentrations of contaminants exiting the PRB are higher

than expected, then an additional wall may be required downgradient of the first wall. In some installations, monitored natural attenuation of contaminants downgradient of the wall is expected and designed into the system to help meet compliance goals.

6.2 Lessons Learned: Site Characterization and PRB Construction

As with any ground-water remediation technology, adequate hydrogeologic characterization must be done to understand flow patterns and the distribution of the contaminant plume. This is particularly important for PRBs as the treatment system is immovable or passive, yet it must intercept and capture the contaminant plume for effective treatment. Information to be obtained includes advective velocity parameters such as the gradient, the hydraulic conductivity, porosity, and other parameters collected as part of a hydrogeologic characterization program. It is also important to understand temporal changes in flow direction and flux due to processes such as recharge, pumping of adjacent wells or other disturbances. Observed changes in flow direction at the Elizabeth City site, for example, have ranged as high as 25 degrees from time to time.

In addition to the hydrology, the stratigraphy and lithology of the site is important to understand and will dictate effective PRB design. If a low permeability layer exists at the site, the PRB can be keyed into this layer. If it does not exist, then a “hanging wall” design must be chosen which may add to the uncertainty of plume capture. If the site has low permeability layers through which the PRB must be constructed, care must be taken during construction to avoid smearing of such layers. This could impact hydraulic contact between the formation and the reactive media. A thorough understanding of site stratigraphy is especially important or helpful in choosing a particular construction method. Use of sheet piling to construct a reactive “gate” may not be a good choice where low permeability layers exist because of the smearing potential and increased difficulty in reestablishing good hydraulic contact between aquifer sediments and the reactive zone.

Characterization of contaminant concentrations in four dimensions is required for successful implementation of a PRB. In addition to knowledge of the plume in the three-dimensional space, it is also imperative to understand variability in plume shape and direction over time. Plumes deviate in direction and location over time and may change shape due to attenuation, degradation, mixing with other plumes, dilution, recharge, and other natural and anthropogenic-induced disturbances.

PRBs are often located within plumes. This requires some understanding of the impact of construction on plume behavior, both upgradient and downgradient of the barrier. For example, it is essential to verify that hydraulic contact between the plume and reactive media is established. If a PRB is located below an impermeable surface structure such as a parking lot, will the surface be repaved immediately or will recharge be allowed to occur over the PRB? Some understanding of natural attenuation processes at the site is important in being able to interpret the subsequent response of the natural system to the presence of the PRB. This is most often manifested in trying to estimate how long the downgradient aquifer will require to achieve cleanup goals. A key question to address is the length of time required before contaminants located downgradient of the barrier flush out of the sediments or degrade naturally.

6.3 Lessons Learned: Long-term Performance Assessments of PRBs

Geochemical characterization of sites for PRBs is important for optimizing the design and performance of a PRB and for predicting longevity. The lifetime of a PRB will depend on the hydrogeochemical nature of the site, flow rate, and contaminant flux, among other factors. It is known that high carbonate waters, high nitrate waters, high dissolved organic carbon waters, or waters with generally high total dissolved solids will have shorter life expectancies than what might be considered for “typical” or “average” composition waters. Decreased life expectancy may be caused by competition for reaction sites, loss of reactive sites due to rapid corrosion or fouling, or precipitation of inorganic minerals due to changes in geochemistry caused by the presence of the reactive media with subsequent loss of permeability.

If zero-valent iron is the reactive media, corrosion reactions together with mineral precipitation will eventually result in loss of permeability and/or reactivity resulting in decreased performance to the point where performance goals are no longer met. Long-term performance studies have documented decreased reactivity at some sites over time as well as loss of porosity, which can affect residence time of contaminants in the reactive media. For inorganic contaminants, such as chromium and arsenic, removal capacities have been calculated for zero valent iron PRBs. These capacities can be quickly reached if waters are rich in species that compete for reaction sites.

Monitoring of geochemical parameters (e.g., pH, Eh, dissolved oxygen [DO], specific conductance, terminal electron acceptors) in iron-based PRBs will verify that the system functions as designed once installed. Within the zero valent iron barriers, the change in these parameters is strikingly different than the natural system (e.g. Eh ~ -400 mV, pH > 9, DO = 0). Trends in these parameters may signal changes in system performance, but no clear correlations between these parameters and decreased performance have been observed to date. Long-term trends for these parameters are consistent with contaminant trends observed in both sites studied and reported on in this document. Spatial and temporal variations in the concentration distribution of terminal electron accepting species (e.g., sulfate), specific

conductance, and Eh suggest that both anaerobic iron corrosion and microbial activity play important roles in controlling the oxidation-reduction potential in iron barriers. Low Eh values (<-100 mV relative to the SHE) and decreases in the specific conductance of ground water between upgradient contaminant plumes and sampling points within reactive iron media are consistently indicative of normally operating PRB systems. Anomalous behavior in these parameters may be useful indicators of problems associated with construction, as observed in gate 2 at the Denver Federal Center.

Performance monitoring also focuses on the rate of mineral buildup within the reactive media. This may lead to decreased permeability and clogging. For zero valent iron systems, the reactive media is a long-term sink for C, S, Ca, Si, Mg, and N. The buildup of mineral precipitates is related to influent ground-water chemistry and flow rate. Mineral precipitates and microbial biomass accumulate the fastest near the upgradient aquifer-Fe⁰ interface. Porosity loss in the iron media due to precipitation of inorganic carbon and sulfur minerals can be estimated by integrating the concentrations of inorganic carbon and sulfur as a function of distance in the iron and estimating the volume loss by using the molar volumes of zero-valent iron, calcium carbonate, iron carbonate, and iron sulfide. The rate of mineral accumulation and the rate of iron corrosion varies spatially, therefore, so does the rate of porosity infilling. Porosity loss estimates have ranged from 1 to 4 % per year in this study. Based on these estimates, the average porosity of the PRB at Elizabeth City would not be expected to approach that of the surrounding aquifer for 15 to 30 years. The highest concentrations of mineral precipitates and rates of porosity loss are found adjacent to upgradient interfaces, and at Elizabeth City, there is a vertically localized zone which corresponds to the higher specific conductance portion of the plume. As these zones lose porosity, flow may be diverted to other locations along the face of the wall, thus extending lifetime estimates based on worst-case scenarios. As corrosion minerals form on the surface of the iron media, reactive surfaces are coated, presumably decreasing the effective reactive surface area. However, corrosion products formed include some minerals which themselves are highly reactive and capable of transforming inorganic and organic contaminants into immobile or non-toxic species. This phenomenon must also be factored into lifetime projections.

Microbiological impacts are important to understand in order to better predict how long PRB systems will remain effective. The presence of a large reservoir of iron, coupled with abundant substrate supports the metabolic activity of iron-reducing, sulfate-reducing, and/or methanogenic bacteria. These populations may have either beneficial or detrimental effects on system performance. Enhanced biodegradation of contaminants is possible where growth is stimulated by the presence of the reactive media, but biofouling may lead to permeability reduction within the reactive media or immediately upgradient. Additional research is required to assess changes in microbial ecology associated with the installation of these systems. Indications from Elizabeth City are that enhanced treatment some distance away from the PRB occurs, and it will be interesting to follow this development over extended periods of time.

While long-term performance observations of the Elizabeth City and Denver Federal Center site are now approaching seven years, there has still not been sufficient time to adequately predict the lifetime of these PRBs. It is clear that lifetimes exceeding 10 years are reasonable to expect, and they may function adequately for much longer. Continued studies are needed to better predict longevity based on ground-water composition, flow rate, and contaminant flux.

6.3.1 Recommendations for Future Research

The research conducted to date on the long-term performance of permeable reactive barriers has uncovered a number of new questions that require further investigation. In addition, several complex outstanding issues still require further study. Topical areas of research are outlined below where continued efforts will lead to more successful implementation of PRB technology for ground-water remediation.

- Tools are needed to more quantitatively relate ground-water chemistry to porosity loss, changes in hydraulic performance, and changes in Fe⁰ reactivity.
- An improved understanding is needed of how the reactivity and removal capacity of iron-based media changes with time and continued ground-water exposure, with respect to various inorganic and organic contaminants of concern, and over a range of hydrogeological and geochemical conditions.
- Research is needed on the microbial ecology of iron-based PRBs, especially with respect to potential benefits and deleterious effects, and the factors that control biomass accumulation.
- A better understanding and development of approaches are needed to determine flow patterns through reactive barriers in three-dimensions.
- Application of the PRB technology in conjunction with other subsurface treatment technologies is needed (e.g., monitored natural attenuation, source zone treatment).
- New methods are needed for regeneration of the reactive medium *in situ*, without having to excavate and entirely or partially replace the PRB.



7.0 References

- Agrawal, A. and Tratnyek, P. G. (1996). Reduction of nitro-aromatic compounds by zero-valent iron metal. *Environmental Science and Technology*, v. 30, p. 153-160.
- Agrawal, A., Ferguson, W. J., Gardner, B. O., Christ, J. A., Bandstra, J. Z., and Tratnyek, P. G. (2002). Effects of carbonate species on the kinetics of dechlorination of 1,1,1-trichloroethane by zero-valent iron. *Environmental Science and Technology*, v. 36, p. 4326-4333.
- Alowitz, M. J. and Scherer, M. M. (2002). Kinetics of nitrate, nitrite, and Cr(VI) reduction by iron metal. *Environmental Science and Technology*, v. 36, p. 299-306.
- Arnold, W. A. and Roberts, A. L. (2000). Pathways and kinetics of chlorinated ethylene and chlorinated acetylene reaction with Fe(0) particles. *Environmental Science and Technology*, v. 34, p. 1794-1805.
- Benner, S. G., Blowes, D. W., and Ptacek, C. J. (1997). A full-scale porous reactive wall for the prevention of acid mine drainage. *Ground Water Monitoring and Remediation*, fall, p. 99-107.
- Benner, S. G., Blowes, D. W., and Molson, J. W. H. (2001). Modeling preferential flow in reactive barriers: Implications for performance and design. *Ground Water*, v. 39, p. 371-379.
- Benning, L. G., Wilkin, R. T., and Barnes, H. L. (2000). Reaction pathways in the Fe-S system below 100°C. *Chemical Geology*, v. 167, p. 25-51.
- Berner, R. A. (1975). The role of magnesium in the crystal growth of calcite and aragonite from sea water. *Geochimica et Cosmochimica Acta*, v. 39, 489-504.
- Blengino, J. M., Keddum, M., Labbe, J. P., and Robbiola, L. (1995). Physico-chemical characterization of corrosion layers on iron in a sodium carbonate-bicarbonate containing environment. *Corrosion Science*, v. 37, p. 621-643.
- Blowes, D. W., Ptacek, C. J., Benner, S. G., McRae, C. W. T., Bennet, T., and Puls, R. W. (2000). Treatment of inorganic contaminants using permeable reactive barriers. *Journal of Contaminant Hydrology*, v. 45, p. 123-137.
- Blowes, D. W., Gillham, R. W., Ptacek, C. J., Puls, R. W., Bennett, T. A., O'Hannesin, S. F., Hanton-Fong, C. J., and Bain, J. G. (1999a). An In Situ Permeable Reactive Barrier for the Treatment of Hexavalent Chromium and Trichloroethylene in Ground Water, Volume 1: Design and Installation. U.S. Environmental Protection Agency, EPA/600/R-99/095a.
- Blowes, D. W., Puls, R. W., Gillham, R. W., Ptacek, C. J., Bennett, T. A., Bain, J. G., Hanton-Fong, C. J., and Paul, C. J. (1999b). An In Situ Permeable Reactive Barrier for the Treatment of Hexavalent Chromium and Trichloroethylene in Ground Water, Volume 2: Performance Monitoring. U.S. Environmental Protection Agency, EPA/600/R-99/095b.
- Blowes, D. W. and Mayer, K. U. (1999). An In Situ Permeable Reactive Barrier for the Treatment of Hexavalent Chromium and Trichloroethylene in Ground Water, Volume 3: Multicomponent Reactive Transport Modeling. U.S. Environmental Protection Agency, EPA/600/R-99/095c.
- Blowes, D. W., Ptacek, C. J., and Jambor, J. L. (1997). In-situ remediation of Cr(VI)-contaminated groundwater using permeable reactive walls: laboratory studies. *Environmental Science and Technology*, v. 31, p. 3348-3357.
- Bonin, P. M. L., Odziemkowski, M. S., Reardon, E. J., and Gillham, R. W. (2000). In situ identification of carbonate-containing green rust on iron electrodes in solutions simulating groundwater. *Journal of Solution Chemistry*, v. 29, p. 1061-1074.
- Bourrié, G., Trolard, F., Génin, J., Jaffrezic, A., Maître, V., and Abdelmoula, M. (1999). Iron control by equilibria between hydroxy-green rusts and solutions in hydromorphic soils. *Geochimica et Cosmochimica Acta*, v. 63, p. 3417-3427.
- Burriss, D. R., Campbell, T. J., and Manoranjan, V. S. (1995). Sorption of trichloroethylene and tetrachloroethylene in a batch reactive metallic iron-water system. *Environmental Science and Technology*, v. 29, p. 2850-2855.
- Butler, E. C. and Hayes, K. F. (1998). Effects of solution composition and pH on the reductive dechlorination of hexachlorethane by iron sulfide. *Environmental Science and Technology*, v. 32, p. 1276-1284.

-
- Butler, E. C. and Hayes, K. F. (1999). Kinetics of the transformation of trichloroethylene and tetrachloroethylene by iron sulfide. *Environmental Science and Technology*, v. 33, p. 2021-2027.
- Butler, E. C. and Hayes, K. F. (2000). Kinetics of the transformation of halogenated aliphatic compounds by iron sulfide. *Environmental Science and Technology*, v. 34, p. 422-429.
- Butler, E. C. and Hayes, K. F. (2001). Factors influencing rates and products in the transformation of trichloroethylene by iron sulfide and iron metal. *Environmental Science and Technology*, v. 35, p. 3884-3891.
- Cantrell, K. J., Kaplan, D. I., and Wietsma, T. W. (1995). Zero-valent iron for the in situ remediation of selected metals in groundwater. *Journal of Hazardous Materials*, v. 42, p. 201-212.
- Chapelle, F. H., Haack, S. K., Adriaens, P., Henry, M., and Bradley, P. M. (1996). Comparison of Eh and H₂ measurements for delineating redox processes in a contaminated aquifer. *Environmental Science and Technology*, v. 30, p. 3565-3569.
- Das, D. B. (2002). Hydrodynamic modeling for groundwater flow through permeable reactive barriers. *Hydrological Processes*, v. 16, p. 3393-3418.
- Davies, D. H. and Burstein, G. T. (1980). The effects of bicarbonate on the corrosion and passivation of iron. *Corrosion*, v. 36, p. 416-422.
- Deng, B., Burris, D. R., and Campbell, T. J. (1999). Reduction of vinyl chloride in metallic iron-water systems. *Environmental Science and Technology*, v. 33, p. 2651-2656.
- Dowling, J. E., Widdel, F., and White, D. C. (1986). Comparison of the phospholipid ester-linked fatty acid biomarkers of acetate-oxidizing sulphate-reducers and other sulphide-forming bacteria. *Journal of General Microbiology*, v. 132, p. 1815-1825.
- Drissi, S. H., Refait, Ph., Abdelmoula, M., and Génin, J. M. R. (1995). The preparation and thermodynamic properties of Fe(II)-Fe(III) hydroxide-carbonate (green rust I); Pourbaix diagram of iron in carbonate-containing aqueous media. *Corrosion Science*, v. 37, p. 2025-2041.
- Drury, W. J. (1999). Treatment of acid mine drainage with anaerobic solid-substrate reactors. *Water and Environmental Research*, v. 71, p. 1244-1250.
- Dvorak, D. H., Hedin, R. S., Edenborn, H. M., and McIntire, P. E. (1992). Treatment of metal-contaminated water using bacterial sulfate reduction: Results from pilot scale reactors. *Biotechnology and Bioengineering*, v. 40, p. 609-616.
- Edlund, A., Nichols, P. D., Roffey, R., and White, D. C. (1986). Extractible and lipopolysaccharide fatty acid and hydroxy acid profiles from *Desulfovibrio* species. *Journal of Lipid Research*, v. 26, p. 982-988.
- Erdös, V. and Altorfer, H. (1976). Ein dem Malachit ähnliches basisches Eisenkarbonat als Korrosionsprodukt von Stahl. *Werkstoffe und Korrosion*, v. 27, p. 304-312.
- Eykholt, G. R., Elder, C. R., and Benson, C. H. (1999). Effects of aquifer heterogeneity and reaction mechanism uncertainty on a reactive barrier. *Journal of Hazardous Materials*, v. 68, p. 1-24.
- Farrell, J., Kason, M., Melitas, N., and Li, T. (2000). Investigation of the long-term performance of zero-valent iron for reductive dechlorination of trichloroethylene. *Environmental Science and Technology*, v. 34, p. 514-521.
- Fennelly, J. P. and Roberts, A. L. (1998). Reaction of 1,1,1-trichloroethane with zero-valent metals and bimetallic reductants. *Environmental Science and Technology*, v. 32, p. 1980-1988.
- Fiedor, J. N., Bostick, W. D., Jarabek, R. J., and Farrell, J. (1998). Understanding the mechanism of uranium removal from groundwater by zero-valent iron using X-ray photoelectron spectroscopy. *Environmental Science and Technology*, v. 32, p. 1466-1473.
- Furukawa, Y., Kim, J., Watkins, J., and Wilkin, R. T. (2002). Formation of ferrihydrite and associated iron corrosion products in permeable reactive barriers of zero-valent iron. *Environmental Science and Technology*, v. 36, p. 5469-5475.
- Gandhi, S., Oh, B., Schnoor, J. L., and Alvarez, P. J. J. (2002). Degradation of TCE, Cr(VI), sulfate, and nitrate mixtures by granular iron in flow-through columns under different microbial conditions. *Water Research*, v. 36, p. 1973-1982.
- Gavaskar, A., Sass, B., Gupta, N., Drescher, E., Yoon, W., Sminchak, J., Hicks, J., and Condit, W. (2002). Evaluating the longevity and hydraulic performance of permeable reactive barriers at Department of Defense sites. Prepared for Naval Facilities Engineering Service Center, Port Hueneme, CA.
- Gavaskar, A. R., Gupta, N., Sass, B. M., Jansoy, R. J., and O'Sullivan, D. (1998). *Permeable Barriers for Groundwater Remediation Design, Construction, and Monitoring*, Battelle Press, Columbus, OH.

- Geiger, C. L., Ruiz, N. E., Clausen, C. A., Reinhart, D. R., and Quinn, J. W. (2002). Ultrasound pretreatment of elemental iron: kinetic studies of dehalogenation reaction enhancement and surface effects. *Water Research*, v. 36, p. 1342-1350.
- Gillham, R. W., Blowes, D. W., Ptacek, C. J., and O'Hannesin, S. F. (1994). Use of zero-valent metals in in-situ remediation of contaminated groundwater. In *In-situ Remediation: Scientific Basis for Current and Future Technologies*, eds. G. W. Gee and N. R. Wing, Battelle Press, Columbus, Ohio, p. 913-929.
- Gillham, R. W. and O'Hannesin, S. F. (1994). Enhanced degradation of halogenated aliphatics by zero-valent iron. *Ground Water*, v. 32, p. 958-967.
- Gu, B., Phelps, T. J., Liang, L., Dickey, M. J., Roh, Y., Kinsall, B. L., Palumbo, A. V., and Jacobs, G. K. (1999). Biogeochemical dynamics in zero-valent iron columns: implications for permeable reactive barriers. *Environmental Science and Technology*, v. 33, p. 2170-2177.
- Gu, B., Watson, D. B., Wu, L., Phillips, D. H., White, D. C., and Zhou, J. (2002). Microbiological characterization in a zero-valent iron reactive barrier. *Environmental Monitoring and Assessment*, v. 77, p. 293-307.
- Gui, J. and Devine, T. M. (1994). The influence of sulfate ions on the surface enhanced Raman spectra of passive films formed on iron. *Corrosion Science*, v. 36, p. 441-462.
- Gupta, N. and Fox, T. C. (1999). Hydrogeologic modeling for permeable reactive barriers. *Journal of Hazardous Materials*, v. 68, p. 19-39.
- Hassan, S. A. (2000). Reduction of halogenated hydrocarbons in aqueous media: I. Involvement of sulfur in iron catalysis. *Chemosphere*, v. 40, p. 1357-1363.
- Huang, C. P., Wang, H. W., and Chiu, P. C. (1998). Nitrate reduction by metallic iron. *Water Research*, v. 32, p. 2257-2264.
- Hurlbut, C. S. and Klein, C. (1977). *Manual of Mineralogy*, 19th Edition. John Wiley & Sons, New York, 532 pp.
- Johnson, T. L. and Tratnyek, P. G. (1994). A column study of geochemical factors affecting reductive dechlorination of chlorinated solvents by zero-valent iron. In *In-situ Remediation: Scientific Basis for Current and Future Technologies*, eds. G.W. Gee and N. R. Wing, Volume 2, Battelle Pacific Northwest Laboratories, Pasco, WA, p. 931-947.
- Johnson, T. L., Scherer, M. M., and Tratnyek, P. G. (1996). Kinetics of halogenated organic compound degradation by iron metal. *Environmental Science and Technology*, v. 30, p. 2634-2640.
- Kamolpornwijit, W., Liang, L., West, O., Moline, G., and Sullivan, A. (2002). Heterogeneity development and its influence on long-term PRB performance. In RTDF Permeable Reactive Barriers Action Team Meeting (November 6-7, Washington, DC).
- Kamolpornwijit, W., Liang, L., West, O., Moline, G., and Sullivan, A. (2003). Heterogeneity development and its influence on long-term PRB performance: A column study. *Journal of Contaminant Hydrology*, in press.
- Köber, R., Schlicker, O., Ebert, M., and Dahmke, A. (2002). Degradation of chlorinated ethylenes by Fe⁰: inhibition process and mineral precipitation. *Environmental Geology*, v. 41, p. 644-652.
- Lackovic, J. A., Nikolaidis, N. P., Dobbs, G. M. (2000). Inorganic arsenic removal by zero-valent iron. *Environmental Engineering and Science*, v. 17, p. 29-39.
- Langmuir, D. (1997). *Aqueous Environmental Geochemistry*. Prentice Hall, Upper Saddle River, NJ, 600 pp.
- Lee, W. and Batchelor, B. (2002a). Abiotic reductive dechlorination of chlorinated ethylenes by iron-bearing soil minerals. 1. Pyrite and magnetite. *Environmental Science and Technology*, v. 36, p. 5147-5154.
- Lee, W. and Batchelor, B. (2002b). Abiotic reductive dechlorination of chlorinated ethylenes by iron-bearing soil minerals. 2. Green rust. *Environmental Science and Technology*, v. 36, p. 5348-5354.
- Liang, L., Sullivan, A., West, O., Kamolpornwijit, W., Moline, G. (2003). Predicting the precipitation of mineral phases in permeable reactive barriers. *Environmental Science and Technology*, in press.
- Liang, L., Moline, G., Kamolpornwijit, W., Gu, B., Sullivan, A., and West, O. (2002). Performance Assessment of Zero-valent Iron Permeable Reactive Barriers, Environmental Sciences Division, Oak Ridge National Laboratory Report TTP No. ORO-9-SS-30.
- Liang, L., Korte, N., Gu, B., Puls, R., and Reeter, C. (2000). Geochemical and microbiological reactions affecting the long-term performance of in situ barriers. *Advances in Environmental Research*, v. 4, p. 273-286.
- Lien, H. and Wilkin, R. T. (2002). Reductive activation of dioxygen for degradation of methyl tert-butyl ether by bifunctional aluminum. *Environmental Science and Technology*, v. 36, p. 4436-4440.
- Mackenzie, P. D., Horney, D. P., and Sivavec, T. M. (1999). Mineral precipitation and porosity losses in granular iron columns. *Journal of Hazardous Materials*, v. 68, p. 1-17.

-
- Matheson, L. J. and Tratnyek, P. G. (1994). Reductive dehalogenation of chlorinated methanes by iron metal. *Environmental Science and Technology*, v. 28, p. 2045-2053.
- Matheson, L. J. (1994). Abiotic and biotic reductive dehalogenation of halogenated methanes. Unpublished Ph.D. Dissertation, Oregon Graduate Institute of Science and Technology.
- Mayer, K. U., Blowes, D. W., and Frind, E. O. (2001). Reactive transport modeling of an in situ reactive barrier for the treatment of hexavalent chromium and trichloroethylene. *Water Resources Research*, v. 37, p. 3091-3103.
- McGill, I. R., McEnaney, B., and Smith, D. C. (1976). Crystal structure of green rust formed by corrosion of cast iron. *Nature*, v. 259, p. 200-201.
- McMahon, P. B., Dennehy, K. F., and Sandstrom, M. W. (1999). Hydraulic and geochemical performance of a permeable reactive barrier containing zero-valent iron, Denver Federal Center. *Ground Water*, v. 37, p. 396-404.
- Melitas, N., Chuffe-Moscoco, O., and Farrell, J. (2001). Kinetics of soluble chromium removal from contaminated water by zerovalent iron media: Corrosion inhibition and passive oxide effects. *Environmental Science and Technology*, v. 35, p. 3948-3953.
- Moline, G., Liang, L., Kamolpornwijit, W., and West, L. (2002). Data Acquisition Report Long-term Monitoring of Permeable Reactive Barrier, Environmental Sciences Division, Oak Ridge National Laboratory Report TTP No. ORO-9-SS-30.
- Morrison, S. J., Metzler, D. R., and Carpenter, C. E. (2001). Uranium precipitation in a permeable reactive barrier by progressive irreversible dissolution of zerovalent iron. *Environmental Science and Technology*, v. 35, p. 385-390.
- Morrison, S. J., Metzler, D. R., and Dwyer, B. P. (2002). Removal of As, Mn, Mo, Se, U, V and Zn from groundwater by zero-valent iron in a passive treatment cell: reaction progress modeling. *Journal of Contaminant Hydrology*, v. 56, p. 99-116.
- Nam, S. and Tratnyek, P. G. (2000). Reduction of azo dyes with zero-valent iron. *Water Research*, v. 34, p. 1837-1845.
- Odziemkowski, M. S., Schumacher, T. T., and Reardon, E. J. (1998). Mechanism of oxide film formation on iron in simulated groundwater solutions. *Corrosion Science*, v. 40, p. 371-389.
- Oh, B., Just, C. L., and Alvarez, P. J. J. (2001). Hexahydro-1,3,5-trinitro-1,3,5-triazine mineralization by zerovalent iron and mixed anaerobic cultures. *Environmental Science and Technology*, v. 35, p. 4341-4346.
- O'Hannesin, S. F. and Gillham, R. W. (1998). Long-term performance of an in situ "Iron Wall" for remediation of VOCs. *Ground Water*, v. 36, p. 164-172.
- Orth, W. S. and Gillham, R. W. (1996). Dechlorination of trichloroethene in aqueous solution using Fe⁰. *Environmental Science and Technology*, v. 30, p. 66-71.
- Pacific Western Technologies, Ltd. 2000. 1999 Performance Evaluation of the Interim Groundwater Remediation Measure, Denver Federal Center. Prepared for Federal Highway Administration and General Services Administration, Denver CO.
- Parkes, R. J., Dowling, N. J. E., White, D. C., Herbert, R. A., and Gibson, G. R. (1993). Characterization of sulphate-reducing bacterial populations within marine and estuarine sediments with different rates of sulphate reduction. *FEMS Microbiology Ecology*, v. 102, p. 235-250.
- Phillips, D. H., Gu, B., Watson, D. B., Roh, Y., Liang, L., and Lee, S. Y. (2000). Performance evaluation of a zero-valent iron reactive barrier: mineralogic characteristics. *Environmental Science and Technology*, v. 34, p. 4169-4176.
- Postma, D., Boesen, C., Kristiansen, H., and Larsen, F. (1991). Nitrate reduction in an unconfined sandy aquifer: Water chemistry, reduction processes, and geochemical modeling. *Water Resources Research*, v. 27, p. 255-263.
- Powell, R. M., Puls, R. W., Hightower, S. K., and Sabatini, D. A. (1995). Coupled iron corrosion and chromate reduction: Mechanisms for subsurface remediation. *Environmental Science and Technology*, v. 29, p. 1913-1922.
- Powell, R. M., Blowes, D. W., Gillham, R. W., Schultz, D., Sivavec, T., Puls, R. W., Vogan, J. L., Powell, P. D., and Landis, R. (1998). Permeable reactive barrier technologies for contaminant remediation, EPA/600/R-98/125, 94 pp.
- Pratt, A. R., Blowes, D. W., and Ptacek, C. J. (1997). Products of chromate reduction on proposed subsurface remediation material. *Environmental Science and Technology*, v. 31, p. 2492-2498.
- Puls, R. W., Blowes, D. W., and Gillham, R. W. (1999a). Long-term performance monitoring for a permeable reactive barrier at the U.S. Coast Guard Support Center, Elizabeth City, North Carolina. *Journal of Hazardous Materials*, v. 68, p. 109-124.
- Puls, R. W., Paul, C. J., and Powell, R. M. (1999b). The application of in situ permeable reactive (zero-valent iron) barrier technology for the remediation of chromate-contaminated groundwater: A field test. *Applied Geochemistry*, v. 14, p. 989-1000.

-
- Reardon, E. J. (1995). Anaerobic corrosion of granular iron: Measurement and interpretation of hydrogen evolution rates. *Environmental Science and Technology*, v. 29, p. 2936-2945.
- Refait, Ph., Géhin, A., Abdelmoula, M., and Génin, J. M. R. (2003). Coprecipitation thermodynamics of iron (II-III) hydroxysulphate green rust from Fe(II) and Fe(III) salts. *Corrosion Science*, v. 45, p. 659-676.
- Ritter, K., Odziemkowski, M. S., Gillham, R. W. (2002). An in situ study of the role of surface films on granular iron in the permeable iron wall technology. *Journal of Contaminant Hydrology*, v. 55, p. 87-111.
- Roberts, A. L., Totten, L. A., Burris, A. W., and Campbell, T. J. (1996). Reductive elimination of chlorinated ethylenes by zero-valent metals. *Environmental Science and Technology*, v. 30, p. 2654-2659.
- Roh, Y., Lee, S. Y., and Elless, M. P. (2000). Characterization of corrosion products in the permeable reactive barriers. *Environmental Geology*, v. 40, p. 184-194.
- Ruiz, N., Seal, S., and Reinhart, D. (2000). Surface chemical reactivity in selected zero-valent iron samples used in groundwater remediation. *Journal of Hazardous Materials*, v. B80, p. 107-117.
- Sarr, D. (2001). Zero-valent-iron permeable reactive barriers-How long will they last? *Remediation*, v. 11, p. 1-18.
- Scherer, M. M., Johnson, K. M., Westall, J. C., and Tratnyek, P. G. (2001). Mass transport effects on the kinetics of nitrobenzene reduction by iron metal. *Environmental Science and Technology*, v. 35, p. 2804-2811.
- Scherer, M. M., Balko, B. A., and Tratnyek, P. G. (1998). The role of oxides in reduction reactions at the metal-water interface. In *Kinetics and Mechanisms of Reactions at the Mineral-Water Interface*, Ch. 15, eds. D. L. Sparks and T. Grundl, American Chemical Society, Washinton, D.C.
- Scherer, M. M., Richter, S., Valentine, R. L., and Alvarez, P. J. (2000). Chemistry and microbiology of permeable reactive barriers for in situ groundwater cleanup. *Critical Reviews in Environmental Science and Technology*, v. 30, p. 363-411.
- Schlicker, O., Ebert, M., Fruth, M., Weidner, M., Wüst, W., and Dahmke, A. (2000). Degradation of TCE with iron: The role of competing chromate and nitrate reduction. *Ground Water*, v. 38, p. 403-409.
- Siantar, D. P., Schreier, C. G., Chou, C. S., and Reinhard, M. (1996). Treatment of 1,2-dibromo-3-chloropropane and nitrate-contaminated water with zero-valent iron or hydrogen-palladium catalysts. *Water Research*, v. 30, p. 2315-2322.
- Su, C. and Puls, R.W. (1999). Kinetics of trichloroethene reduction by zerovalent iron and tin: pretreatment effect, apparent activation energy, and intermediate products. *Environmental Science and Technology*, v. 33, p. 163-168.
- Su, C. and Puls, R.W. (2001). Arsenate and arsenite removal by zerovalent iron: kinetics, redox transformation, and implications for in situ groundwater remediation. *Environmental Science and Technology*, v. 35, p. 1487-1492.
- Taylor, R. M. (1973). Crystal structures of some double hydroxide minerals. *Mineralogical Magazine*, v. 39, p. 377-389.
- Taylor, S. W., Milly, P. C. D., and Jaffé, P. R. (1990a). Biofilm growth and the related changes in the physical properties of a porous medium 2. Permeability. *Water Resources Research*, v. 26, p. 2161-2169.
- Taylor, S. W. and Jaffé, P. R. (1990b). Biofilm growth and the related changes in the physical properties of a porous medium 1. Experimental investigation. *Water Resources Research*, v. 26, p. 2153-2159.
- Thullner, M., Mauclaire, L., Schroth, M. H., Kinzelbach, W., and Zeyer, J. (2002). Interaction between water flow and spatial distribution of microbial growth in a two-dimensional flow field in saturated porous media. *Journal of Contaminant Hydrology*, v. 58, p. 169-189.
- Till, B. A., Weathers, L. J., and Alvarez, P. J. (1998). Fe(0)-supported autotrophic denitrification. *Environmental Science and Technology*, v. 32, p. 634-639.
- Tratnyek, P. G., Johnson, T. L., Scherer, M. M., and Eykholt, G. R. (1997). Remediating ground water with zero-valent metals: Chemical considerations in barrier design. *Ground Water Monitoring and Remediation*, v. 17, p. 108-114.
- Trudinger, P. A., Chambers, L. A., and Smith, J. W. (1985). Low-temperature sulphate reduction: Biological versus abiological. *Canadian Journal of Earth Sciences*, v. 22, p. 1910-1918.
- Tunlid, A. and White, D. C. (1991). Biochemical analysis of biomass, community structure, nutritional status and metabolic activity of microbial communities in soil. In *Soil Biochemistry*, Volume 7, eds. J. M. Bollag and G. Stotzky, New York, p. 229-262.
- USGS (1999). Performance evaluation of the interim ground-water remediation measure and distribution trench, Denver Federal Center. Prepared for Federal Highway Administration and General Services Administration, Denver, CO.
- Vandevivere, P. and Baveye, P. (1992). Relationship between transport of bacteria and their clogging efficiency in sand columns. *Applied and Environmental Microbiology*, v. 58, p. 2523-2530.

-
- Vaughan, D. J. and Craig, J. R. (1978). *Mineral Chemistry of Metal Sulfides*. Cambridge University Press, London, 493 pp.
- Vikesland, P. J., Klausen, J., Kohn, T., Burris, D. R., Ball, W. P., and Roberts, L. (2002). Co-solute effects on the reactivity of iron with groundwater contaminants. In *The Third International Conference on Remediation of Chlorinated and Recalcitrant Compounds*, Eds. A. Gavaskar and S. Chen (May 20-23, Monterey, CA).
- Vogan, J. L., Focht, R. M., Clark, D. K., and Graham, S. L. (1999). Performance evaluation of a permeable reactive barrier for remediation of dissolved chlorinated solvents in groundwater. *Journal of Hazardous Materials*, v. 68, p. 97-108.
- Waybrant, K. R., Blowes, D. J., and Ptacek, C. J. (1998). Selection of reactive mixtures for use in permeable reactive walls for treatment of mine drainage. *Environmental Science and Technology*, v. 32, p. 1972-1979.
- Waybrant, K. R., Ptacek, C. J., and Blowes, D. W. (2002). Treatment of mine drainage using permeable reactive barriers: Column experiments. *Environmental Science and Technology*, v. 36, p. 1349-1356.
- Weathers, L. J., Parkin, G. F., and Alvarez, P. J. (1997). Utilization of cathodic hydrogen as electron donor for chloroform cometabolism by a mixed, methanogenic culture. *Environmental Science and Technology*, v. 31, p. 880-885.
- Wilkin, R.T., Puls, R.W., and Sewell, G.W. (2002). Long-Term Performance of Permeable Reactive Barriers for Ground Water Remediation: An Evaluation at Two Sites. EPA Environmental Research Brief, EPA/600/S-02/001, 18 pp.
- Wilkin, R.T. (2002). Permeable reactive barrier performance monitoring: Long-term trends in geochemical parameters at two sites. In *The Third International Conference on Remediation of Chlorinated and Recalcitrant Compounds*, Eds. A. Gavaskar and S. Chen (May 20-23, Monterey, CA).
- Wilkin, R.T., Puls, R.W., and Sewell, G.W. (2003). Long-term performance of permeable reactive barriers using zero-valent iron: Geochemical and microbiological effects. *Ground Water*, v. 41, p. 493-503.
- Wolery, T.J. (1979). Calculation of chemical equilibrium between aqueous solution and minerals: The EQ3/6 software package. Lawrence Livermore National Laboratory Report UCRL-52658.
- Wüst, W.F., Köber, R., Schlicker, O., and Dahmke, A. (1999). Combined zero- and first-order kinetic model of the degradation of TCE and cis-DCE with commercial iron. *Environmental Science and Technology*, v. 33, p. 4304-4309.
- Yabusaki, S., Cantrell, K., Sass, B., and Steefel, C. (2001). Multicomponent reactive transport in an in situ zero-valent iron cell. *Environmental Science and Technology*, v. 35, p. 1493-1503.
- Zhabina, N.N. and Volkov, I.I. (1978). A method of determination of various sulfur compounds in sea sediments and rocks. In *Environmental Biogeochemistry and Geomicrobiology*, W. Krumbein (ed.), v. 3, Ann Arbor, Ann Arbor Science Publishers, p. 735-746.

Appendix A

Table A1. Inorganic Carbon and Sulfur Concentrations in Elizabeth City Cores

Sample ID	Location	Section	Interval cm	Date	Total IC µg/g	Total S µg/g
EC050801-1	Upgradient	5	0-10.2	May-01	56	80
EC050801-1	Upgradient	4	10.2-20.4	May-01	31	110
EC050801-1	Upgradient	3	20.4-30.6	May-01	83	170
EC050801-1	Upgradient	2	30.6-40.8	May-01	121	330
EC050801-1	Upgradient	1	40.8-51.0	May-01	315	620
EC050801-1	Upgradient	-1	51.0-56.1	May-01	1850	468
EC050801-1	Upgradient	-2	56.1-61.2	May-01	384	240
EC050801-1	Upgradient	-3	61.2-66.3	May-01	264	90
EC050801-1	Upgradient	-4	66.3-71.4	May-01	153	70
EC050801-1	Upgradient	-5	71.4-76.5	May-01	151	70
EC050801-1	Upgradient	-6	76.5-81.6	May-01	23	100
EC050801-1	Upgradient	-7	81.6-86.7	May-01	44	70
EC050801-1	Upgradient	-8	86.7-91.8	May-01	71	50
EC050801-1	Upgradient	-9	91.8-96.9	May-01	106	60
EC050801-1	Upgradient	-11	102-107.1	May-01	7	100
EC050801-3	Upgradient	5	0-10.2	May-01	4	130
EC050801-3	Upgradient	4	10.2-20.4	May-01	53	410
EC050801-3	Upgradient	3	20.4-30.6	May-01	176	1510
EC050801-3	Upgradient	2	30.6-40.8	May-01	14	190
EC050801-3	Upgradient	1	40.8-51.0	May-01	10	160
EC050801-3	Upgradient	-1	51.0-56.1	May-01	4633	3880
EC050801-3	Upgradient	-2	56.1-61.2	May-01	5867	1100
EC050801-3	Upgradient	-3	61.2-66.3	May-01	4000	590
EC050801-3	Upgradient	-4	66.3-71.4	May-01	2100	340
EC050801-3	Upgradient	-5	71.4-76.5	May-01	1086	210
EC050801-3	Upgradient	-6	76.5-81.6	May-01	381	150
EC050801-3	Upgradient	-7	81.6-86.7	May-01	453	110
EC050801-3	Upgradient	-8	86.7-91.8	May-01	176	80
EC050801-3	Upgradient	-9	91.8-99.4	May-01	149	90
EC050801-4	Upgradient	5	0-10.2	May-01	5	60
EC050801-4	Upgradient	4	10.2-20.4	May-01	7	100
EC050801-4	Upgradient	3	20.4-30.6	May-01	29	140
EC050801-4	Upgradient	2	30.6-40.8	May-01	20	170
EC050801-4	Upgradient	1	40.8-51.0	May-01	500	690
EC050801-4	Upgradient	-1	51.0-56.1	May-01	1672	2140
EC050801-4	Upgradient	-2	56.1-61.2	May-01	3337	2080
EC050801-4	Upgradient	-3	61.2-66.3	May-01	1167	570
EC050801-4	Upgradient	-4	66.3-71.4	May-01	401	240
EC050801-4	Upgradient	-5	71.4-76.5	May-01	174	216
EC050801-4	Upgradient	-6	76.5-81.6	May-01	136	232
EC050801-4	Upgradient	-7	81.6-86.7	May-01	129	285
EC050801-4	Upgradient	-8	86.7-91.8	May-01	155	189
EC050801-4	Upgradient	-9	91.8-96.9	May-01	60	1
EC050801-4	Upgradient	-10	96.9-107.1	May-01	46	1

Table A1. (continued) Inorganic Carbon and Sulfur Concentrations in Elizabeth City Cores

Sample ID	Location	Section	Interval	Date	Total IC	Total S
			cm		µg/g	µg/g
EC050801-5	Upgradient	5	0-12.7	May-01	274	768
EC050801-5	Upgradient	4	12.7-25.4	May-01	150	620
EC050801-5	Upgradient	3	25.4-38.1	May-01	1023	720
EC050801-5	Upgradient	2	38.1-50.8	May-01	126	420
EC050801-5	Upgradient	1	50.8-63.5	May-01	258	640
EC050801-5	Upgradient	-1	63.5-68.6	May-01	468	1370
EC050801-5	Upgradient	-2	68.6-73.7	May-01	4491	1830
EC050801-5	Upgradient	-3	73.7-78.8	May-01	2370	2680
EC050801-5	Upgradient	-4	78.8-83.9	May-01	4000	2210
EC050801-5	Upgradient	-5	83.9-89.0	May-01	4520	709
EC050801-5	Upgradient	-6	89.0-94.1	May-01	1824	303
EC050801-6	Upgradient	5	0-12.7	May-01	0	10
EC050801-6	Upgradient	4	12.7-25.4	May-01	2	10
EC050801-6	Upgradient	3	25.4-38.1	May-01	20	20
EC050801-6	Upgradient	2	38.1-50.8	May-01	28	10
EC050801-6	Upgradient	1	50.8-63.5	May-01	69	20
EC050801-6	Upgradient	-1	63.5-68.6	May-01	231	180
EC050801-6	Upgradient	-2	68.6-73.7	May-01	223	160
EC050801-6	Upgradient	-3	73.7-78.8	May-01	172	100
EC050801-6	Upgradient	-4	78.8-83.9	May-01	186	110
EC050801-6	Upgradient	-5	83.9-89.0	May-01	110	90
EC050801-6	Upgradient	-6	89.0-94.1	May-01	76	80
EC050801-6	Upgradient	-7	94.1-101.7	May-01	121	70
EC050801-7	Upgradient	5	0-12.7	May-01	65	151
EC050801-7	Upgradient	4	12.7-25.4	May-01	8	149
EC050801-7	Upgradient	3	25.4-38.1	May-01	45	93
EC050801-7	Upgradient	2	38.1-50.8	May-01	78	280
EC050801-7	Upgradient	1	50.8-63.5	May-01	55	129
EC050801-7	Upgradient	-1	63.5-68.6	May-01	1542	1610
EC050801-7	Upgradient	-2	68.6-73.7	May-01	3615	926
EC050801-7	Upgradient	-3	73.7-78.8	May-01	3636	278
EC050801-7	Upgradient	-4	78.8-83.9	May-01	1219	212
EC050801-7	Upgradient	-5	83.9-89.0	May-01	383	168
EC050801-7	Upgradient	-6	89.0-94.1	May-01	162	122
EC050801-7	Upgradient	-7	94.1-99.2	May-01	206	95
EC050801-7	Upgradient	-8	99.2-104.3	May-01	158	76
EC050801-7	Upgradient	-9	104.3-109.4	May-01	256	147

Table A1. (continued) Inorganic Carbon and Sulfur Concentrations in Elizabeth City Cores

Sample ID	Location	Section	Interval cm	Date	Total IC μg/g	Total S μg/g
EC050901-8	Vertical	-1	0-5.1	May-01	59	98
EC050901-8	Vertical	-3	10.2-15.3	May-01	80	87
EC050901-8	Vertical	-5	20.4-25.6	May-01	51	70
EC050901-8	Vertical	-8	35.8-40.9	May-01	112	88
EC050901-8	Vertical	-11	51.1-56.2	May-01	49	80
EC050901-8	Vertical	-13	61.3-66.4	May-01	46	58
EC050901-8	Vertical	-15	71.5-76.6	May-01	90	84
EC050901-8	Vertical	-17	81.7-86.8	May-01	98	84
EC050901-8	Vertical	-18	86.8-91.9	May-01	201	90
EC050901-8	Vertical	-19	91.9-97.0	May-01	333	93
EC050901-8	Vertical	-20	97-102.1	May-01	285	101
EC050901-9	Vertical	-1	0-5.1	May-01	100	100
EC050901-9	Vertical	-3	10.2-15.3	May-01	122	103
EC050901-9	Vertical	-5	20.4-25.6	May-01	118	121
EC050901-9	Vertical	-7	30.7-35.8	May-01	204	93
EC050901-9	Vertical	-9	40.9-46.0	May-01	160	95
EC050901-9	Vertical	-11	51.1-56.2	May-01	242	104
EC050901-9	Vertical	-13	61.3-66.4	May-01	272	132
EC050901-9	Vertical	-15	71.5-76.6	May-01	276	116
EC050901-9	Vertical	-17	81.7-86.8	May-01	513	165
EC050901-9	Vertical	-18	86.8-91.9	May-01	517	174
EC050901-9	Vertical	-19	91.9-97.0	May-01	523	169
EC050901-9	Vertical	-20	97.0-102.1	May-01	854	121
EC050901-9	Vertical	-22	107.2-112.3	May-01	355	70
EC060200-1	Upgradient	4	0-10.2	Jun-00	7	50
EC060200-1	Upgradient	3	10.2-20.4	Jun-00	4	69
EC060200-1	Upgradient	2	20.4-30.6	Jun-00	3	70
EC060200-1	Upgradient	1	30.6-40.8	Jun-00	8	141
EC060200-1	Upgradient	-1	40.8-45.9	Jun-00	308	756
EC060200-1	Upgradient	-2	45.9-51.0	Jun-00	1740	588
EC060200-1	Upgradient	-3	51.0-56.1	Jun-00	244	230
EC060200-1	Upgradient	-4	56.1-61.2	Jun-00	175	168
EC060300-4	Upgradient	3	0-10.2	Jun-00	9	147
EC060300-4	Upgradient	2	10.2-20.4	Jun-00	8	143
EC060300-4	Upgradient	1	20.4-30.6	Jun-00	65	187
EC060300-4	Upgradient	-1	30.6-35.7	Jun-00	2339	1179
EC060300-4	Upgradient	-2	35.7-40.8	Jun-00	3210	466
EC060300-4	Upgradient	-3	40.8-45.9	Jun-00	2141	279
EC060300-4	Upgradient	-4	45.9-51.0	Jun-00	234	301
EC060300-4	Upgradient	-5	51.0-56.1	Jun-00	194	166
EC060300-4	Upgradient	-6	56.1-61.2	Jun-00	119	161
EC060300-4	Upgradient	-7	61.2-66.3	Jun-00	73	130
EC060300-4	Upgradient	-8	66.3-71.4	Jun-00	72	104
EC060300-4	Upgradient	-9	71.4-76.5	Jun-00	107	128

Table A1. (continued) Inorganic Carbon and Sulfur Concentrations in Elizabeth City Cores

Sample ID	Location	Section	Interval cm	Date	Total IC μg/g	Total S μg/g
EC060300-6	Downgradient	9	0-7.6	Jun-00	<1	265
EC060300-6	Downgradient	8	7.6-15.2	Jun-00	<1	296
EC060300-6	Downgradient	6	22.8-30.4	Jun-00	<1	194
EC060300-6	Downgradient	4	38.0-45.6	Jun-00	1	157
EC060300-6	Downgradient	2	53.2-60.8	Jun-00	41	125
EC060300-6	Downgradient	1	60.8-68.4	Jun-00	81	239
EC060300-6	Downgradient	-1	68.4-73.5	Jun-00	92	196
EC060300-6	Downgradient	-2	73.5-78.6	Jun-00	66	106
EC060300-6	Downgradient	-3	78.6-83.7	Jun-00	81	163
EC060300-6	Downgradient	-4	83.7-88.8	Jun-00	80	161
EC060300-6	Downgradient	-5	88.8-93.9	Jun-00	242	218
EC060300-5	Vertical	8	0-7.6	Jun-00	2	151
EC060300-5	Vertical	7	7.6-15.2	Jun-00	10	97
EC060300-5	Vertical	6	15.2-22.8	Jun-00	16	155
EC060300-5	Vertical	5	22.8-30.4	Jun-00	12	138
EC060300-5	Vertical	4	30.4-38.0	Jun-00	4	126
EC060300-5	Vertical	3	38.0-45.6	Jun-00	10	114
EC060300-5	Vertical	2	45.6-53.2	Jun-00	19	79
EC060300-5	Vertical	1	53.2-60.8	Jun-00	7	133
EC060300-5	Vertical	-1	60.8-68.4	Jun-00	66	239
EC060300-5	Vertical	-2	68.4-76.0	Jun-00	57	173
EC060300-5	Vertical	-3	76.0-83.6	Jun-00	80	174
EC060500-7A	Vertical	5	0-7.6	Jun-00	na	88
EC060500-7A	Vertical	4	7.6-15.2	Jun-00	na	81
EC060500-7A	Vertical	3	15.2-22.8	Jun-00	na	166
EC060500-7A	Vertical	2	22.8-30.4	Jun-00	na	104
EC060500-7A	Vertical	1	30.4-38.0	Jun-00	na	160
EC060500-7A	Vertical	-1	38.0-43.1	Jun-00	na	106
EC060500-7A	Vertical	-2	43.1-48.2	Jun-00	na	148
EC060500-7A	Vertical	-3	48.2-53.3	Jun-00	na	76
EC060500-7A	Vertical	-4	53.3-58.4	Jun-00	na	269
EC060500-7A	Vertical	-5	58.4-63.5	Jun-00	na	165
EC060500-7A	Vertical	-6	63.5-68.6	Jun-00	na	161
EC030616	Upgradient	1	0-10.2	Jun-99	571	289
EC030616	Upgradient	-1	10.2-20.4	Jun-99	1392	303
EC030616	Upgradient	-2	20.4-30.6	Jun-99	1345	292
EC030616	Upgradient	-3	30.6-40.8	Jun-99	1500	231
EC030616	Upgradient	-4	40.8-51.0	Jun-99	97	101
EC030616	Upgradient	-5	51.0-61.2	Jun-99	274	94

Table A1. (continued) Inorganic Carbon and Sulfur Concentrations in Elizabeth City Cores

Sample ID	Location	Section	Interval cm	Date	Total IC μg/g	Total S μg/g
EC90903	Upgradient	2	0-7.6	Sep-98	4	18
EC90903	Upgradient	1	7.6-15.2	Sep-98	55	211
EC90903	Upgradient	-1	15.2-22.8	Sep-98	2350	1019
EC90903	Upgradient	-2	22.8-30.4	Sep-98	357	315
EC90903	Upgradient	-3	30.4-38.0	Sep-98	174	137
EC90903	Upgradient	-4	38.0-45.6	Sep-98	117	183
EC90903	Upgradient	-5	45.6-53.2	Sep-98	110	178
EC90903	Upgradient	-6	53.2-60.8	Sep-98	50	142
EC6101	Upgradient	-1	0-7.6	Jun-98	1800	228
EC6101	Upgradient	-2	7.6-15.2	Jun-98	792	195
EC6101	Upgradient	-3	15.2-22.8	Jun-98	550	157
EC6101	Upgradient	-4	22.8-30.4	Jun-98	451	117
EC6101	Upgradient	-5	30.4-38.0	Jun-98	65	64
EC6101	Upgradient	-6	38.0-45.6	Jun-98	106	96
EC6101	Upgradient	-7	45.6-53.2	Jun-98	208	39
EC6101	Upgradient	-8	53.2-60.8	Jun-98	419	34
EC6101	Upgradient	-9	60.8-68.4	Jun-98	541	36

Table A2. Reduced Sulfur Speciation in Elizabeth City and Denver Federal Center Cores

Sample ID	Site	Section	Interval	Date	AVS	CRS	Total S
			cm		μg/g	μg/g	μg/g
EC060300-4	EC	1	20.4-30.6	Jun-00	17	6	187
EC060300-4	EC	-1	30.6-35.7	Jun-00	1200	nd	1179
EC060300-4	EC	-2	35.7-40.8	Jun-00	612	39	466
EC060300-4	EC	-3	40.8-45.9	Jun-00	303	nd	279
EC060300-4	EC	-4	45.9-51.0	Jun-00	351	nd	301
EC060300-4	EC	-6	56.1-61.2	Jun-00	222	nd	161
EC060300-4	EC	-7	61.2-66.3	Jun-00	155	nd	130
EC060300-4	EC	-9	71.4-76.5	Jun-00	145	nd	128
C2-12-71300	DFC	-1	0-10.2	Jul-00	3089	120	3239
C2-12-71300	DFC	-3	20.4-30.6	Jul-00	4333	198	4597
C2-12-71300	DFC	-5	40.8-51.0	Jul-00	3019	55	3356
C2-12-71300	DFC	-7	61.2-71.4	Jul-00	3976	230	4084
C2-12-71300	DFC	-9	81.6-91.8	Jul-00	3746	250	3833
C2-13-71300	DFC	-1	0-10.2	Jul-00	3382	504	3844
C2-13-71300	DFC	-3	20.4-30.6	Jul-00	3434	130	3527
C2-13-71300	DFC	-5	40.8-51.0	Jul-00	2807	227	3172
C2-13-71300	DFC	-7	61.2-71.4	Jul-00	4033	422	3935
C2-13-71300	DFC	-9	81.6-91.8	Jul-00	3254	105	3189
C2-14-71300	DFC	-1	0-10.2	Jul-00	1538	205	1627
C2-14-71300	DFC	-3	20.4-30.6	Jul-00	1275	193	1519
C2-14-71300	DFC	-5	40.8-51.0	Jul-00	2128	25	1957
C2-14-71300	DFC	-7	61.2-71.4	Jul-00	1829	25	1878
C2-17-71300	DFC	-1	0-5.1	Jul-00	3590	197	3799
C2-17-71300	DFC	-3	10.2-15.3	Jul-00	3365	262	3366
C2-17-71300	DFC	-5	20.4-25.5	Jul-00	2445	337	2324
C2-17-71300	DFC	-7	30.6-35.7	Jul-00	1752	148	1867

Notes: nd, not determined.

Table A3. Inorganic Carbon and Sulfur Concentrations in Denver Federal Center Cores

Sample ID	Location	Section	Interval	Date	Total IC	Total S
			cm		µg/g	µg/g
C1-1-71701	Upgradient	-1	0-5.1	Jul-01	8700	2203
C1-1-71701	Upgradient	-2	5.1-10.2	Jul-01	2500	2066
C1-1-71701	Upgradient	-3	10.2-15.3	Jul-01	2200	1966
C1-1-71701	Upgradient	-4	15.3-20.4	Jul-01	1444	1545
C1-1-71701	Upgradient	-5	20.4-25.5	Jul-01	395	928
C1-1-71701	Upgradient	-6	25.5-30.6	Jul-01	442	820
C1-1-71701	Upgradient	-7	30.6-35.7	Jul-01	392	1187
C1-1-71701	Upgradient	-8	35.7-40.8	Jul-01	348	874
C1-1-71701	Upgradient	-9	40.8-45.9	Jul-01	629	889
C1-1-71701	Upgradient	-10	45.9-51.0	Jul-01	352	899
C1-1-71701	Upgradient	-11	51.0-56.1	Jul-01	162	448
C1-1-71701	Upgradient	-12	56.1-61.2	Jul-01	125	463
C1-1-71701	Upgradient	-13	61.2-66.3	Jul-01	95	393
C1-1-71701	Upgradient	-14	66.3-71.4	Jul-01	102	359
C1-1-71701	Upgradient	-15	71.4-76.5	Jul-01	115	347
C1-1-71701	Upgradient	-16	76.5-81.6	Jul-01	95	326
C1-1-71701	Upgradient	-17	81.6-86.7	Jul-01	111	282
C1-1-71701	Upgradient	-18	86.7-91.8	Jul-01	146	242
C1-1-71701	Upgradient	-19	91.8-102	Jul-01	87	318
C1-2-71701	Upgradient	4	0-10.2	Jul-01	10300	390
C1-2-71701	Upgradient	3	10.2-20.4	Jul-01	358	279
C1-2-71701	Upgradient	2	20.4-30.6	Jul-01	31	72.6
C1-2-71701	Upgradient	1	30.6-40.8	Jul-01	42	151
C1-2-71701	Upgradient	-1	40.8-45.9	Jul-01	9000	3570
C1-2-71701	Upgradient	-2	45.9-51.0	Jul-01	3700	2790
C1-2-71701	Upgradient	-3	51.0-56.1	Jul-01	1800	1450
C1-2-71701	Upgradient	-4	56.1-61.2	Jul-01	4400	3160
C1-2-71701	Upgradient	-5	61.2-66.3	Jul-01	2500	3180
C1-2-71701	Upgradient	-6	66.3-71.4	Jul-01	3407	2440
C1-2-71701	Upgradient	-7	71.4-79.0	Jul-01	1347	1940
C1-3-71701	Upgradient	3	0-7.6	Jul-01	10	<5
C1-3-71701	Upgradient	2	7.6-15.2	Jul-01	19	<5
C1-3-71701	Upgradient	1	15.2-22.8	Jul-01	38	137
C1-3-71701	Upgradient	-1	22.8-27.9	Jul-01	8	138
C1-3-71701	Upgradient	-2	27.9-33.0	Jul-01	726	149
C1-3-71701	Upgradient	-3	33.0-38.1	Jul-01	2600	4321
C1-3-71701	Upgradient	-4	38.1-43.2	Jul-01	8900	5680
C1-3-71701	Upgradient	-5	43.2-48.3	Jul-01	4200	4860
C1-3-71701	Upgradient	-6	48.3-53.4	Jul-01	3000	4400
C1-3-71701	Upgradient	-7	53.4-58.5	Jul-01	3000	3290
C1-3-71701	Upgradient	-8	58.5-63.6	Jul-01	3600	5110
C1-3-71701	Upgradient	-9	63.6-68.7	Jul-01	3200	4640
C1-3-71701	Upgradient	-10	68.7-73.8	Jul-01	2000	2570
C1-3-71701	Upgradient	-11	73.8-81.4	Jul-01	775	1570

Table A3. (continued) Inorganic Carbon and Sulfur Concentrations in Denver Federal Center Cores

Sample ID	Location	Section	Interval cm	Date	Total IC µg/g	Total S µg/g
C1-4-71801	Downgradient	3	0-5.1	Jul-01	187	144
C1-4-71801	Downgradient	2	5.1-10.2	Jul-01	692	142
C1-4-71801	Downgradient	1	10.2-15.3	Jul-01	1500	237
C1-4-71801	Downgradient	-1	15.3-20.4	Jul-01	1700	787
C1-4-71801	Downgradient	-2	20.4-25.5	Jul-01	5800	2780
C1-4-71801	Downgradient	-3	25.5-30.6	Jul-01	9800	5290
C1-4-71801	Downgradient	-4	30.6-35.7	Jul-01	14100	7520
C1-4-71801	Downgradient	-5	35.7-40.8	Jul-01	8900	5450
C1-4-71801	Downgradient	-6	40.8-45.9	Jul-01	9500	5210
C1-4-71801	Downgradient	-7	45.9-51.0	Jul-01	11600	4430
C1-4-71801	Downgradient	-8	51.0-56.1	Jul-01	10400	4170
C1-4-71801	Downgradient	-9	56.1-61.2	Jul-01	7400	4690
C1-4-71801	Downgradient	-10	61.2-66.3	Jul-01	7000	3720
C1-4-71801	Downgradient	-11	66.3-71.4	Jul-01	3100	3010
C1-4-71801	Downgradient	-12	71.4-76.5	Jul-01	707	1096
C1-4-71801	Downgradient	-13	76.5-81.6	Jul-01	206	472
C1-4-71801	Downgradient	-14	81.6-86.7	Jul-01	124	580
C1-4-71801	Downgradient	-15	86.7-91.8	Jul-01	80	274
C1-4-71801	Downgradient	-16	91.8-96.9	Jul-01	226	280
C1-4-71801	Downgradient	-17	96.9-102	Jul-01	117	197
C1-4-71801	Downgradient	-18	102-107.1	Jul-01	65	220
C1-4-71801	Downgradient	-19	107.1-112.2	Jul-01	154	217
C2-1-71801	Upgradient	2	0-5.1	Jul-01	224	1580
C2-1-71801	Upgradient	1	5.1-10.2	Jul-01	13700	4930
C2-1-71801	Upgradient	-1	10.2-15.3	Jul-01	7500	5650
C2-1-71801	Upgradient	-2	15.3-20.4	Jul-01	4700	4460
C2-1-71801	Upgradient	-3	20.4-25.5	Jul-01	5200	3950
C2-1-71801	Upgradient	-4	25.5-30.6	Jul-01	5200	3320
C2-1-71801	Upgradient	-5	30.6-35.7	Jul-01	2200	3420
C2-1-71801	Upgradient	-6	35.7-40.8	Jul-01	3000	2820
C2-1-71801	Upgradient	-7	40.8-45.9	Jul-01	3500	3550
C2-1-71801	Upgradient	-8	45.9-51.0	Jul-01	3300	4260
C2-1-71801	Upgradient	-9	51.0-56.1	Jul-01	3300	2880
C2-1-71801	Upgradient	-10	56.1-61.2	Jul-01	1800	2590
C2-1-71801	Upgradient	-11	61.2-66.3	Jul-01	1404	2090
C2-1-71801	Upgradient	-12	66.3-71.4	Jul-01	1383	2460
C2-1-71801	Upgradient	-13	71.4-76.5	Jul-01	2600	3330
C2-1-71801	Upgradient	-14	76.5-81.6	Jul-01	3300	3530
C2-1-71801	Upgradient	-15	81.6-86.7	Jul-01	2700	2270
C2-1-71801	Upgradient	-16	86.7-91.8	Jul-01	2200	2200
C2-1-71801	Upgradient	-17	91.8-96.9	Jul-01	1035	1750
C2-1-71801	Upgradient	-18	96.9-102	Jul-01	774	1450
C2-1-71801	Upgradient	-19	102-107.1	Jul-01	499	1210
C2-1-71801	Upgradient	-20	107.1-112.2	Jul-01	189	580
C2-1-71801	Upgradient	-21	112.2-117.3	Jul-01	1146	2130

Table A3. (continued) Inorganic Carbon and Sulfur Concentrations in Denver Federal Center Cores

Sample ID	Location	Section	Interval cm	Date	Total IC μg/g	Total S μg/g
C2-3-71801	Upgradient	-1	0-5.1	Jul-01	7700	2718
C2-3-71801	Upgradient	-2	5.1-10.2	Jul-01	5900	2041
C2-3-71801	Upgradient	-3	10.2-15.3	Jul-01	4100	2111
C2-3-71801	Upgradient	-4	15.3-20.4	Jul-01	2100	1785
C2-3-71801	Upgradient	-5	20.4-25.5	Jul-01	1324	1464
C2-3-71801	Upgradient	-6	25.5-30.6	Jul-01	331	582
C2-3-71801	Upgradient	-7	30.6-35.7	Jul-01	137	495
C2-3-71801	Upgradient	-8	35.7-40.8	Jul-01	150	561
C2-3-71801	Upgradient	-9	40.8-45.9	Jul-01	128	520
C2-3-71801	Upgradient	-10	45.9-51.0	Jul-01	118	506
C2-3-71801	Upgradient	-11	51.0-56.1	Jul-01	91	547
C2-3-71801	Upgradient	-12	56.1-61.2	Jul-01	115	300
C2-3-71801	Upgradient	-13	61.2-66.3	Jul-01	90	320
C2-3-71801	Upgradient	-14	66.3-71.4	Jul-01	108	440
C2-3-71801	Upgradient	-15	71.4-76.5	Jul-01	122	425
C2-3-71801	Upgradient	-16	76.5-81.6	Jul-01	144	501
C2-3-71801	Upgradient	-17	81.6-86.7	Jul-01	111	736
C2-3-71801	Upgradient	-18	86.7-91.8	Jul-01	107	637
C2-3-71801	Upgradient	-19	91.8-96.9	Jul-01	135	375
C2-4-71801	Upgradient	2	0-7.6	Jul-01	147	<5
C2-4-71801	Upgradient	1	7.6-15.2	Jul-01	4100	<5
C2-4-71801	Upgradient	-1	15.2-20.3	Jul-01	5900	1110
C2-4-71801	Upgradient	-2	20.3-25.4	Jul-01	2500	1460
C2-4-71801	Upgradient	-3	25.4-30.5	Jul-01	1036	758
C2-4-71801	Upgradient	-4	30.5-35.6	Jul-01	398	727
C2-4-71801	Upgradient	-5	35.6-40.7	Jul-01	435	611
C2-4-71801	Upgradient	-6	40.7-45.8	Jul-01	296	580
C2-4-71801	Upgradient	-7	45.8-50.9	Jul-01	1600	1550
C2-4-71801	Upgradient	-8	50.9-56.0	Jul-01	1205	1250
C2-4-71801	Upgradient	-9	56.0-61.1	Jul-01	1385	1414
C2-4-71801	Upgradient	-10	61.1-66.2	Jul-01	1498	1485
C2-4-71801	Upgradient	-11	66.2-71.3	Jul-01	1161	1234
C2-4-71801	Upgradient	-12	71.3-76.4	Jul-01	1308	1189
C2-4-71801	Upgradient	-13	76.4-81.5	Jul-01	1012	1062
C2-4-71801	Upgradient	-14	81.5-86.6	Jul-01	755	925
C2-4-71801	Upgradient	-15	86.6-91.7	Jul-01	438	716
C2-4-71801	Upgradient	-16	91.7-96.8	Jul-01	382	619

Table A3. (continued) Inorganic Carbon and Sulfur Concentrations in Denver Federal Center Cores

Sample ID	Location	Section	Interval cm	Date	Total IC	Total S
					µg/g	µg/g
C2-1-71901	Vertical	-1	0-7.6	Jul-01	417	920
C2-1-71901	Vertical	-2	7.6-15.2	Jul-01	567	1192
C2-1-71901	Vertical	-3	15.2-22.8	Jul-01	384	1220
C2-1-71901	Vertical	-4	22.8-30.4	Jul-01	960	1742
C2-1-71901	Vertical	-5	30.4-38.0	Jul-01	1203	2150
C2-1-71901	Vertical	-6	38.0-45.6	Jul-01	1523	2807
C2-1-71901	Vertical	-7	45.6-53.2	Jul-01	1116	2621
C2-1-71901	Vertical	-8	53.2-60.8	Jul-01	1349	1879
C2-1-71901	Vertical	-9	60.8-68.4	Jul-01	1283	2291
C2-1-71901	Vertical	-10	68.4-76.0	Jul-01	2600	2995
C2-1-71901	Vertical	-11	76.0-83.6	Jul-01	2050	3108
C2-1-71901	Vertical	-12	83.6-91.2	Jul-01	2850	3175
C2-1-71901	Vertical	-13	91.2-98.8	Jul-01	2700	3803
C2-1-71901	Vertical	-14	98.8-106.4	Jul-01	2600	2493
C2-1-71901	Vertical	-15	106.4-114.0	Jul-01	4500	3374
C2-2-71901	Vertical	-1	0-7.6	Jul-01	212	814
C2-2-71901	Vertical	-2	7.6-15.2	Jul-01	184	755
C2-2-71901	Vertical	-3	15.2-22.8	Jul-01	217	546
C2-2-71901	Vertical	-4	22.8-30.4	Jul-01	249	628
C2-2-71901	Vertical	-5	30.4-38.0	Jul-01	365	499
C2-2-71901	Vertical	-6	38.0-45.6	Jul-01	352	380
C2-2-71901	Vertical	-7	45.6-53.2	Jul-01	1700	613
C2-2-71901	Vertical	-8	53.2-60.8	Jul-01	253	633
C2-2-71901	Vertical	-9	60.8-68.4	Jul-01	291	210
C2-2-71901	Vertical	-10	68.4-76.0	Jul-01	176	694
C2-2-71901	Vertical	-11	76.0-83.6	Jul-01	172	551
C2-2-71901	Vertical	-12	83.6-91.2	Jul-01	124	687
C2-2-71901	Vertical	-13	91.2-98.8	Jul-01	216	232
C2-2-71901	Vertical	-14	98.8-106.4	Jul-01	146	782
C2-3-71901	Vertical	1	0-7.6	Jul-01	2500	122
C2-3-71901	Vertical	2	7.6-15.2	Jul-01	7900	269
C2-3-71901	Vertical	-1	15.2-22.8	Jul-01	1299	831
C2-3-71901	Vertical	-2	22.8-30.4	Jul-01	1113	971
C2-3-71901	Vertical	-3	30.4-38.0	Jul-01	2500	1590
C2-3-71901	Vertical	-4	38.0-45.6	Jul-01	5600	1910
C2-3-71901	Vertical	-5	45.6-53.2	Jul-01	4500	1750
C2-3-71901	Vertical	-6	53.2-60.8	Jul-01	4100	1660
C2-3-71901	Vertical	-7	60.8-68.4	Jul-01	2800	1730
C2-3-71901	Vertical	-8	68.4-76.0	Jul-01	3000	1840
C2-3-71901	Vertical	-9	76.0-83.6	Jul-01	4000	1490
C2-3-71901	Vertical	-10	83.6-91.2	Jul-01	3300	1420

Table A3. (continued) Inorganic Carbon and Sulfur Concentrations in Denver Federal Center Cores

Sample ID	Location	Section	Interval	Date	Total IC	Total S
			cm		µg/g	µg/g
C3-2-71801	Upgradient	-1	0-5.1	Jul-01	1800	231
C3-2-71801	Upgradient	-2	5.1-10.2	Jul-01	594	203
C3-2-71801	Upgradient	-3	10.2-15.3	Jul-01	452	152
C3-2-71801	Upgradient	-4	15.3-20.4	Jul-01	429	133
C3-2-71801	Upgradient	-5	20.4-25.5	Jul-01	693	146
C3-2-71801	Upgradient	-6	25.5-30.6	Jul-01	1037	149
C3-2-71801	Upgradient	-7	30.6-35.7	Jul-01	1900	881
C3-2-71801	Upgradient	-8	35.7-40.8	Jul-01	640	401
C3-2-71801	Upgradient	-9	40.8-45.9	Jul-01	1200	547
C3-2-71801	Upgradient	-10	45.9-51.0	Jul-01	2000	649
C3-2-71801	Upgradient	-11	51.0-56.1	Jul-01	2800	1180
C3-2-71801	Upgradient	-12	56.1-61.2	Jul-01	3900	1940
C3-2-71801	Upgradient	-13	61.2-66.3	Jul-01	6300	2320
C3-2-71801	Upgradient	-14	66.3-71.4	Jul-01	4900	2290
C3-2-71801	Upgradient	-15	71.4-76.5	Jul-01	4100	1051
C3-2-71801	Upgradient	-16	76.5-81.6	Jul-01	5800	2120
C1-2-71000	Upgradient	-1	0-5.1	Jul-00	593	702
C1-2-71000	Upgradient	-2	5.1-10.2	Jul-00	854	1141
C1-2-71000	Upgradient	-3	10.2-15.3	Jul-00	1390	1377
C1-2-71000	Upgradient	-4	15.3-20.4	Jul-00	1559	1328
C1-2-71000	Upgradient	-5	20.4-25.5	Jul-00	1056	1107
C1-2-71000	Upgradient	-6	25.5-30.6	Jul-00	563	681
C1-2-71000	Upgradient	-7	30.6-35.7	Jul-00	493	648
C1-2-71000	Upgradient	-8	35.7-40.8	Jul-00	361	437
C1-2-71000	Upgradient	-9	40.8-45.9	Jul-00	202	431
C1-2-71000	Upgradient	-10	45.9-51.0	Jul-00	306	460
C1-2-71000	Upgradient	-11	51.0-56.1	Jul-00	235	421
C1-2-71000	Upgradient	-12	56.1-61.2	Jul-00	118	306
C1-2-71000	Upgradient	-13	61.2-66.3	Jul-00	144	267
C1-2-71000	Upgradient	-14	66.3-73.9	Jul-00	125	278
C1-2-71000	Upgradient	-15	73.9-81.5	Jul-00	167	284
C1-3-71100	Downgradient	3	0-7.6	Jul-00	2656	4143
C1-3-71100	Downgradient	2	7.6-15.2	Jul-00	906	2518
C1-3-71100	Downgradient	1	15.2-22.8	Jul-00	769	1199
C1-3-71100	Downgradient	-1	22.8-27.9	Jul-00	245	717
C1-3-71100	Downgradient	-2	27.9-33.0	Jul-00	218	464
C1-3-71100	Downgradient	-3	33.0-38.1	Jul-00	161	412
C1-3-71100	Downgradient	-4	38.1-43.2	Jul-00	154	413
C1-3-71100	Downgradient	-5	43.2-48.3	Jul-00	158	303
C1-3-71100	Downgradient	-6	48.3-53.4	Jul-00	160	232
C1-3-71100	Downgradient	-7	53.4-58.5	Jul-00	174	233
C1-3-71100	Downgradient	-8	58.5-63.6	Jul-00	126	169
C1-3-71100	Downgradient	-9	63.6-68.7	Jul-00	139	128
C1-3-71100	Downgradient	-10	68.7-73.8	Jul-00	128	143
C1-3-71100	Downgradient	-11	73.8-81.4	Jul-00	143	106

Table A3. (continued) Inorganic Carbon and Sulfur Concentrations in Denver Federal Center Cores

Sample ID	Location	Section	Interval	Date	Total IC	Total S
			cm		µg/g	µg/g
C2-17-71300	Upgradient	-1	0-5.1	Jul-00	5987	3799
C2-17-71300	Upgradient	-2	5.1-10.2	Jul-00	4324	3546
C2-17-71300	Upgradient	-3	10.2-15.3	Jul-00	4772	3366
C2-17-71300	Upgradient	-4	15.3-20.4	Jul-00	4817	2838
C2-17-71300	Upgradient	-5	20.4-25.5	Jul-00	3704	2324
C2-17-71300	Upgradient	-6	25.5-30.6	Jul-00	3481	2092
C2-17-71300	Upgradient	-7	30.6-35.7	Jul-00	2367	1867
C2-17-71300	Upgradient	-8	35.7-43.3	Jul-00	2769	1678
C2-16-71300	Downgradient	1	0-7.6	Jul-00	871	913
C2-16-71300	Downgradient	-1	7.6-12.7	Jul-00	793	1320
C2-16-71300	Downgradient	-2	12.7-17.8	Jul-00	2299	2034
C2-16-71300	Downgradient	-3	17.8-22.9	Jul-00	4243	3830
C2-16-71300	Downgradient	-4	22.9-28.0	Jul-00	5949	3362
C2-12-71300	Vertical	-1	0-10.2	Jul-00	5470	3239
C2-12-71300	Vertical	-2	10.2-20.4	Jul-00	6048	3966
C2-12-71300	Vertical	-3	20.4-30.6	Jul-00	7233	4597
C2-12-71300	Vertical	-4	30.6-40.8	Jul-00	7201	3886
C2-12-71300	Vertical	-5	40.8-51.0	Jul-00	7391	3356
C2-12-71300	Vertical	-6	51.0-61.2	Jul-00	7506	3493
C2-12-71300	Vertical	-7	61.2-71.4	Jul-00	4613	4084
C2-12-71300	Vertical	-8	71.4-81.6	Jul-00	6556	4453
C2-12-71300	Vertical	-9	81.6-91.8	Jul-00	6692	3833
C2-12-71300	Vertical	-10	91.8-102	Jul-00	8969	2044
C2-13-71300	Vertical	-1	0-10.2	Jul-00	5178	3844
C2-13-71300	Vertical	-2	10.2-20.4	Jul-00	6786	3761
C2-13-71300	Vertical	-3	20.4-30.6	Jul-00	6602	3527
C2-13-71300	Vertical	-4	30.6-40.8	Jul-00	5603	2923
C2-13-71300	Vertical	-5	40.8-51.0	Jul-00	4035	3172
C2-13-71300	Vertical	-6	51.0-61.2	Jul-00	3850	3354
C2-13-71300	Vertical	-7	61.2-71.4	Jul-00	7058	3935
C2-13-71300	Vertical	-8	71.4-81.6	Jul-00	5073	3324
C2-13-71300	Vertical	-9	81.6-91.8	Jul-00	5637	3189
C2-14-71300	Vertical	-1	0-10.2	Jul-00	1523	1627
C2-14-71300	Vertical	-2	10.2-20.4	Jul-00	476	1207
C2-14-71300	Vertical	-3	20.4-30.6	Jul-00	799	1519
C2-14-71300	Vertical	-4	30.6-40.8	Jul-00	1360	1474
C2-14-71300	Vertical	-5	40.8-51.0	Jul-00	2495	1957
C2-14-71300	Vertical	-6	51.0-61.2	Jul-00	3577	1883
C2-14-71300	Vertical	-7	61.2-71.4	Jul-00	3284	1878



Appendix B

Table B1. Phospholipid Fatty-acid (PLFA) Extract Data from Elizabeth City Cores

Sample ID	Section	Date	Biomass			Community Structure (% of total PLFA)										Eukaryotes (Polyenes)	Physiological Status
			PLFA pM/g	PLFA cells/g	PLFA pM/g	Prokaryote PLFA pM/g	Eukaryotic PLFA pM/g	Prokaryote/Eukaryote	Gram-/Anaerobic Gram- (TerB/Sats)	Gram-/Monos)	Anaerobic Metal Reducers (B/Monos)	Actinomyces (MidBr/Sats)	Genera Nests	Eukaryotes (Polyenes)			
EC050801-5	3	May-01	155	3.11E+06	154	1	174	19.2	27.7	28.2	6.9	17.5	0.6	0.00			
EC050801-5	2	May-01	248	4.95E+06	245	2	100	17.7	30.6	26.1	7.0	17.7	1.0	0.00			
EC050801-5	1	May-01	348	6.96E+06	3341	7	52	18.3	28.9	27.2	5.5	18.3	1.9	0.00			
EC050801-5	-1	May-01	782	1.56E+07	782	ND	NC	28.3	29.4	23.6	0.4	18.4	0.0	0.03			
EC050801-5	-2	May-01	2614	5.23E+07	2614	ND	NC	42.1	17.1	30.3	0.0	10.6	0.0	0.00			
EC050801-5	-3	May-01	1809	3.62E+07	1809	ND	NC	38.1	19.0	29.3	2.8	10.9	0.0	0.00			
EC050801-5	-4	May-01	2406	4.81E+07	2406	ND	NC	41.1	18.8	28.5	0.0	11.7	0.0	0.00			
EC050801-5	-5	May-01	260	5.20E+06	260	ND	NC	28.3	20.9	37.8	0.9	12.1	0.0	0.00			
EC050801-5	-6	May-01	24	4.72E+05	24	ND	NC	21.9	33.1	27.9	0.0	17.2	0.0	0.00			
EC050801-6	3	May-01	27	5.38E+05	27	ND	NC	0.0	0.0	0.0	0.0	100.0	0.0	0.00			
EC050801-6	2	May-01	8	1.66E+05	8	ND	NC	0.0	59.9	0.0	0.0	40.1	0.0	0.00			
EC050801-6	1	May-01	5	1.06E+05	5	ND	NC	0.0	52.6	0.0	0.0	47.4	0.0	0.00			
EC050801-6	-1	May-01	54	1.07E+06	50	4	13	12.8	41.9	16.6	2.0	19.4	7.2	0.00			
EC050801-6	-2	May-01	9	1.86E+05	9.3	ND	NC	0.0	69.0	0.0	0.0	31.0	0.0	0.00			
EC050801-6	-3	May-01	5	1.09E+05	5.4	ND	NC	0.0	69.0	0.0	0.0	31.1	0.0	0.00			
EC050801-6	-4	May-01	6	1.24E+05	6.2	ND	NC	0.0	71.5	0.0	0.0	28.5	0.0	0.00			
EC050801-6	-5	May-01	4	8.77E+04	4.4	ND	NC	0.0	50.8	0.0	0.0	49.3	0.0	0.00			
EC050801-6	-6	May-01	3	6.95E+04	3.5	ND	NC	0.0	53.8	0.0	0.0	46.2	0.0	0.00			
EC050801-6	-7	May-01	ND	ND	ND	ND	NC	0.0	0.0	0.0	0.0	0.0	0.0	0.00			
EC050801-7	3	May-01	25	5.05E+05	25	ND	NC	16.5	30.6	26.4	0.0	26.6	0.0	0.00			
EC050801-7	2	May-01	5	9.28E+04	5	ND	NC	0.0	22.2	29.8	0.0	48.1	0.0	0.00			
EC050801-7	1	May-01	18	3.56E+05	17	1	16	10.1	37.8	20.7	0.0	25.6	5.8	0.00			
EC050801-7	-1	May-01	913	1.83E+07	913	ND	NC	18.1	31.3	26.5	0.0	24.2	0.0	0.00			
EC050801-7	-2	May-01	196	3.92E+06	196	ND	NC	16.0	35.2	27.4	1.1	20.4	0.0	0.00			
EC050801-7	-3	May-01	25	5.00E+05	25	ND	NC	14.1	45.0	20.7	3.3	16.9	0.0	0.00			
EC050801-7	-4	May-01	9	1.77E+05	9	ND	NC	5.3	73.5	0.0	0.0	21.2	0.0	0.00			
EC050801-7	-7	May-01	6	1.19E+05	6	ND	NC	0.0	74.8	0.0	0.0	25.2	0.0	0.00			
EC050801-7	-9	May-01	6	1.15E+05	6	ND	NC	0.0	58.9	0.0	0.0	41.1	0.0	0.00			
EC060200-1	4	Jun-00	4	7.10E+04	3	Trace	17	0.0	34.2	0.0	6.3	53.9	5.7	0.00			
EC060200-1	3	Jun-00	3	5.44E+04	3	ND	19	0.0	29.8	0.0	7.0	58.2	5.0	0.00			
EC060200-1	2	Jun-00	9	1.87E+05	9	ND	NC	0.0	34.7	0.0	0.0	65.3	0.0	0.00			
EC060200-1	1	Jun-00	89	1.78E+06	88	1	148	5.8	37.2	0.5	6.0	49.9	0.7	0.10			
EC060200-1	-1	Jun-00	875	1.75E+07	875	ND	NC	7.4	57.7	3.6	4.0	27.3	0.0	0.10			
EC060200-1	-2	Jun-00	309	6.18E+06	309	1	555	12.6	50.9	12.7	9.5	14.2	0.2	0.20			
EC060200-1	-3	Jun-00	44	8.73E+05	44	Trace	832	7.5	30.1	4.8	3.9	53.6	0.1	0.04			
EC060200-1	-4	Jun-00	51	1.02E+06	51	Trace	178	3.8	16.5	2.5	2.2	74.5	0.6	0.18			
EC060200-4	3	Jun-00	4	7.56E+04	4	ND	NC	0.0	37.0	0.0	0.0	63.0	0.0	0.00			
EC060200-4	2	Jun-00	5	9.52E+04	5	Trace	27	8.1	34.7	0.0	12.3	41.3	3.6	0.00			
EC060200-4	1	Jun-00	51	1.02E+06	51	Trace	138	4.5	15.1	0.4	3.7	75.6	0.7	0.00			
EC060200-4	-1	Jun-00	570	1.14E+07	569	1	434	24.8	17.6	8.0	18.5	30.9	0.2	0.38			
EC060200-4	-2	Jun-00	203	4.07E+06	203	Trace	525	32.5	17.4	12.7	30.3	7.0	0.2	0.94			
EC060200-4	-3	Jun-00	173	3.46E+06	173	Trace	666	27.7	14.4	13.6	38.9	5.2	0.2	0.85			
EC060200-4	-4	Jun-00	41	8.24E+05	41	ND	NC	22.0	20.4	12.8	28.9	15.9	0.0	0.51			
EC060200-4	-5	Jun-00	13	2.67E+05	13	ND	NC	12.4	35.8	4.8	7.9	39.1	0.0	0.27			
EC060200-4	-6	Jun-00	4	7.73E+04	4	ND	NC	13.2	41.4	2.6	4.1	38.8	0.0	0.00			
EC060200-4	-7	Jun-00	3	6.55E+04	3	ND	NC	2.7	22.7	0.0	2.7	74.6	0.0	0.00			
EC060200-4	-8	Jun-00	42	8.46E+05	42	Trace	249	0.0	10.1	0.4	1.0	85.9	0.4	0.00			
EC060200-4	-9	Jun-00	5	9.63E+04	5	ND	NC	16.8	30.7	0.0	0.0	52.6	0.0	0.00			

Table B1. Phospholipid Fatty-acid (PLFA) Extract Data from Elizabeth City Cores

Sample ID	Section	Date	PLFA		Biomass		Prokaryote/ Eukaryote	Prokaryotic PLFA	Eukaryotic PLFA	Prokaryote/ Eukaryote	Community Structure (% of total PLFA)						Eukaryotes (Polyenols)	Physiological Status
			cells/g	pM/g	Prokaryote pM/g	PLFA pM/g					Gram-/ Anaerobic Gram- (TerB/Sats)	Gram- (Monos)	Gram- (Monos)	Metal Reducers (BiMonos)	Actinomyces (MidB/Sats)	Genera Nsats		
EC060300-5	8	Jun-00	4	8.51E+04	4	8.51E+04	14	Trace	14	NC	21.8	0.0	0.0	0.0	67.4	6.8	0.00	
EC060300-5	7	Jun-00	12	2.33E+05	11	2.33E+05	43	Trace	43	NC	18.1	0.0	0.0	0.0	71.0	2.3	0.00	
EC060300-5	6	Jun-00	2	4.18E+04	2	4.18E+04	21.3	Trace	21.3	NC	26.1	0.0	0.0	0.0	69.2	9.5	0.00	
EC060300-5	5	Jun-00	12	2.40E+05	12	2.40E+05	38	Trace	38	NC	26.1	0.0	0.0	0.0	66.3	2.6	0.00	
EC060300-5	4	Jun-00	11	2.12E+05	10	2.12E+05	20	Trace	20	NC	12.1	0.0	0.0	0.0	78.0	4.7	0.00	
EC060300-5	3	Jun-00	9	1.80E+05	9	1.80E+05	34	Trace	34	NC	9.8	0.0	0.0	0.0	73.6	2.9	0.00	
EC060300-5	2	Jun-00	6	1.20E+05	6	1.20E+05	24	Trace	24	NC	16.7	0.0	0.0	0.0	51.2	4.1	0.00	
EC060300-5	1	Jun-00	57	1.13E+06	56	1.13E+06	59	Trace	59	NC	16.0	0.4	0.4	3.5	67.2	1.7	0.13	
EC060300-5	-1	Jun-00	14	2.79E+05	14	2.79E+05	146	Trace	146	NC	13.7	0.0	0.0	0.0	82.1	0.7	0.00	
EC060300-5	-2	Jun-00	7	1.42E+05	7	1.42E+05	NC	ND	NC	23.5	0.0	0.0	0.0	68.4	0.0	0.00		
EC060300-5	-3	Jun-00	21	4.25E+05	21	4.25E+05	NC	ND	NC	12.5	0.0	0.0	0.0	86.9	0.0	0.00		
EC060300-6	9	Jun-00	22	4.39E+05	22	4.39E+05	56	Trace	56	NC	25.7	0.0	0.0	0.0	58.6	1.8	0.20	
EC060300-6	8	Jun-00	41	8.13E+05	40	8.13E+05	64	Trace	64	NC	17.2	2.1	2.1	9.1	74.2	1.6	0.00	
EC060300-6	7	Jun-00	1	2.98E+04	1	2.98E+04	NC	ND	NC	0.0	0.0	1.3	3.0	100.0	0.0	0.00		
EC060300-6	6	Jun-00	0	2.51E+03	0	2.51E+03	NC	ND	NC	0.0	0.0	0.0	0.0	100.0	0.0	0.00		
EC060300-6	5	Jun-00	0	6.92E+03	0	6.92E+03	NC	ND	NC	0.0	0.0	0.0	0.0	100.0	0.0	0.00		
EC060300-6	4	Jun-00	1	1.88E+04	1	1.88E+04	NC	ND	NC	0.0	0.0	0.0	0.0	100.0	0.0	0.00		
EC060300-6	3	Jun-00	6	1.14E+05	6	1.14E+05	NC	ND	NC	17.2	2.8	2.8	0.0	80.1	0.0	0.00		
EC060300-6	2	Jun-00	54	1.07E+06	54	1.07E+06	NC	ND	NC	63.0	5.2	5.2	4.2	15.6	0.0	0.00		
EC060300-6	1	Jun-00	5	1.09E+05	5	1.09E+05	NC	ND	NC	25.0	0.0	0.0	0.0	69.8	0.0	0.00		
EC060300-6	-1	Jun-00	15	3.06E+05	15	3.06E+05	75	Trace	75	NC	14.1	0.6	0.6	0.0	84.6	1.3	0.00	
EC060300-6	-2	Jun-00	25	4.91E+05	24	4.91E+05	121	Trace	121	NC	32.7	0.0	0.0	0.0	64.2	0.8	0.10	
EC060300-6	-3	Jun-00	9	1.82E+05	9	1.82E+05	50	Trace	50	NC	33.1	0.0	0.0	0.0	64.9	2.0	0.19	
EC060300-6	-4	Jun-00	6	1.23E+05	6	1.23E+05	NC	ND	NC	17.5	0.0	0.0	0.0	82.5	0.0	0.00		
EC060300-6	-5	Jun-00	92	1.85E+06	92	1.85E+06	131	Trace	131	NC	13.3	1.5	1.5	0.0	80.9	0.8	0.26	
EC90902	8	Sep-99	5	9.19E+04	5	9.19E+04	NC	ND	NC	50.9	0.0	0.0	0.0	49.1	0.0	0.00		
EC90902	7	Sep-99	1	2.98E+04	1	2.98E+04	NC	ND	NC	50.1	0.0	0.0	0.0	49.9	0.0	0.00		
EC90902	6	Sep-99	1	1.93E+04	1	1.93E+04	NC	ND	NC	33.6	0.0	0.0	0.0	66.4	0.0	0.00		
EC90902	5	Sep-99	2	4.19E+04	2	4.19E+04	NC	ND	NC	46.6	0.0	0.0	0.0	53.4	0.0	0.00		
EC90902	4	Sep-99	1	1.88E+04	1	1.88E+04	NC	ND	NC	30.4	0.0	0.0	0.0	69.6	0.0	0.00		
EC90902	3	Sep-99	1	1.77E+04	1	1.77E+04	NC	ND	NC	38.7	0.0	0.0	0.0	60.3	0.0	0.00		
EC90902	2	Sep-99	3	5.79E+04	3	5.79E+04	NC	ND	NC	38.9	0.0	0.0	0.0	61.2	0.0	0.00		
EC90902	1	Sep-99	4	7.77E+04	4	7.77E+04	NC	ND	NC	47.7	0.0	0.0	0.0	52.3	0.0	0.00		
EC90903	2	Sep-99	51	1.02E+06	559	1.02E+06	NC	ND	NC	38.7	6.3	6.3	17.1	24.1	0.0	0.39		
EC90903	1	Sep-99	219	4.38E+06	1541	4.38E+06	NC	ND	NC	40.0	2.2	2.2	8.2	34.2	0.0	0.13		
EC90903	-1	Sep-99	2610	5.22E+07	2610	5.22E+07	NC	ND	NC	23.5	6.8	6.8	17.3	12.4	0.0	0.00		
EC90903	-2	Sep-99	114	2.28E+06	114	2.28E+06	NC	ND	NC	22.6	3.3	3.3	6.3	29.5	0.0	0.30		
EC90903	-3	Sep-99	53	1.06E+06	53	1.06E+06	NC	ND	NC	63.3	2.8	2.8	1.2	22.7	0.0	0.38		
EC90903	-4	Sep-99	22	4.40E+05	22	4.40E+05	NC	ND	NC	21.1	2.4	2.4	0.0	25.6	0.0	0.00		
EC90903	-5	Sep-99	11	2.26E+05	11	2.26E+05	NC	ND	NC	66.9	0.0	0.0	0.0	33.1	0.0	0.00		
EC90903	-6	Sep-99	15	3.03E+05	15	3.03E+05	NC	ND	NC	60.0	1.2	1.2	0.0	25.3	0.0	0.00		
EC01061899	-1	Jun-99	128	2.55E+06	125	2.55E+06	47	3	47	NC	30.6	12.3	8.1	31.1	31.1	2.1	0.07	
EC01061899	-2	Jun-99	39	7.82E+05	38	7.82E+05	34	1	34	NC	10.3	3.1	2.3	75.8	2.8	0.10		
EC01061899	-3	Jun-99	38	7.54E+05	33	7.54E+05	12	3	12	NC	5.5	1.3	1.1	77.6	7.5	0.00		
EC03061699	-1	Jun-99	474	9.48E+06	463	9.48E+06	41	11	41	NC	36.3	11.7	11.6	17.9	2.4	0.07		
EC03061699	-2	Jun-99	1171	2.34E+07	1159	2.34E+07	101	11	101	NC	32.4	14.2	14.1	12.8	1.0	0.07		
EC03061699	-4	Jun-99	130	2.60E+06	61	2.60E+06	64	1	64	NC	14.0	1.0	1.0	29.5	49.6	0.00		
EC03061699	-5	Jun-99	69	1.38E+06	30	1.38E+06	1	37	1	NC	10.0	1.2	1.4	28.4	53.7	0.00		

Table B1. Phospholipid Fatty-acid (PLFA) Extract Data from Elizabeth City Cores

Sample ID	Section	Date	Biomass			Community Structure (% of total PLFA)										Physiological Status	
			PLFA pM/g	Prokaryote PLFA pM/g	Eukaryotic PLFA pM/g	Prokaryote/Eukaryote	Anaerobic Gram- (TerB/Sats)	Gram+/- (TerB/Sats)	Gram- (Mones)	Aerobic Metal Reducers (BtMones)	SRB/Actinomyces (MidB/Sats)	Genera Nsats	Eukaryotes (Polyenics)				
EC6102	4	Jun-99	1	1.99E+04	1	ND	NC	0.0	31.0	1.0	0.0	69.0	0.0	0.0	0.0	0.0	NC
EC6102	3	Jun-99	3	5.21E+04	3	ND	NC	0.0	45.9	1.0	0.0	54.1	0.0	0.0	0.0	0.0	NC
EC6102	2	Jun-99	1	1.32E+04	1	ND	NC	0.0	57.0	1.0	0.0	43.0	0.0	0.0	0.0	0.0	NC
EC6102	1	Jun-99	2	3.06E+04	2	ND	NC	0.0	0.0	0.0	0.0	100.0	0.0	0.0	0.0	0.0	NC
EC6101	-1	Jun-99	795	1.59E+07	795	ND	NC	15.7	39.8	7.0	7.9	29.7	0.0	0.0	0.0	0.0	0.17
EC6101	-2	Jun-99	85	1.70E+06	85	ND	NC	9.9	59.5	4.8	6.5	19.2	0.0	0.0	0.0	0.0	0.14
EC6101	-3	Jun-99	14	2.72E+05	14	ND	NC	7.1	77.2	0.0	0.0	15.7	0.0	0.0	0.0	0.0	0.00
EC6101	-4	Jun-99	6	1.26E+05	6	ND	NC	0.0	66.9	0.0	0.0	33.1	0.0	0.0	0.0	0.0	0.00
EC6101	-5	Jun-99	5	1.05E+05	5	ND	NC	0.0	65.9	0.0	0.0	34.1	0.0	0.0	0.0	0.0	0.00
EC6101	-6	Jun-99	2	3.59E+04	2	ND	NC	0.0	29.3	0.0	0.0	70.7	0.0	0.0	0.0	0.0	NC
EC6101	-7	Jun-99	1	1.25E+05	1	ND	NC	0.0	0.0	0.0	0.0	100.0	0.0	0.0	0.0	0.0	0.00
EC6101	-8	Jun-99	3	6.90E+04	3	ND	NC	0.0	37.5	0.0	0.0	62.5	0.0	0.0	0.0	0.0	0.00
EC6101	-9	Jun-99	1	2.03E+04	1	ND	NC	0.0	18.1	0.0	0.0	81.9	0.0	0.0	0.0	0.0	0.00
EC6101	-10	Jun-99	96	1.92E+06	70	26	3	1.4	51.9	0.0	0.1	19.4	0.0	0.0	27.3	0.0	0.30
EC6114	4	Jun-99	412	8.24E+06	412	ND	NC	27.5	37.9	7.6	12.1	14.9	0.0	0.0	0.0	0.0	0.10
EC6114	3	Jun-99	39	7.84E+05	39	ND	NC	11.5	56.1	4.2	5.4	22.8	0.0	0.0	0.0	0.0	0.00
EC6114	2	Jun-99	8	1.62E+05	8	ND	NC	21.1	54.4	0.0	0.0	24.4	0.0	0.0	0.0	0.0	0.00
EC6114	1	Jun-99	6	1.17E+05	6	ND	NC	0.0	58.1	0.0	0.0	41.9	0.0	0.0	0.0	0.0	0.00
EC6114	-1	Jun-99	21	4.21E+05	21	ND	NC	3.3	58.5	0.0	2.2	36.0	0.0	0.0	0.0	0.0	0.20
EC6114	-2	Jun-99	8	1.59E+05	8	ND	NC	1.6	31.6	0.0	7.4	59.5	0.0	0.0	0.0	0.0	0.00
EC6114	-3	Jun-99	2	3.27E+04	2	ND	NC	0.0	0.0	0.0	0.0	100.0	0.0	0.0	0.0	0.0	NC
EC6114	-4	Jun-99	3	6.11E+04	3	ND	NC	14.4	18.6	0.0	0.0	66.9	0.0	0.0	0.0	0.0	NC

The number of cells is calculated based on 2.0×10^{12} cells per gram dry weight of cells and 10^6 picomoles of phospholipid per gram dry weight of cells. Microbial Insights (G. Davis, pers. comm.) points out that the number of cells/gram of dry weight may vary and is dependent on the environmental conditions from which the microorganisms were recovered. Physiological status is based on ratios of fatty acid biomarkers that indicate a metabolic response to environmentally induced stress evidenced by decreased membrane permeability (w7/w7c). The biomarker indicators generally suggest that the samples have slow to moderate rates of turnover. Sample locations are shown in Figure 3.19. ND, not detected; NC not calculated.

Table B2. Phospholipid Fatty-acid (PLFA) Extract Data from Denver Federal Center Cores

Sample ID	Section	Date	Biomass				Community Structure (% of total PLFA)										Eukaryotes (Polyenols)	Physiological Status
			PLFA pM/g	PLFA cells/g	Prokaryote PLFA pM/g	Eukaryotic PLFA pM/g	Prokaryote PLFA pM/g	Eukaryote PLFA pM/g	Gram- (Monos)	Gram- (DiBifSats)	Gram- (TriBifSats)	Anaerobic Gram- (TerBifSats)	Gram- (Monos)	Metal Reducers (BifMonos)	Anaerobic Metal Reducers (BifMonos)	Actinomycetes (MidBifSats)		
C1-1-71701	-1	Jul-02	1533	3.07E+07	1499	34	44	9.3	51.6	9.8	6.2	20.9	2.2	0.26				
C1-1-71701	-2	Jul-02	979	1.96E+07	959	25	38	8.1	56.7	7.9	4.8	21.0	2.6	0.26				
C1-1-71701	-3	Jul-02	775	1.55E+07	758	17	44	10.0	51.5	8.0	4.8	23.4	2.2	0.24				
C1-1-71701	-4	Jul-02	858	1.72E+07	838	20	42	11.4	47.1	10.9	6.0	22.2	2.3	0.21				
C1-1-71701	-6	Jul-02	222	4.43E+06	213	9	24	9.1	53.5	10.7	5.9	16.8	4.1	0.17				
C1-1-71701	-8	Jul-02	27	2.55E+06	123	4	28	6.5	60.0	8.1	4.7	17.3	3.5	0.17				
C1-1-71701	-12	Jul-02	27	5.42E+05	26	1	28	4.0	72.2	4.3	0.0	16.0	3.5	0.00				
C1-1-71701	-18	Jul-02	22	4.33E+05	20	2	10	2.5	71.0	0.0	0.0	17.1	9.4	0.00				
C2-1-71801	2	Jul-02	68	1.36E+06	66	1	46	8.7	51.9	10.3	8.5	18.5	2.1	0.16				
C2-1-71801	-1	Jul-02	1439	2.88E+07	1410	29	50	17.1	41.4	12.9	10.9	15.8	2.0	0.42				
C2-1-71801	-2	Jul-02	1091	2.18E+07	1066	25	42	18.3	43.2	12.2	9.0	15.1	2.3	0.32				
C2-1-71801	-3	Jul-02	1100	2.20E+07	1084	17	67	20.5	42.2	12.4	8.3	15.0	1.5	0.32				
C2-1-71801	-4	Jul-02	1561	3.12E+07	1527	34	45	17.8	47.8	10.4	6.0	15.8	2.2	0.27				
C2-1-71801	-5	Jul-02	1517	3.03E+07	1477	40	37	17.6	46.9	11.3	6.4	15.2	2.6	0.28				
C2-1-71801	-7	Jul-02	1556	3.11E+07	1533	24	64	13.8	55.3	8.9	5.0	15.6	1.5	0.26				
C2-1-71801	-11	Jul-02	984	1.97E+07	970	14	69	14.2	55.8	9.6	5.2	13.8	1.4	0.15				
C2-1-71801	-15	Jul-02	1372	2.74E+07	1348	24	54	14.1	54.1	7.8	4.3	18.0	1.7	0.24				
C2-1-71801	-19	Jul-02	332	6.63E+06	324	8	43	11.9	54.9	8.4	10.6	11.8	2.3	0.13				
C2-3-71801	-1	Jul-02	1869	3.74E+07	1853	16	119	26.4	31.6	12.2	9.4	19.7	0.8	0.25				
C2-3-71801	-2	Jul-02	773	1.55E+07	767	6	124	22.1	39.4	11.9	7.9	17.9	0.8	0.23				
C2-3-71801	-3	Jul-02	533	1.07E+07	526	6	60	20.3	44.3	10.3	6.5	17.4	1.2	0.18				
C2-3-71801	-4	Jul-02	463	9.25E+06	455	8	67	17.2	51.5	8.6	5.6	15.4	1.6	0.19				
C2-3-71801	-6	Jul-02	125	2.51E+06	121	4	27	8.5	72.2	3.0	2.0	10.9	3.5	0.05				
C2-3-71801	-9	Jul-02	111	2.22E+06	105	6	18	5.5	56.3	1.8	21.2	10.1	5.1	0.06				
C2-3-71801	-12	Jul-02	58	1.17E+06	58	1	68	3.4	85.3	0.0	0.0	9.9	1.5	0.04				
C2-3-71801	-15	Jul-02	61	1.23E+06	59	3	21	4.0	78.2	1.1	0.0	12.2	4.6	0.05				
C2-3-71801	-17	Jul-02	114	2.29E+06	112	2	47	6.8	81.2	1.0	0.0	8.9	2.1	0.04				
C2-3-71801	-19	Jul-02	50	1.00E+06	49	1	52	7.2	79.1	1.3	0.0	10.6	1.9	0.06				
C2-1-71901	-2	Jul-02	363	7.26E+06	345	17	20	9.3	62.7	9.4	4.4	9.4	4.8	0.06				
C2-1-71901	-4	Jul-02	1326	2.65E+07	1303	23	56	20.3	42.4	15.2	6.2	14.3	1.7	0.34				
C2-1-71901	-6	Jul-02	1075	2.15E+07	1053	22	48	15.3	43.9	14.8	9.1	14.9	2.1	0.13				
C2-1-71901	-10	Jul-02	1909	3.82E+07	1883	23	74	19.4	36.1	16.5	10.0	16.7	1.3	0.17				
C2-1-71901	-12	Jul-02	2874	5.75E+07	2835	38	74	20.2	41.2	15.3	4.6	17.4	1.3	0.46				
C2-1-71901	-14	Jul-02	1527	3.06E+07	1497	30	49	15.5	44.1	15.4	8.9	14.1	2.0	0.21				
C2-2-71901	-2	Jul-02	42	8.50E+05	39	3	13	4.0	77.7	1.0	0.0	10.2	7.2	0.00				
C2-2-71901	-6	Jul-02	24	4.73E+05	19	4	4	3.1	61.7	3.6	0.0	13.2	18.4	0.00				
C2-2-71901	-9	Jul-02	60	1.20E+06	55	5	12	3.6	76.1	0.0	3.6	8.6	8.0	0.05				
C2-2-71901	-12	Jul-02	42	8.38E+05	39	3	14	4.3	74.9	1.1	0.0	12.9	6.9	0.06				
C2-2-71901	-14	Jul-02	86	1.72E+06	85	1	59	14.0	72.5	1.4	0.0	10.5	1.7	0.16				
C2-3-71901	-1	Jul-02	208	4.16E+06	191	17	11	17.8	49.6	2.6	2.2	19.6	8.2	0.12				
C2-3-71901	-2	Jul-02	100	2.00E+06	94	6	16	10.1	67.0	3.7	2.6	10.8	5.8	0.08				
C2-3-71901	-6	Jul-02	337	6.74E+06	331	6	57	17.8	32.3	9.6	8.2	30.6	1.7	0.17				
C2-3-71901	-9	Jul-02	656	1.31E+07	617	38	16	17.8	36.5	9.9	14.3	13.8	5.8	0.15				
C3-2-71801	-5	Jul-02	234	4.68E+06	220	14	16	13.8	52.4	11.7	3.4	12.9	5.8	0.32				
C3-2-71801	-6	Jul-02	655	1.31E+07	638	17	37	18.4	47.0	12.8	5.6	13.6	2.6	0.44				
C3-2-71801	-12	Jul-02	977	1.95E+07	965	12	82	21.4	34.0	15.8	8.9	18.7	1.2	0.56				
C3-2-71801	-14	Jul-02	1439	2.88E+07	1431	8	178	22.5	30.6	15.9	7.4	23.0	0.6	0.50				
C3-2-71801	-16	Jul-02	1301	2.60E+07	1294	7	195	22.3	30.9	14.5	5.3	26.6	0.5	0.36				

Table B2. Phospholipid Fatty-acid (PLFA) Extract Data from Denver Federal Center Cores

Sample ID	Section	Date	Biomass			Community Structure (% of total PLFA)						Eukaryotes (Polyenols)	Physiological Status
			PLFA pM/g	Prokaryote PLFA pM/g	Eukaryotic PLFA pM/g	Gram-/Anaerobic Gram- (TerB/Sats)	Gram- (Monos)	Anaerobic Metal Reducers (BtMonos)	Actinomycetes (MidBt/Sats)	Genera Nsats			
C1-2-71000	-1	Jul-00	1904	3.81E+07	1776	14	3.5	62.4	2.0	2.1	23.2	6.7	0.59
C1-2-71000	-2	Jul-00	95	1.89E+06	93	69	3.4	68.9	11.1	3.4	12.0	1.4	0.08
C1-2-71000	-3	Jul-00	693	1.39E+07	691	1	5.3	68.3	8.5	3.0	14.8	0.2	0.08
C1-2-71000	-4	Jul-00	506	1.01E+07	505	1	2.7	77.3	5.6	1.9	12.3	0.2	0.02
C1-2-71000	-5	Jul-00	103	2.07E+06	103	0.4	1.7	80.2	4.6	1.3	11.9	0.4	0.04
C1-2-71000	-8	Jul-00	15	3.03E+05	15	0.4	1.5	71.8	8.9	2.7	12.7	2.6	0.00
C1-2-71000	-13	Jul-00	22	4.48E+05	22	1	0.0	87.8	1.7	0.0	7.8	2.7	0.00
C1-3-71100	3	Jul-00	124	2.49E+06	122	2	8.5	52.0	11.7	6.7	19.5	1.6	0.00
C1-3-71100	1	Jul-00	306	6.13E+06	304	2	7.7	59.2	10.9	6.7	14.8	0.8	0.03
C1-3-71100	-1	Jul-00	80	1.59E+06	79	1	2.1	82.8	3.3	1.8	8.7	1.2	0.12
C1-3-71100	-2	Jul-00	19	3.85E+05	19	30	0.8	84.3	1.9	1.2	8.6	3.2	0.00
C1-3-71100	-4	Jul-00	30	6.00E+05	29	1	0.0	86.2	0.6	0.0	9.7	3.5	0.00
C2-13-71300	-1	Jul-00	2752	5.50E+07	2752	ND	11.2	52.9	13.5	7.0	15.4	0.0	0.34
C2-13-71300	-3	Jul-00	4182	8.36E+07	4177	5	768	48.5	16.1	6.7	13.2	0.1	0.32
C2-13-71300	-5	Jul-00	1827	3.65E+07	1821	7	262	57.0	11.9	5.3	14.2	0.4	0.32
C2-13-71300	-7	Jul-00	1115	2.23E+07	1115	ND	16.8	45.0	14.3	7.0	16.9	0.0	0.27
C2-13-71300	-9	Jul-00	2296	4.59E+07	2297	ND	10.7	54.7	10.5	4.8	19.4	0.0	0.22
C2-14-71300	-1	Jul-00	601	1.20E+07	599	2	356	14.8	9.5	5.3	10.5	0.3	0.25
C2-14-71300	-3	Jul-00	576	1.15E+07	574	2	66.2	66.2	4.8	1.6	10.1	0.4	0.08
C2-14-71300	-5	Jul-00	283	5.66E+06	282	1	45.3	53.4	13.0	6.6	16.4	0.2	0.29
C2-14-71300	-7	Jul-00	916	1.83E+07	913	3	344	57.8	10.5	5.2	15.1	0.3	0.34
C2-17-71300	-1	Jul-00	3851	7.70E+07	3842	9	416	52.7	13.2	4.7	17.5	0.2	0.19
C2-17-71300	-2	Jul-00	3760	7.52E+07	3752	8	454	53.4	13.3	5.3	17.7	0.2	0.22
C2-17-71300	-3	Jul-00	4066	8.13E+07	4061	6	666	51.8	13.8	4.9	18.1	0.2	0.14
C2-17-71300	-5	Jul-00	3916	7.83E+07	3905	10	384	51.2	14.3	4.7	18.3	0.3	0.17
C2-17-71300	-7	Jul-00	1820	3.64E+07	1819	ND	9.7	54.3	13.1	4.9	18.1	0.0	0.16
C1-2-52199	1	May-99	592	1.18E+07	559	33	12.1	24.3	3.5	26.9	23.0	5.5	0.17
C1-3-52199	-1	May-99	2584	5.17E+07	2537	48	10.4	56.9	9.4	4.0	17.5	1.9	0.10
C1-3-52199	-3	May-99	3554	7.11E+07	3476	78	13.4	50.9	11.0	4.7	17.9	2.2	0.10
C1-3-52199	-4	May-99	3455	6.91E+07	3395	59	13.0	52.9	10.6	4.1	17.6	1.7	0.10
C2-1-52299	4	May-99	1629	3.26E+07	1541	89	13.2	43.2	3.2	15.6	19.4	5.4	0.03
C2-1-52299	-1	May-99	4523	9.05E+07	4485	38	6.0	62.1	4.8	1.8	24.4	0.8	NC
C2-1-52299	-2	May-99	4924	9.86E+07	4859	65	8.8	54.8	6.3	2.7	26.1	1.3	0.10

The number of cells is calculated based on 2.0×10^{10} cells per gram dry weight of cells and 10^6 picomoles of phospholipid per gram dry weight of cells. Microbial Insights (G. Davis, pers. comm.) points out that the number of cells/gram of dry weight may vary and is dependent on the environmental conditions from which the microorganisms were recovered. Physiological status is based on ratios of fatty acid biomarkers that indicate a metabolic response to environmentally induced stress evidenced by decreased membrane permeability (w7/w7c). The biomarker indicators generally suggest that the samples have slow to moderate rates of turnover. Sample locations are shown in Figures 4.1 to 4.3. ND, not detected; NC not calculated.



United States
Environmental Protection
Agency

National Risk Management
Research Laboratory
Cincinnati, OH 45268

Official Business
Penalty for Private Use
\$300

EPA/600/R-03/045a
August 2003

Please make all necessary changes on the below label,
detach or copy, and return to the address in the upper
left-hand corner.

If you do not wish to receive these reports CHECK HERE ;
detach, or copy this cover, and return to the address in the
upper left-hand corner.

PRESORTED STANDARD
POSTAGE & FEES PAID
EPA
PERMIT No. G-35